

**THE MODELLING, SIMULATION AND CONTROL OF  
HELICOPTERS OPERATING WITH EXTERNAL LOADS**

Thesis submitted in accordance with the requirements of the  
University of Liverpool for the degree of Doctor in Philosophy

by

Stephen Albert Kendrick

November 2007

## ABSTRACT

The idea of using helicopters to transport loads externally is almost as old as the helicopter itself and is now commonplace, with applications both in civil and military environments. The concept allows heavy or bulky loads to be transported rapidly for point-to-point deployment, often to remote places that are inaccessible by ground transport. This useful ability makes helicopter slung load transport an extremely valuable asset to have, both in a civil and military context.

This thesis takes a holistic view of helicopters operating with external loads and investigates novel ways of expanding the operational effectiveness of helicopter slung load operations. The main research activity focussed on co-operative lift, a concept that uses multiple helicopters to carry extremely heavy or bulky loads that cannot be transported using a single helicopter alone.

Before tackling the complex problem of co-operative lift, the handling qualities and stability characteristics of a helicopter similar in type to the Sikorsky UH-60 were assessed using the US Army's ADS-33 handling qualities design criteria. This was to examine the effects that the external load had on the handling qualities of a single helicopter before multiple helicopter operations were explored. The single helicopter slung load configuration was also used to develop a novel multivariable  $H_{\infty}$  control scheme that provided pitch attitude regulation and load stabilisation. The system successfully increased the external load stability at the cost of reduced aircraft agility.

Co-operative lift trials in the past with traditionally augmented helicopters cited overwhelmingly high pilot work load as the main limitation, reducing the handling qualities and operational flight envelope of the co-operative lift system to a level below that of a single helicopter alone. To address this problem an extremely effective automatic co-operative lift controller (ACLC) was developed that allowed one pilot in the co-operative lift configuration to control both helicopters. The separation distance between the helicopters and the flight formation of the co-operative lift system was maintained automatically by the ACLC which proved to

decrease the pilot workload dramatically and improve the handling qualities. Piloted simulation with the HELIFLIGHT motion simulator at The University of Liverpool was carried out to test and compare the ACLC configuration with a manually controlled co-operative lift configuration using selected mission task elements (MTEs) from ADS-33. The configuration was simulated in a novel manner using commercial modelling software and a distributed simulation architecture. For the MTEs examined in this research, the ACLC improved the Cooper-Harper handling qualities ratings of the manual co-operative lift configuration from a system with major handling qualities deficiencies (Level 3), to a system with highly desirable handling qualities (Level 1). The augmented system also reduced the pilot workload from an extremely high level, with no spare capacity to complete additional tasks, to a level with insignificant workload. The handling qualities of the co-operative lift system were also compared with a non-linear Boeing CH-47 helicopter simulation model that was developed within this project using FLIGHTLAB modelling software. The piloted simulation results indicated that future co-operative lift operations would need an ACLC type controller to compete with a dedicated heavy lift cargo helicopter such as the CH-47.

# CONTENTS

<b>ABSTRACT .....</b>	<b>I</b>
<b>CONTENTS.....</b>	<b>III</b>
<b>ACKNOWLEDGMENTS.....</b>	<b>VIII</b>
<b>NOTATIONS AND ABBREVIATIONS .....</b>	<b>IX</b>
List of Symbols.....	ix
Greek Symbols.....	x
Subscripts .....	xi
Abbreviations.....	xi
<b>CHAPTER 1 .....</b>	<b>1</b>
INTRODUCTION .....	1
1.1 Overview of Slung Load Operations .....	1
1.2 Thesis Objective .....	4
1.3 Thesis Structure .....	5
1.4 Original Contribution .....	7
1.5 Literature Review .....	8
1.6 Co-operative Lift .....	13
1.7 Economic and Operational Benefits of Co-operative Lift.....	19
1.8 Conclusions to Chapter.....	22
<b>CHAPTER 2 .....</b>	<b>24</b>
HELICOPTER AND SLUNG LOAD MODELLING.....	24
2.1 Introduction.....	24
2.2 Helicopter Slung Load Model Configurations .....	25
2.3 Modelling Software .....	27
2.4 The FLIGHTLAB Generic Rotorcraft Model .....	28
2.5 The F-CH-47B Chinook Model .....	29
2.6 The Agusta Westland EH-101 Model.....	33
2.7 Slung Load Model Development .....	34

2.8 Co-operative Lift Model Development.....	37
2.8.1 <i>SimMechanics Co-operative Lift Model Validation</i> .....	40
2.8.2 <i>Co-operative Lift Separation Limits</i> .....	44
2.9 Conclusions to Chapter.....	48
<b>CHAPTER 3 .....</b>	<b>49</b>
EXPERIMENTAL SIMULATION SETUP .....	49
3.1 Introduction.....	49
3.2 The HELIFLIGHT Motion Simulator .....	49
3.3 The Fixed Base XPIT Simulator .....	53
3.4 Co-operative Lift Simulation .....	55
3.5 Co-operative Lift Model Operational Modes .....	57
3.5.1 <i>Fully Manual Control Mode</i> .....	57
3.5.2 <i>Data Driven Control Mode</i> .....	57
3.5.3 <i>Automated Control Mode</i> .....	58
3.6 Conclusions to Chapter.....	58
<b>CHAPTER 4 .....</b>	<b>59</b>
HANDLING QUALITIES ANALYSIS.....	59
4.1 Introduction.....	59
4.2 Mission Task Elements .....	63
4.3 FGR Handling Qualities Analysis.....	64
4.3.1 <i>Hover and Low Speed Requirements</i> .....	64
4.3.2 <i>The Bandwidth Criterion</i> .....	65
4.3.3 <i>The Attitude Quickness Criterion</i> .....	74
4.3.4 <i>The Large Amplitude Criterion</i> .....	78
4.4 Conclusion to Chapter .....	80
<b>CHAPTER 5 .....</b>	<b>82</b>
HELICOPTER AND EXTERNAL SLUNG LOAD ANALYSIS.....	82
5.1 Introduction.....	82
5.2 Single Helicopter Linear Stability Analysis .....	82
5.3 Piloted Simulation with Non-linear Model.....	89
5.4 Closed Loop Frequency Analysis .....	92
5.5 Load Stabilisation using SCAS.....	95

5.6 H-infinity Control .....	98
5.6.1 <i>H-infinity Control Design</i> .....	102
5.6.2 <i>Controller Robustness</i> .....	108
5.7 Conclusions to Chapter.....	110
<b>CHAPTER 6 .....</b>	<b>111</b>
THE AUTOMATIC CO-OPERATIVE LIFT CONTROL SYSTEM .....	111
6.1 Introduction.....	111
6.2 The Automatic Co-operative Lift Controller Objectives .....	115
6.3 Design Procedure.....	116
6.4 Control System Architecture .....	117
6.4.1 <i>Inner Control Loop Design</i> .....	118
6.5 Inner Loop ACAH Handling Qualities Analysis.....	122
6.5.1 <i>Inner Loop Attitude Quickness Results</i> .....	123
6.5.2 <i>Inner Loop Small Amplitude Results</i> .....	126
6.5.3 <i>Stability Analysis of the ACLC Inner Loop and the Industrial Clearance of Flight Control Laws</i> .....	129
6.5.4 <i>Stability Margin Criterion</i> .....	130
6.5.5 <i>Unstable Eigenvalue Criterion</i> .....	132
6.6 The ACLC Outer Control Loop .....	134
6.7 Master-Slave and Separation Maintenance Control .....	138
6.7.1 <i>Controller Objectives</i> .....	138
6.7.2 <i>Controller Data Link</i> .....	140
6.7.3 <i>The Desired Separation Point</i> .....	140
6.7.4 <i>Separation Maintenance Control</i> .....	143
6.7.5 <i>Controller Envelope</i> .....	145
6.7.6 <i>Tau Based Gap Closure System</i> .....	148
6.7.7 <i>Tau Based Visual Guidance</i> .....	151
6.8 Controller Implementation .....	153
6.9 Conclusions to Chapter.....	155
<b>CHAPTER 7 .....</b>	<b>156</b>
CO-OPERATIVE LIFT PILOTED SIMULATION TRIAL .....	156
7.1 Introduction.....	156

7.2 The Piloted Simulation Trial Objective .....	156
7.3 The Mission Task Elements .....	157
7.4 The Acceleration and Deceleration MTE .....	158
7.4.1 <i>The MTE Test Conditions</i> .....	161
7.4.2 <i>Single Helicopter Results</i> .....	163
7.4.3 <i>MCLC Load Results</i> .....	164
7.4.4 <i>MCLC without Load Results</i> .....	165
7.4.5 <i>ACLC Load Results</i> .....	165
7.4.6 <i>Task Performance</i> .....	167
7.4.7 <i>Load Dynamics</i> .....	174
7.4.8 <i>Control Activity</i> .....	176
7.5 F-CH-47B Acceleration and Deceleration MTE .....	178
7.6 The Pirouette MTE .....	183
7.6.1 <i>The MTE Test Conditions</i> .....	185
7.6.2 <i>Single Helicopter Results</i> .....	185
7.6.3 <i>MCLC Load Results</i> .....	185
7.6.4 <i>ACLC Load Results</i> .....	186
7.6.5 <i>Task Performance</i> .....	186
7.7 Conclusions to Chapter.....	189
<b>CHAPTER 8 .....</b>	<b>191</b>
CONCLUSIONS AND RECOMMENDATIONS.....	191
<b>REFERENCES.....</b>	<b>195</b>
<b>APPENDIX 1 .....</b>	<b>201</b>
F-CH-47B CHINOOK MODEL .....	201
A1.1 Rotor System Properties .....	201
A1.2 Fuselage Properties.....	203
A1.3 Engine Properties.....	206
A1.4 Mechanical Control System .....	206
A1.5 Stability Augmentation System.....	208
A1.6 F-CH-47B Model Validation .....	210

**APPENDIX 2 ..... 214**

    SIMMECHANICS MULTI-BODY SIMULATION ..... 214

        A2.1 SimMechanics ..... 214

        A2.2 SimMechanics Example ..... 216

**APPENDIX 3 ..... 219**

    PILOT RATING SCALES ..... 219



## ACKNOWLEDGMENTS

I would like to begin by expressing my appreciation to Prof. Gareth Padfield for introducing me to the interesting world of rotorcraft flight when I was an undergraduate student and for giving me the opportunity to fulfil an ambition in completing a PhD in aerospace engineering.

I would also like to express my gratitude to my project supervisor, Dr. Daniel Walker, who has supported me throughout the project, sharing his expertise in modern control techniques and for giving me the freedom to steer the project in the direction I deemed most suitable.

This project was supported by Westland Helicopters and would not have been as successful without their involvement. I would like to express my sincere gratitude to Mr. Paul Brinson for giving me the opportunity to work with his department at Yeovil and sharing with me his invaluable expertise. I would also like to thank the Technology and Simulation department who provided me with technical assistance and helpful advice.

Simulators invariably require more than one person to prepare and operate and HELIFLIGHT is no exception. I would therefore like to thank all of my colleagues at the Flight Science and Technology research group who have helped with the various simulation aspects of the project. Special appreciation must also be made to Mr. Gary Ireland who provided valuable experience in computer programming and system integration.

The final mention must go to my family and friends who have supported me throughout, providing me with sound advice and regular reality checks.

The research described in this thesis has been made possible by the UK Engineering and Physical Sciences Research Council (EPSRC) and Westland Helicopters.

## Notations and Abbreviations

### List of Symbols

a	Acceleration	[ft/s <sup>2</sup> , m/s <sup>2</sup> ]
a <sub>1s</sub>	Lateral cyclic pitch angle	[rad, deg]
A	State Matrix	
b <sub>1s</sub>	Longitudinal cyclic pitch angle	[rad, deg]
B	Control input matrix	
c	Chord	[ft, m]
C	Output matrix	
C <sub>m</sub>	Pitching moment coefficient	[-]
D	Direct matrix	
e	Error signal	
E	East	
g	Gravitational acceleration	[ft/s <sup>2</sup> , m/s <sup>2</sup> ]
h	Height	[ft, m]
J	Inertia	Kg m <sup>2</sup>
K	Proportional gain or controller gain	
l	Length	[ft, m]
L	Lift force	[N]
L <sub>p</sub>	Rolling moment due to roll rate derivative	
m	Mass	[lb, kg]
M <sub>q</sub>	Pitching moment due to pitch rate derivative	[-]
N	North	
N <sub>r</sub>	Yawing moment due to yaw rate derivative	[-]
p	Roll rate	[deg/s, rad/s]
P	Generalised plant model	
q	Pitch rate	[deg/s]
r	Yaw rate	[deg/s, rad/s]
R	Rotor radius	[ft, m]

## Notations and Abbreviations

---

t	Time	[s]
T	Total duration time	[s]
u	Body axes forward airspeed	[ft/s, kts, m/s]
u	Control signal	
v	Body axes sideward airspeed	[ft/s, kts, m/s]
v	Controller inputs	
w	Body axes heave airspeed	[ft/s, kts, m/s]
w	Exogenous inputs	
W	Weight	[lbs, kg]
x	Distance	[ft, m]
xa	Pilot lateral stick input	[inches, %]
X <sub>u</sub>	X force due to forward velocity derivative	[-]
xb	Pilot longitudinal stick input	[inches, %]
xc	Pilot collective stick input	[inches, %]
xp	Pilot pedal input	[inches, %]
X	State Vector	
y	Output vector	
Y <sub>v</sub>	Side force due to sideways velocity derivative	[-]
z	Exogenous outputs	
Z <sub>w</sub>	Vertical force due to vertical velocity derivative	[-]

## Greek Symbols

$\gamma$	H <sub>∞</sub> norm	
$\phi$	Roll attitude	[rad, deg]
$\theta$	Pitch attitude	[rad, deg]
$\theta_{\text{long}}$	longitudinal sling angle	[rad, deg]
$\theta_{\text{lat}}$	lateral sling angle	[rad, deg]
$\tau$	Tau, time to contact	[s]
$\omega$	Frequency	[rad/s, deg/s]
$\psi$	Yaw attitude	[rad, deg]

### **Subscripts**

b	Body axis
bw	Bandwidth
e, N	Earth axis
lh	Local helicopter axis
min	Minimum
max	Maximum
Pk	Peak
xb	body axis x component
yb	body axis y component
zb	body axis z component

### **Abbreviations**

ACAH	Attitude command, attitude hold
ACLC	Automatic co-operative lift controller
ACSR	Active vibration control of structural response
AUM	All up mass
AFCS	Automatic flight control system
CAA	Civil Aviation Authority
CFD	Computational Fluid Dynamics
CG	Centre of gravity
CSGE	Control system graphical editor
DADC	Dual air data computer
DLR	German Aerospace Centre
DCPT	Differential-collective-pitch-trim
DOF	Degrees of freedom
DSP	Desired separation point
DVE	Degraded visual environment
EGI	Embedded GPS and inertial sensor
FBW	Fly-by-wire
FBL	Fly-by-light
FCL	Flight control law
FGR	FLIGHTLAB Generic Rotorcraft

FLME	FLIGHTLAB model editor
GCP	Guidance and control point
GPS	Global positioning system
GSCOPE	Graphical scope
GVE	Good visual environment
HH	Hover hold
HIL	Hardware in the loop
HQ	Handling qualities
HQR	Handling qualities rating
IMU	Inertial measurement unit
LAN	Local area network
LCT	Longitudinal cyclic trim
LTI	Linear time invariant
MCLC	Manual co-operative lift control
MFCS	Mechanical flight control system
MIMO	Multiple input multiple output
MTE	Mission task element
NOE	Nap-of-the-earth
OFE	Operational flight envelope
PC	Position command
PH	Position hold
PI	Proportional, integral
PID	Proportional, integral, derivative
PIO	Pilot induced oscillation
RC	Rate command
SAS	Stability augmentation system
SCAS	Stability, control augmentation system
SISO	Single input, single output
SMC	Separation maintenance control
TC	Turn co-ordination
TFT	Thin film transistor display
TRC	Translational rate command
TSCS	Tau separation closure system

## Notations and Abbreviations

---

UCE	Usable cue environment
UDP	Universal data package
VRML	Virtual reality modelling language

# Chapter 1

## INTRODUCTION

### 1.1 Overview of Slung Load Operations

The idea of using helicopters to carry loads externally is almost as old as the helicopter itself and is now commonplace, with applications both in civil and military environments. The concept allows heavy or bulky loads to be transported to remote places that are often inaccessible by ground transport. Most conventional fixed wing aircraft require existing infrastructure in the form of runways to deliver or pick up their payload. Some dedicated transport aircraft can be operated from rough temporary runways but these are often labour intensive to create, take time to setup and require level ground. The ability to deploy resources rapidly for point-to-point deployment means that helicopter slung load configurations are an extremely valuable resource to the battlefield commander. The operational importance is mirrored in peace time operations where helicopter slung load configurations are used in specialist roles where point-to-point transportation is extremely important from an economic or humanitarian perspective. Humanitarian relief, fire suppression and construction operations are just a few examples of peace time missions where helicopters are used routinely to transport resources externally from point-to-point.

The addition of an externally slung load to a helicopter modifies the original flight dynamics and stability of the helicopter, altering the flight handling qualities throughout the operational flight envelope (OFE). Essentially, the external load behaves like a pendulum, changing the natural frequencies and modal shapes of the helicopter's low frequency modes. The slung load attachment point or cargo hook is not usually located at the same location as the helicopter centre of gravity (CG) and is usually offset both vertically and horizontally, further adding to the complexity of the dynamic system. Modern multi-body dynamic synthesis and modelling software allows these complex slung load systems to be modelled and analysed in a fraction of the time that it would take to derive and model mathematically from first principles.

The research in this thesis uses this approach to model and analyse a wide range of systems from simple point mass slung load models to more complex configurations that use multiple helicopters to carry extremely heavy loads. This design philosophy allowed more time to be spent on designing, implementing and simulating novel automatic flight control systems (AFCS) and slung load configurations.

The externally slung load introduces three main effects to the dynamics of the system. These include:

1. Additional pendulum-like rigid body modes.
2. Load aerodynamics.
3. Sling stretching.

The slung load introduces two additional rigid body modes to the system; a mode representing the longitudinal dynamics and a mode representing the lateral dynamics of the external load. These modes couple with the longitudinal and lateral modes of the helicopter most noticeably during low speed flight regime and hover [1], changing the dynamics and characteristics of the helicopter phugoid and Dutch roll mode. The aerodynamic shape of the load also contributes to the helicopter slung load dynamics. For example, loads that are spherical in shape, cubes and loads with good weathercock stability such as aeroplane fuselages with empennage still attached are usually dynamically stable up to high speed. However, many loads are not so regular in shape and will begin to oscillate as the aerodynamic forces increase. The ensuing oscillation of the load due to unsteady aerodynamics can build up to such high amplitudes that the pilot may be forced to jettison the load to prevent the safety of the helicopter and crew being endangered. Other loads such as slender rectangular loads on a single line cable will first orientate themselves broadside to the wind and then go into a steady oscillation with combined yawing and side-to-side motion. These effects degrade the system stability and handling qualities, reducing the operational flight envelope of the slung-load system to below that of a single helicopter operating without a load. Modern fly-by-wire control and AFCS that are usually employed to provide helicopter dynamic stabilisation and envelope protection can also be used to augment the helicopter-load system to provide additional load stabilisation. Novel



multivariable  $H_\infty$  control techniques were developed within this research using this concept and are described later in this thesis in Chapter 5.

Multiple helicopters can be used to transport an extremely heavy or bulky load that cannot be carried using a single helicopter alone. This concept is known as co-operative lift or twin lift and forms one of the primary research areas in this thesis. The concept allows increased productivity and efficiency for heavy lift operations without the need for large helicopters, which are more expensive to purchase, operate and maintain. Previous research which is outlined later in Section 1.5 has indicated that the limiting factor in co-operative lift operations is the extremely high workload encountered by the pilots of the multiple helicopter configurations. The pilots must co-ordinate their control strategy to fly in close formation with a separation distance between the helicopters equivalent to only two rotor diameters. Pilots find formation flying with this separation distance difficult enough, but with the addition of the spreader bar and external load that make the system highly coupled the piloting task is made much more difficult. With this in mind, one of the main research activities was to design a twin-lift AFCS where one pilot controls both of the helicopters in the co-operative lift configuration. Piloted simulation trials described later in Chapter 7 indicate that the incorporation of the twin-lift AFCS, designated the automatic co-operative lift control (ACLC) model, significantly reduced the pilot workload by automatically maintaining the separation and formation of the helicopters in the configuration. The work completed in this thesis can be categorised into four main activities:

1. The modelling of helicopters and external slung load configurations including a co-operative lift system.
2. The desktop and piloted simulation of conventional and novel co-operative lift helicopter slung load models using the HELIFLIGHT six-axis motion simulator located at The University of Liverpool.
3. The application of novel AFCS that stabilise the external load, improve the helicopter handling qualities and allow safe, productive operation of co-operative lift configurations.

4. The handling qualities analysis of the different non-augmented and augmented helicopter external slung load configurations using the ADS-33 design standard [2].

The four main activities listed were inter-connected and had to be explored in parallel to gain a complete understanding of helicopter slung load system. In this manner, for example, the helicopter and externally slung load were modelled and simulated using desktop and real-time piloted simulation in order to assess the handling qualities of the un-augmented system. Once the handling qualities were assessed and the behaviour of the system was fully understood, control theory was applied to stabilise the load and improve the helicopter handling qualities.

## **1.2 Thesis Objective**

The research objective was to take a holistic view of helicopters operating with externally slung loads and to investigate novel ways of using helicopters to transport loads and to develop novel control concepts that alleviate handling qualities problems and ensure safe flight. The main activity of the project was to develop a co-operative lift system that could be simulated in real-time and used for the application and subsequent analysis of a novel co-operative lift AFCS that improved handling qualities and reduced the pilot workload ensuring safe flight during the hazardous mode of flight. Previous research outlined later in this chapter indicated that co-operative lift was only suitable for low speed taxi manoeuvres due to extremely high pilot workload and the objective was to expand the flight envelope using modern AFCS, making co-operative lift a viable alternative to operating with one dedicated heavy lift helicopter such as the Boeing CH-47 Chinook. The main flight control objective was to develop an ACLC where one pilot controls both helicopters in the configuration and the controller ensures that the separation distance between the helicopters and the physical formation of the system are maintained automatically. The co-operative lift system investigated consisted of two helicopters carrying an external load supported by a horizontal rigid spreader bar. The handling qualities and system characteristics of conventional helicopter slung load operations had to be investigated first before the complex problem of co-operative lift could be tackled and this foundation work forms a considerable portion of this thesis. The approach

adopted in this research was to develop helicopter slung load models using non-linear modelling software where possible rather than developing models mathematically from first principles. This design philosophy allowed more time to be devoted to AFCS design and handling qualities analysis of the models developed.

### **1.3 Thesis Structure**

The idea of using helicopters to transport externally slung loads is introduced in this chapter with a detailed literature review of the relevant research that has already been carried out in this area. The concept of co-operative lift, including the important strategic and economic advantages are also detailed in this chapter, giving a broad overview of the project and research areas that will be addressed later on in the thesis.

Chapter 2 introduces the three helicopter types and non-linear flight mechanics models that were used in the research to investigate different aspects of helicopter slung load operations. The models include; the FLIGHTLAB Generic Rotorcraft (FGR), the Boeing CH-47 Chinook and the Agusta Westland EH-101 Merlin helicopter. The chapter also describes the modelling methods employed and the development of the co-operative lift model, including an introduction to the distributed simulation architecture. The simulation architecture and hardware is described in more detail in Chapter 3 with a detailed description of the HELIFLIGHT motion simulator and the XPIT fixed base simulator that were networked together to allow multiple helicopter operations. The novel method of simulating co-operative lift systems in real-time using commercial software and distributed simulation is also described in Chapter 3.

Handling qualities analysis forms an integral and important part of the work in this thesis and consequently has a whole chapter devoted to the subject in Chapter 4. Suitable handling qualities criteria from the United States ADS-33 design standard [2] were selected for assessing helicopter slung load configurations and the handling qualities of two of the helicopter flight mechanics models used in the research were investigated to give a pragmatic overview of the subject area. The concept of handling qualities analysis is developed further in Chapter 5 when the effects that an

external load has on the handling qualities of a medium lift utility helicopter similar in configuration to the Sikorsky UH-60 were investigated. The effect that conventional classical stability and control augmentation systems (SCAS) has on the load dynamics is also described in this chapter before examining the merits of more modern control techniques including a novel multi-variable  $H_\infty$  control system that gives an ACAH response type and stabilises the sling load angle.

The main research activity involved developing a co-operative lift model and applying a novel automatic co-operative lift control (ACLC) system that allowed one pilot to control both helicopters in the twin lift configuration using automatic separation and formation maintenance control. The co-operative lift model developed is described in Chapter 6 and includes the offline handling qualities analysis of the ACLC that was applied to two EH-101 models. The ACLC featured many novel features that improved the handling qualities allowing safer and more productive operation of the co-operative lift configuration.

Chapter 7 reports the results from two piloted co-operative lift simulation trials that were carried out using the HELIFLIGHT motion simulator. The trials were performed using two different piloting methods, these included: the manual co-operative lift control (MCLC) method where one pilot manually tracked the other helicopter in the twin lift configuration and the ACLC method where one pilot controlled both helicopters in the formation. Chapter 7 also describes a trial that was performed with a CH-47B Chinook helicopter model that was developed specifically for this research and designated the F-CH-47B. The aim of the trial was to compare the handling qualities and pilot workload of the dedicated heavy lift CH-47 cargo helicopter with the co-operative lift configuration to ascertain if co-operative lift is a viable alternative for transporting heavy external loads in the region of 5 to 10 tonnes.

Finally Chapter 8 states the conclusions drawn from the research and lists the recommendations for future work that could not be carried out within this research due to time constraints.

## 1.4 Original Contribution

This section emphasises the original contributions to learning made in this research. A PhD thesis should exhibit substantial evidence of original scholarship and material worthy of publication. The University of Liverpool ordinance for the degree of PhD states that the degree may be conferred upon:

*“A graduate of this or any other approved University or Institution, or a candidate who holds a qualification deemed by the Senate to be equivalent to an Honours degree of this University, who has submitted a thesis embodying the results of his/her individual research which is adjudged to make an original contribution to learning; which is coherently structured and clearly presented; and which shows evidence of systematic study and of ability to relate the results of such study to the general body of knowledge in the subject...”*

In general original scholarship can be an entirely new contribution to the research field, or an interpretation or application of existing work in a new way not considered before. The work presented in this thesis falls into both of these categories, with examples of novel modern control techniques and novel applications of existing concepts including co-operative lift control and simulation techniques. The original contributions to the area of helicopter slung load operations are summarised in the following list:

1. A co-operative lift configuration was modelled and simulated in a novel manner using commercial software and a distributed simulation network which included the HELIFLIGHT six-axis motion simulator.
2. An automatic co-operative lift control system (ACLC) was developed with some innovative features including; separation and flight formation maintenance control.
3. The handling qualities and pilot workload of the co-operative lift system were compared directly to a dedicated heavy lift CH-47B cargo helicopter carrying the same payload. This was achieved using piloted simulation and selected ADS-33 mission task elements (MTEs).

4. A multi-objective  $H_\infty$  AFCS was applied to a helicopter slung load system in a novel manner to simultaneously achieve an attitude regulation response type and slung load stabilisation.
5. Tau optical guidance theory [3] was used to develop an automatic gap closure system and guidelines were made for an innovative head-up-display (HUD) that would help to maintain separation between the helicopters in a co-operative lift configuration.

## 1.5 Literature Review

Early theoretical studies of the dynamics of a helicopter and slung load configuration focussed on the stability characteristics of simplified system models. One of the earliest studies was performed by Lucassen and Sterk in 1965 [4]. The model used in their investigations was a simple 3-degree of freedom model of the hover and longitudinal dynamics of the helicopter with angular displacement of the load. The model consisted of single cable suspension and neglected any aerodynamic forces and moments on the load. They concluded that the pole of the load pendulum mode was stable and the phugoid mode remained unstable as the cable length was increased. The multi-body system investigated was found to be sensitive to parameter change and for some combinations of parameters the helicopter mode was destabilised while the load mode was stabilised suggesting that a more comprehensive model of the system was required.

In 1971 Szustak and Jenny [5] examined the control and operational issues of the control of large crane helicopters. They investigated several load suspension systems including one design which had retractable load cables that allowed the load to be retracted so that it was 'snug' with the helicopter. This was found to increase the stability of the system and allowed the load to be transported at increased speed but with expense of an increased complexity and dry mass. The authors also outlined five operational criteria aimed at increasing the efficiency and safety of slung load operations.

The operational criteria are still relevant and can be used as design targets:

1. Fast hook-up and release by a minimum ground crew are required.
2. Maximum speed is desired with the load in a 'snug' position (cables retracted), without load oscillations in still air.
3. For rapid turn-around and operation in winds, a maximum speed without load instabilities is required with the load suspended below the aircraft (cables extended).
4. Emergency release is required.
5. Failure of a single cable should not produce un-safe aircraft motions (assuming normal pilot reaction times).

They also pointed out in their study that a conventional stability augmentation system was not adequate for precision hover and load release due to the susceptibility of pilot induced oscillations (PIO) and that further control augmentation of the helicopter through stability and control augmentation systems (SCAS) would be required. Dukes [6] used similar approximations to Lucassen and Sterk to investigate the basic stability characteristics of a helicopter with a slung load and explored various feedback and open-loop control systems for damping the pendulous helicopter-load motion. Several feedback stabilisation schemes and appropriate piloting strategies were investigated. Positive pitch damping, from the rotor alone or also by a flight control system was not found necessarily to increase the stability of the pendulum mode of the load and increased pitch damping only provided a small increase in the damping of the mode. A novel feedback scheme in which the attachment point actively moved longitudinally along the helicopter fuselage was proven effective but the practical feasibility was not investigated.

The preceding work focussed on hover and low speed flight regimes where the load dynamics did not play a significant role. In reality however slung loads are rarely aerodynamically shaped bodies and are more likely to resemble bluff bodies that can be susceptible to dynamic instabilities triggered by unsteady aerodynamics. Poli and Cromack [7] studied the stability of a helicopter carrying two different loads; an 8ft × 8ft × 20ft container and a 20ft long × 5.4ft diameter cylindrical container. They

concluded that the stability of the system was increased by using longer cables, flying at high speeds and transporting lighter weights. Cliff and Bailey [8] confirmed Poli and Cromack's results to an extent by proving that decreasing the weight improved the stability, but longer cables were found to be destabilising and lowering drag was found to increase stability. Although the authors were able to make some deductions regarding the stability effects of various parameters such as mass ratio and tether length, they suggested that more complete dynamical models were required for further investigation.

Feaster [9] and Feaster *et al* [10] attempted to increase the fidelity of the aerodynamic load model using a yaw-damping coefficient that was determined through experiment. The coefficient was used in a linearised small perturbation stability analysis, which considered single and two-cable tandem suspension systems. The results from their study agreed with full-scale tests and demonstrated that two-cable tandem suspension was a practical way of transporting the standard cargo container investigated. A year later in 1976 Prabhakar and Sheldon [11, 12] completed a theoretical study of a Westland Sea King helicopter carrying a standard cargo container on a two point longitudinal suspension. The aerodynamic stability derivatives used in the model were again determined through experiment and they concluded that the pitch and yaw rate derivatives were strongly destabilising. The lateral-directional and longitudinal stability were governed by the same parameters, but the conditions for lateral stability proved to be more complex.

A decade later, Nagabhushan [13, 14] and Nagabhushan and Cliff [15] revisited the dynamics, stability and control of low speed single-point suspension load configurations. The helicopter model used was more sophisticated than the ones used in the studies previously mentioned and included the full linear equations for rigid body aircraft motion and rotor flapping dynamics. The equations were used for stability analysis and the effects of several configuration parameters were investigated. These included cable length, fore/aft and vertical position of suspension point, and load weight. Some of the system modes could be stabilised depending on the combination of parameters but overall all the instabilities were found to be small in amplitude and frequency.



Cicolani and Kanning [16] derived general simulation equations for the rigid body motion of slung load systems, motivated by an interest in trajectory control for slung loads carried by co-operative lift configurations. The equations for the general systems of  $n$  rigid bodies were obtained using Newton Euler rigid-body equations with the introduction of generalised velocity co-ordinates [16]. These are illustrated below in equations 1.1 and 1.2:

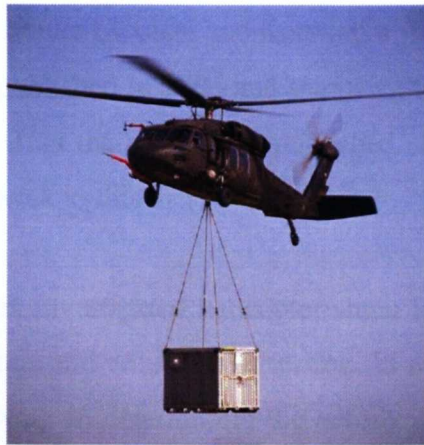
$$mig_N + FAi_N + FCi_N - mi\dot{V}i^*_N = 0 \quad \text{eqn 1.1}$$

$$MAi_b + MCi_b - Ji\omega_i_b - S(\omega_i_b) Ji\omega_i_b = 0; \quad \text{eqn 1.2}$$

$$i = 1, 2, \dots, n$$

Equation 1.1 above represents the balance of translational forces in the system, where the subscript  $N$  denotes the inertial axes. Equation 1.2 represents the sum of moments about each body's CG, where the subscript  $b$  denotes the corresponding body axes. The first term,  $mig_N$  is the gravity force acting through each CG,  $FAi_N$  and  $MAi_b$  are the aerodynamic forces and moments respectively,  $FCi_N$  and  $MCi_b$  are the cable forces and moment respectively. The terms  $mi\dot{V}i^*_N$  and  $Ji\omega_i_b$  represent the inertial reaction force of each body and the term  $S(\omega_i_b) Ji\omega_i_b$  is the moment induced by the Coriolis effect [16]. Three forms of the general equations were obtained: two generic case specific results for single helicopter systems with elastic and inelastic suspension respectively and a third new formulation for inelastic suspensions. The work completed by Cicolani and Kanning did not consider the effects of cable collapse which could occur during large unstable excursions from the nominal configuration or during load pick up and drop off.

In 1998 Cicolani et al. [17] reported the results of flight tests of a UH-60 helicopter carrying a CONNEX container load which is illustrated in figure 1.1. This was the first time that detailed flight test results were published that included useful frequency domain analysis. The study focused on the frequency domain and in particular on system identification and validation.



**Figure 1.1: Sikorsky UH-60 carrying a CONNEX container [16]**

Increasing the load weight was found to reduce the lateral bandwidth and further increases in weight reduced the bandwidth to a value below that of the pendulum frequency. Longitudinal stability margins were not particularly sensitive to changes to the external load parameters, but lateral stability margins were degraded. Both the bandwidth and phase delay were found to be highly variable depending on the load configuration, i.e. combination of cable lengths and load mass.

In 2001 Stuckey [18] used mathematical modelling to assist in defining the operating limits of the Australian Army CH-47D Chinook when carrying mixed density slung loads. General system equations of motion were obtained from the Newton-Euler equations in terms of generalised coordinates and velocities. The model was verified using simple pendulum approximations and the open-loop characteristics of the system were examined with respect to changes of multiple parameters including: helicopter-load mass ratio, suspension configuration and the number of loads.

Bisgaard *et al* [19] modelled and verified a generic slung load system using a small-scale helicopter. The model was intended for use in simulation, pilot training and control application and was derived using a redundant co-ordinate formulation based on Gauss' Principle of Least Constraint using the Udeadia-Kalaba equation. The model was capable of modelling all body to body suspension types and was augmented with the ability to detect and respond to collapsing and tightening of wires in a dynamic way using simple impulse based collision theory. The model was also shown to extend to multi-lift systems in a generic way for modelling multiple

helicopters and loads and unlike Cicolani and Kanning's work [16] could model cable collapse. This work was published in 2006 and seems an ideal method for modelling co-operative lift systems. Had the work been published earlier, the approach would have been applied to the work in this thesis.

Most of the previous work investigated helicopter slung load behaviour through the use of mathematical models and wind tunnel testing. In comparison, there has been very little experimental work in determining the aerodynamic behaviour of various slung loads through full scale flight testing. Gabel and Wilson [20] addressed the problems of aerodynamic yaw instability, vertical bounce and sling-web flapping through extensive simulation, wind-tunnel and flight tests in 1968. Several years later Hone [21] used data from flight tests on a Sikorsky CH-54 heavy lift helicopter to investigate the validity of a model developed by Briczinski and Karas [22]. The purpose of carrying out this work was to investigate the carriage of externally suspended loads and to establish more reliable strength requirement data for the load slings and attachment points.

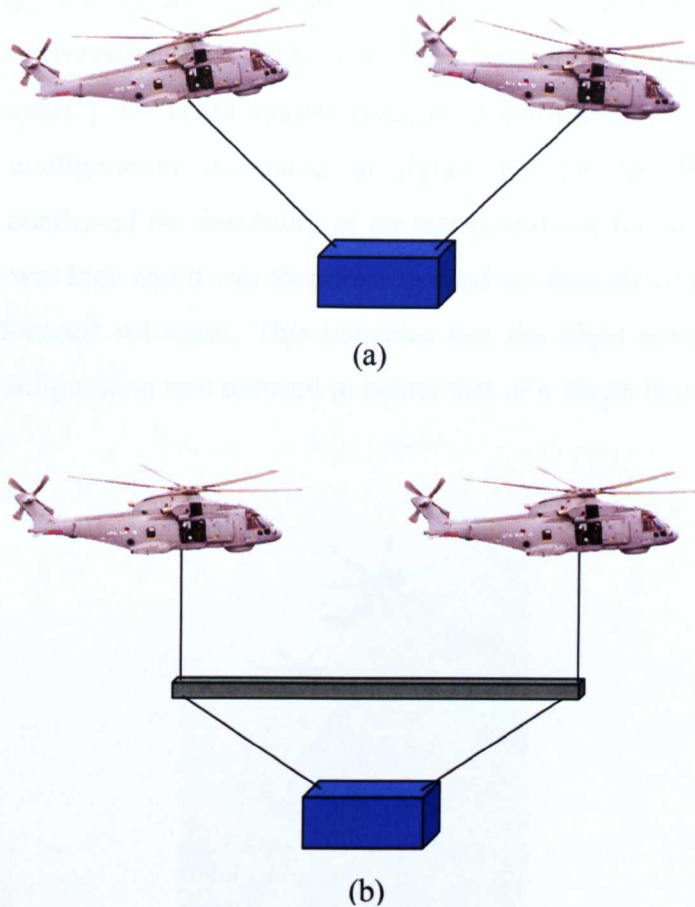
More recently in 2005 Hamers [23] flight tested a flight director for a BO105 helicopter carrying a slung load. The flight director gave the pilot a convenient aid to effectively damp the load pendulum motion and to allow manoeuvring without exciting oscillatory load modes.

## **1.6 Co-operative Lift**

Co-operative or multi-lift utilises multiple helicopters to transport extremely heavy or bulky loads that could not be transported using a single helicopter alone. The concept has been in existence for at least five decades [24], but a successful configuration that is effective across a wide flight envelope does not appear to have been implemented successfully. This is primarily due to the extremely high pilot workload involved in manoeuvring the highly coupled system. Co-operative lift allows increased lifting efficiency and productivity without the need for large rotorcraft, which are more expensive to acquire and maintain. Beyond a certain payload capacity, the economics of the helicopter performance follows the law of diminishing returns [25].

The potential for extending the capabilities of medium payload commercial helicopters using twin lift has also been suggested because of the difficulties involved in ferrying dedicated heavy lift helicopters such as the Russian MI-26 to a given location for a unique, one-off heavy lift operation. Imaginative operators have already used a multi helicopter technique to a limited degree. Examples include operations in South America for carrying transmission cable which is beyond the capacity of available helicopters in the area and an operation in Scotland where 15m utility poles weighing as much as 800kg were transported by suspending them between two Jet Rangers in a spreader bar configuration. In this example a payload 1.8 times the nominal helicopter payload was carried using a tip path separation of 40% of a rotor diameter. The poles were moved in this way for 3 miles at speeds up to 60 knots [28].

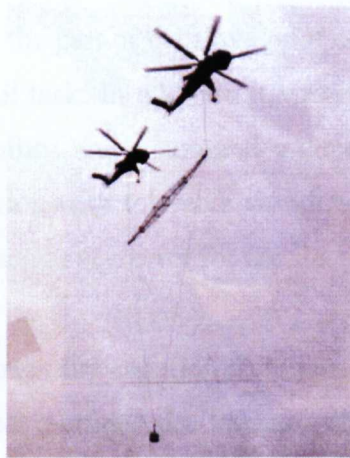
Cicolani and Kanning [16] proposed several co-operative lift configurations. The most common type investigated over recent years involves the use of two helicopters – often referred to as the twin-lift system. Two main twin-lift configurations have emerged over the years and are illustrated in figure 1.2.



**Figure 1.2: The two most common types of twin lift configuration**

Configuration (a) in figure 1.2 is referred to as the pendant arrangement and is most flexible from a logistics point of view. The external load is rigged directly to the two lifting helicopters via the two tether cables. Configuration (b) uses a horizontal rigid separation beam known as a spreader bar. Without the spreader bar, the helicopters would have to adopt a pitch and roll trim attitude that eliminates the tendency for the helicopters to be drawn together by the forces and moments created by the tether cables that are attached directly to the load, as illustrated in figure 1.2 (a). The spreader bar therefore reduces the control activity and pilot workload required permitting nominally zero trim pitch and roll attitudes in the hover. The main disadvantage of the spreader bar is that, logistically, it is inconvenient especially in the context of a rapid reaction situation such as a battlefield operation or humanitarian response. The spreader bar also takes up some of the payload capacity and introduces additional dynamics to the system including an additional unstable mode in the hover [25].

In 1968 Sikorsky was funded for studies of possible twin lift techniques and these studies led to a demonstration in 1970 of a 20-ton twin lift configuration using two CH-54B helicopters [25]. These studies considered many options and selected the spreader bar configuration illustrated in figure 1.3 for the flight trial. The demonstration confirmed the feasibility of air taxi operations for short distances but pilot workload was high and it was therefore deemed not feasible or safe to transition to significant forward velocities. This indicates that the flight envelope of the cooperative lift configuration was reduced to below that of a single helicopter operating alone.



**Figure 1.3: Two CH-54 helicopters sharing a 16,000kg load [25]**

In 1986 Rodriguez and Athans [26] presented guidelines for developing a multivariable centralised automatic flight control system (AFCS) for a twin lift helicopter system. The linear model used was a Sikorsky UH-60A Blackhawk and only the longitudinal dynamics were considered near a hover trim condition. Singular value ideas were used to formulate performance and stability robustness specifications and a Linear-Quadratic-Gaussian with Loop-Transfer-Recovery (LQG, LTR) design was obtained and evaluated. The methodology proved that it was possible to design a centralised multiple input, multiple output (MIMO) AFCS for a twin lift system addressing several feedback issues including low frequency command following, disturbance rejection as well as being robust to high frequency modelling and the attenuation of high frequency sensor noise.

In 1988 Hess and Tran [27] carried out a pilot/vehicle analysis of a twin-lift helicopter configuration in hover carrying a load suspended from a rigid spreader bar. They made one of the first references to “master-slave” twin-lift control where the pilot manoeuvres the master vehicle in response to internally generated position commands and the pilot of the slave visually senses master helicopter translational motion and uses it as a position command for his own vehicle. The pilot equalisation in all feedback loops was established using classical frequency domain pilot/vehicle analysis techniques based upon the crossover model of the human pilot. Hess and Tran concluded that in addition to the high bandwidth roll control that was essential for stabilising the entire twin lift system, the necessity of sensing and using the lateral helicopter separation rate on the part of the slave pilot defined the workload intensive elements of the flight control task. In addition it was recommended that an attitude command/attitude hold stability and command augmentation system would be a necessity for twin-lift operation with tolerable workload. The inclusion of a cockpit display of quickened lateral separation error for the slave pilot was also advised.

Menon *et al* [28] used feedback linearization techniques to investigate the nonlinear control of a twin lift helicopter configuration constrained to the transversal plane. The controller performance, together with the sensitivity to a few parameter variations, was studied in a nonlinear simulation. Two distinct operational modes were identified including a completely automatic mode where the pilot sets up the desired final conditions and the flight computer then flies the twin lift configuration automatically using an internally generated trajectory. This scenario could be used for takeoff and landings as well as flying in a degraded visual environment. In the second mode of operation, one or both pilots would operate three axis control columns to continuously command the payload position. The twin lift autopilot would then track these commands in real time while maintaining adequate separation between the helicopters. Two control philosophies were investigated, in the first, each helicopter was charged with the task of controlling specific sets of output variables. For example, one of the helicopters could be assigned the responsibility for payload positioning, while the other helicopter maintains the separation between the two vehicles. This type of philosophy was referred to as role-assigned control and is equivalent to “master-slave” control used in previous literature [26], [28]. In the

second control philosophy termed the co-operative control concept, both helicopters were jointly responsible for the control of all of the flight variables. The co-operative control concept was shown to be more robust than the role assigned control concept in the presence of relative helicopter performance degradation.

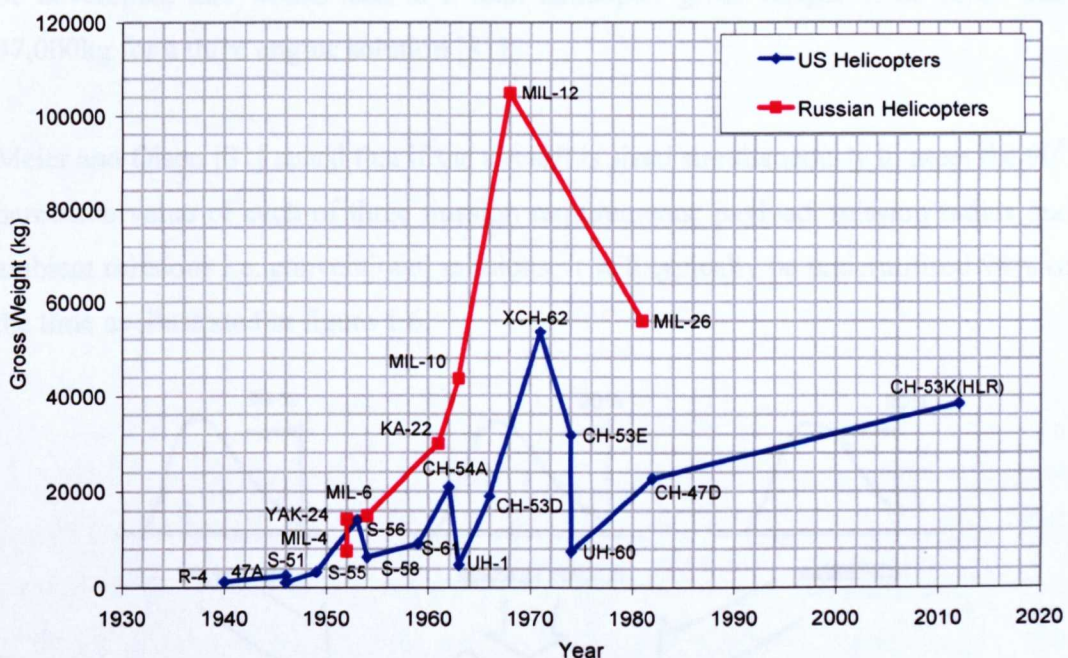
Reynolds and Rodriguez [29] presented two  $H_\infty$  controller designs for a twin lift helicopter system. The configuration consisted of two Sikorsky UH-60A helicopters jointly carrying a load supported by a horizontal spreader bar. The first design considered the tethers connecting the helicopters to be an equal length and the second considered them to be un-equal. Both designs used a seven degree of freedom model linearised about the hover. They concluded that both  $H_\infty$  designs provided adequate stabilisation of the helicopter pitch attitudes and required reasonable amounts of control action to achieve this. The equal tether configuration appeared to slightly outperform the unequal system in terms of overshoot and settling time, however the unequal tether system offered the benefits of reduced control action and the additional feature of increased safety by increasing the separation between the main rotors of the master and slave helicopters.

Mittal and Prasad [30] developed the first three-dimensional nonlinear dynamical simulation capable model of the twin-lift system in 1993. The model included; the rigid-body dynamics of the two helicopters, spreader bar and the load. The mathematical model for the helicopter aerodynamics consisted of generic, nonlinear, force and moment models for each helicopter component; the main rotor, tail rotor, fuselage and empennage. A nonlinear controller based on an approximate input-output feedback linearization was synthesised where the nonlinear feedback laws formed an outer loop for the twin lift flight control system and was used in conjunction with the existing stability augmentation systems of the helicopters, which constitute the inner loop for the flight control system. For the specific command trajectory considered, the simulation results show that the nonlinear controller designed enabled stable load transportation with tight tolerances and reasonable control magnitude.



## 1.7 Economic and Operational Benefits of Co-operative Lift

This section develops the advantages of co-operative lift from an economic and operational perspective based on a paper produced in 1987 by Meier and Olson [31]. Their intention was to challenge U.S. Army's decision to design a new cargo rotorcraft sized to meet the most demanding of the future combat airlift requirements, warning the programme would be unnecessarily large and expensive. They recommended that overall requirements could be satisfied more efficiently with a smaller aircraft by using co-operative lift for infrequent peak payload demands. Figure 1.4 shows that after 60 years of steadily increasing gross weight, the maximum rotorcraft size appears to be levelling off with the exception of the unique MIL-12 which did not make it into operational service (figure 1.5). Meier and Olson [31] cited the main reason for this trend reversal was due to economic and operational factors rather than technology limitations.



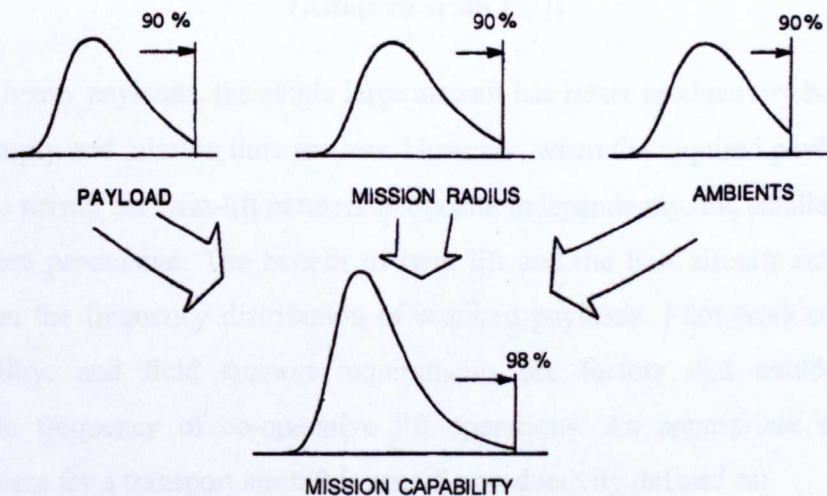
**Figure 1.4: Historical helicopter size trends (adapted from [31])**



**Figure 1.5: MIL-12 Helicopter [31]**

In theory economies of scale should make a larger aircraft more efficient to build and operate, however in reality costs for the same total fleet lift capability are actually higher because of the greater initial investment for development, qualification, and tooling. A large aircraft is also easier to detect than a smaller helicopter and less able to out manoeuvre threats, reducing its combat survivability and making it less likely to be deployed by field commanders. The practical limit to the size of future large cargo rotorcraft can be defined in terms of the availability of large enough engines capable of generating sufficient power. Assuming an engine producing 8000 hp could be developed, this would lead to a total helicopter gross weight of no more than 37,000kg for a three engine solution [31].

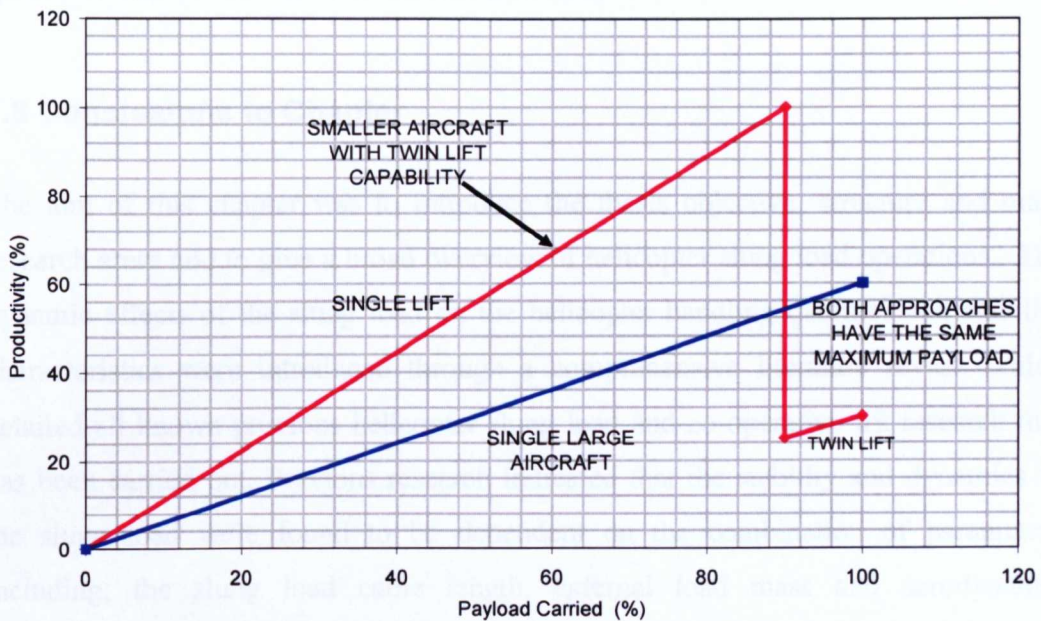
Meier and Olson [31] stated that if the aircraft is sized simultaneously to meet the 90<sup>th</sup> percentile value of each of three mission requirements; payload, mission radius and ambient missions i.e. conventional missions, it will typically be underutilised 98% of the time as illustrated in figure 1.6.



**Figure 1.6: Typical distribution of mission requirements (adapted from [31])**

A smaller aircraft can be considerably more effective when effectiveness is measured by average productivity rather than by maximum theoretically achievable productivity and twin lift provides a way to take advantage of this without sacrificing the peak mission demands.

The relationship between mission productivity and payload carried is compared notionally in figure 1.7 for single and twin lift solutions having the same maximum payload capability.



**Figure 1.7: Relative productivity of single and twin-lift approaches having the same maximum lift capability as a function of payload actually carried (Adapted from [31])**

For very heavy payloads, the single large aircraft has better productivity because total weight empty and mission time are less. However, when the required payload is light enough to permit the twin-lift partners to operate independently, the smaller aircraft is much more productive. The benefit of twin lift and the best aircraft size therefore depend on the frequency distribution of required payloads. Pilot workload, combat vulnerability, and field support requirements are factors that could limit the acceptable frequency of co-operative lift operations. An appropriate measure of effectiveness for a transport aircraft is specific productivity defined as:

$$\text{Specific productivity} = \frac{\text{payload} \times \text{radius of action}}{\text{mission time} \times \text{weight empty}}$$

This definition is similar to the productivity index used in [32] with the exception that maximum cruise speed is replaced by mission block speed (radius of action divided by total mission time), assuming the payload is carried one way only. The mission time also includes an allowance for load acquisition and drop off. For co-operative lift, weight empty is simply the sum of individual aircraft weight empties and payload is less than the sum of individual aircraft lift capabilities due to the addition of spreader bars, tethers and additional mission fuel.

## **1.8 Conclusions to Chapter**

The aim of this chapter was to introduce the thesis objective, structure and main research areas and to give a broad overview of helicopter slung load operations. The dynamic effects of the slung load on the helicopter handling qualities and stability characteristics were introduced through a comprehensive literature review which detailed all known previous helicopter slung load and co-operative lift research that has been carried out. Previous research indicated that the stability and dynamics of the slung load were found to be dependent on the combination of parameters including; the slung load cable length, external load mass and aerodynamic properties. The effects that different permutations of these parameters have on the stability and helicopter handling qualities will be investigated later in Chapter 5.

The main research interest, co-operative lift, was also introduced in this chapter with details about the operational benefits that make this unique configuration so desirable in a strategic context. Co-operative lift operations in theory allow increased efficiency and productivity without the need for large expensive rotorcraft which are more expensive to purchase, operate and maintain. A previous co-operative lift trial performed by Sikorsky in the 1970's indicated that the flight envelope of the configuration was reduced to below that of a single helicopter alone. This area will be explored later in Chapter 7 when a co-operative model developed within this research will be assessed through piloted simulation using ADS-33 MTEs.

The following chapter describes the helicopter and slung load modelling carried out including; the three helicopter models used, the software environments utilised and the methods employed to simulate the co-operative lift configuration via a distributed simulation network.

## Chapter 2

### HELICOPTER AND SLUNG LOAD MODELLING

#### 2.1 Introduction

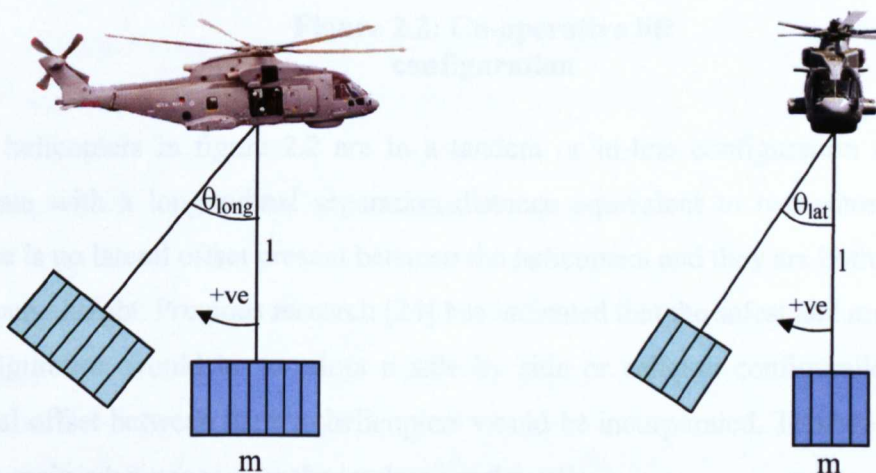
The modern multi-body synthesis software used in this research meant that advanced helicopter slung load models could be developed in a fraction of the time it would take to derive and model the configurations mathematically from first principles. FLIGHTLAB [33] and Matlab SimMechanics both enabled non-linear multi-body aerospace models to be developed in a modular fashion utilising existing components that can be linked together in a hierarchical manner. This meant that more time could be spent on the handling qualities analysis of the helicopter slung load systems and development and implementation of novel AFCS. The disadvantage of this approach this approach is that the model is less flexible and it is difficult to incorporate user specified functions. To ensure that the SimMechanics modelling approach gave accurate representations of the mechanical systems, a series of validation models were created for comparison with mathematical models, one of which is described in Appendix 2.2. This chapter describes the three different helicopter models used in this research ranging from the FLIGHTLAB Generic Rotorcraft (FGR) which was a fully validated, finished product, to the F-CH-47B model that was developed from a blank canvas using the FLIGHTLAB Model Editor (FLME). The three different models used and their specific research functions are summarised in the list below:

1. **The FGR model**, used for the initial handling qualities analysis of a helicopter operating with externally slung load.
2. **The FLIGHTLAB F-CH-47B Chinook model**, used for heavy lift slung load handling qualities analysis and as a benchmark performance comparison with the co-operative lift model.
3. **The Westland Helicopters EH-101 Merlin**, used for co-operative lift modelling, handling qualities analysis and ACLC research.

This chapter also describes the novel development and validation of the EH-101 co-operative lift model which was used for twin-lift handling qualities assessment and the application of the novel ACLC.

## 2.2 Helicopter Slung Load Model Configurations

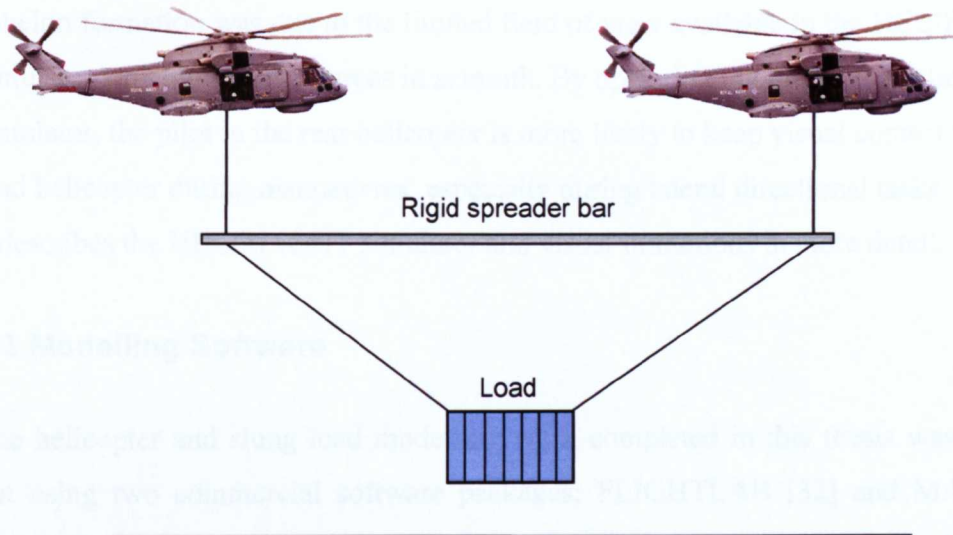
The general helicopter slung-load system falls into a class of multi-body dynamic systems consisting of two or more rigid bodies connected by massless cables. The cables can either be modelled as elastic or inelastic. The system is characterised by the configuration geometry, mass, inertia, aerodynamic loads and elastic properties of the links. Two main types of slung load system have been considered in this research; single helicopter, single point suspension and co-operative lift, multi-helicopter, multi-cable suspension. The general single helicopter, single-point suspension system with one tether cable is illustrated below in figure 2.1. The longitudinal and lateral sling angles ( $\theta_{\text{long}}$  and  $\theta_{\text{lat}}$ ) are defined as positive aft and right in helicopter body axis.



**Figure 2.1: Single helicopter, single point suspension convention**

The model comprises  $n$  rigid bodies with  $m$  straight line cables (suspension links), supporting a single force in the direction of the link. This is strictly a tensile force with respect to the cables and cable collapse will not be considered within this research. If the links are modelled as inelastic, then  $c$  ( $\leq m$ ) holonomic constraints [17] are imposed on the motion of the bodies (where  $c$  is the number of constraints due to inelastic suspension) and the system has  $d = 6n - c$  degrees of freedom (DOF). If the

links are modelled as elastic there are  $6n$  DOF. A holonomic constraint occurs when the number of controllable degrees of freedom is equal to the total number of degrees of freedom of the system. Figure 2.2 illustrates the co-operative lift system investigated in this research, which consists of two helicopters and an externally slung load supported by a rigid horizontal spreader bar.



**Figure 2.2: Co-operative lift configuration**

The helicopters in figure 2.2 are in a tandem or in-line configuration and usually operate with a longitudinal separation distance equivalent to two rotor diameters. There is no lateral offset present between the helicopters and they are both operated at the same height. Previous research [24] has indicated that the safest and most efficient configuration would be to adopt a side by side or echelon configuration where a lateral offset between the two helicopters would be incorporated. This would provide three main advantages over the tandem configuration:

1. The formation would provide an additional margin of safety by allowing a run off area if the rear helicopter did not decelerate in synchronisation with the lead helicopter.
2. The rear pilot in the formation would receive better visual cues because the pitch attitude of the lead helicopter can be better judged from a partial side on view, as opposed to only being able to see the empennage of the lead helicopter in the tandem configuration illustrated in figure 2.2.



3. The lateral offset would also ensure that there was minimum vortex wake interaction and interference from the lead helicopter onto the rear helicopter during low speed manoeuvring.

The main reason for adopting the tandem configuration in the research and not an echelon formation was due to the limited field of view available in the HELIFLIGHT simulator which was 140 degrees in azimuth. By operating in tandem formation in the simulator, the pilot in the rear helicopter is more likely to keep visual contact with the lead helicopter during manoeuvres, especially during lateral directional tasks. Chapter 3 describes the HELIFLIGHT simulator and visual limitations in more detail.

### **2.3 Modelling Software**

The helicopter and slung load modelling work completed in this thesis was carried out using two commercial software packages; FLIGHTLAB [32] and MATLAB. FLIGHTLAB is a modelling tool that allows analysis and real time simulation of multi-body dynamic systems, through an intuitive graphical user interface known as SCOPE. Complex nonlinear aerospace models of varying levels of simulation fidelity can be modelled quickly using the component library and FLME which features reconfigurable modules including: rotor systems, inflow models and aerodynamic drag models. Models are created hierarchically in FLME, with a complete vehicle being built up from lower level subsystems, which in turn are collections of primitive components. For example a typical rotorcraft model will utilise the following top level components:

- Two rotor models representing the main and tail rotor
- A rigid body fuselage model with 3D aerodynamic loads
- Physical environment model with atmospheric data
- Engine model with varying degrees of complexity
- A control system representing the mechanical interlinks and AFCS

Each subsystem has variable fidelity options that are specified by the user. For example the engine model can be specified as either an ideal engine (constant rpm), a

simple engine or as a gas turbine which utilises thermodynamic data. This feature is useful when the details about a particular subsystem are not well defined for example if there is no-public domain data available. FLIGHTLAB is also provided with two additional pieces of software; the Control System Graphical Editor (CSGE) for modelling mechanical elements and AFCS and GSCOPE for modelling multi-body dynamic systems.

FLIGHTLAB was already pre-configured for use with the HELIFLIGHT simulator and real-time simulation before the work on this project commenced and required no additional experimental setup or modification. In contrast, considerable time was spent in configuring the simulation hardware and software so that piloted real-time simulation was possible with MATLAB Simulink models. This upgrade greatly enhanced the capability of the simulator and allowed advanced co-operative lift simulation using multiple computers on a distributed simulation network to take place. The main motivation behind this development was because the time FLIGHTLAB did not allow this type of multi-entity simulation. A detailed description of how the simulator was adapted for compatibility with MATLAB Simulink is can be found in Chapter 3.

## **2.4 The FLIGHTLAB Generic Rotorcraft Model**

The FLIGHTLAB software comes complete with a high fidelity, validated helicopter model called the FGR. The model closely resembles the Sikorsky UH-60 Black Hawk medium lift utility helicopter (figure 1.1) in terms of physical attributes and dynamic response. The UH-60 helicopter carries 11 fully equipped troops using two General Electric T700-GE-700 turbo shaft engines providing the aircraft with a maximum usable power of 2,828 shaft horse power [34], allowing the helicopter to carry external loads of up to 3,500kg. The nominal cruise speed of the helicopter is 140kts, although the aircraft is capable of 160kts straight and level. The helicopter features a fully articulated rotor system consisting of four SC-1095 aerofoils [35]. The FGR model is a total force, large angle representation, featuring rotor blade flapping, lagging and hub rotational degrees of freedom. The main rotor blades which rotate anti-clockwise are modelled using a blade element model which divides each

rotor into six individual elements for aerodynamic and load calculation and the tail rotor is modelled as a Bailey rotor [36]. The aerodynamic loads are modelled as quasi-steady and the inflow model used is the three-state Peters/He Model [37]. The airframe includes a fuselage, and empennage, all modelled using aerodynamic lookup tables valid for an angle of incidence of  $-90^\circ$  to  $90^\circ$  and a side slip angle of  $-180^\circ$  to  $180^\circ$ . The engine is modelled as a turbo shaft engine and utilises thermodynamic data. The model has a flight control system that consists of the mechanical flight control system (MFCS) and AFCS. The MFCS features a longitudinal and lateral cyclic control mixing unit, collective mixing unit and tail rotor mixing unit. The FGR SCAS is a 3-axis control unit which gives a rate command response type in pitch, roll and yaw.

## 2.5 The F-CH-47B Chinook Model

FLIGHTLAB was also used to model a Boeing CH-47 tandem rotor helicopter for heavy slung load handling quality analysis and for a benchmark comparison against a co-operative lift slung load system carrying a similar payload in the region of 1 to 10 tonnes. The CH-47 is a twin-engine, tandem rotor helicopter designed for transportation of cargo, troops, and weapons during day, night, and degraded visual environment (DVE) conditions. The maximum airspeed is 170 knots with a normal cruise speed of 130 knots. The helicopter is equipped with two T55-L-712 turbo shaft engines from Honeywell, which are pod-mounted on either side of the rear pylon under the rear rotor blades. The engine provides a continuous power of 3,000shp and maximum power of 3,750shp enabling it to lift 12,000kg of external load. The Chinook has a unique triple-hook system, which provides stability to large external loads or the capacity for multiple external loads. Large external loads such as 155mm howitzers can be transported at speeds up to 140kts using the triple-hook load configuration. Multiple external loads can be delivered to three separate destinations in one sortie. The central hook is rated to carry the maximum 12,000kg and the other two hooks 7,500kg each. Development of the medium lift Boeing Vertol (models 114 and 414) CH-47 Series Chinook began in 1956. Since then the effectiveness of the Chinook has been continually upgraded by successive product improvements, the

CH-47A, CH-47B, CH-47C, and CH-47D. Figure 2.3 shows a CH-47 helicopter transporting 2 slung loads.



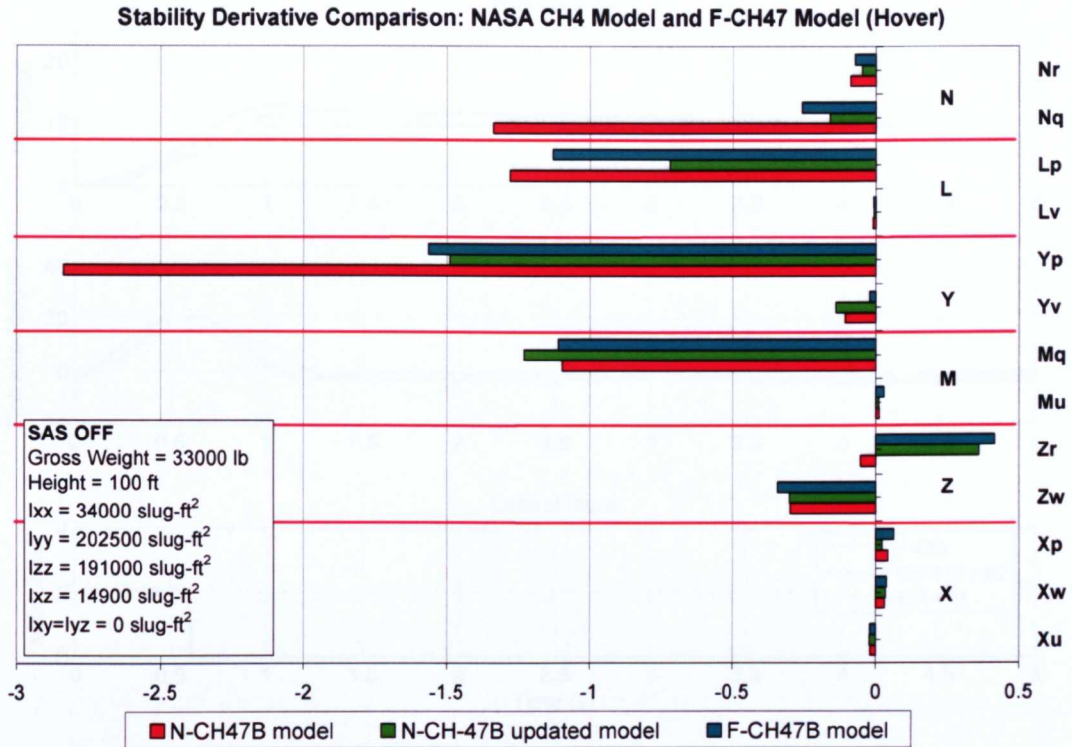
**Figure 2.3: CH-47 tandem rotor helicopter with dual hook suspension [38]**

The high fidelity model developed within this research was based on the ‘B’ model and was designated the F-CH-47B. Unlike the ‘off the shelf’ FGR which was already developed and fully validated by FLIGHTLAB, the F-CH-47B simulation model was developed from a blank canvas, based on detailed data from a NASA simulation model (N-CH-47B) [34]. The main features that have been included in the model are as follows:

1. Three dimensional aerodynamic loads derived from rotor off wind tunnel tests performed by NASA Ames.
2. An articulated blade element rotor with equivalent hinge offset and hinge lag dynamics.
3. A Peter’s three state rotor inflow and rotor interference model that simulates rotor interaction.
4. An accurate representation of the mechanical mixing control system.
5. A simple engine model with power dynamics based on T55-L-712 data.
6. The complete CH-47B SAS including: the longitudinal and lateral SAS, longitudinal cyclic trim (LCT), differential-collective-pitch-trim (DCPT) and directional SAS with sideslip, turn co-ordination and yaw rate damping.

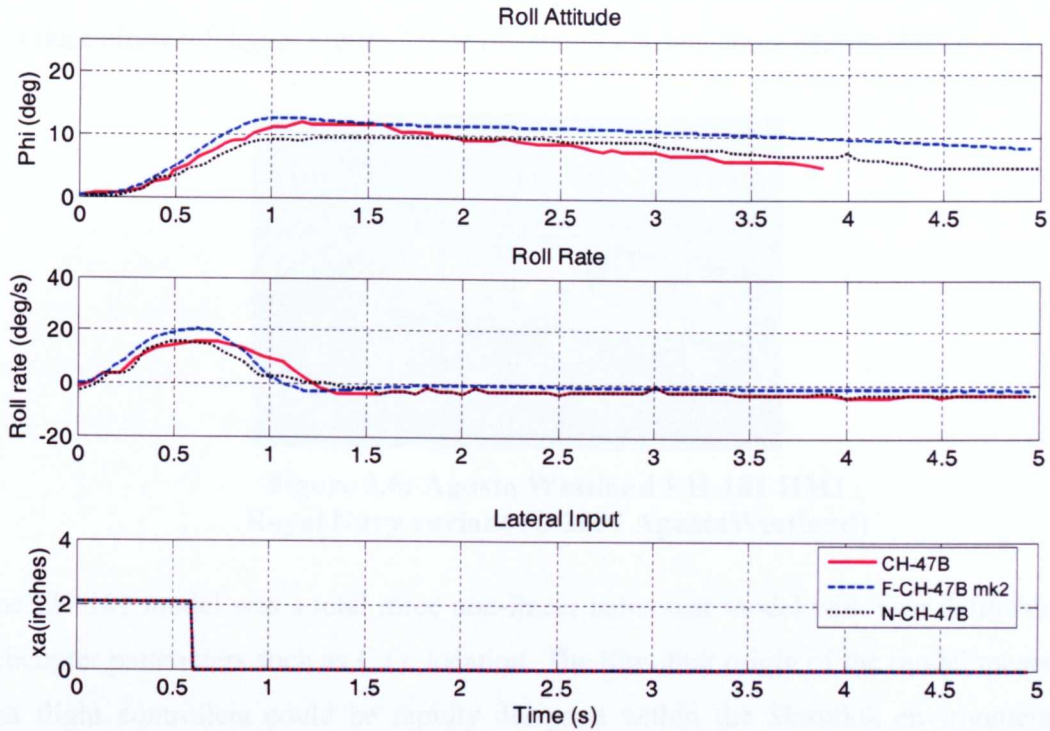
In order to compare how closely the F-CH-47B flight dynamics compared with the original N-CH-47B NASA model, the F-CH-47B model was linearised using FLIGHTLAB in a hover condition, with an all up mass (AUM) of 33000lb, SAS off. Figure 2.4 shows a comparison plot of the stability derivatives of the F-CH-47B and two different N-CH-47B models; the original N-CH-47B and an updated model that was modelled two years after the original N-CH-47B. The main update included a higher order rotor interference model. The X-axis of the figure shows the derivative value and the Y-axis shows the following stability derivatives:

$L_p$	roll moment due to roll rate
$L_v$	roll moment due to lateral velocity
$M_q$	pitch moment due to pitch rate
$M_u$	pitch moment due to forward velocity
$N_r$	yaw moment due to yaw rate
$N_q$	yaw moment due to pitch rate
$X_u$	X force due to forward velocity
$X_p$	X force due to roll rate
$X_w$	X force due to vertical velocity
$Y_p$	Y force due to roll rate
$Y_v$	Y force due to lateral velocity
$Z_r$	Z force due to yaw rate
$Z_w$	Z force due to vertical velocity



**Figure 2.4: Stability derivative comparison for F-CH-47B and N-CH-47B models**

The linear analysis shows that the F-CH-47B on-axis stability derivatives correlate well with the updated NASA model. The F-CH-47B was also validated by comparing non-linear responses from the updated N-CH-47B model. The data from NASA report [38] was originally obtained from the CH-47 Airworthiness and Qualification Test [39] and Boeing Company simulation report [40]. The F-CH-47B used advanced Flightlab components including an improved rotor interference model which featured rotor wake velocity decay constants and rotor skew geometry which meant it was a much higher fidelity model than the N-CH-47B. Figure 2.5 shows the roll response to lateral stick step input performed at 35knots. The figure shows the response from CH-47 flight test and the two simulation models. Appendix 1 describes the model development and validation in more detail.



**Figure 2.5: 35 knots lateral step input,  
33,000lb AUM, SAS on**

Figure 2.5 shows that all three models reach the same roll attitude within 2 degrees after 1 second and that the F-CH-47B mk2 had a higher roll rate indicating more control power. The linear and non-linear results indicate that the F-CH-47B model is sufficiently accurate for the handling qualities assessment required in this project.

## 2.6 The Agusta Westland EH-101 Model

The third rotorcraft used in the research was the Agusta Westland EH-101 Merlin. The non-linear MATLAB Simulink model was supplied by Agusta Westland and was used to construct the primary co-operative lift model (CLM) for offline analysis and piloted real-time simulation. The Agusta Westland EH-101 is a medium-lift helicopter for military applications but also marketed for civil use. The military version of the EH-101 is powered by three Rolls-Royce Turbomeca RTM322 rated at 2,000hp. The rugged modular structure incorporates crashworthy and damage-tolerant features, including a five blade main rotor, a four bladed teetering tail rotor and main lift frame which includes multiple primary and secondary load paths. The fuselage is mainly of aluminium-lithium construction. Active vibration control of the structural response

(ACSR) uses a vibration cancelling technique to reduce cabin vibration which helps to reduce aircrew fatigue. Figure 2.6 below shows a Royal Navy Merlin HM1.



**Figure 2.6: Agusta Westland EH-101 HM1  
Royal Navy variant (© 2007 AgustaWestland)**

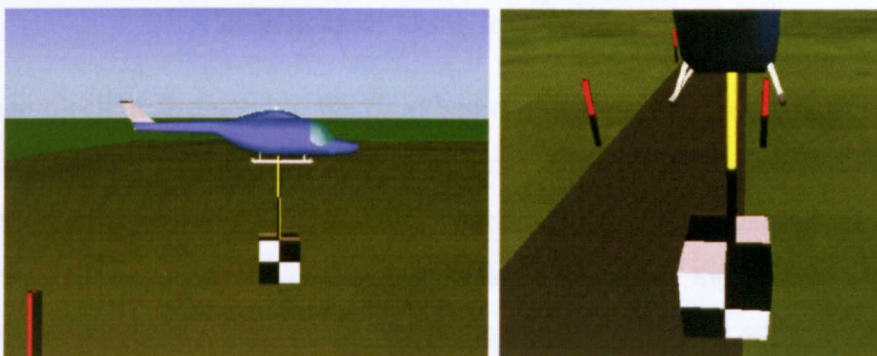
The EH-101 model was a total force non-linear helicopter model with user definable helicopter parameters such as C.G. location. The Simulink origin of the model meant that flight controllers could be rapidly designed within the Simulink environment taking advantage of the Simulink control toolbox. Designs could then be tested offline before being tested in real-time on the HELIFLIGHT simulator allowing rapid prototyping and hardware-in-the-loop (HIL) development.

## **2.7 Slung Load Model Development**

In a similar fashion to the helicopter models, the slung load models created in this research were developed using FLIGHTLAB and MATLAB Simulink software. FLIGHTLAB features a slung load component option that can be incorporated in helicopter flight models to create a single helicopter slung load system. Varying complexity loads can be modelled from single cable, simple point mass loads with one dimensional aerodynamic drag models to more complex rigid body loads with multi-line suspension, elastic cables and three dimensional aerodynamic loads that use look up tables. This meant that systems that would usually take months to derive and model mathematically from first principles could be modelled efficiently using FLME and analysed thoroughly in a fraction of the time utilising the existing FLIGHTLAB slung load component. The FLIGHTLAB slung load models were applied to both the FGR and F-CH-47B models for handling qualities and stability analysis.



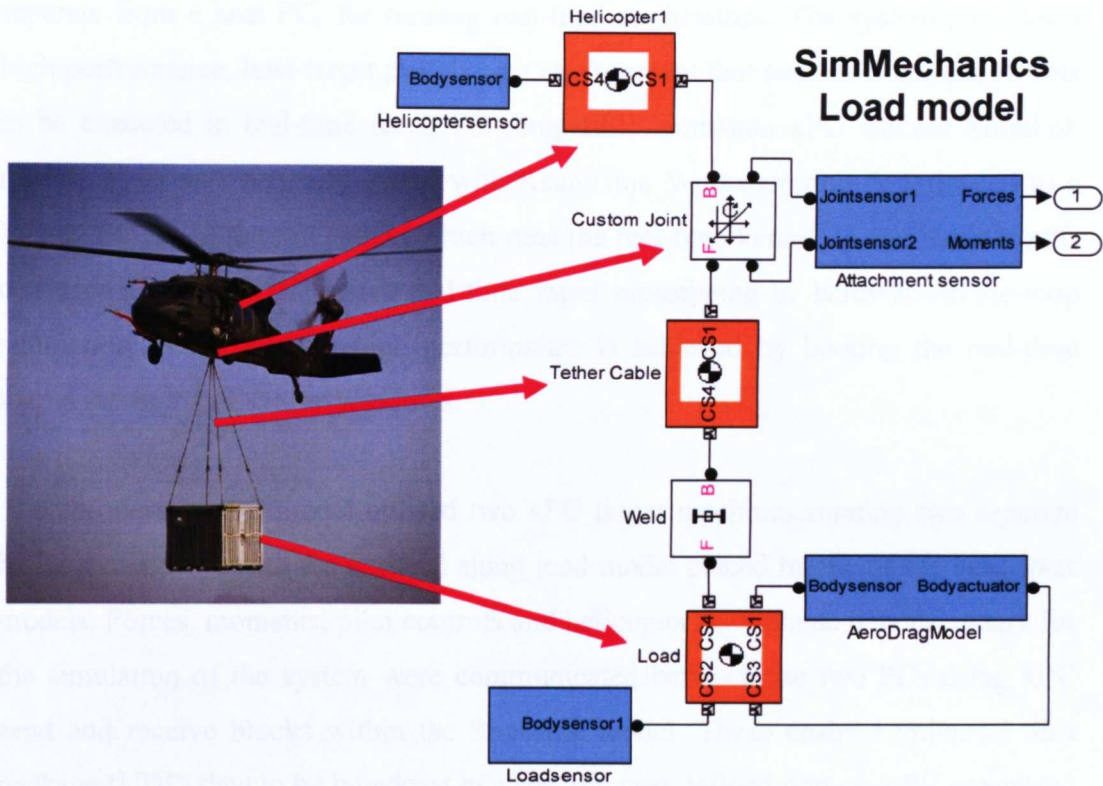
The co-operative lift slung load model was developed in MATLAB using the SimMechanics modelling tool. The main reason for using this software and not FLIGHTLAB was because FLIGHTLAB did not allow multi-entity simulation in a distributed simulation manner that was required to model two helicopters and an externally slung load. SimMechanics is a block diagram modelling environment for the engineering design and simulation of rigid body machines and their motions, using the standard Newtonian dynamics of forces and torques. SimMechanics enables the modelling and simulation of mechanical systems using a suite of tools to specify bodies and their mass properties, their possible motions, kinematic constraints, and coordinate systems, and to initiate and measure body motions. The mechanical system is represented by a connected block diagram allowing subsystems to be created in a hierarchical manner. SimMechanics is part of Simulink Physical Modelling, encompassing the modelling and design of systems according to basic physical principles. Physical Modelling runs within the Simulink environment and interfaces seamlessly with the rest of Simulink and with MATLAB. Unlike other Simulink blocks, which represent mathematical operations or operate on signals, Physical Modelling blocks represent physical components or relationships directly. SimMechanics also features visualisation tools allowing the user to view and display simplified 3-D renderings of mechanical systems during simulation, using the MATLAB Graphics system as shown in figure 2.7:



**Figure 2.7: Matlab 3-D visual representation**

Rigid bodies are connected to each other by a selection of joints including prismatic, revolute and spherical which represent the desired number of degrees of freedom. The rigid bodies and joints in turn can be driven by a collection of actuators including linear and revolute actuators. Elastic damping, friction effects and body sensors can

also be incorporated using additional SimMechanics blocks and in this way the whole system can be developed. Figure 2.8 shows how a helicopter slung load system can be modelled using a simple SimMechanics model. The main components of the helicopter and load combination have been highlighted.



**Figure 2.8: SimMechanics representation of helicopter slung load system**

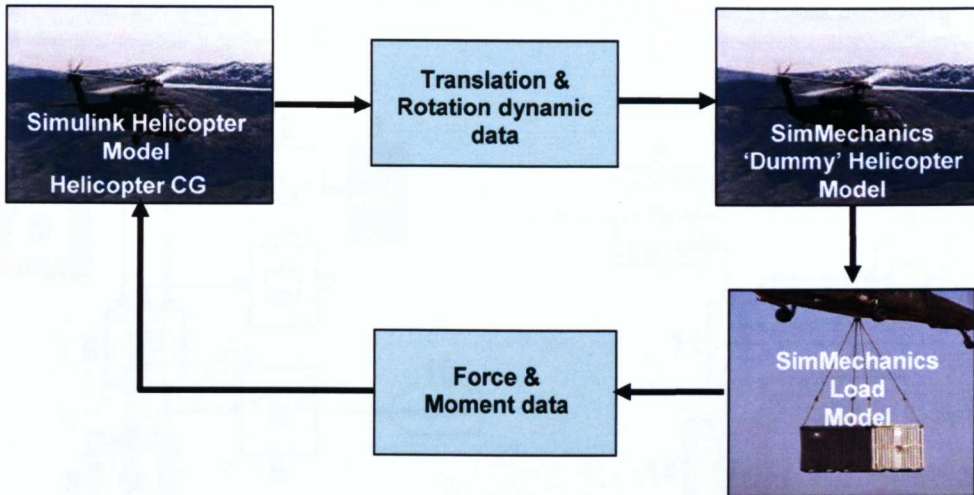
The orange blocks correspond to the rigid bodies that represent the helicopter, tether cable and external load. The mass, inertia tensors and co-ordinate systems of the rigid bodies can all be specified within these subsystem blocks. The white blocks represent the degrees of freedom between the rigid bodies. For example, the first revolute joint represents the slung load cable attachment point with the helicopter and the weld joint represents a simplified fixed attachment method between the tether cable and load for simple point mass analysis. The blue blocks represent joint sensor components used for measuring and feeding back the reaction forces and moments to the helicopter. This particular model also features a simple aerodynamic drag model that uses body actuator blocks to simulate drag on the external load based on simple drag equations using the projected side area of the load.

## 2.8 Co-operative Lift Model Development

The co-operative lift model utilised MATLAB xPC for desktop and piloted real-time simulation. xPC is a solution for rapid prototyping, testing, and deploying real-time systems using standard PC hardware. It is an environment that uses a target PC, separate from a host PC, for running real-time applications. The system provides a high performance, host-target prototyping environment that enables Simulink models to be executed in real-time using PC-compatible hardware. xPC enables Simulink models to be automatically coded with Real-Time Workshop and downloaded to a second PC called the xPC target which runs the real-time kernel. In this manner xPC converts a standard PC into a real-time rapid prototyping or hardware-in-the-loop simulation tool where the high performance is achieved by booting the real-time kernel rather than DOS or Windows.

The co-operative lift model utilised two xPC target machines running two separate helicopter models with the external slung load model placed in one of the helicopter models. Forces, moments, pilot controls and helicopter co-ordinate data necessary for the simulation of the system were communicated between the two PCs using xPC send and receive blocks within the Simulink model. These enabled universal data package (UDP) data to be broadcast to a specific user defined port on a PC connected within the local intranet via an Ethernet cable link. The latency in the communication between the helicopter models was found to be negligible, 0.05ms, in comparison to the simulation time step (5.6ms). More detailed information on the experimental setup of the arrangement can be found in Chapter 3.

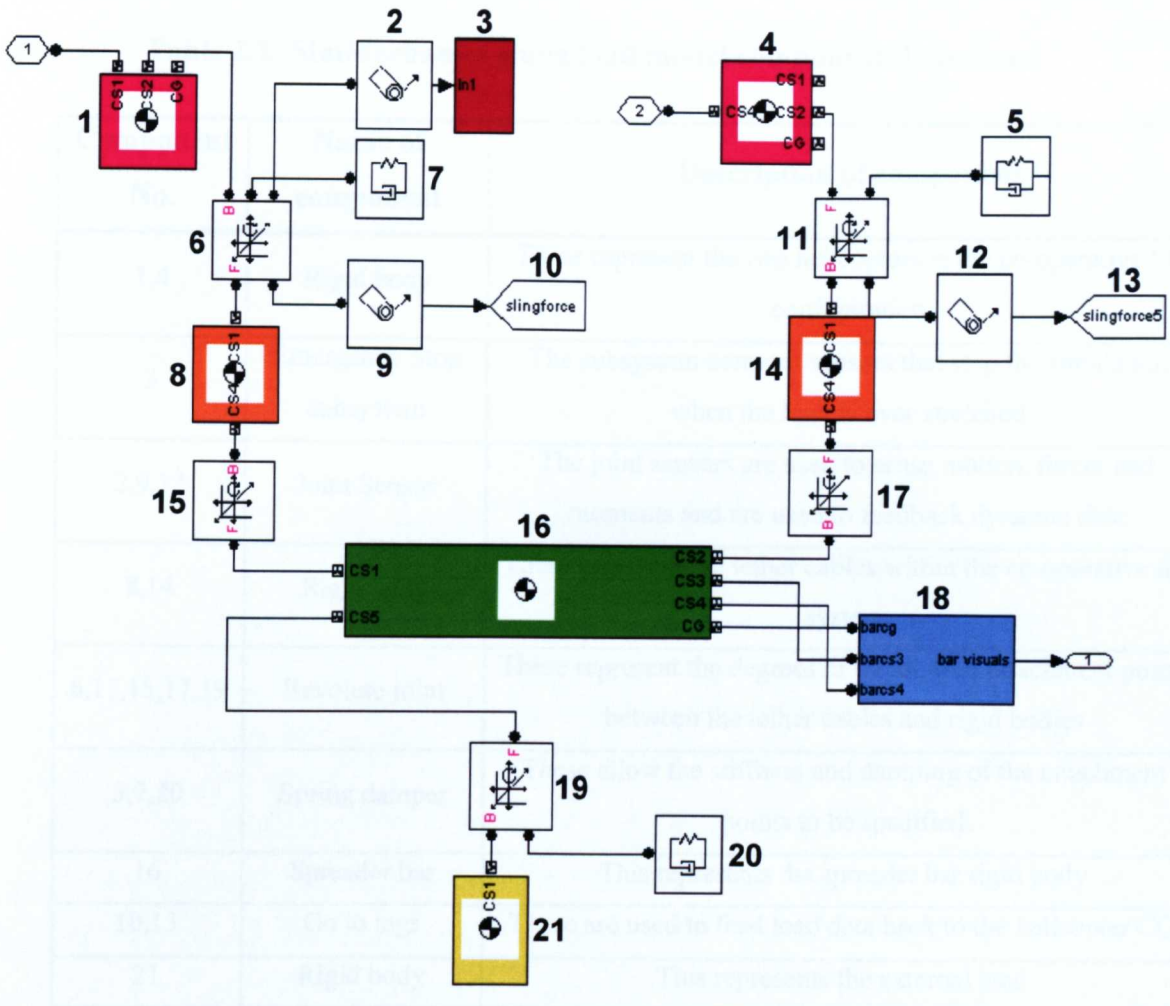
A novel approach using a Simulink helicopter model and SimMechanics underslung load model was used to model the helicopter-load system. The model slung load dynamics were modelled by driving a mass-less body or 'dummy helicopter' in SimMechanics with the dynamic output signals from the Simulink helicopter model as illustrated in figure 2.9.



**Figure 2.9: Simulink SimMechanics configuration**

The forces and moments at the cable attachment point were measured using a SimMechanics force and moment sensor block and fed back into the Simulink helicopter CG with a correction to represent the physical offset distance between the cable attachment point and CG of the helicopter.

Figure 2.10 shows the Simulink block diagram of the SimMechanics co-operative lift underslung load model developed. Note this is a simplified representation of the system and omits secondary subsystems. The arrangement of the Simulink model conveniently represents the physical structure of the actual system which made the construction of the model more intuitive. The resulting complex multi-body system that would normally require the solutions to numerous equations of motion can be simply designed and implemented in Simulink in a fraction of the time that it would take to model and derive the system mathematically by hand.



**Figure 2.10: SimMechanics co-operative lift slung load model (labels on the following page)**

Figure 2.10 shows a similar structure to the example illustrated in figure 2.9, the main difference being the inclusion of two helicopter rigid bodies, extra tether cables and the spreader bar. The model also includes body spring damper blocks which were used to model joint damping and simulate the elastic tether cables. The type of joints used in the model were revolute joints with three degrees of freedom representing spherical joints. The joint sensors labelled 9 and 12 in figure 2.10 were used to measure the reaction forces and moments at the helicopter cable attachment point before feeding them back to the helicopter CG. Table 2.1 lists the names of the

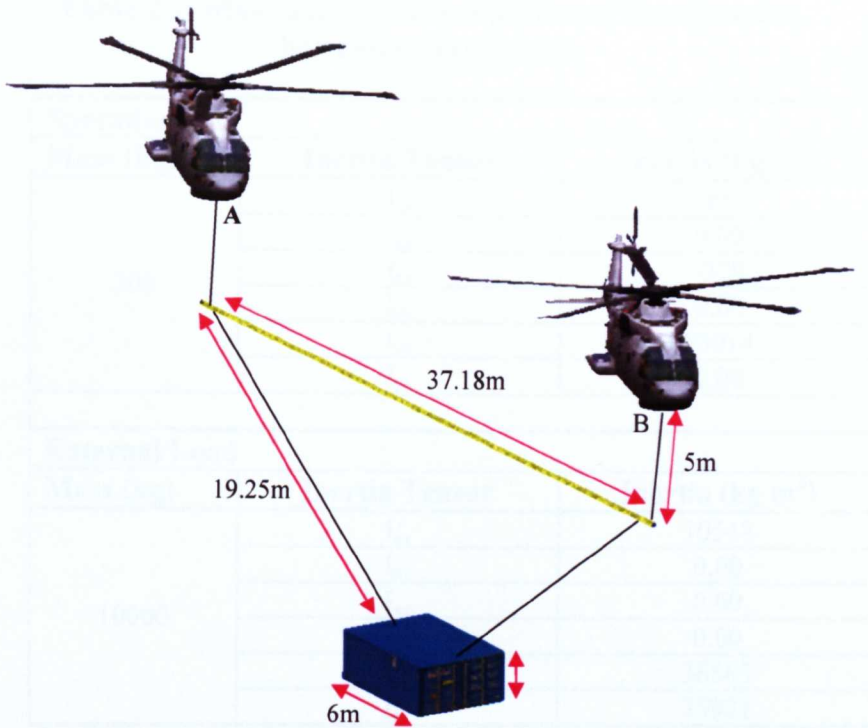
SimMechanics component blocks labelled in figure 2.10 along with a description of the purpose of each block:

**Table 2.1: SimMechanics slung load model component definitions**

<b>Component No.</b>	<b>Name of component</b>	<b>Description of component</b>
1,4	Rigid body	These represent the two helicopters in the co-operative lift configuration
3	Emergency Stop subsystem	The subsystem contains sensors that stop the simulation when the load is over stretched
2,9,12	Joint Sensor	The joint sensors are used to sense motion, forces and moments and are used to feedback dynamic data
8,14	Rigid body	These represent the tether cables within the co-operative lift system
6,11,15,17,19	Revolute joint	These represent the degrees of freedom or attachment points between the tether cables and rigid bodies
5,7,20	Spring damper	These allow the stiffness and damping of the attachment points to be specified
16	Spreader bar	This represents the spreader bar rigid body
10,13	Go to tags	These are used to feed load data back to the helicopter CG
21	Rigid body	This represents the external load

### **2.8.1 SimMechanics Co-operative Lift Model Validation**

The SimMechanics co-operative lift slung load model was validated by exciting the model and comparing the ensuing dynamic response with another model produced separately by the project partners Westland Helicopters. The Westland Helicopters model was produced using a completely different software package and was developed using the Euler equations of motion for rigid bodies with the incorporation of spring damping terms to account for the elastic steel cables. Figure 2.11 shows the common co-operative configuration used in the validation exercise:



**Figure 2.11: Co-operative lift slung load configuration used for model validation**

The spreader bar and external load were modelled as a triangular space frame and a cargo container, the mass, inertia and aerodynamic properties of which are shown in tables 2.2 and 2.3. This data was based on a known configuration and supplied by Westland Helicopters.

The SimMechanics and Westland external load models were defined from the helicopter models and the top tether attachment points, labelled A and B in figure 2.11, which usually attach to the helicopter cargo hooks, were fixed in space at identical starting co-ordinates 10m above sea level. The attachment points were then translated a specified distance (5m) about the X-axis with all other axes held in place to allow a hover to hover response manoeuvre performed by a helicopter with a translational rate command (TRCT) response type. Figures 2.12 and 2.13 show the translational input and resulting change in the spreader bar and load CG throughout the manoeuvre.

**Table 2.2: Mass and inertia properties of the spreader bar and external load**

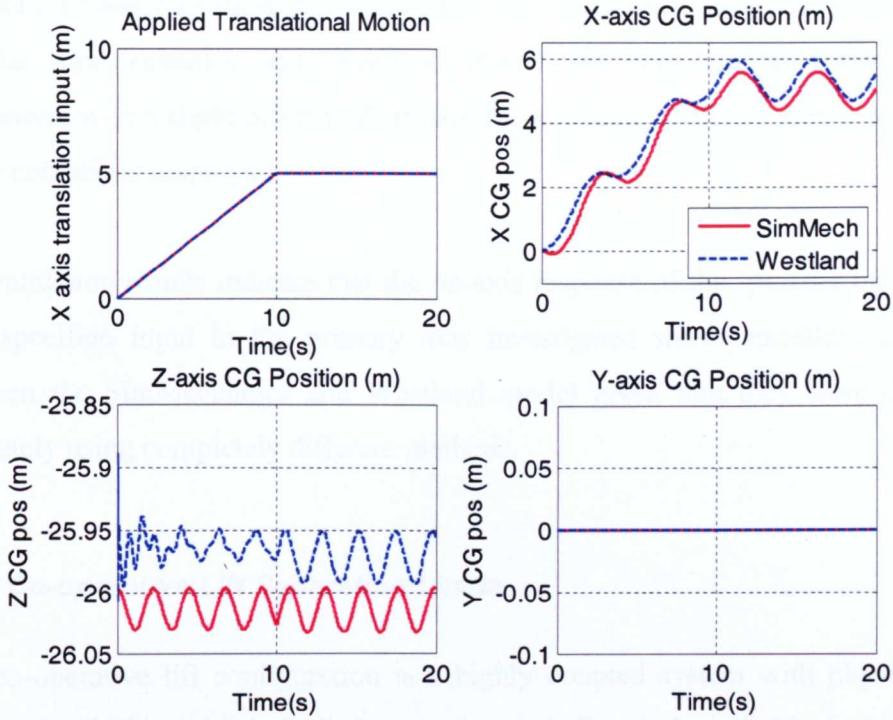
<b>Spreader Bar</b>		
<b>Mass (kg)</b>	<b>Inertia Tensor</b>	<b>Inertia (kg m<sup>2</sup>)</b>
300	$I_{xx}$	88
	$I_{xy}$	0.00
	$I_{xz}$	-329
	$I_{yx}$	0.00
	$I_{yy}$	93014
	$I_{zz}$	0.00
<b>External Load</b>		
<b>Mass (kg)</b>	<b>Inertia Tensor</b>	<b>Inertia (kg m<sup>2</sup>)</b>
10000	$I_{xx}$	10548
	$I_{xy}$	0.00
	$I_{xz}$	0.00
	$I_{yx}$	0.00
	$I_{yy}$	36563
	$I_{zz}$	35921

**Table 2.3: Aerodynamic properties of the external load**

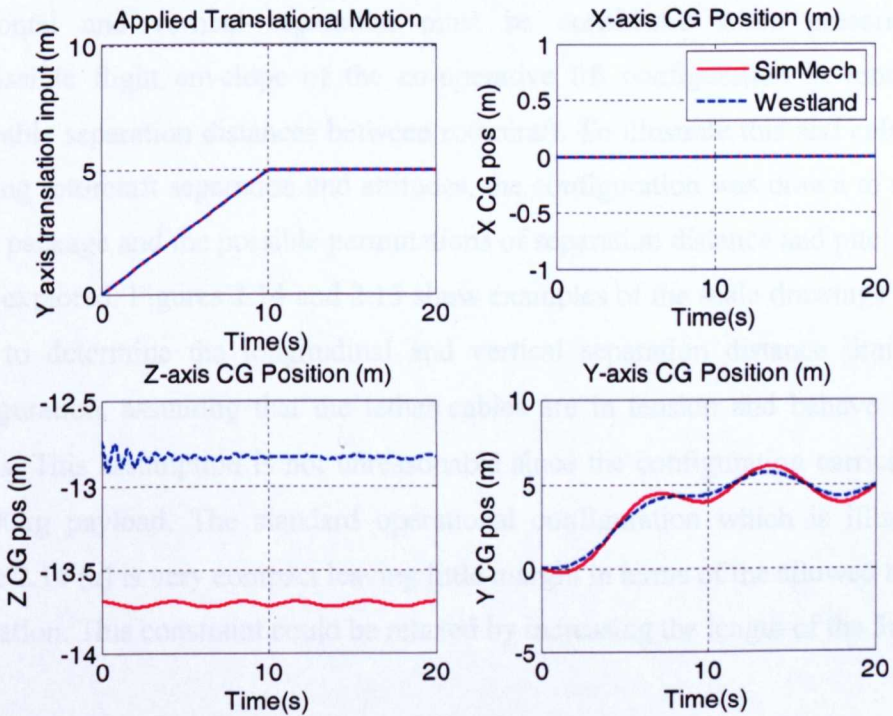
<b>External Load</b>			
<b>Surface Area (x-y plane) (m<sup>2</sup>)</b>	<b>Surface Area (y-z plane) (m<sup>2</sup>)</b>	<b>Surface Area (x-z plane) (m<sup>2</sup>)</b>	<b>Drag Coefficient</b>
14.86	6.32	15.79	1

The SimMechanics and Westland external load models were isolated from the helicopter models and the top tether attachments points, labelled A and B in figure 2.11, which usually attach to the helicopter cargo hooks, were fixed in space at identical starting co-ordinates 33m above-sea-level. The attachment points were then translated a specified distance (5m) about the X-axis with all other axes fixed to simulate a hover to hover re-position manoeuvre performed by a helicopter with a translational rate command (TRC) response type. Figures 2.12 and 2.13 show the translational input and resulting change in the spreader bar and load CG throughout the manoeuvre.





**Figure 2.12: Change in spreader bar CG co-ordinates throughout the manoeuvre**



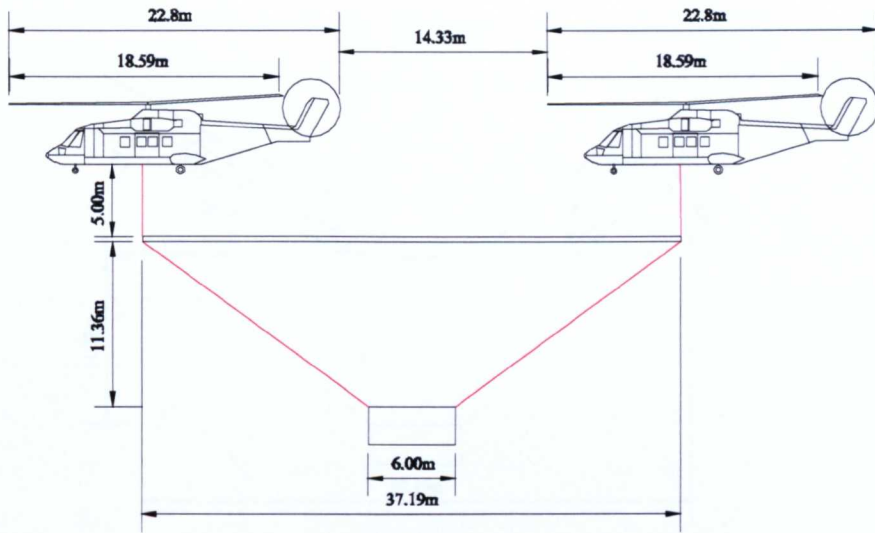
**Figure 2.13: Change in Load CG co-ordinates throughout the manoeuvre**

Figures 2.12 and 2.13 show that the X and Y co-ordinates of the spreader bar and load for the SimMechanics and Westland model are very similar throughout the manoeuvre with a slight offset in Z (0.5m) due to slightly different spring models and initial conditions employed.

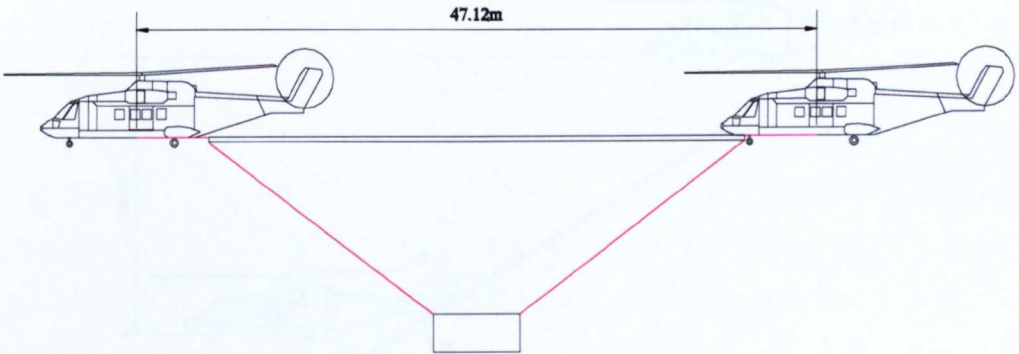
The validation results indicate that the on-axis response of the spreader bar and load to a specified input in the primary axis investigated shows excellent correlation between the SimMechanics and Westland model given that they were developed separately using completely different methods.

### ***2.8.2 Co-operative Lift Separation Limits***

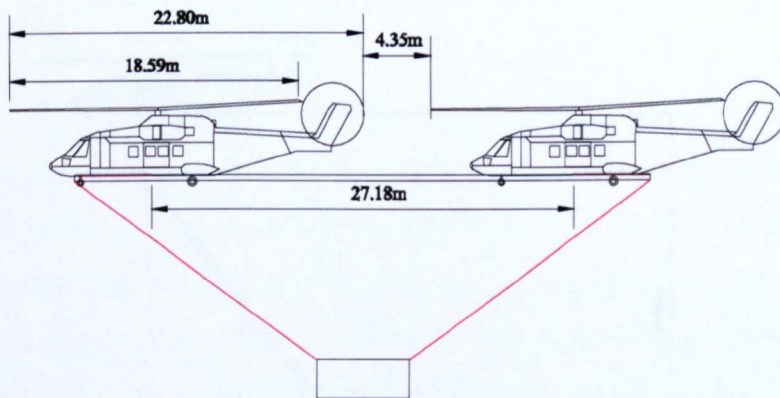
The co-operative lift configuration is a highly coupled system with physical cable constraints limiting the independence of each helicopter's individual motion. The addition of the spreader bar and connecting tether cables apply restrictions on the allowable separation between the helicopters in the X, Y and Z planes and also on the pitch attitudes of the helicopters. The different permutations of pitch attitudes and horizontal and vertical separation must be considered when prescribing the permissible flight envelope of the co-operative lift configuration in terms of the allowable separation distances between rotorcraft. To illustrate this and calculate the limiting rotorcraft separation and attitudes, the configuration was drawn to scale in a CAD package and the possible permutations of separation distance and pitch attitudes were explored. Figures 2.14 and 2.15 show examples of the scale drawings that were used to determine the longitudinal and vertical separation distance limits of the configuration, assuming that the tether cables are in tension and behave like rigid beams. This assumption is not unreasonable since the configuration carries a heavy 10,300kg payload. The standard operational configuration which is illustrated in figure 2.14 (a) is very compact leaving little margin in terms of the allowed horizontal separation. This constraint could be relaxed by increasing the length of the 5m cables.



(a) Standard trim condition

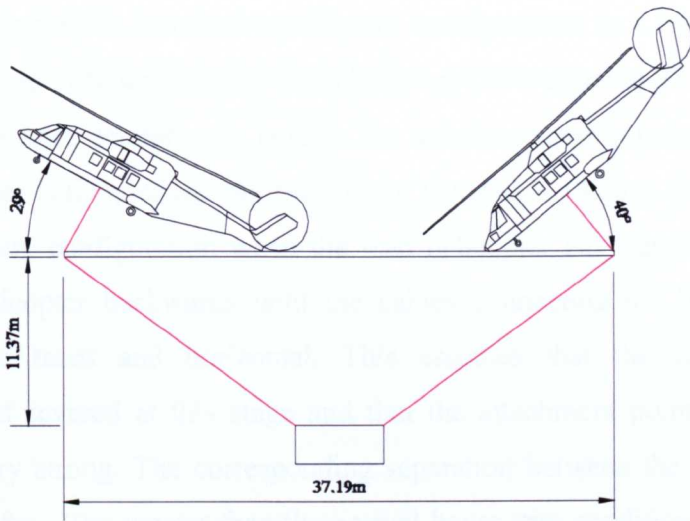


(b) Stretched condition

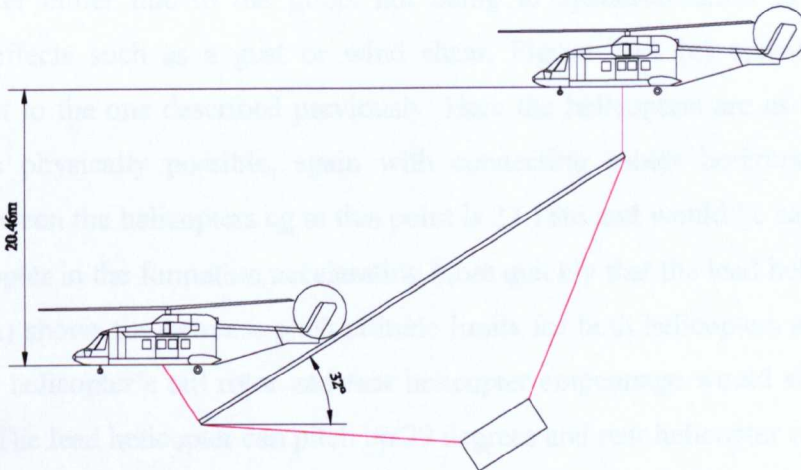


(c) Compressed condition

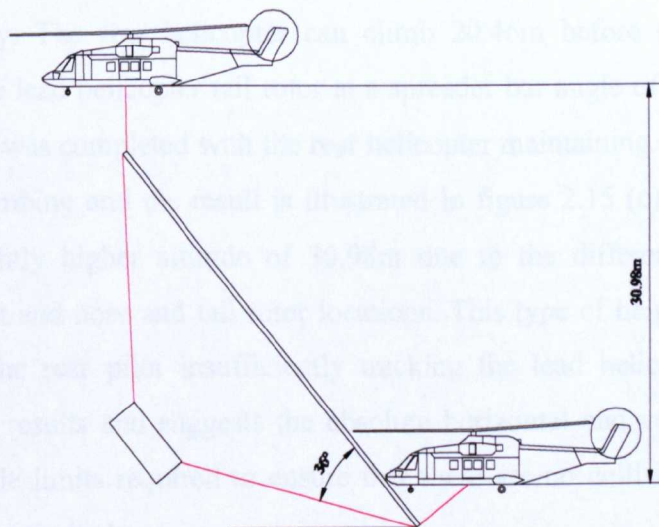
Figure 2.14: Scale CAD drawings used to determine maximum allowable separation distance



(a) Pitch attitude limits



(b) Master height limit



(c) Slaver height limit

Figure 2.15: Pitch attitude limits

Figure 2.14 (a) shows the standard equilibrium configuration in a hover condition where the separation distance between the helicopters CG is equal to 37.18m which is equivalent to two rotor diameters in length. The actual separation between the main rotor tip of the rear helicopter and tail rotor tip of the lead is 14.33m. Figure 2.14 (b) shows the resulting configuration when the lead helicopter has translated forwards and the rear helicopter backwards until the cables connecting the helicopter and spreader bar are taut and horizontal. This assumes that the cable has not overstretched and severed at this stage and that the attachment point between the helicopters is very strong. The corresponding separation between the helicopters at this point is 47.18m, 10m greater than the normal hover trim condition. This type of situation would occur when the lead helicopter accelerates more quickly than the slave helicopter either due to the pilots not being in synchronisation or due to atmospheric effects such as a gust or wind shear. Figure 2.14 (c) considers the opposite effect to the one described previously. Here the helicopters are as close to each other as physically possible, again with connecting cables horizontal. The separation between the helicopters cg at this point is 27.18m and would be caused by the rear helicopter in the formation accelerating more quickly than the lead helicopter. Figure 2.15 (a) shows the extreme pitch attitude limits for both helicopters at which point the lead helicopter's tail rotor and rear helicopter empennage would strike the spreader bar. The lead helicopter can pitch up 29 degrees and rear helicopter can pitch down by 40 degrees before striking the spreader bar. Figure 2.15 (b) shows what happens if the lead helicopter maintains a constant height whilst the rear helicopter climbs vertically. The rear helicopter can climb 20.46m before the spreader bar collides with the lead helicopter tail rotor at a spreader bar angle of 32 degrees. The same procedure was completed with the rear helicopter maintaining a constant height and the lead climbing and the result is illustrated in figure 2.15 (c). The lead could climb to a slightly higher altitude of 30.98m due to the difference between the attachment point and nose and tail rotor locations. This type of height change could be caused by the rear pilot insufficiently tracking the lead helicopter. Table 2.4 summarises the results and suggests the absolute horizontal and vertical separation and pitch attitude limits required to ensure that there are no collisions between the helicopters and spreader bar.

**Table 2.4: Absolute helicopter separation and pitch attitude limits**

<b>Constraint</b>	<b>Limiting value</b>
Horizontal separation	+ 47.18m -27.18m
Vertical separation	+20.46m -20.46m
Pitch attitude limit	+32.0° -40.0°

## 2.9 Conclusions to Chapter

This chapter has described the two main packages and methods used in this research to model slung load configurations; FLIGHTLAB and Matlab SimMechanics. The software packages allowed helicopter and slung load configurations to be modelled and simulated in a fraction of the time it would usually take to derive and model mathematically. The three main helicopter types used in the research were also introduced with a section describing the model development of the F-CH-47B tandem rotor simulation model. The implementation techniques and hardware modifications employed to allow Matlab Simulink models to run in real-time on the HELIFLIGHT motion simulator were also described and the novel method of creating and simulating the co-operative lift system using a distributed simulation network was introduced. The co-operative lift system developed using Simulink and SimMechanics was validated against another model developed separately by the project partners Westland Helicopters.

The following chapter describes the HELIFLIGHT motion simulator and the distributed simulation system architecture necessary for co-operative lift operations.

## Chapter 3

### EXPERIMENTAL SIMULATION SETUP

#### 3.1 Introduction

The following Chapter describes the HELIFLIGHT motion simulation facility at The University of Liverpool and details the significant modifications made to the simulation software and hardware architecture that were required to implement the co-operative lift Simulink models. The Chapter also describes the XPIT fixed base simulator which was adapted for the co-operative lift research to enable the twin-lift configuration to be flown by two pilots. This upgrade greatly enhanced the capability of the simulator and allowed advanced novel co-operative lift simulation operations using multiple computers on a distributed simulation network.

#### 3.2 The HELIFLIGHT Motion Simulator

The real-time simulation and analysis was performed using the HELIFLIGHT simulator at the University of Liverpool [41]. The simulator was nominally configured to execute FLIGHTLAB non-linear models using the PILOTSTATION interface and considerable work was spent in adapting the system architecture to allow real-time simulation of MATLAB Simulink models. The main features of the simulator include:

1. Selective fidelity, aircraft-specific, interchangeable flight dynamics modelling software (FLIGHTLAB) with a real time interface (PILOTSTATION),
2. Six degree of freedom motion platform (Maxcue),
3. Four axis dynamic control loading (Loadcue),
4. A three channel collimated visual display for forward view, plus two flat panel chin windows, providing a wide field of view visual system (Optivision), each channel running a visual database,

5. A re-configurable, computer-generated instrument display panel and head-up-display (HUD).

Figure 3.1 shows the simulator cockpit room, capsule and simulator control room.



**Figure 3.1: HELIFLIGHT pod and simulator control room**

The flight dynamics models are an important part of a flight simulator, the detail and accuracy of which will ultimately define the fidelity level of the simulation. The environment into which a pilot is immersed is an equally important factor. HELIFLIGHT uses a Maxcue 600 series motion platform together with Optivision collimated displays and Loadcue electronic control loading systems supplied by Motionbase plc (now QueSim) to create a realistic and immersive experience. Pilots interpret information about the vehicle behaviour from a number of different sensory cues. The basic mechanisms are visual perception, perception through the vestibular system of the inner ears and perception through the proprioceptors distributed throughout the body [43]. Each of these mechanisms provides important information or “cues” to the pilot. Visual perception is probably the most important sense since it is the human’s only means of directly sensing one of the primary motion cues - translational velocity [43]. In the vestibular system, the non-auditory portion of the inner ear, is an important and sensitive sensor of motion and position [44]. The semi-circular canals detect angular velocity and acceleration and the otholiths detect linear acceleration. There are three such canals in each ear which can detect angular acceleration in laboratory experiments as low as  $0.1 \text{ degree/s}^2$  [45]. The otoliths of the inner ear are the linear motion sensors which detect specific force – the external or non-gravity force acting on the body. Their threshold has been measured as low as

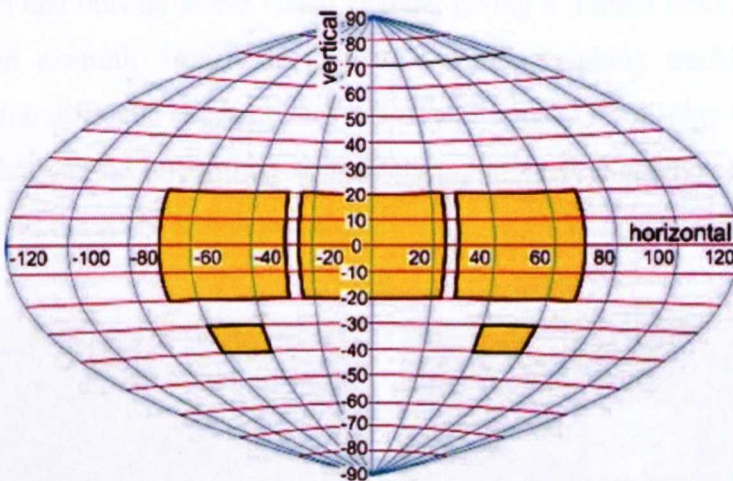


0.02 m/s<sup>2</sup> [45]. The otoliths can also detect a tilt of about 2 degrees and can detect head motion whether it is caused by the whole body or motion of the head with respect to the rest of the body [45]. The HELIFLIGHT simulator is capable of rotational speeds of 40 deg/s in pitch and roll and 60 deg/s in yaw with translational accelerations of 5.89 m/s<sup>2</sup> making it suitable for the work in this thesis.

The sensation of motion in HELIFLIGHT is generated using the Maxcue platform, which has a significant movement envelope. This is a six-axis, electrically actuated platform with a position range of 0.6 m. One area where the motion platform was found to be especially useful was during helicopter slung load operations. The motion cueing gave the pilot additional kinaesthetic cues on the behaviour of the under slung load dynamics which was previously underestimated by the author. This was particularly apparent during the co-operative lift operations where the pilot could feel if the configuration was being stretched – an indication that the separation distance between the helicopters and the spreader bar was too large. To ensure that the pilot does not receive “false” cues and that the motion was realistic, the motion cueing algorithms can be tuned to correspond with the desired vehicle performance. A major limitation with motion platforms is the amount of stroke available from the Stewart platform actuators. To maximise the usable motion envelope, the drive algorithms feature conventional washout filters that return the simulator to its neutral position at acceleration rates below the perception thresholds, after a period of simulator motion. The HELIFLIGHT motion platform required the vehicle specific force and angular velocity respectively in a frame of reference whose origin is approximately at the mid point between the pilot’s two vestibular sensors.

For an immersive simulation experience the cues for these mechanisms must be included and operated in a positive manner. Three collimated visual displays are used to provide infinity optics for enhanced depth perception, which is particularly important for hovering and low speed flying tasks. A series of spherical mirrors positioned in front of the visual displays ensure that the light rays entering the pilot’s eye are horizontal and the image outside the cockpit is located at infinity [44].

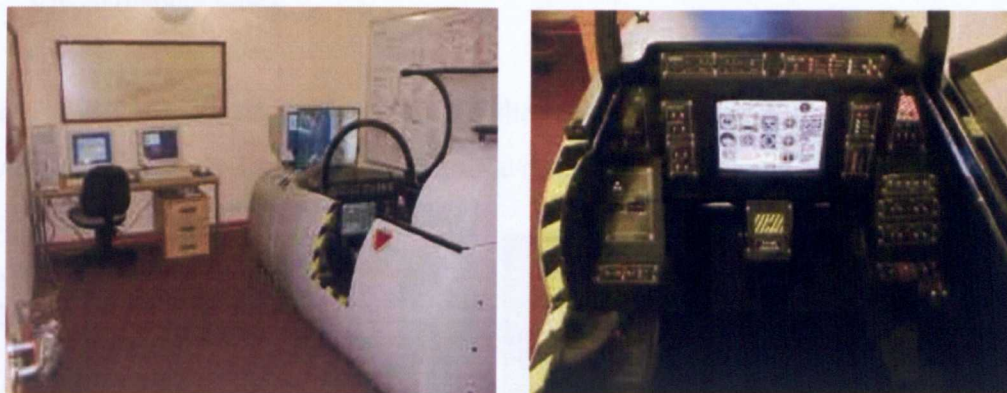
The visual displays in HELIFLIGHT provide  $135^\circ$  horizontal by  $40^\circ$  vertical field of view which is extended to  $60^\circ$  vertical field of view using two flat screen displays in the footwell chin windows (figure 3.2). The displays have a  $1024 \times 768$  pixel resolution, refreshing at 60 Hz which is suitable for flight simulation [44]. The rather limited field of view did affect the type of co-operative lift missions that were possible and in particular made helicopter tracking in formation difficult during pitch up and roll manoeuvres. These factors and solutions are described in more detail in Chapter 7.



**Figure 3.2: HELIFLIGHT visual field of view [41]**

### 3.3 The Fixed Base XPIT Simulator

The fixed base XPIT simulator was necessary for co-operative lift simulation during completely manual twin-lift operations where two piloted helicopter models were required. In contrast to the sophisticated HELIFLIGHT simulator, XPIT is a low cost single seat simulator that was built in house at The University of Liverpool. It features three axis controllers consisting of side-stick, directional pedals and throttle/collective. In comparison to HELIFLIGHT, XPIT has a more limited field-of-view and uses one outside world visual channel giving a limited field of view of  $\pm 30$  degrees in azimuth  $\pm 20$  degrees in elevation, making tracking tasks and formation flying difficult. The simulator has an additional TFT display for the aircraft instruments that can be re-configured and tailored to each simulation model. Figure 3.3 below shows the XPIT simulator setup:



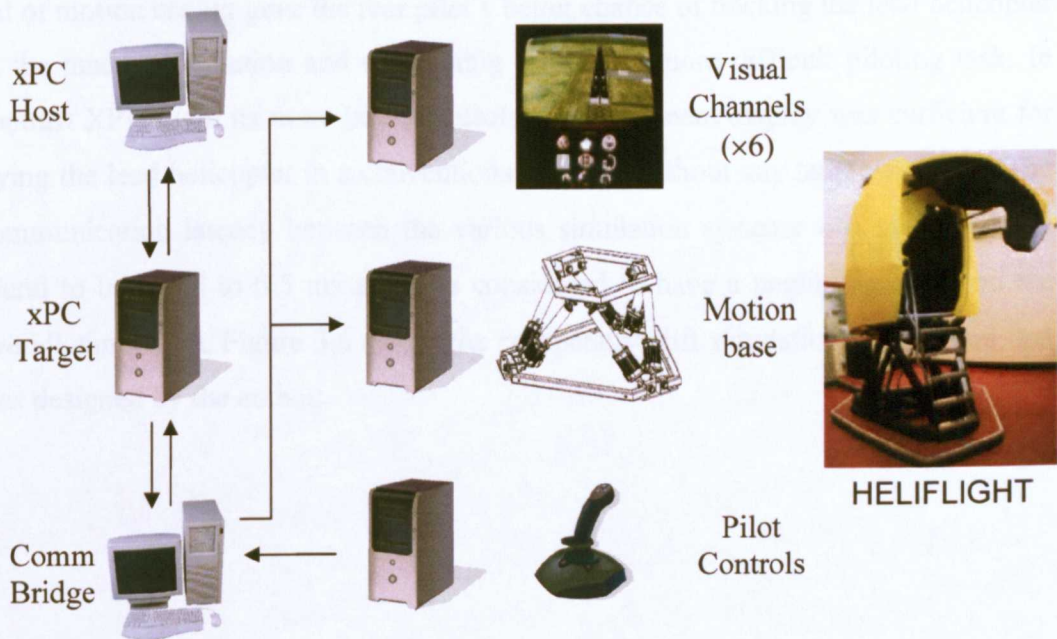
**Figure 3.3: XPIT fixed base simulator**

XPIT was originally designed for fixed wing simulation and had to be adapted for rotary wing simulation by the author. This involved replacing the throttle control with a collective type controller and centralising the location of the control stick to represent the helicopter cyclic control. The simulation architecture consisted of four main systems; an xPC host computer, xPC target computer, a communications bridge computer and the HELIFLIGHT systems (see Section 2.6.2 for more details on xPC). The simulation was developed, and controlled on a Pentium IV 3GHz host machine running Microsoft Windows. When real-time simulation was required, Matlab Real-Time Workshop was used to generate a simulation executable application by auto-

coding the Simulink model using a Microsoft Visual Studio compiler. The application was automatically downloaded to the xPC target computer via a local area network (LAN) using TCP/IP protocol. The simulation data was broadcast on the xPC Target computer and the UDP data was converted into a HELIFLIGHT compatible data form using the communication bridge computer and a C++ coded application. The C++ application, which was developed by a programmer working in the simulation laboratory at The University of Liverpool, converted the raw UDP data from the model into reflective shared memory which was organised into memory blocks that were visible by the HELIFLIGHT systems. In this manner the following shared memory blocks were created:

- Body states block
- Motion platform block
- Instruments block
- Visual display block

The HELIFLIGHT systems consisted of the motion base, pilot controls, and visual environment. Figure 3.4 shows a schematic of the simulation architecture:

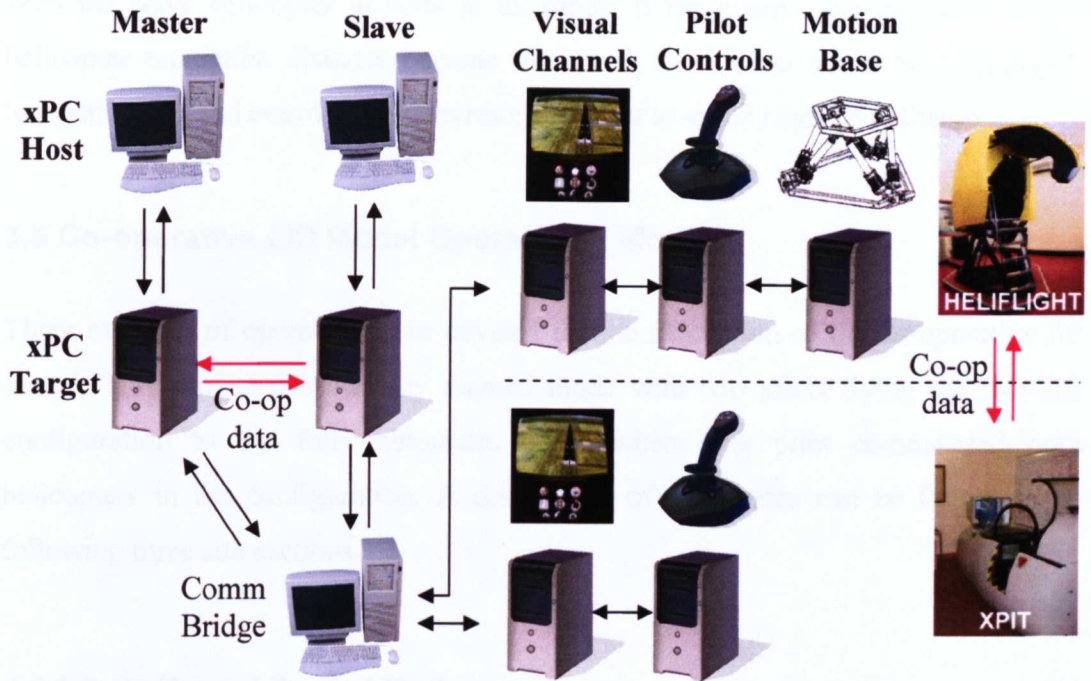


**Figure 3.4: HELIFLIGHT hardware simulation architecture for single model operation**

### 3.4 Co-operative Lift Simulation

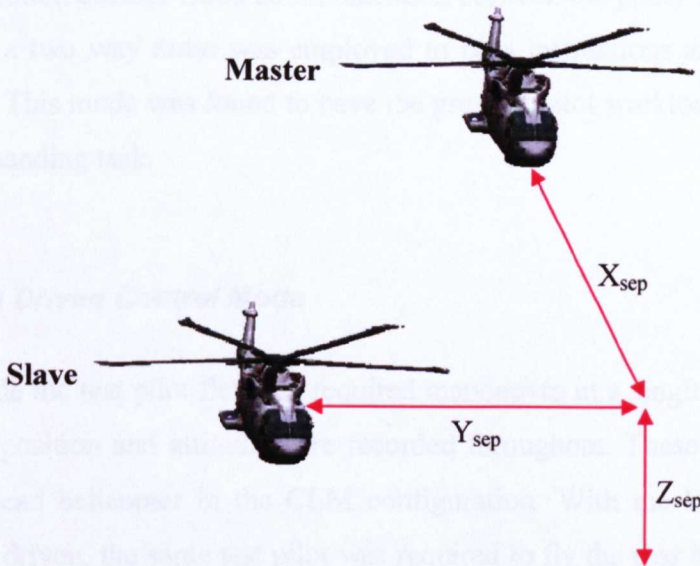
Co-operative lift was simulated using two xPC Target machines running two separate helicopter models with the external slung load model placed in one of the helicopter models as described in section 2.5. This enabled the models to be run with a simulation real-time step of 33.3 ms (30Hz). Experience and medical evidence [44] show that, when a pilot is flying an aircraft, the threshold at which human sensory organs detect a non-continuous effect varies depending on the rate of change, but is typically above a rate of 20Hz [44]. Modern training simulators are designed to have a maximum iteration time interval between 33.3 ms and 50 ms depending on the manufacturer. This means that the fastest computation can take place at a frequency of 30 Hz or 20 Hz, respectively [44].

The two simulators at the University of Liverpool; HELIFLIGHT and XPIT were used for real-time simulation involving two pilots. In this manner, the HELIFLIGHT full motion simulator was used for the rear helicopter in the twin-lift formation and the fixed base XPIT was used for the lead helicopter. The main reason for this was because HELIFLIGHT had better controls, a better instrument display and with the aid of motion cueing gave the rear pilot a better chance of tracking the lead helicopter in the tandem formation and completing this much more difficult piloting task. In contrast XPIT with its more basic controls and instrument display was sufficient for flying the lead helicopter in a conventional manner without any target tracking. The communication latency between the various simulation systems was measured and found to be equal to 0.5 ms and was considered to have a negligible effect on the overall simulation. Figure 3.5 shows the co-operative lift simulation architecture that was designed by the author:



**Figure 3.5: Co-operative Lift simulation configuration with two flight models**

The axes convention used for describing the co-operative system is shown below in figure 3.6:



**Figure 3.6: Co-operative lift convention**

The  $X_{sep}$ ,  $Y_{sep}$ ,  $Z_{sep}$  separation between the helicopters is defined in an inertial earth-axis frame. The formation adopted was based on the assumption that it would be much more beneficial for the pilot to fly the aft helicopter in the formation in order to

keep the slave helicopter in view at all times. If the control system failed or the helicopter separation distance became too small, the system could be disengaged, load jettisoned and evasive manoeuvres carried out to avoid possible collision.

### **3.5 Co-operative Lift Model Operational Modes**

Three methods of operation were devised for the simulation of the co-operative lift model. This ranged from a fully manual mode with two pilots flying the twin-lift configuration to the fully automatic mode where one pilot commanded both helicopters in the configuration. A description of the modes can be found in the following three sub sections.

#### **3.5.1 Fully Manual Control Mode**

In the fully manual control mode, two pilots were required to fly the co-operative lift configuration. One pilot flew the lead or master helicopter, using the XPIT simulator and the second pilot flew the slave helicopter using the HELIFLIGHT simulation pod with full motion cueing. Good communication between the pilots was essential in this mode and a two way radio was employed to pass instructions and comments from each pilot. This mode was found to have the greatest pilot workload and proved to be a very demanding task.

#### **3.5.2 Data Driven Control Mode**

In this mode the test pilot flew the required manoeuvre in a single helicopter and the helicopter position and attitude were recorded throughout. These were then used to drive the lead helicopter in the CLM configuration. With the lead helicopter now being data driven, the same test pilot was required to fly the rear helicopter and track the lead. The disadvantage of this configuration is that the forces and moments from the external load cannot be fed back to the data driven lead helicopter and the slave pilot found it difficult to anticipate what the lead helicopter was about to do due to a lack of two way communication.

### **3.5.3 Automated Control Mode**

In the automated mode the pilot controls both helicopters in the co-operative lift configuration. The pilot actually flies the master helicopter and the slave helicopter is fully automated using the ACLC. The master pilot control inputs and helicopter inertial position data are fed into the slave helicopter ACLC via a UDP data link, which the control system uses to track and maintain the desired separation and formation between the two helicopters. The communication latency in the master/slave data link was 0.011s. One area or recommended future research that could not be considered in this research would be to examine the minimal data link latency required for successful operation. For more detailed information concerning this mode please refer to Chapter 6.

### **3.6 Conclusions to Chapter**

This chapter has described the hardware and software specifications of the HELIFLIGHT motion and XPIT fixed base simulator at The University of Liverpool. The important components necessary for high fidelity flight simulation were also discussed including visual and kinaesthetic cueing. The chapter outlined the xPC distributed simulation architecture and described the three different control modes used to simulate the co-operative lift configuration.

The following chapter uses the simulation tools detailed in this chapter and the flight mechanics models described in Chapter 2 to introduce the reader to the important concept of handling qualities which forms one of the main components of this research.



## Chapter 4

### HANDLING QUALITIES ANALYSIS

#### 4.1 Introduction

Handling qualities analysis is a core component of the work completed in this research and a thorough understanding of the topic was essential in the development and the handling qualities assessment of the flight mechanics models and AFCS designed. The effect that the under slung load had on the stability, dynamics and handling qualities of the helicopter was one of the primary research interests. The purpose of this chapter is to introduce the reader to the concept of handling qualities through the qualitative assessment of two of the helicopters that were used in the research; the FGR and F-CH-47B. Chapter 5 then builds upon the work completed in this chapter and investigates the effect that a cargo container load has on the handling qualities of the FGR.

One of the earliest handling qualities definitions was made in 1969 by Cooper and Harper [42]. They defined handling qualities as:

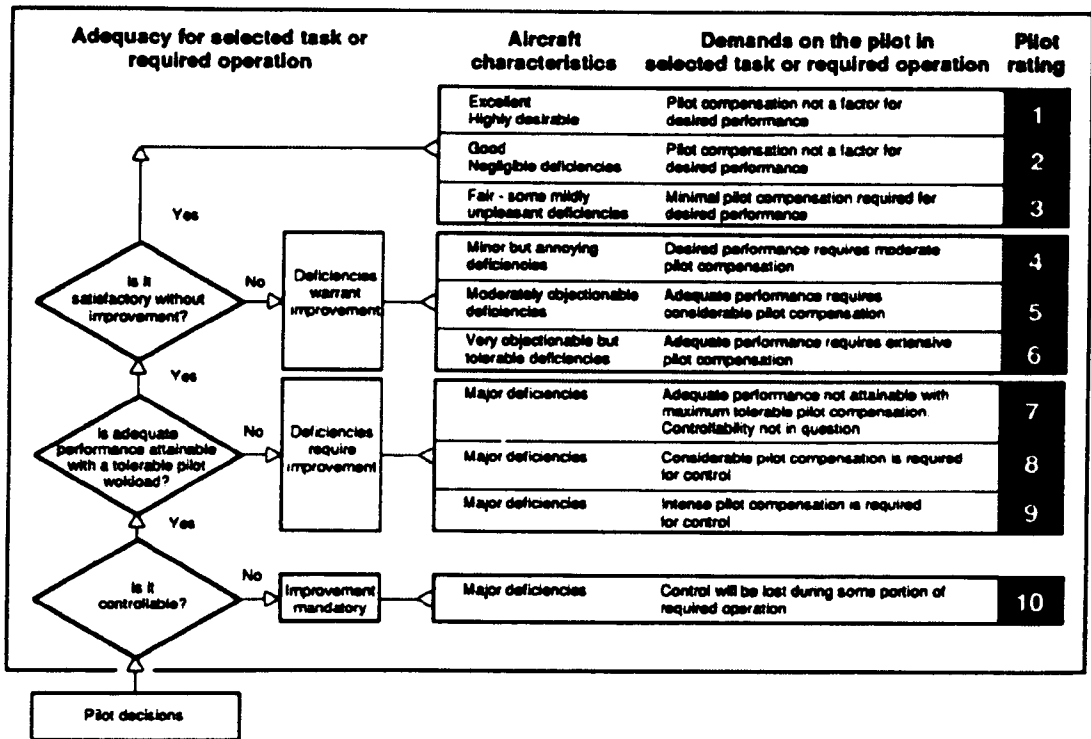
*‘Those qualities or characteristics of an aircraft that govern the ease and precision with which a pilot is able to perform the tasks required in support of an aircraft role.’*

The definition is often referred to as being the ‘original’ handling quality definition [46]. However, the definition does need expanding to increase its relevance to present day and future application. It is ambiguous to talk about flying qualities without a complete description of the influencing factors. In broad terms, the range of influences can be categorised into two groups – those external to and those internal to the aircraft and pilot.

Comprehensive handling qualities analysis is important during the early design and definition phases of a new development programme because a large proportion of the

life-cycle cost of an aircraft is committed during this early stage. The desired handling qualities that define the mission capability of the aircraft are also committed during these early stages and thorough design standards are therefore extremely important in achieving the desired level of performance and avoiding unnecessary programme cost. With this in mind, the United States Army published Aeronautical Design Standard 33B (ADS-33B) in 1988 [2]. The criteria in ADS-33 provided a performance target for the RAH-66 Comanche which was under development in that period. Although the helicopter was later withdrawn before production, a lot was learnt from the programme about how to develop helicopters with highly desirable handling qualities. The Army specification introduced several new concepts to handling quality criteria. ADS-33B introduced the concept of using quantitative criteria to supplement qualitative handling qualities criteria. The qualitative data was in the form of pilot evaluations and subjective comment of handling qualities using well-defined demonstration manoeuvres. Quantitative data was in the form of various handling qualities criteria that quantified the performance and handling qualities of the aircraft. Other new features of the criteria included the dependence of the criteria on the pilot attention state, the available cue environment, the mission task element (MTE) and the helicopter response type. ADS-33 has continued to evolve since 1988 and the latest version ADS-33E-PRF [2] incorporates a few innovations including a reference table that lists the recommended MTE for each rotorcraft type (scout, attack, utility or cargo).

The most developed and widely used handling quality scale is the Cooper-Harper handling qualities rating scale, which is illustrated in figure 4.1.



**Figure 4.1: Cooper-Harper handling qualities rating scale [42]**

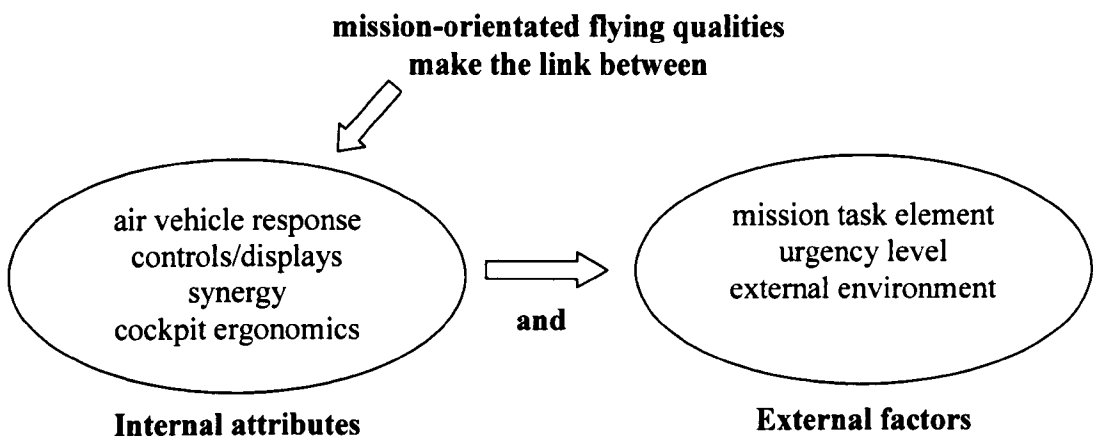
Goodness or quality according to Cooper-Harper can be measured in a scale spanning three levels. Level 1 corresponds to pilot ratings 1-3 in figure 4.1, Level 2 corresponds to 4-5 and Level 3 corresponds to 7-9. Aircraft are normally required to meet Level 1 handling qualities throughout the OFE. Level 2 is acceptable in failed and emergency situations, but Level 3 is considered unacceptable. Result ratings that are not between the decision points on the scale (i.e. 3.5, 6.5, and 9.5) are not allowed. During qualitative assessments, pilots are instructed to clearly follow the decision path dictated by the scale.

When talking about handling qualities reference should be made to the particular mission context, consequently handling qualities are very mission orientated. For example, a helicopter that meets Level 1 requirements in a good visual environment (GVE) may only meet Level 2 or even 3 requirements in a degraded visual environment (DVE).

There are four reference points that must be considered when discussing the handling qualities of a rotorcraft. They are:

1. The mission and the associated piloting tasks.
2. The operational environment.
3. The vehicle configuration, dynamics and flight envelope.
4. The pilot and pilot-vehicle interface.

The vehicle dynamics can be regarded as internal attributes, the mission and environment as the external influences and the pilot-vehicle interface as the connecting human factors. The relationship between internal attributes, MTE, and external factors is shown in figure 4.2.



**Figure 4.2: Relationship between internal attributes, MTE and external factors  
(adapted from Ref [46])**

Care must be taken when using the terms flying qualities and handling qualities. Key [47] made the distinction that flying qualities are defined as the aircraft stability and control characteristics while handling qualities are defined with the task environment included. Padfield [46] uses the terms interchangeably and argues that; *'there seems no good reason to relegate flying to be a sub-set of handling.'* This explanation is reasonable and will be adopted throughout this project. Handling qualities depend on the aircraft's flying characteristics, the Usable Cue Environment (UCE), the piloting task being performed, wind and turbulence, and any additional demands on the pilot.

Objective measurements and assessments in the form of quantitative data from desktop simulation and analysis are very important for demonstrating compliance with quality standards like ADS-33. However, quantitative data alone are not sufficient to guarantee that a new helicopter will be safe in achieving operational objectives. Objective assessment may cover up gaps or potential handling cliff edges in the overall handling qualities, one of which was encountered during a flight trial which is described later in Chapter 7. A handling quality cliff edge is an unknown and untested area in the flight envelope where it is possible for the pilot to unexpectedly lose control of the aircraft. Some handling qualities cliff edges can arise because the ADS-33 criteria handling qualities requirements are based on pilot empirical opinion from previous flight trials with different helicopters. ADS-33 represents the minimum levels to ensure Level 1 in normal operation. Future designs will perform much better than Level 1 requirements due to advancements in technology, materials and control and the absence of upper limits on the majority of handling parameters means there is little indication of the handling qualities deteriorating. Additional piloted tests with a subjective orientation are therefore extremely important and can expose handling problems that were not apparent when considering quantitative data alone. Visiting test pilots were asked to fly specified ADS-33 mission task elements (MTEs) on the HELIFLIGHT simulator to assess the handling qualities of different helicopter load configurations and AFCS and gave subjective comments and pilot ratings.

## **4.2 Mission Task Elements**

ADS-33 has a selection of flight test manoeuvres that are provided in the form of precisely defined MTEs. The MTEs provide a basis for an overall assessment of the helicopter's ability to perform certain critical tasks. A MTE is a collection of individual manoeuvres and will have a definite start and finish point with prescribed temporal and spatial constraints. Some examples of ADS-33 MTEs include the acceleration and deceleration manoeuvre, hover, pirouette, slope landing, slalom, and sidestep manoeuvre.

### **4.3 FGR Handling Qualities Analysis**

The handling qualities of the FGR and F-CH47B models were analysed in order to obtain a broad view of the characteristics of typical rotorcraft prior to future analysis that would include the addition of an external slung load model. The handling qualities of both aircraft were analysed in the temporal and frequency domain to show a comparison of the medium lift utility FGR (UH-60 type) and heavy lift CH-47B Chinook helicopter.

#### **4.3.1 Hover and Low Speed Requirements**

The hover and low speed mission requirements are of particular importance to helicopters operating with external loads. Helicopters carrying out slung load operations usually have to pick up and drop off loads within spatial and temporal constraints in hover or low speed flight. This is of particular importance in a combat or degraded visual environment (DVE) where pilot workload increases significantly and pilot's spare mental capacity to carry out ancillary tasks is reduced endangering safety, especially during nap-of-the-earth (NOE) operations [46]. The DVE encompasses reduced visibility due to weather conditions such as rain and fog and near zero visibility during dark moonless night operations. In such a situation the pilot misses important visual cues pertaining to the flight trajectory [46].

Active control technologies (ACT) can be employed to provide better handling qualities through advanced control laws using fly-by-wire (FBW) or fly-by-light (FBL) control systems. Often the aircraft response is augmented in such a way to reduce pilot workload during a specific task. Augmented response types include attitude-command and hold (ACAH), translational rate command (TRC) and positional command (PC) for hover and station keeping.

The two main ADS-33 handling qualities criteria that were selected for the analysis of the FGR and F-CH-47B during hover and low speed flight were the bandwidth and attitude quickness criteria. The bandwidth criterion was selected because it addresses the short term small amplitude handling qualities which are important for high gain

tasks and also in measuring the susceptibility to pilot induced oscillations (PIOs). These two issues are important to helicopter slung load operations where pilots may use high gain for the accurate pick up or delivery of loads and will prove to be significant factors later on for the high performance automatic co-operative lift system described in Chapter 6. The rear tracking pilot in the co-operative lift tandem configuration uses high gain control in order to keep the separation between the two helicopters within the desired limit and the bandwidth criterion is an excellent predictor of the likely performance that will be achieved.

The attitude quickness criterion is a measure of the rotorcraft's agility and was selected for primarily for the co-operative lift operation specification (the attitude quickness parameter is defined in more detail in Section 4.3.3). The helicopters in the co-operative lift formation have to be agile with a quick response in order to maintain constant separation and correct for any disturbances. This is particularly important for an automatic co-operative controller where the agility and speed of response of the controller is important for eliminating any separation errors [28].

### **4.3.2 The Bandwidth Criterion**

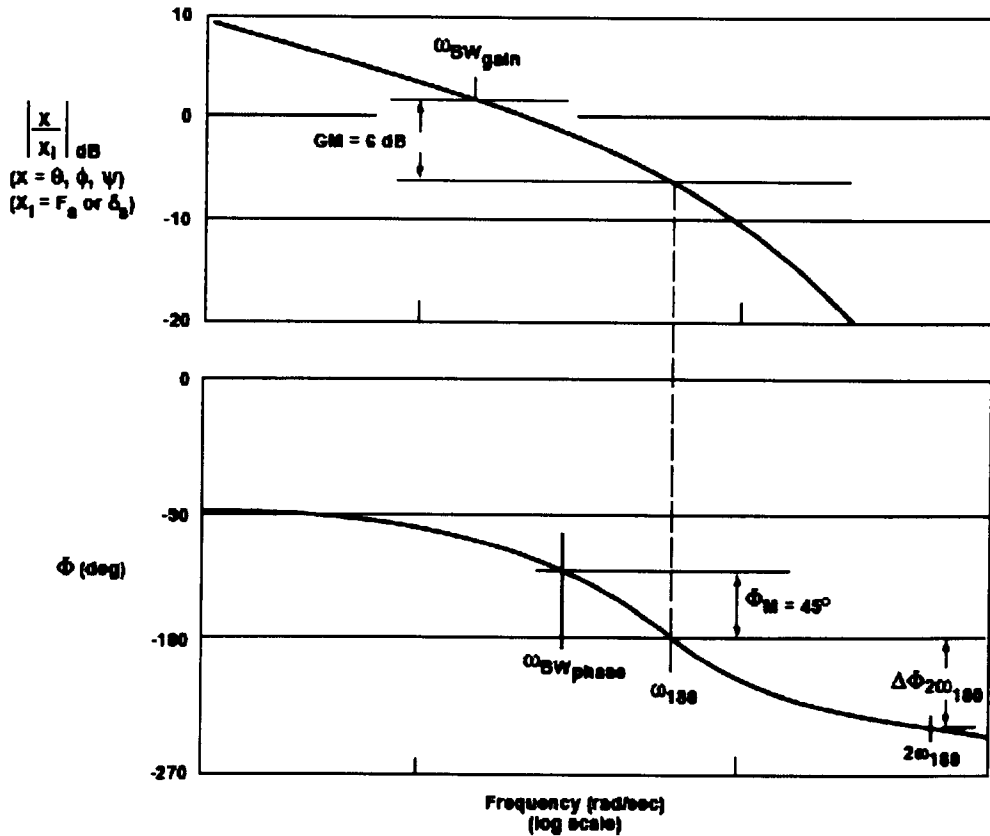
The bandwidth criterion addresses the short term, small amplitude handling qualities [2, 48]. These are of particular importance for high pilot gain tasks such as NOE flying, confined area manoeuvring and tracking tasks which are all applicable to slung load operations. The bandwidth criterion also examines the susceptibility to pilot induced oscillations (PIOs) and the workload expected during very precise manoeuvring tasks. The short term, small amplitude roll response criteria are formulated in the frequency domain using the parameters: bandwidth,  $\omega_{BW}$ , and phase delay,  $\tau_p$ . The parameters can be calculated from a frequency response plot of the aircraft pitch attitude to pilot controller inputs using the definitions illustrated in figure 4.3 [2].

## BANDWIDTH

$$\text{Phase delay} = \tau_p = \frac{\Delta\phi_{2\omega_{180}}}{57.3(2\omega_{180})}$$

For rate command systems  $\omega_{BW}$  is the lesser of  $\omega_{BW_{gain}}$  and  $\omega_{BW_{phase}}$

For attitude command systems  $\omega_{BW} = \omega_{BW_{phase}}$



**Figure 4.3: Definitions of bandwidth and phase delay (adapted from [2])**

The definition of bandwidth considers the human pilot to be an element in a closed loop system for compensatory tracking. When the pilot operates as a pure gain system, the neutral stability frequency ( $\omega_{180}$  = the frequency where the phase lag reaches 180 degrees) is the frequency beyond which the closed loop is unstable [48]. The bandwidth frequency is defined as that frequency where a 45 degree phase margin and a 6 dB gain margin exist with respect to the neutral stability frequency [2]. The bandwidth is therefore an indicator of the maximum closed loop frequency a pure gain pilot can achieve without threatening stability (i.e. without approaching the  $\omega_{180}$  point). The pilot can control the aircraft beyond the bandwidth frequency using



lead-compensation however this increases pilot workload and results in degraded handling qualities ratings [48]. In ADS-33E two bandwidth frequencies are defined:

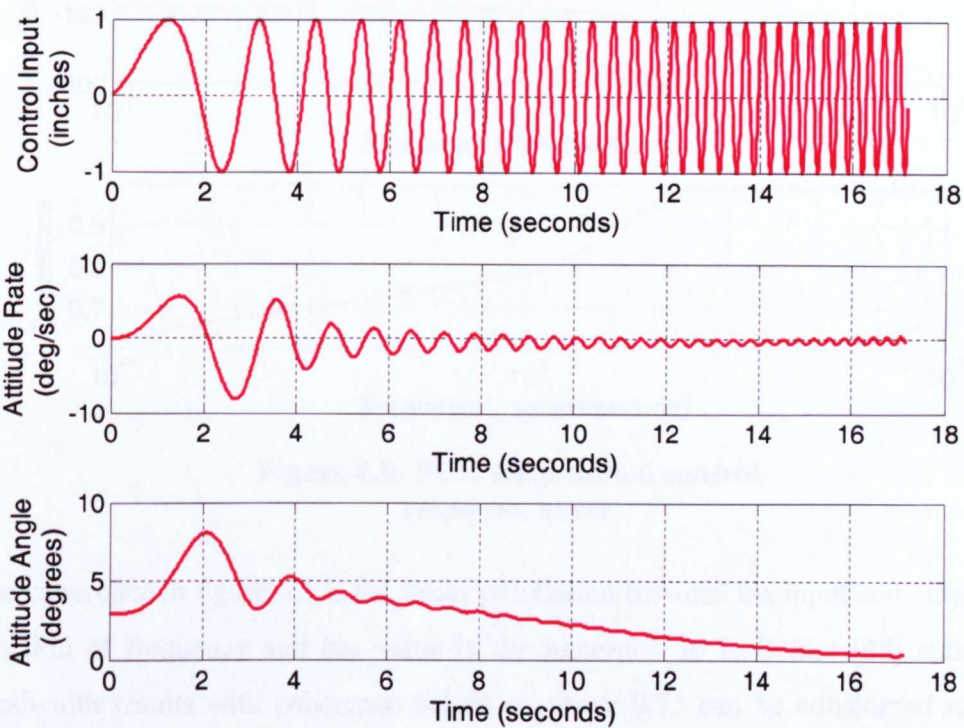
1. The phase bandwidth,  $\omega_{BW_{phase}}$ , where a 45 degree phase margin exists with respect to the neutral stability frequency  $\omega_{180}$ .
2. The gain bandwidth,  $\omega_{BW_{gain}}$ , where a 6 dB gain margin exists with respect to the gain at  $\omega_{180}$ .

The physical meaning of the phase bandwidth is simple; when the bandwidth decreases the helicopter response is perceived by the pilot as being increasingly sluggish [48]. The physical interpretation of the gain bandwidth is more complicated. The 6 dB gain margin means that the pilot can increase his or her feedback gain by a factor of two before going unstable. Increases in feedback gain are common during close loop tasks such as dropping off a slung load at a target point where there is progressive increase in aggressiveness. Helicopters that have an inherently low gain bandwidth may be perceived as having desirable handling qualities providing the phase bandwidth is sufficiently high. These types of systems could be prone to PIOs when the pilot ‘tightens up’ in a close loop situation [48]. For helicopters with a rate-command type system (including non-augmented helicopters) the bandwidth is defined as the minimum of  $\omega_{BW_{gain}}$  and  $\omega_{BW_{phase}}$ . Attitude command helicopters generally allow the pilot to ‘back off’ and use a low gain on attitude and therefore the bandwidth for an attitude command type system only considers  $\omega_{BW_{phase}}$ .

The phase delay parameter in ADS-33E describes the helicopter dynamics beyond the bandwidth frequency where the pilot introduces lead-compensation. The pilot increases the cross-over frequency and can control the helicopter beyond the bandwidth and neutral stability frequencies. The phase margin relates to how much lead-compensation the pilot can apply. A large phase lag results in the pilot no longer being able to compensate, resulting in instabilities and PIOs. The phase delay parameter is defined as the phase margin at the  $2\omega_{BW_{180}}$  frequency divided by  $2\omega_{BW_{180}}$  [2]. When the phase delay is large, there is only a narrow margin between the bandwidth frequency and inevitable instabilities. Small phase delay values relate to an increased margin for the pilot to increase his or her input frequency while adding lead-compensation. Time delays, filters, actuator dynamics all contribute to larger

phase delays, but the phase delay does not measure non-linear phase effects such as those caused by rate limiting.

The bandwidth of the FGR and F-CH-47B was calculated by applying a non-linear sinusoidal input to a trimmed non-linear simulation model in FLIGHTLAB. These were carried out in a hover and 30 knots forward flight condition. The type of input used ranges from an initial frequency of 0.1 to a final frequency of 4 Hz. Figure 4.4 shows an example of the longitudinal sinusoid input applied to the FGR along with the resulting pitch rate and attitude:

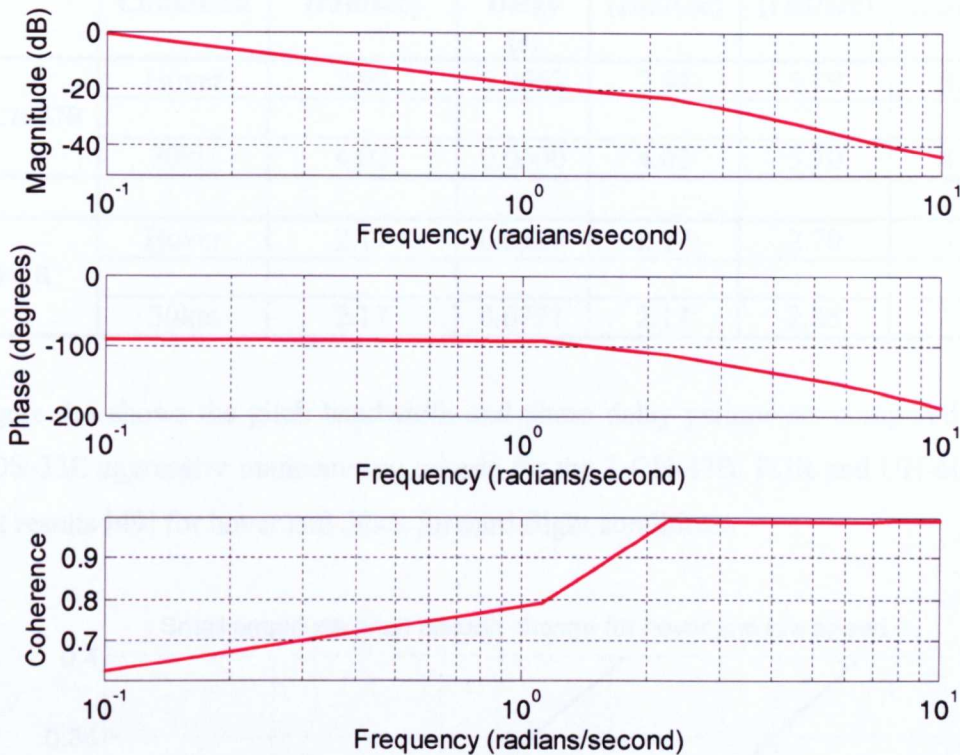


**Figure 4.4: F-CH-47B sinusoid longitudinal step input and pitch response**

To increase the reliability of the results and maximise the information contained in the frequency sweeps, sinusoidal inputs of varying amplitudes and frequencies were applied and an average bandwidth and phase delay parameter calculated.

The frequency responses were computed using a conditioned frequency response program that originated in the German Aerospace Centre (DLR) [48] and was later adapted at The University of Liverpool. The program featured overlapping windows

with varying length that increased the quality of the frequency response around the frequency range of interest. Figure 4.5 below shows the pitch axis response for the FGR in the hover corresponding to the input data shown in figure 4.4:



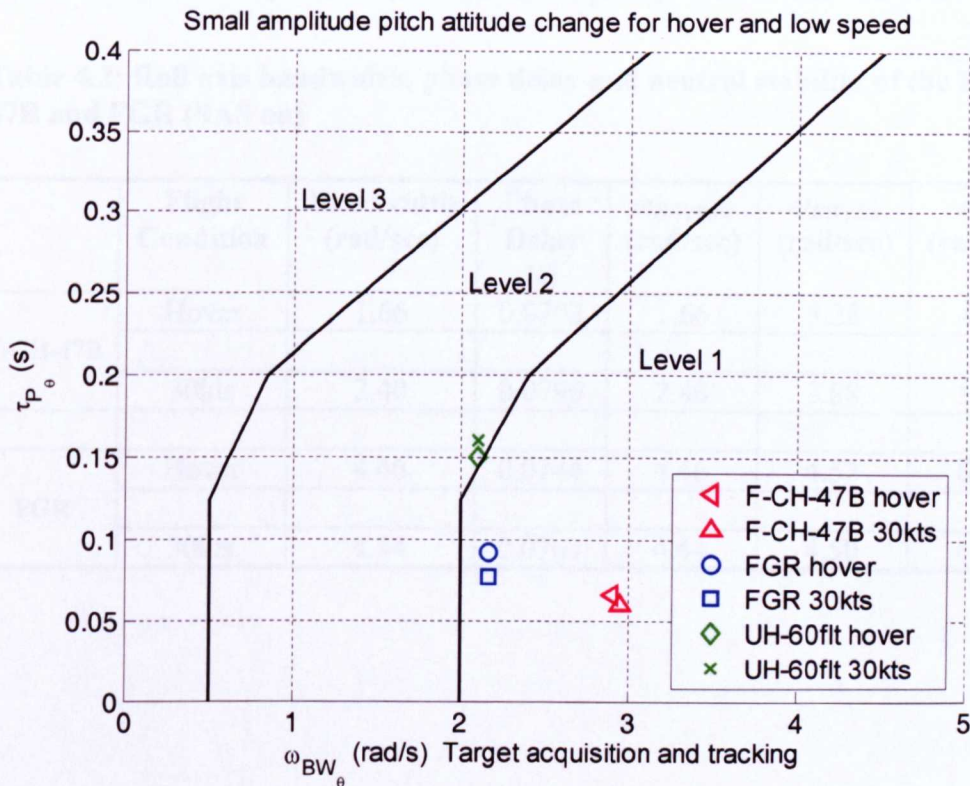
**Figure 4.5: FGR longitudinal control response, hover**

The coherence in figure 4.5 is the linear correlation between the input and output as a function of frequency and has value in the interval 0 to 1. Ockier [48] states that bandwidth results with coherence values of above 0.75 can be considered reliable. Coherence over the frequency range 1.5–10rad/sec is good but drops severely below 1rad/s (coherence is only acceptable between 0.7–4.0rad/sec) in spite of conscious attempts to start the sweeps at a very low frequency. Table 4.1 shows the pitch axis bandwidth, phase delay and neutral stability frequency of the F-CH-47B and FGR. The handling qualities assessment performed in this chapter used the helicopter's empty mission weights. This was 22,450lb for the F-CH-47B and 11,516lb for the FGR [38].

**Table 4.1: Pitch axis bandwidth, phase delay and neutral stability of the F-CH-47B and FGR (SAS on)**

	Flight Condition	Bandwidth (rad/sec)	Phase Delay (s)	$\omega_{BW_{phase}}$ (rad/sec)	$\omega_{BW_{gain}}$ (rad/sec)	$\omega_{180}$ (rad/sec)
F-CH-47B	Hover	2.94	0.0662	2.94	5.79	8.83
	30kts	4.02	0.0600	4.02	5.70	8.90
FGR	Hover	2.17	0.0920	2.17	2.70	3.66
	30kts	2.17	0.0771	2.17	2.85	3.81

Figure 4.6 shows the pitch bandwidth and phase delay parameters compared to the ADS-33E aggressive manoeuvring criteria for the F-CH-47B, FGR and UH-60 flight test results [49] for hover and 30kts forward flight conditions.



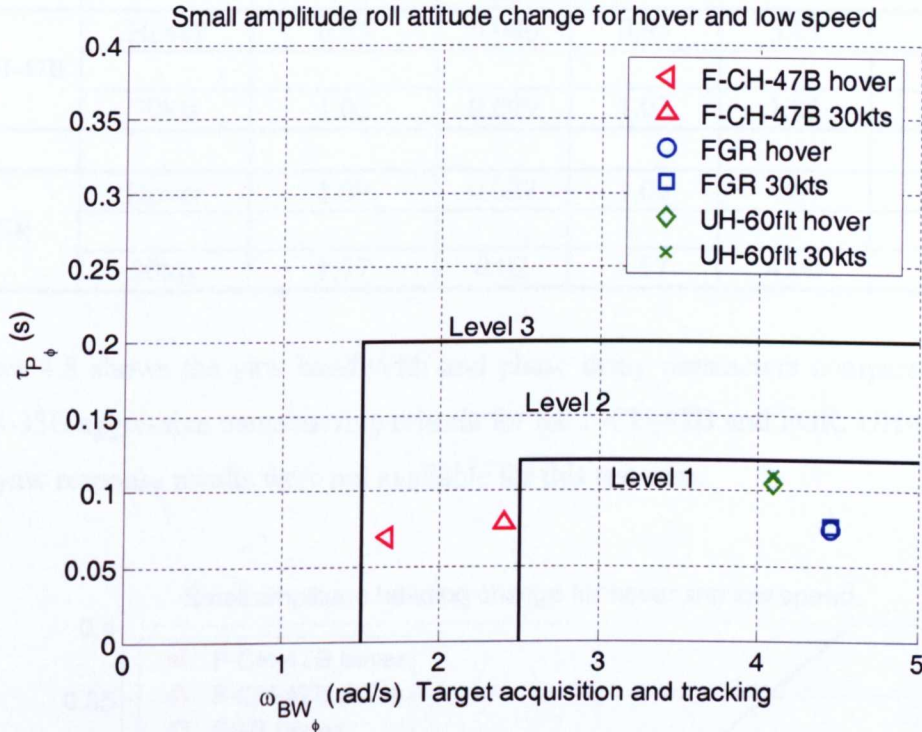
**Figure 4.6: ADS-33E pitch bandwidth criteria for the F-CH-47B, FGR, UH-60 (SAS on) [2]**

The difference in hover bandwidth between the similar FGR and UH-60 rotorcraft is about 0.2 rad/s showing good correlation between the FLIGHTLAB model and UH-60 flight test results. The correlation in the phase delay between the FGR and UH-60 is less positive with a difference equal to 0.05s. This is often the case when flight test derived bandwidth results are compared to those derived from simulation. The FGR simulation model did not model features that contribute to time delays in the system including the mechanical pitch links and delays from filters and the SCAS. Additional time delays could have been incorporated into the models at this stage to better match flight data, but it was decided not to because this might introduce further uncertainties into the system, especially since reliable bandwidth results are difficult to compute. The F-CH-47B was found to have the largest pitch bandwidth (2.9 rad/sec) which is a result of the large control power from the differential collective pitch control. Figure 4.6 shows that the FGR and F-CH-47B predict Level 1 and the UH-60 flight test data predicts borderline high Level 2 handling qualities. Table 4.2 shows the roll axis bandwidth, phase delay and neutral stability frequency of the F-CH-47B and FGR.

**Table 4.2: Roll axis bandwidth, phase delay and neutral stability of the F-CH-47B and FGR (SAS on)**

	<b>Flight Condition</b>	<b>Bandwidth (rad/sec)</b>	<b>Phase Delay (s)</b>	$\omega_{BWphase}$ (rad/sec)	$\omega_{BWgain}$ (rad/sec)	$\omega_{180}$ (rad/sec)
<b>F-CH-47B</b>	Hover	1.66	0.0702	1.66	3.28	4.75
	30kts	2.40	0.0790	2.40	3.88	5.27
<b>FGR</b>	Hover	4.46	0.0744	4.46	4.52	6.62
	30kts	4.44	0.0763	4.44	4.50	6.65

Figure 4.7 shows the roll bandwidth and phase delay parameters compared to the ADS-33E aggressive manoeuvring criteria for the F-CH-47B, FGR and UH-60 flight test results [49] (labelled UH-60ft) for hover and 30kts forward flight conditions.



**Figure 4.7: ADS-33E roll bandwidth criteria for the F-CH-47B, FGR, UH-60 (SAS on) [2]**

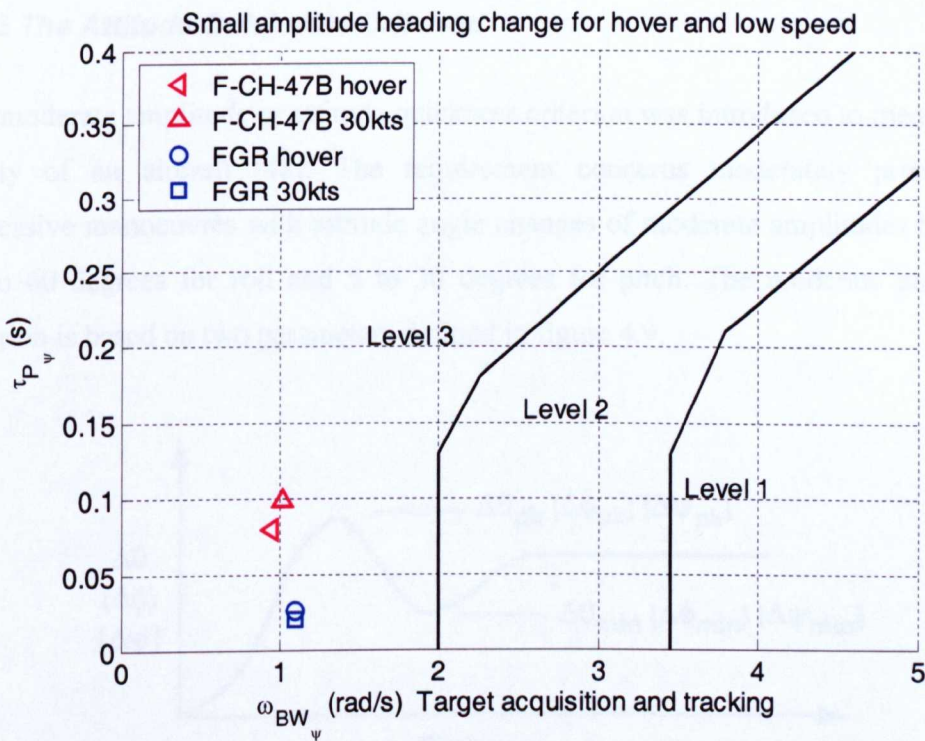
Figure 4.7 shows that the FGR and UH-60 bandwidth results are similar with a difference equal to 0.4rad/sec. This again indicates good correlation between the FLIGHTLAB model and real helicopter. The difference in phase delay between the two sets of results is approximately 0.035s and again can be contributed to a lack of significant time delays in the FGR model. The results indicate that the FGR and UH-60 predict Level 1 and the F-CH-47B predicts Level 2 handling qualities. The F-CH-47B model's lower roll bandwidth result (1.5-2.5rad/sec) was probably due to the high inertia associated with the large cargo helicopter. The Chinook uses combined lateral cyclic to achieve roll control.

Table 4.3 shows the yaw axis bandwidth, phase delay and neutral stability frequency of the F-CH-47B and FGR.

**Table 4.3: Yaw axis bandwidth, phase delay and neutral stability of the F-CH-47B and FGR**

	Flight Condition	Bandwidth (rad/sec)	Phase Delay (s)	$\omega_{BWphase}$ (rad/sec)	$\omega_{BWgain}$ (rad/sec)	$\omega_{180}$ (rad/sec)
F-CH-47B	Hover	0.95	0.080	0.95	3.19	4.64
	30kts	1.02	0.099	1.02	1.83	2.99
FGR	Hover	1.09	0.027	1.09	4.65	6.42
	30kts	1.57	0.02	1.57	4.90	7.21

Figure 4.8 shows the yaw bandwidth and phase delay parameters compared to the ADS-33E aggressive manoeuvring criteria for the F-CH-47B and FGR. UH-60 flight test yaw response results were not available for this test case.



**Figure 4.8: ADS-33E heading bandwidth criteria for the F-CH-47B, FGR, UH-60 (SAS on) [2]**

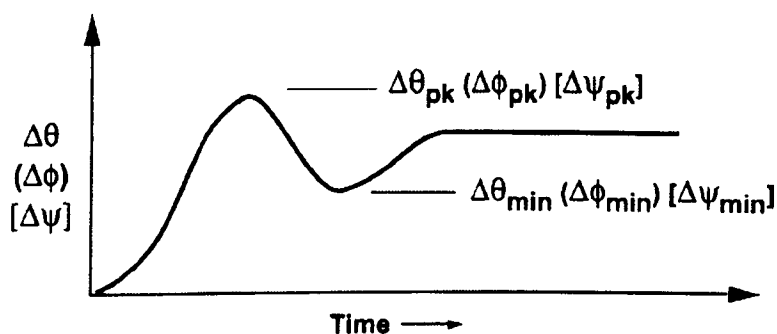
Figure 4.8 shows that the F-CH-47B and FGR yaw bandwidth results were very similar with a difference of 0.1rad/sec. The difference in phase delay between the two

sets of results is approximately 0.06s. The results indicate that the F-CH47B and FGR predict Level 3 handling qualities for target acquisition and tracking MTEs and Level 2 handling qualities for all other MTEs. Target acquisition and tracking describes the process of a pilot being able to visually track either a fixed point in space or another moving object such as another helicopter.

It is important to note that the bandwidth results presented in this section were compared to the ADS-33 requirements for target acquisition and tracking. Usually cargo rotorcraft carrying externally slung loads do not need to achieve the demanding target tracking performance criterion. The reason for adopting this high standard was because later on in the thesis, the automatic co-operative lift system uses the criterion as the benchmark due to the demanding tracking requirements that are necessary for co-operative operations and separation maintenance control.

### 4.3.3 The Attitude Quickness Criterion

The moderate amplitude or attitude quickness criterion was introduced to measure the agility of an aircraft [48]. The requirement concerns moderately precise but aggressive manoeuvres with attitude angle changes of moderate amplitudes between 10 to 60 degrees for roll and 5 to 30 degrees for pitch. The moderate amplitude criterion is based on two parameters defined in figure 4.9.

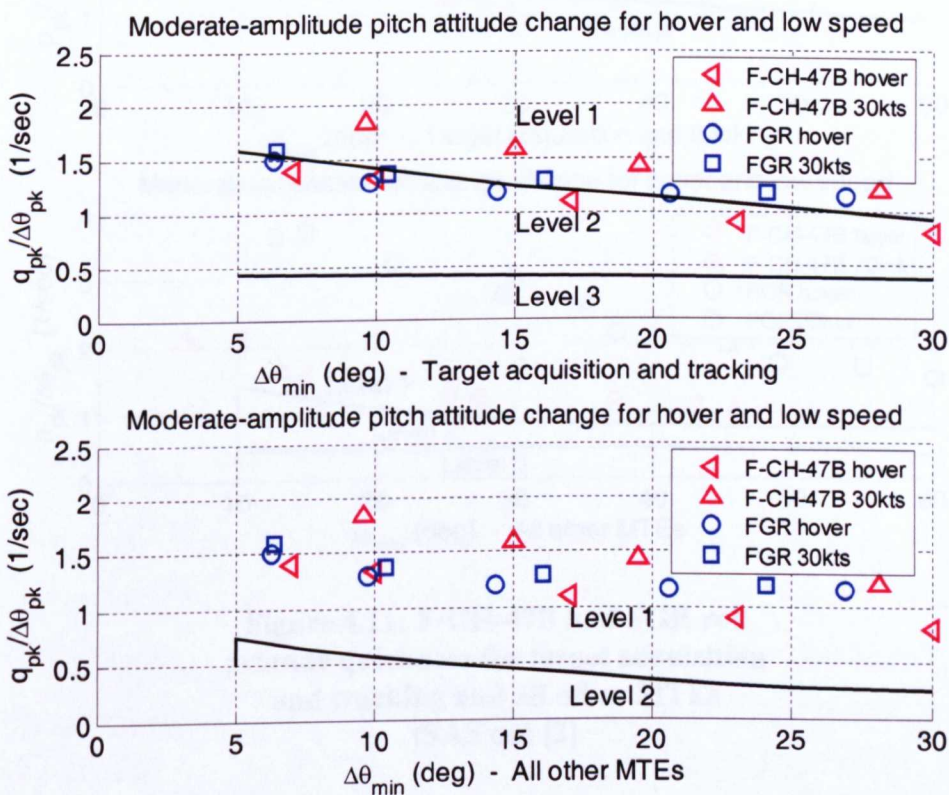


**Figure 4.9: Definition of the attitude quickness parameters [2]**

The parameters are the attitude quickness (the ratio of the maximum angular rate to the peak pitch angle change),  $q_{pk}/\Delta\theta_{pk}$ , and the minimum attitude change during



transition from one pitch angle to another,  $\Delta\theta_{\min}$ . The minimum attitude change parameter was introduced to penalise oscillatory responses (compared to ‘first order’-like responses). For a given pitch change, there will be a maximum value of achievable quickness defined by the limit of the vehicle capability. The attitude quickness parameter was calculated for the FGR and F-CH-47B offline using the FLIGHTLAB software. The models were trimmed in a hover or low speed forward flight condition and the maximum pilot stick control deflection was applied as a step input and the  $q_{pk}$  and  $\Delta\theta_{pk}$  were recorded. The step input duration was varied to obtain the attitude quickness for different  $\Delta\theta_{\min}$ . Figure 4.10 shows the pitch attitude quickness criteria defined for forward flight and hover with the ADS-33E target acquisition and all other MTE requirements overlaid.

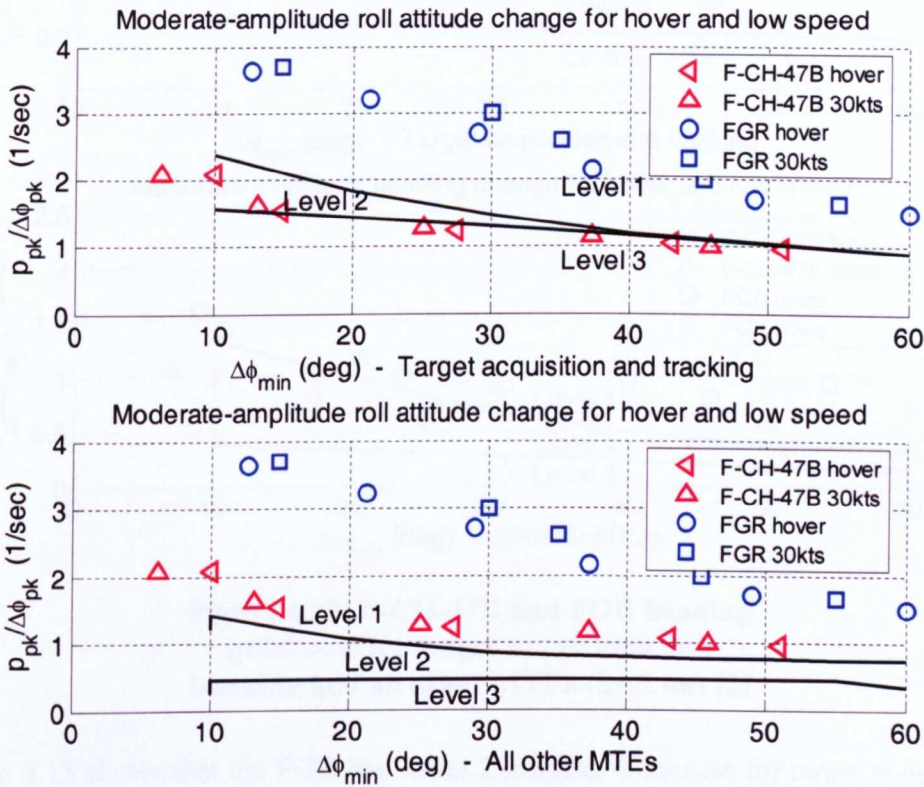


**Figure 4.10: F-CH-47B and FGR pitch attitude quickness for target acquisition and tracking and all other MTEs (SAS on) [2]**

Figure 4.10 shows that the F-CH-47B and FGR has borderline Level 1–Level 2 handling qualities for target acquisition and tracking MTEs (Level 1 for all other MTEs). The F-CH-47B has similar pitch attitude quickness results to the FGR in hover and higher pitch attitude quickness results at 30 knots. Initially this seemed

surprising as the F-CH-47B is much larger than the medium lift utility FGR, however the F-CH-47B has high pitch control power due to the differential collective pitch used for pitch.

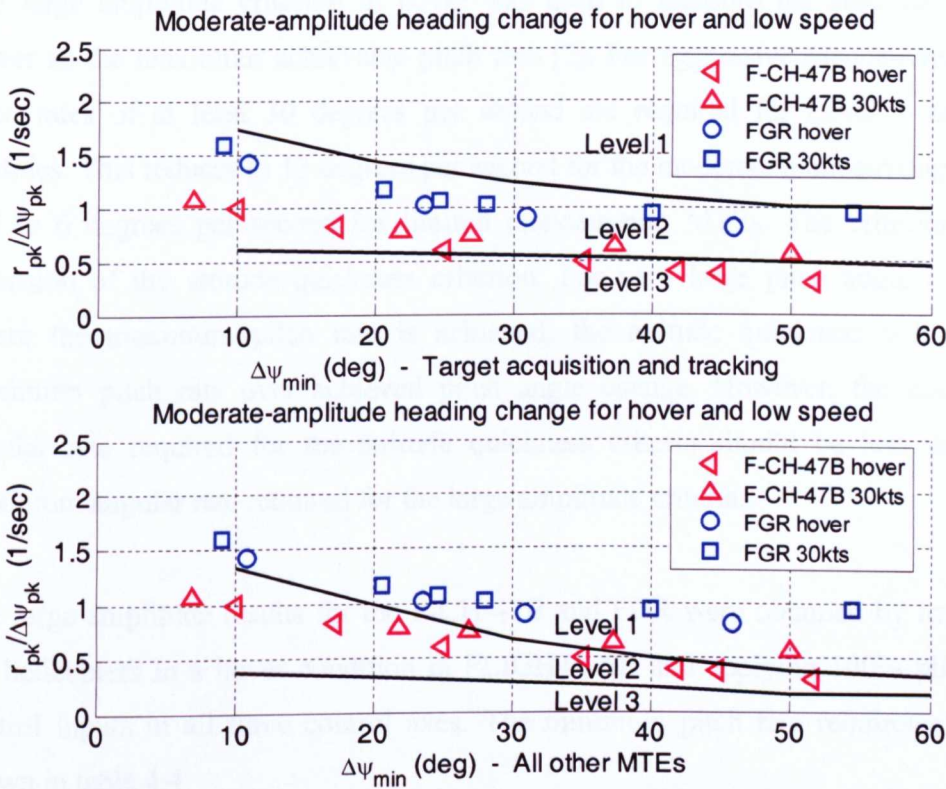
Figure 4.11 shows the roll attitude quickness criteria defined for forward flight and hover with the ADS-33E target acquisition and all other MTE requirements overlaid.



**Figure 4.11: F-CH-47B and FGR roll attitude quickness for target acquisition and tracking and all other MTEs (SAS on) [2]**

Figure 4.11 shows that the FGR has Level 1 roll attitude for target acquisition and tracking and all other MTE requirements. The F-CH-47B has Level 2-Level 3 roll attitude quickness results for target acquisition and tracking and Level 1 handling qualities for all other MTEs. This was expected since the F-CH-47B is much larger than the FGR and has larger roll inertia with less control power. Roll in the F-CH-47B is controlled using combined lateral cyclic on both rotors which gives less control power than the differential collective control used for pitch.

Figure 4.12 shows the yaw attitude quickness criteria defined for forward flight and hover with the ADS-33E target acquisition and all other MTE requirements overlaid.



**Figure 4.12: F-CH-47B and FGR heading quickness for target acquisition and tracking and all other MTEs (SAS on) [2]**

Figure 4.12 shows that the FGR has Level 2 heading quickness for target acquisition and tracking and Level 1 for all other MTE requirements. The F-CH-47B has Level 2-Level 3 heading quickness results for target acquisition and tracking and Level 2 handling qualities for all other MTEs. Unlike a conventional helicopter that uses a tail rotor to control yaw, the F-CH-47B uses differential lateral cyclic to control yaw attitude.

### 4.3.4 The Large Amplitude Criterion

The large amplitude criterion in hover was used to measure the absolute control power as the maximum achievable pitch rate [2]. For aggressive manoeuvres MTE pitch rates of at least 30 degrees per second are required for Level 1 handling qualities. This reduces to 13 degrees per second for the moderate manoeuvring MTEs and to 6 degrees per second for limited manoeuvring MTEs. The criterion is an extension of the attitude quickness criterion. For very large pitch angle changes, where the maximum pitch rate is achieved, the attitude quickness will be the maximum pitch rate over achieved pitch angle change. However, the maximum angular rate required for the attitude quickness criteria should be less than the maximum angular rate required for the large amplitude criteria.

The large amplitude results for the F-CH-47B and FGR were obtained by trimming the helicopters in a hover condition in FLIGHTLAB and applying 100% pilot step control inputs in all three control axes. The minimum pitch rate requirements are shown in table 4.4:

**Table 4.4: Requirements for the larger amplitude criteria for the pitch axis in hover [2]**

	Minimum pitch rate (deg/sec) [rate command systems]		Minimum pitch attitude (deg) [attitude command systems]	
	LEVEL 1	LEVEL 2-3	LEVEL 1	LEVEL 2-3
Aggressive Manoeuvring MTEs	30	13	30	+20/-30
Moderate Manoeuvring MTEs	13	6	+20/-30	13
Limited Manoeuvring MTEs	6	3	15	7

The maximum pitch rates measured in hover for the F-CH-47B and FGR were 30deg/sec and 40deg/sec respectively placing both helicopters in the Level 1 range for all MTEs.

Table 4.5 shows the minimum roll rate requirements for all MTEs.

**Table 4.5: Requirements for the larger amplitude criteria for the roll axis in hover [2]**

	Minimum roll rate (deg/sec) [rate command systems]		Minimum roll attitude (deg) [attitude command systems]	
	LEVEL 1	LEVEL 2-3	LEVEL 1	LEVEL 2-3
Aggressive Manoeuvring MTEs	50	50	60	30
Moderate Manoeuvring MTEs	50	21	60	30
Limited Manoeuvring MTEs	21	15	15	10

In hover the F-CH-47B and FGR achieved roll rates of 51.6deg/sec and 85.9deg/s respectively placing both aircraft in the Level 1 range for all MTEs. The roll attitude quickness and large amplitude control power indicate that the smaller FGR is much more agile than the larger F-CH-47B.

Table 4.6 shows the minimum yaw rate requirements for all MTEs.

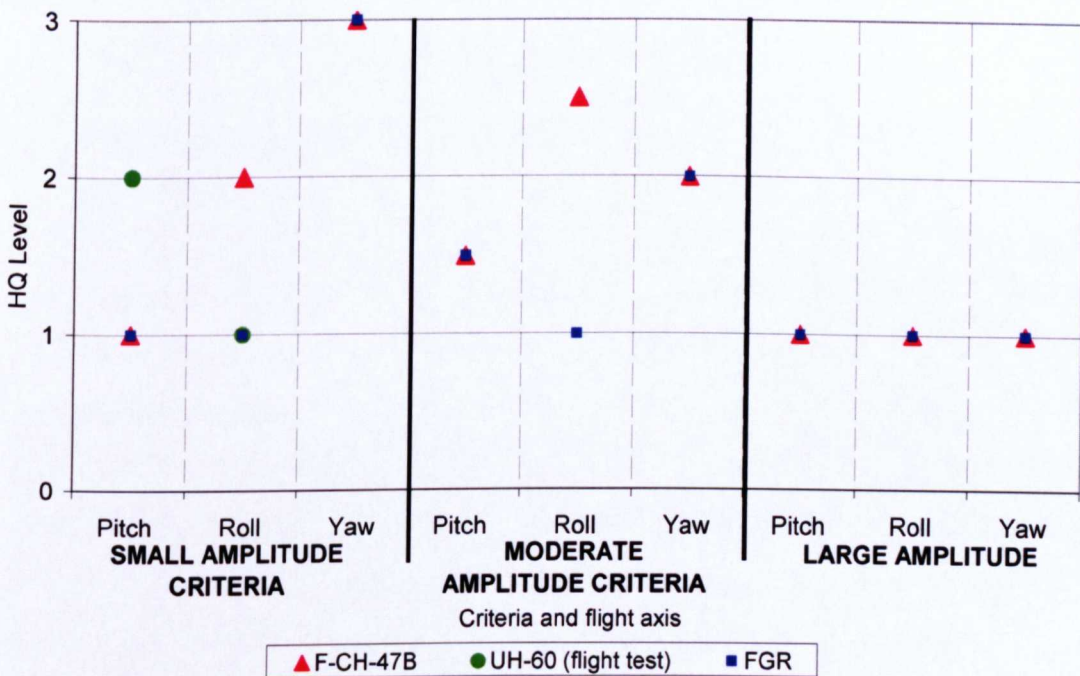
**Table 4.6: Requirements for the larger amplitude criteria for the yaw axis in hover [2]**

	Minimum yaw rate (deg/sec) [rate command systems]	
	LEVEL 1	LEVEL 2-3
Aggressive Manoeuvring MTEs	60	22
Moderate Manoeuvring MTEs	22	9.5
Limited Manoeuvring MTEs	9.5	5

In hover the F-CH-47B and FGR achieved yaw rates of 26.35deg/sec and 51deg/s respectively placing the F-CH-47B in the Level 1 range for moderate and limited manoeuvring MTEs and Level 2-3 for aggressive MTEs. The FGR achieved Level 1 handling qualities for all MTEs with the exception of aggressive manoeuvring MTEs where it achieved Level 2-3 large amplitude yaw handling qualities.

#### 4.4 Conclusion to Chapter

The aim of this chapter was to introduce the important concept of handling qualities analysis which forms one of the key components of this research. The chapter described the methodology and importance of the ADS-33 handling qualities criteria and described the internal attributes and external factors that can influence handling qualities. The important role of ADS-33 MTEs and the Cooper-Harper handling qualities rating scales was highlighted with emphasis made on how important it is to complement objective data derived from offline simulation with subjective pilot comment using piloted simulation trials and ADS-33 MTEs. The handling qualities of two helicopters models: the FGR and F-CH-47, were assessed and compared to flight test results where possible using the ADS-33 bandwidth, attitude quickness and large amplitude criteria. The ADS-33 small and medium amplitude criteria were described in detail and highlighted as being particularly pertinent to slung load operations. Figure 4.13 summarises the handling qualities results from this chapter for the three different configurations considered in comparison to the target acquisition and tracking requirements. The large amplitude results in the figure were based on the moderate manoeuvring MTE requirements. Only bandwidth data was available for the UH-60, hence the limited number of flight test data points.



**Figure 4.13: Summary of handling qualities results**

The handling qualities criteria covered in this chapter will be used again later on in the thesis in Chapters 6 and 7 when examining the handling qualities of the EH-101 ACLC.

The following chapter will build upon the handling qualities assessment introduced here and assess how the dynamic stability and handling qualities of the FGR are modified by the inclusion of an externally slung load. The handling qualities will be assessed using piloted simulation focussed on the ADS-33 hover board MTE.

## Chapter 5

### HELICOPTER AND EXTERNAL SLUNG LOAD ANALYSIS

#### 5.1 Introduction

This chapter builds on the handling qualities analysis work introduced in the previous chapter and examines what effect the externally slung load has on the handling qualities and dynamic stability of the FGR. The sensitivity of the handling qualities to a change in various helicopter and slung load parameters including airspeed, cable length and external load mass will be explored offline and online through piloted simulation undertaken by a qualified test pilot. The chapter includes the results from an ADS-33 hover board MTE where the external load mass and cable length were varied to examine how the helicopter handling qualities were modified. The offline simulation analysis presented was completed in the time and frequency domain using ADS-33 to gain a complete picture of the underlying dynamics. Load stabilisation using conventional classical systems and modern techniques including multi-variable  $H_\infty$  control are also explored later in the chapter.

#### 5.2 Single Helicopter Linear Stability Analysis

The FGR model was used to investigate the dynamic stability of the single load model as a function of:

- Airspeed
- Cable length
- External load mass

The FGR was trimmed at a number of different speeds, at sea level, and linearised using the following 13 states: roll attitude ( $\phi$ ), pitch attitude ( $\theta$ ), heading angle ( $\psi$ ), roll rate ( $p$ ), pitch rate ( $q$ ), yaw rate ( $r$ ), body axis x component of velocity ( $v_{xb}$ ), body axis y component of velocity ( $v_{yb}$ ), body axis z component of velocity ( $v_{zb}$ ), the longitudinal sling trail angle,  $\theta_{long}$ , lateral sling trail angle  $\theta_{lat}$ , and sling trail angle



rates  $\dot{\theta}_{\text{long}}$  and  $\dot{\theta}_{\text{lat}}$ . The linearization was performed using FLIGHTLAB software and allowed any of the aircraft states to be defined by the user. The analysis completed in the remainder of this section was focussed on the eigenvalue and eigenvector analysis using the s-plane. To understand eigenvectors and eigenvalues, one must first consider a square-matrix transformation that has the property that vectors exist whose components are only scaled by the transformation. If  $v$  is such an “invariant” vector, its components must satisfy the equation [50]:

$$Av = \lambda v, \quad v(n \times 1), \quad \text{eqn 5.1}$$

where  $A$  is the transformation matrix and  $\lambda$  is a (scalar) constant of proportionality. A rearrangement of eqn 5.1 gives the set of homogenous linear equations:

$$(A - \lambda I)v = 0, \quad \text{eqn 5.2}$$

Which has a non-null solution for  $v$  if, and only if, the determinant of the coefficient matrix is zero:

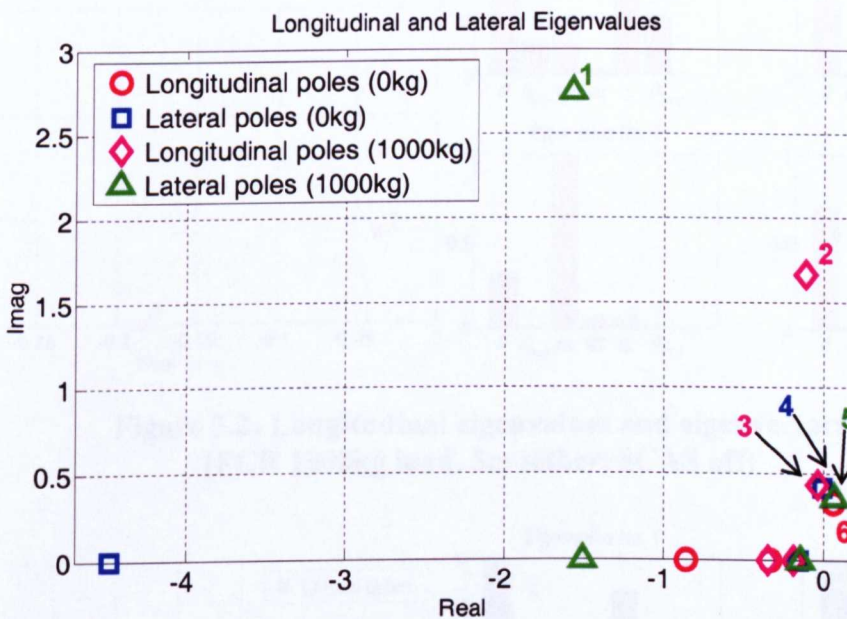
$$|A - \lambda I| = 0 \quad \text{eqn 5.3}$$

This determinant is an  $n$ -th order polynomial in  $\lambda$ , called the characteristic polynomial of  $A$ , so there may be up to  $n$  distinct solutions for  $\lambda$ . Each solution,  $\lambda_i$ , is known as an eigenvalue or characteristic value of the matrix  $A$ . The associated invariant vector defined by equation 5.1 is known as a right eigenvector of  $A$  (the left eigenvectors of  $A$  are the right eigenvectors of its transpose  $A^T$  [50]).

The eigenvalues represent the natural modes of the aircraft which describe the stability of small motions about the trim condition. The eigenvectors represent the mode-shapes, or the ratio of the response contributions in the various degrees of freedom. The modes are linearly independent, meaning that no one can be made up as a collection of others [50].

The s-plane is a mathematical domain where, instead of viewing processes in the time domain modelled with time-based functions, they are viewed as equations in the frequency domain [51]. The poles are plotted on graph with the real part of the pole value as the x-axis and the imaginary part as the y-axis. The more negative the real part of the pole the more rapidly the transient response dies away. The larger the imaginary part of the pole the higher the frequency of the oscillation. A system that has a pole which has a positive real part is unstable [51].

The modes of the aircraft were then de-coupled into longitudinal and lateral sub-sets for identification by separating the longitudinal and lateral states. Figure 5.1 shows an s-plane plot of the coupled helicopter eigenvalues for a helicopter with no load and for a helicopter with a 1000kg load supported by a 5m tether cable in a hover condition with SCAS off.

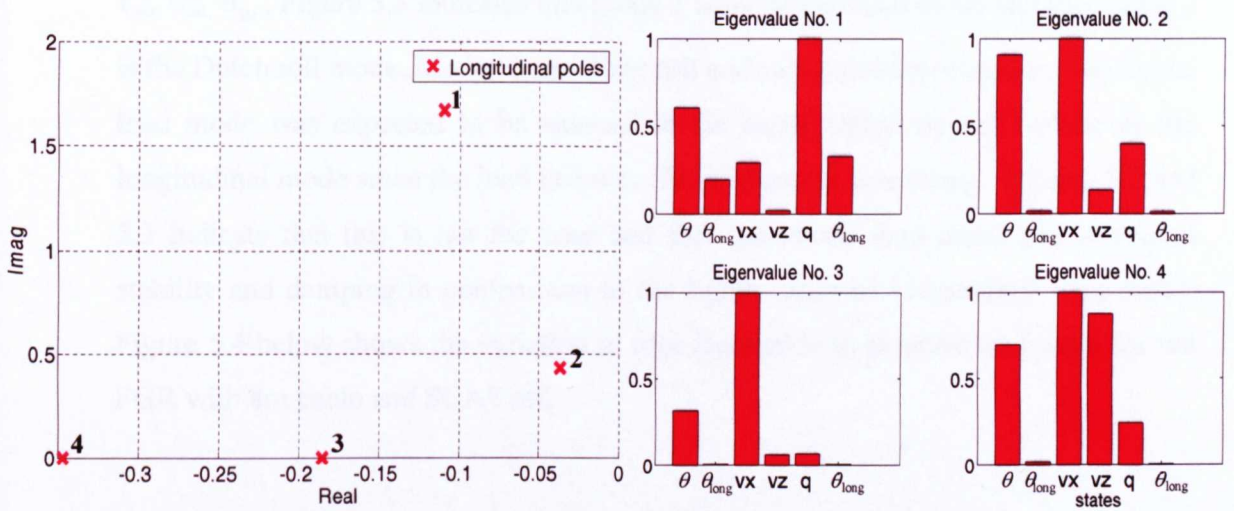


**Figure 5.1: Longitudinal and lateral eigenvalues (FGR 0kg and 1000kg load, 5m tether, SCAS off)**

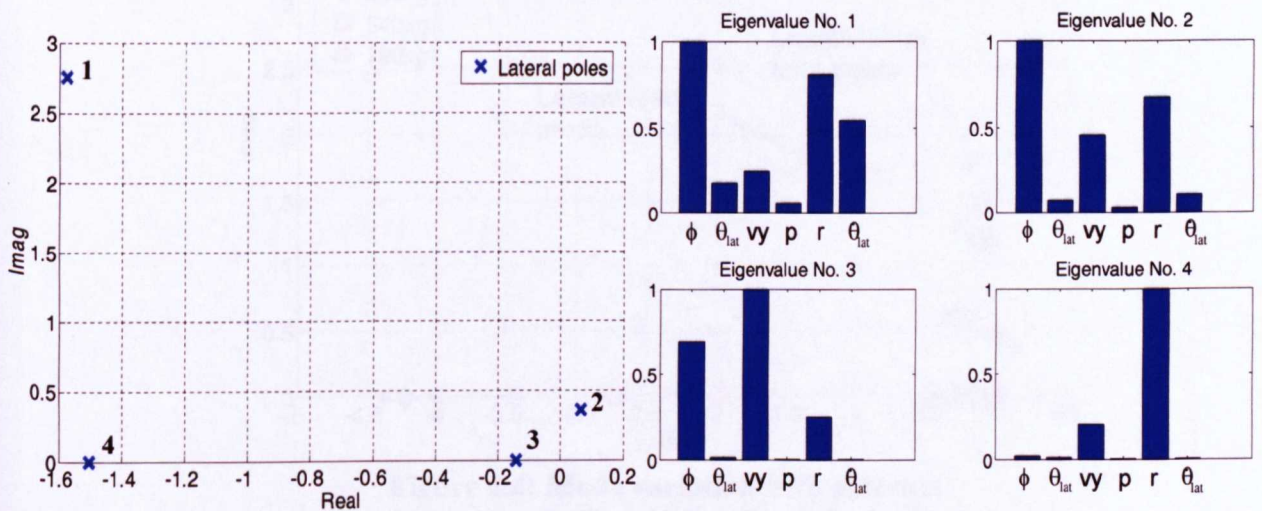
From the figure, it is evident that the external load introduces two additional load modes (i.e. modes dominated by load swinging motion) to the system that represent the lateral (load mode 1) and longitudinal motions (load mode 2) of the external load. In the hover condition, with no external load, the Phugoid and Dutch roll modes (labelled 6 and 4) are unstable and marginally stable respectively. The introduction of

the external load increased the stability of the phugoid mode (mode 3) and decreased the stability of the Dutch roll mode (mode 5) as shown.

The eigenvectors for each eigenvalue of the reduced order aircraft stability matrix were examined to investigate and verify the mode components. The contributions were normalised against the maximum absolute eigenvector for each eigenvalue. Figure 5.2 and 5.3 show the decoupled longitudinal and lateral eigenvalues and corresponding graphical eigenvector contributions obtained using the following states;  $\theta, q, v_{xb}, v_{zb}, \theta_{long}, \dot{\theta}_{long}$ . Each eigenvalue has been numbered and corresponds to the adjacent eigenvector contribution plot.

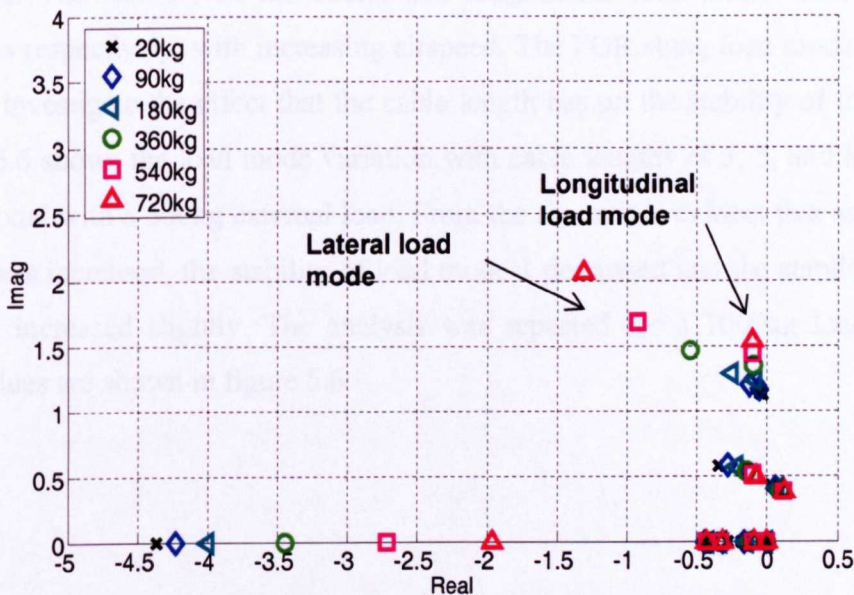


**Figure 5.2: Longitudinal eigenvalues and eigenvectors (FGR 1000kg load, 5m tether, SCAS off)**



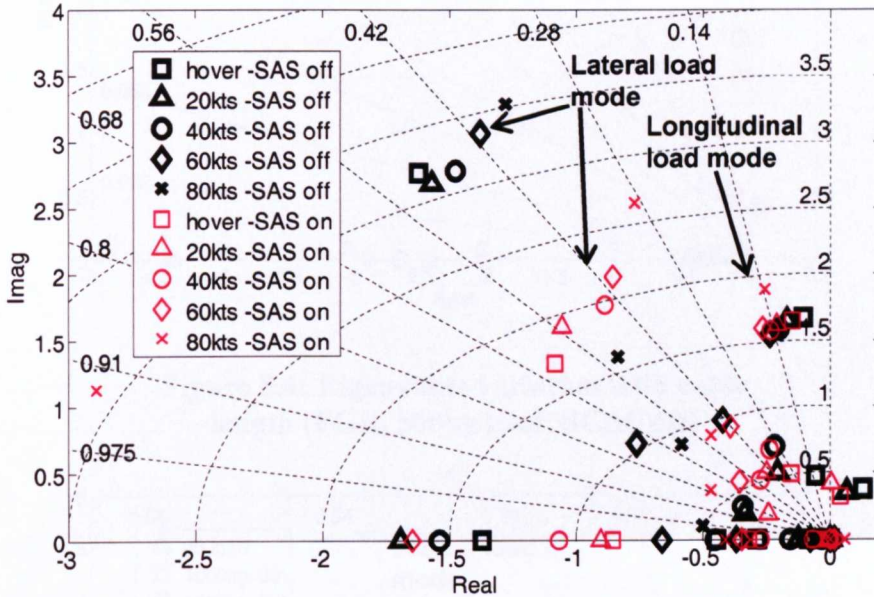
**Figure 5.3: Lateral eigenvalues and eigenvectors (FGR 1000kg load, 5m tether, SCAS off)**

The longitudinal eigenvalue at  $-0.11+1.7i$  (eigenvalue 1) in figure 5.2 is associated principally with the fore and aft swinging of the load. The natural frequency and damping factor of the mode are, respectively, 2 rad/s and 0.046. Note that the natural frequency of the coupled mode is slightly greater than the 1.4 rad/s of a simple pendulum of the same length. By examining the relative eigenvector contribution in figure 5.2, it is evident that mode 1 has the largest longitudinal sling rate contribution and is therefore the longitudinal load mode. By examining the other contributions it is evident that mode 2 is the phugoid and modes 3 and 4 are the heave and pitch subsidence modes. Figure 5.3 shows the decoupled lateral eigenvalues and eigenvector contributions. These were obtained using the following states;  $\phi, \psi, p, r, v_{yb}, \theta_{lat}, \dot{\theta}_{lat}$ . Figure 5.3 indicates that mode 1 is the lateral load mode and that mode 2 is the Dutch roll mode. Modes 3 and 4 are roll and yaw subsidence modes. The lateral load mode was expected to be situated in the same region on the s-plane as the longitudinal mode since the load behaves like a spherical pendulum. Figures 5.2 and 5.3 indicate that this is not the case and that the lateral load mode has increased stability and damping in comparison to the lightly damped longitudinal load mode. Figure 5.4 below shows the variation in root location with external load mass for the FGR with 8m cable and SCAS off.



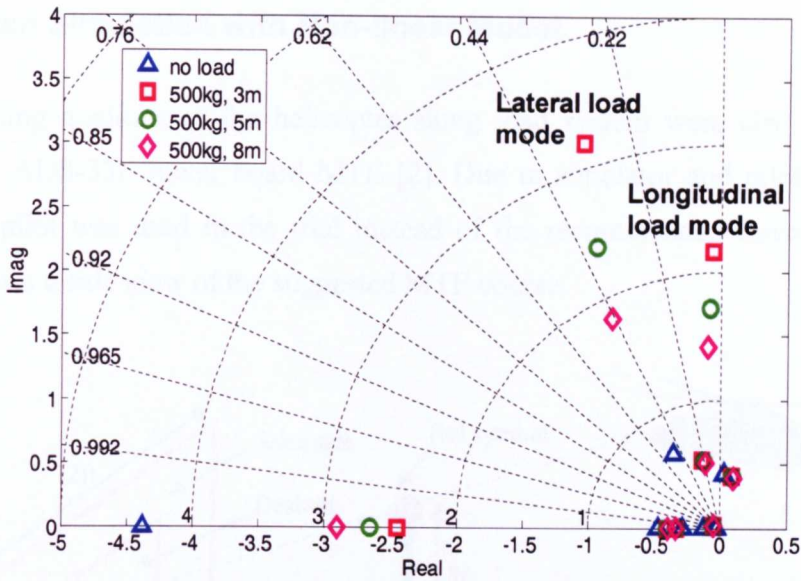
**Figure 5.4: Mode variation with external load mass (FGR, 1000kg, 5m, SCAS off)**

For small load masses, the longitudinal and lateral load modes are located in the same region as expected. However as the mass increases above 180kg the separation between the two load modes increases indicating a coupling effect. Figure 5.5 shows the eigenvalue variation with forward airspeed for SCAS on and off cases.

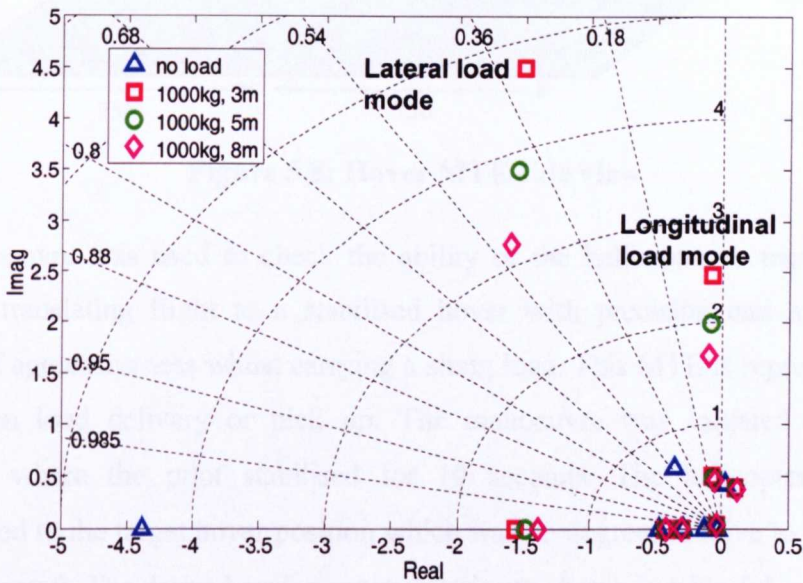


**Figure 5.5: Mode variation with fwd airspeed (FGR, 1000kg load, 5m)**

Figure 5.5 shows that lateral load mode has increased damping with SCAS on below 60 knots. The stability of the lateral and longitudinal load modes decreases and increases respectively, with increasing airspeed. The FGR slung load model was also used to investigate the effect that the cable length has on the stability of the system. Figure 5.6 shows the load mode variation with cable lengths of 3, 5, and 8m for the FGR model with a 500kg external load. From the figure it is evident that as the cable length was increased, the stability of load mode 1 decreased and the stability of load mode 2 increased slightly. The analysis was repeated for a 1000kg load and the eigenvalues are shown in figure 5.6.



**Figure 5.6: Eigenvalue variation with cable length (FGR, 500kg load, SCAS off)**

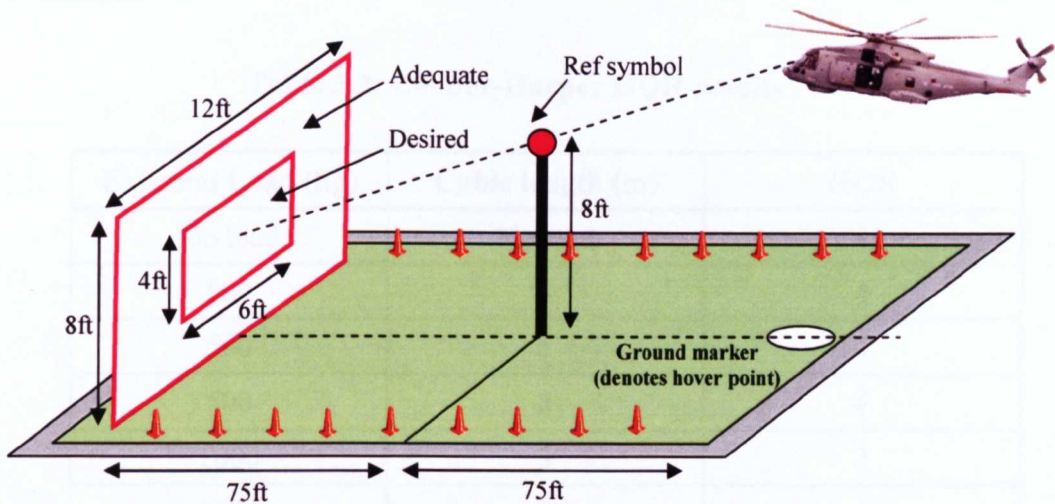


**Figure 5.7: Eigenvalue variation with cable length (FGR, 1000kg load, SCAS off)**

Figure 5.7 shows that as the cable length is increased, the stability of lateral load mode increased which is contrary to the previous 500kg load case where the stability decreased. The load mode damping for the 1000kg external load was higher than the previous 500kg case. This illustrates that the combination of cable length and external load mass determine the stability of the system.

### 5.3 Piloted Simulation with Non-linear Model

The handling qualities of the helicopter slung load system were also assessed by flying the ADS-33E hover board MTE [2]. Due to simulator and pilot availability only one pilot was used in the trial instead of the recommended three. Figure 5.8 below shows a side view of the suggested MTE course.



**Figure 5.8: Hover MTE side view**

The manoeuvre was used to check the ability of the helicopter to transition from hover to translating flight to a stabilised hover with precision and a reasonable amount of aggressiveness whilst carrying a slung load. This MTE is representative of a precision load delivery or pick up. The manoeuvre was initiated in a hover condition where the pilot stabilised for 10 seconds. The helicopter was then manoeuvred to the target hover position which was 45 degrees relative to the heading of the rotorcraft. The desired performance criteria are shown in table 5.1:

**Table 5.1: Desired performance requirements**

Desired Performance
Attain a stabilised hover within 10 seconds of deceleration.
Maintain a stabilised hover for at least 30 seconds
Maintain an altitude of +/- 3 feet
Maintain a heading of +/- 5 degrees
No objectionable oscillations in any axis

The MTE was performed with 500, 1000 and 2000kg external loads with cable lengths of 3, 5 and 8m with SCAS on. The pilot was asked to award each test case a Cooper-Harper HQR [42]. Table 5.2 shows the HQR awarded for each test case. The pilot performed each test case twice with a practice run followed by the actual assessed run. Ideally each test case would have been flown at least three times and an average HQR recorded, but this was not the case due to test pilot availability and time constraints.

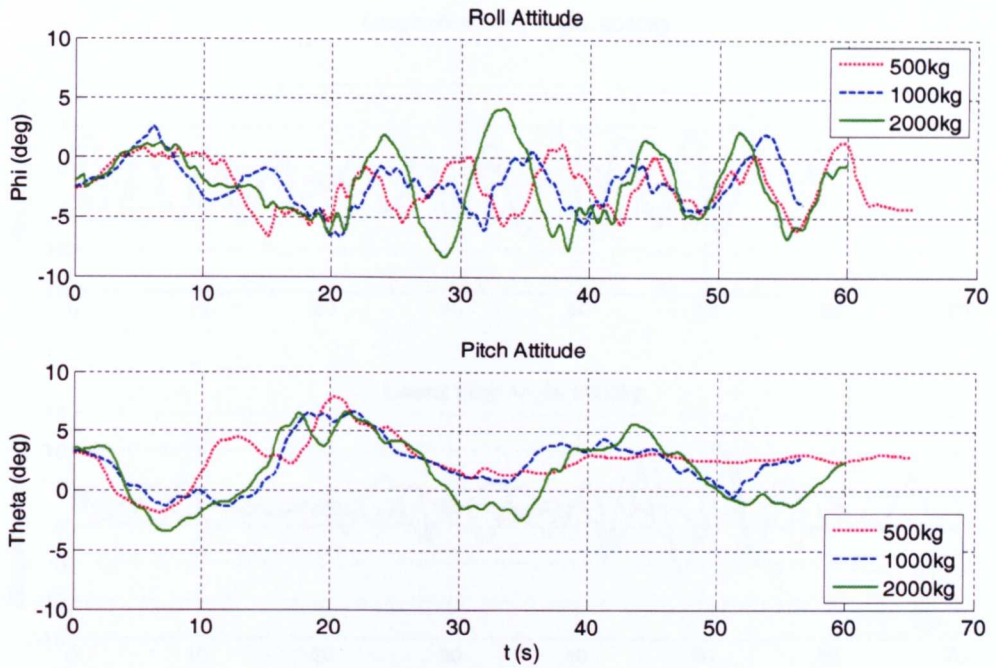
**Table 5.2: Cooper-Harper HQR results**

<b>External Load (kg)</b>	<b>Cable length (m)</b>	<b>HQR</b>
No load	No load	4
500	3	4
500	5	4
500	8	4
1000	3	3
1000	5	4
1000	8	4
2000	3	4
2000	5	4
2000	8	5

Table 5.2 shows that the most common HQR was 4. The pilot felt that the addition of the external load improved the handling qualities due to increased damping in longitudinal and lateral axes.

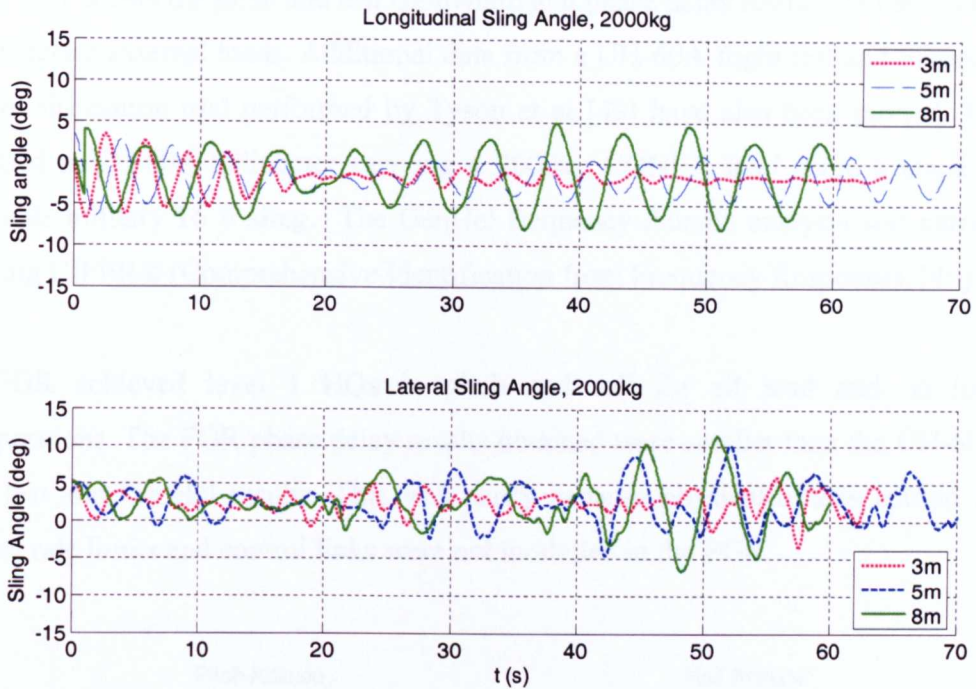
The pilot also indicated that increasing the cable length increased the pilot workload due to the increase in the amplitude of the load oscillations. The worst HQR of 5 was obtained for the 2000 kg 8m load case. Figure 5.9 shows the roll and pitch attitude of the helicopter carrying 500, 1000 and 2000kg external loads with the cable length fixed at 8m. The 2000kg case shows the greatest roll amplitude which contributed to the increased pilot workload.





**Figure 5.9: Helicopter roll and pitch attitude (FGR, SCAS on)**

Figure 5.10 shows the longitudinal and lateral sling angles for a 2000kg external load with cable lengths of 3, 5, and 8m. From the figure it is evident that the oscillation amplitude increases with increasing cable length and the frequency decreases. The pendulum frequencies are determined approximately by the load relative mass and sling length which can be estimated as,  $\omega = \sqrt{g/L(1 + m_2/m_1)}$  [17] where L is the distance between the load and the helicopter attachment point,  $m_1$  and  $m_2$  are the helicopter and load mass respectively. L is in the range 10-26 ft,  $m_2/m_1$  is between 0.06 – 0.27.



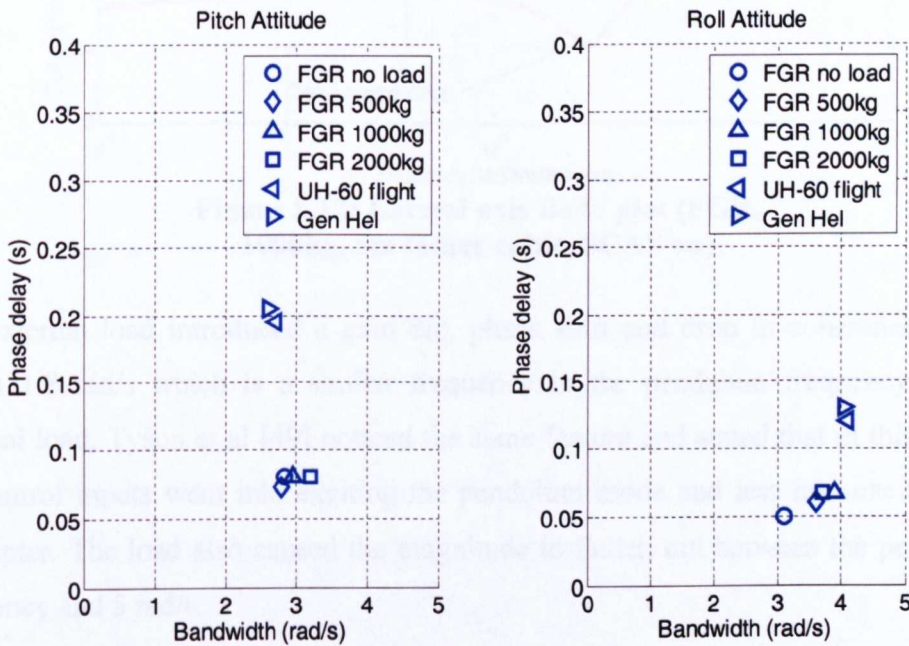
**Figure 5.10: Variation in longitudinal and lateral sling angles with increased cable length (FGR SCAS on)**

#### 5.4 Closed Loop Frequency Analysis

Pitch and roll frequency sweeps were carried out in a hover condition in order to investigate the short term handling qualities. The ADS-33E Bandwidth criteria address the short term, small amplitude handling qualities. These are particularly important for high gain tasks such as confined area manoeuvring and precision load delivery and other tracking tasks. Manual frequency sweeps were used as these generally yield better results than user specified synthetic sweeps [48] like the one illustrated in figure 4.4. This is because the manual sweeps capture the closed loop pilot/aircraft interaction which includes the delays introduced by the pilot due to reaction times [48]. To ensure that the frequency content consisted only of the primary axis being investigated, the pilot was instructed to keep the normal off-axis correctional inputs (such as pedal to collective correction) uncorrelated with on-axis inputs. This was found to be particularly difficult in the hover where off-axis inputs are required to stabilise the naturally unstable aircraft [46].

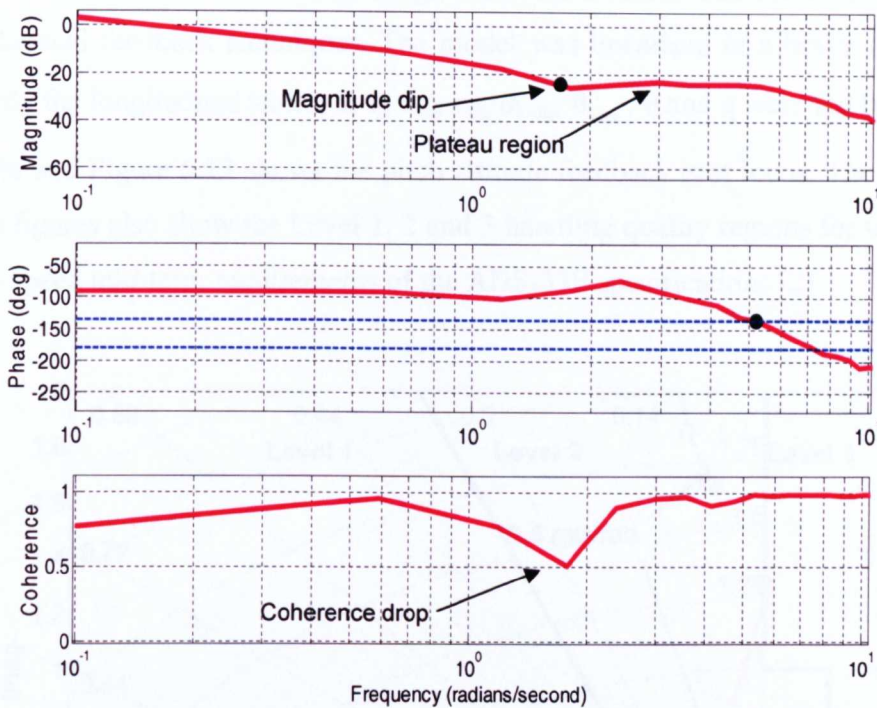
Figure 5.11 shows the pitch and roll bandwidth and phase delay results for the system with different external loads. Additional data from a UH-60A flight test and Sikorsky GenHel simulation trial performed by Tyson et al [49] have also been plotted. The trial used a UH-60A helicopter carrying a 2000kg CONEX load using a standard four-cable military 16 ft sling. The GenHel frequency domain analysis was carried out using CIPHER® (Comprehensive Identification from Frequency Responses, [49]).

The FGR achieved level 1 HQs in pitch and roll for all load and no load configurations. The FGR phase delay results obtained were smaller than the UH-60A flight test and GenHel results. This was partly because physical effects caused by actuator rate limits and control links were not modelled in the FGR.



**Figure 5.11: Pitch and roll attitude short term response [49]**

Figure 5.12 shows an example of the Bode plot obtained from a lateral frequency sweep.

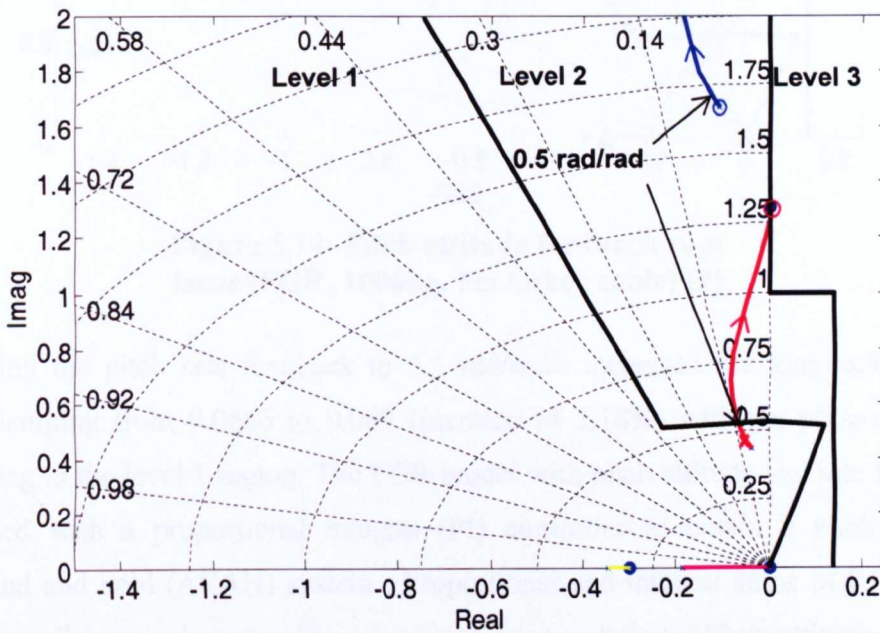


**Figure 5.12: Lateral axis Bode plot (FGR, 1000kg, 5m tether cable, SCAS on)**

The external load introduced a gain dip, phase shift and drop in coherence in the region 1.8 rad/s which is a similar frequency to the pendulum frequency of the external load. Tyson et al [49] noticed the same feature and stated that in this region the control inputs went into exciting the pendulum mode and less into exciting the helicopter. The load also caused the magnitude to flatten out between the pendulum frequency and 5 rad/s.

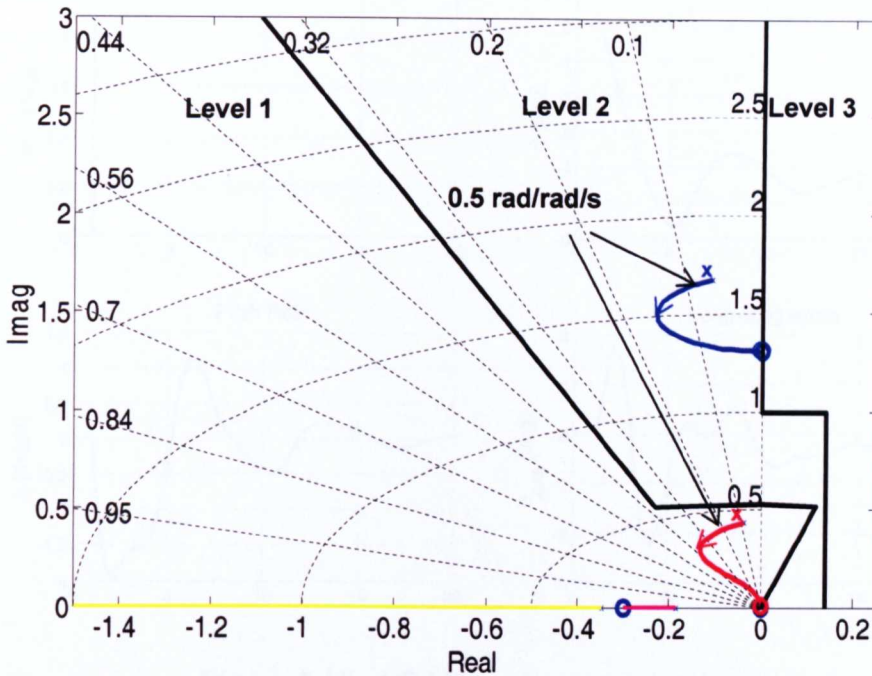
## 5.5 Load Stabilisation using SCAS

The FGR model was also used to investigate how the external load could be stabilised using classical feedback techniques. The model was linearised in a hover condition using only the longitudinal states;  $\theta$ ,  $q$ ,  $v_{xb}$ ,  $v_{zb}$ ,  $\theta_{long}$ ,  $\dot{\theta}_{long}$ .  $\theta$  and  $q$  were fed back with pure gain and Figure 5.13 shows the pitch attitude feedback root locus. The stability analysis figures also show the Level 1, 2 and 3 handling quality regions for the hover and low speed mid-term requirements of the ADS-33E specifications [2].



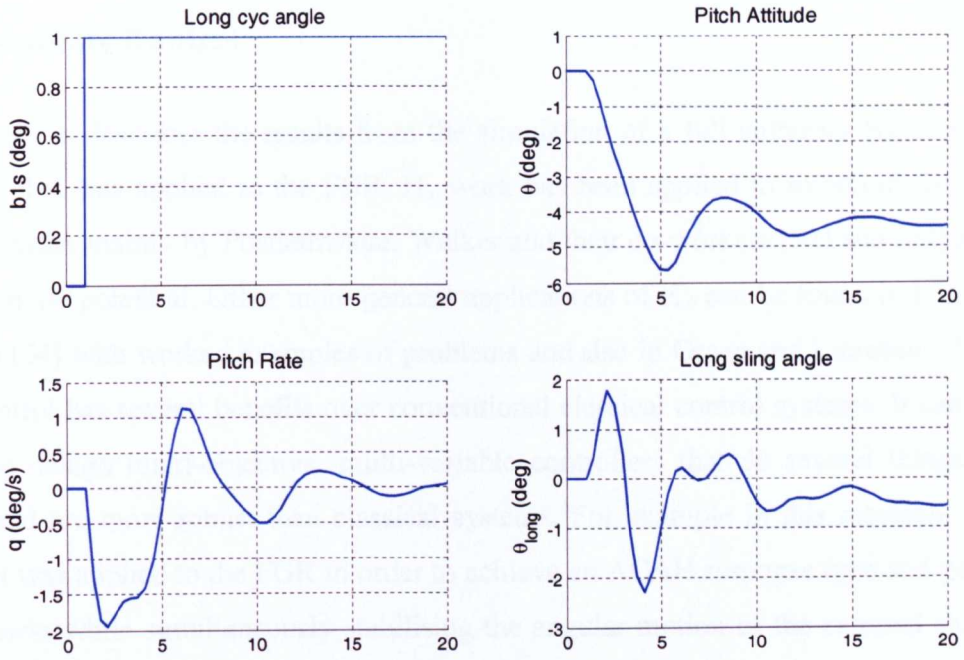
**Figure 5.13: Pitch attitude feedback root locus (FGR, 1000kg, 5m tether cable) [2]**

The Level 1, 2 and 3 handling quality regions for the hover and low speed mid-term requirements of the ADS-33E specifications have been overlaid. Increasing the pitch attitude feedback gain to 0.5 rad/rad has negligible effect on the load damping. The pitch rate feedback loop was also closed, and the root locus plotted in figure 5.14.



**Figure 5.14: Pitch attitude feedback root locus (FGR, 1000kg, 5m tether cable) [2]**

Increasing the pitch rate feedback to 0.5 rad/rad/s increased the longitudinal load mode damping from 0.0656 to 0.069 (increase of 5.18%) with the phugoid mode remaining in the level 1 region. The FGR model with pitch attitude and rate feedback was used with a proportional integral (PI) controller to obtain a pitch attitude command and hold (ACAH) system. Proportional and integral gains of 0.9 rad/rad and 0.5 sec<sup>-1</sup> were selected using a trial and error technique. Pitch attitude and rate feedback gains of 0.5 rad/rad and 0.5 rad/rad/s were selected based on the previous root locus plots. Figure 5.15 shows the type of pitch attitude and load angle obtained for a PI controller that was tuned specifically for an ACAH response type using only the helicopter states (i.e. without considering the external load). The figure shows how the external load influences the helicopter pitch attitude response, introducing pitch oscillations.



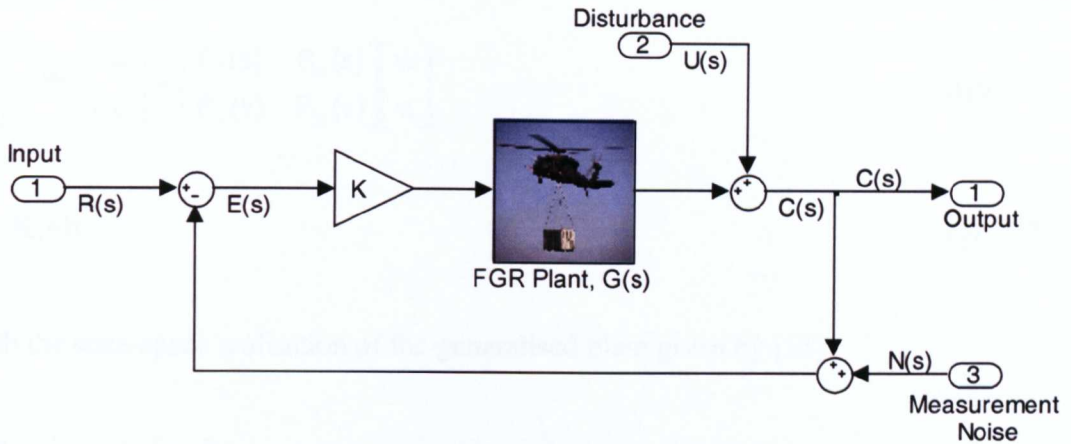
**Figure 5.15: ACAH response to step input  
(FGR, 1000kg load, 5m tether cable)**

## 5.6 H-infinity Control

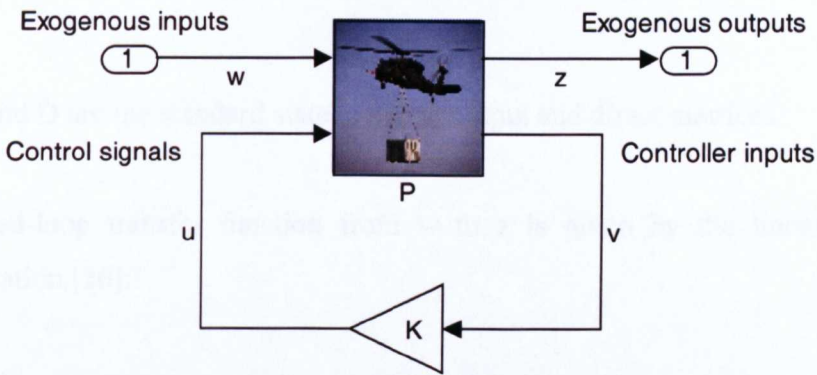
This section describes the results from the simulation of a full authority  $H_\infty$  control system that was applied to the FGR.  $H_\infty$  work has been applied to rotorcraft for the last 20 years mainly by Postlethwaite, Walker and their co-workers [52] and [53] and shows good potential. Other more general applications of  $H_\infty$  can be found in text by Simon [54] with worked examples of problems and also in Green and Limebeer [55].  $H_\infty$  control has several benefits over conventional classical control systems. It can be used to design multi-objective, multi-variable controllers that do several things at once and are more robust than classical systems. For example in this research,  $H_\infty$  control was applied to the FGR in order to achieve an ACAH response type and good robustness while simultaneously stabilising the angular motion of the external slung load. The 'H' in  $H_\infty$  control stands for Hardy space and the ' $\infty$ ' implies that it is designed to accomplish minimax restrictions in the frequency domain [56]. Essentially  $H_\infty$  is a modern control optimisation method that takes a 'worst case' approach to optimisation. The method can guarantee stability against certain forms of uncertainty and is particularly useful when used in a two degree of freedom scenario, for example in obtaining pitch attitude regulation and sling angle rate minimisation.  $H_\infty$  is also useful when there is uncertainty in the simulation model due to a lack of representative data, for example when certain data such as blade elastic properties are not known.

The most widely accepted general control problem formulation applied to H-infinity optimisation problems is known as the general control configuration [56]. This differs slightly from the one degree-of-freedom configuration used in the research up until now. Figure 5.16 and 5.17 show the one degree-of-freedom and general control formulation for comparison.





**Figure 5.16: One degree-of-freedom configuration [56]**



**Figure 5.17: General Control Configuration [56]**

where

- P is the generalised plant model. If P is being used to formulate a design problem, then it will also include the weighting functions
- w are the exogenous inputs; commands, disturbances and noise
- z are the exogenous outputs; the error signal to be minimised ( $y-r$ )
- v are the controller inputs for the general configuration. These include commands, measured plant outputs, measured disturbances
- u are the control signals

where

$$\begin{bmatrix} z \\ v \end{bmatrix} = P(s) \begin{bmatrix} w \\ u \end{bmatrix} = \begin{bmatrix} P_{11}(s) & P_{12}(s) \\ P_{21}(s) & P_{22}(s) \end{bmatrix} \begin{bmatrix} w \\ u \end{bmatrix} \quad \text{eqn 5.1}$$

$$u = K(s)v \quad \text{eqn 5.2}$$

With the state-space realisation of the generalised plant given by [56]:

$$P^s = \begin{bmatrix} A & B_1 & B_2 \\ C_1 & D_{11} & D_{12} \\ C_2 & D_{21} & D_{22} \end{bmatrix} \quad \text{eqn 5.3}$$

where

A, B, C and D are the standard state, control, output and direct matrices.

The closed-loop transfer function from w to z is given by the linear fractional transformation [56]:

$$z = F_1(P, K)w \quad \text{eqn 5.4}$$

where

$$F_1(P, K) = P_{11} + P_{12}K(I - P_{22}K)^{-1}P_{21} \quad \text{eqn 5.5}$$

$H_2$  and  $H_\infty$  control involve the minimisation of the  $H_2$  and  $H_\infty$  norms of  $F_1(P, K)$  (eqn 5.5) respectively. The  $H_\infty$  norm of the transfer function  $F_1(P, K)$  is defined as [56]:

$$\|F_1(P, K)\|_\infty = \sup_w \bar{\sigma}(F_1(P, K)(j\omega)) \quad \text{eqn 5.6}$$

where

$\bar{\sigma}$  is the maximum singular value of the matrix  $F_1(P, K)(j\omega)$

The  $H_\infty$  norm, often labelled  $\gamma$  and the controller which achieves this can be computed using commercially available packages, using a bisection algorithm [56]. It is often

desirable to achieve a slightly sub-optimal controller, due to algorithmic difficulties in calculating  $\gamma$  as it approaches optimality [56].

The most general and widely available algorithms for  $H_2$  and  $H_\infty$  control problems are based on the state-space solutions of Glover and Doyle [57] and Doyle et al [58]. There are many similarities between  $H_2$  and  $H_\infty$  theory, for example both require the solutions to two Riccati equations, they both give controllers of the same state-dimension equal to half of the generalised plant  $P$ , and they both exhibit a separation structure in the controller. For the purpose of this research the solutions to  $H_2$  and  $H_\infty$  Riccati control were solved using commercial software but information on how the Riccati equations can be solved can be found in [56].

The control design architecture pursued in this section was based on a full authority control system. These systems are able to out-perform limited authority systems and are much easier to implement in a control problem allowing controllers to be designed, modified and applied to the system in a shorter time period than limited authority systems, which was the principle reason for pursuing full authority control [59]. As the name suggests, limited authority systems only allow their control signal magnitudes a limited, often small percentage of the actuator's full deflection. This restricts the set of states controllable directly by the control system which could confine the potential benefits of modern control techniques such as  $H$ -infinity. It is worth noting however, that limited authority systems do have several advantages over full authority systems; they are cheaper and easier to install in existing helicopters, they do not need to be built to such high reliability standards and in certain highly non-linear flight regimes such as vortex ring state, it is often difficult to predict how a full authority controller will perform [59].

### 5.6.1 H-infinity Control Design

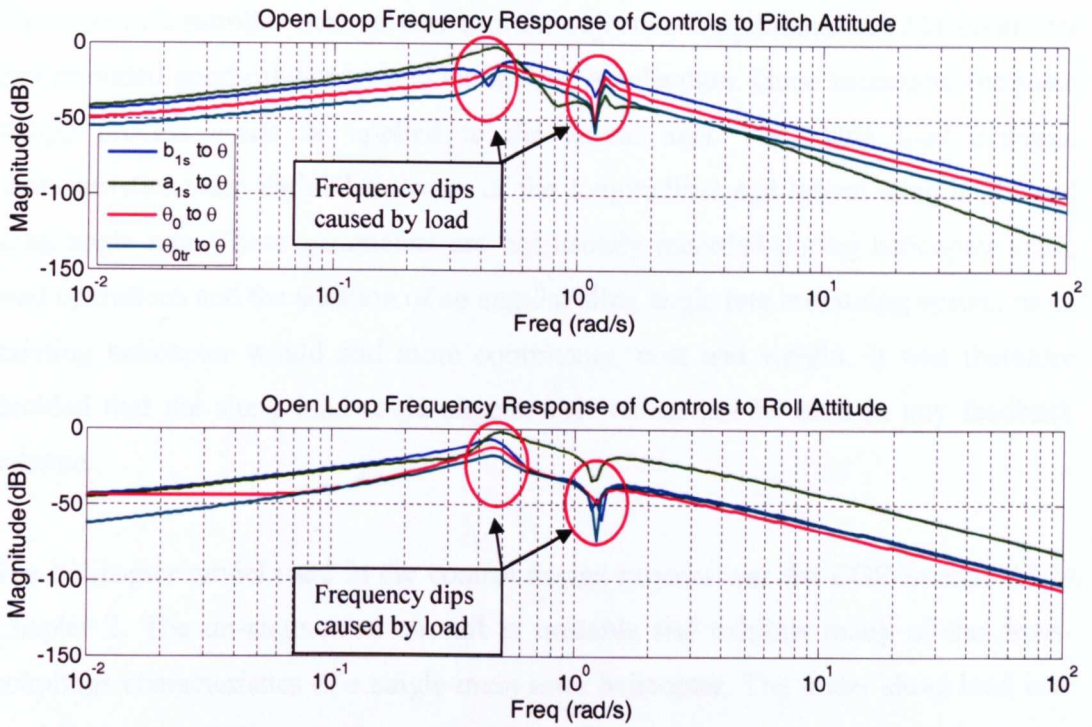
The first step in the design process was to gain an insight into the type of control law structure required. This was achieved by examining the open loop frequency response of the control inputs in terms of cyclic and collective blade angles to the attitude response and sling tether angle rate. Figures 5.17 and 5.18 show the open loop frequency response of the helicopter controls in terms of blade angles to the helicopter pitch and roll attitude and the longitudinal and lateral sling angles. From the figures it is evident that the longitudinal sling angle is affected mainly by longitudinal cyclic as one would imagine but also by collective pitch. This is due to the induced pitching moment caused by the offset between the helicopter centre of gravity and rotor mast. The pitch and roll axes are primarily affected by the longitudinal and lateral cyclic respectively and the lateral sling angle is primarily affected by the lateral cyclic angle. Figure 5.17 show four highlighted regions where there is a magnitude dip corresponding to 0.45rad/s and 1.2rad/s. The first dip corresponds to the phugoid mode of the helicopter coupling with the longitudinal load and has a time period of 14s. To explain the second dip in frequency at 0.25rad/s, the configuration of the helicopter slung load system must be considered. The load model used in the analysis uses a single tether cable to connect the load to the helicopter and can be approximated as single pendulum system. The frequency of such a system can be found using the simple relationship:

$$f = \sqrt{\frac{g}{l}} \quad \text{eqn 5.7}$$

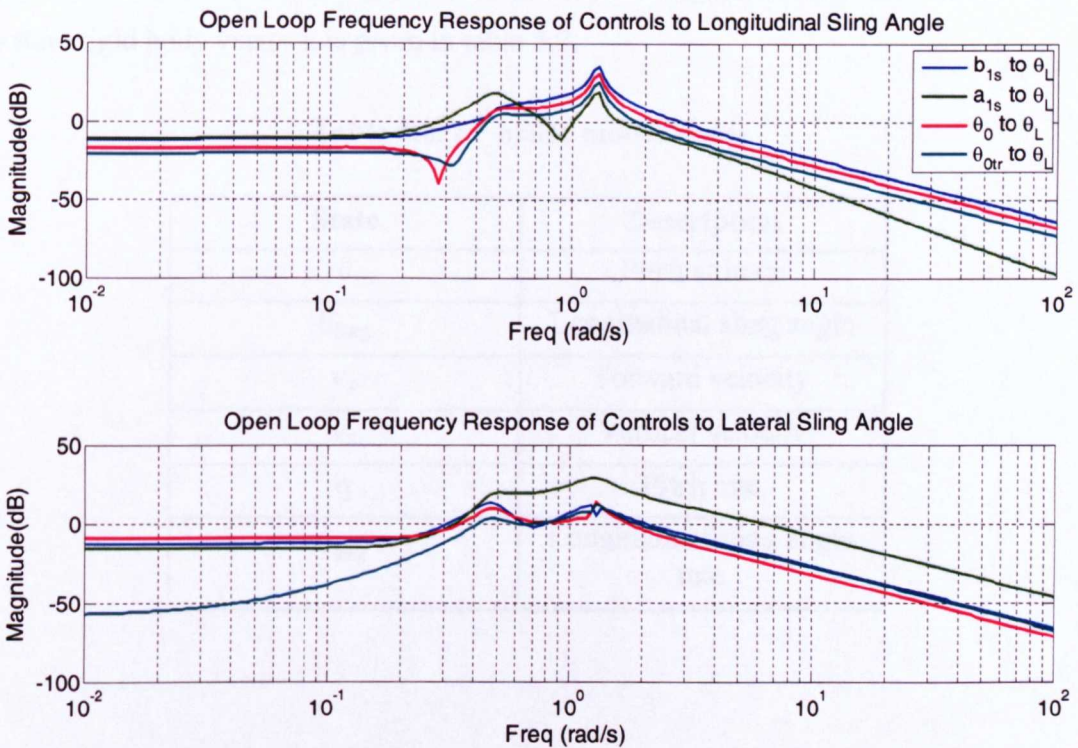
where;

$l$  is the length of the pendulum and  $g$  is the gravitational constant = 9.81m/s<sup>2</sup>.

Substituting the length of the cable used in the model, 8m, the frequency was found to be 1.1rad/s which corresponds to the same frequency as the second dip in magnitude in figure 5.17 indicating helicopter load interaction.



**Figure 5.17: Open loop frequency response of controls to pitch and roll attitudes**



**Figure 5.18: Open loop frequency response of controls to longitudinal and lateral sling angles**

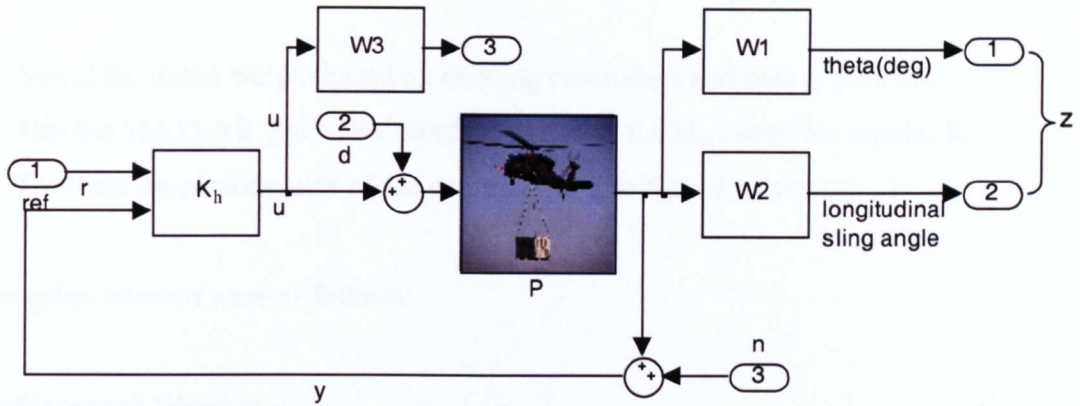
The type of controller desired was a multi-objective longitudinal ACAH controller that provided good robustness and slung load stabilisation. Once successful the same design process could be applied to the lateral axis. The slung load dynamic characteristics were defined in terms of the longitudinal and lateral sling angle and sling angle rate. These parameters are not usually recorded during helicopter slung load operations and the addition of an angular sling angle rate measuring system to an existing helicopter would add more complexity, cost and weight. It was therefore decided that the slung load cable angular rate would not be used in any feedback scheme.

The helicopter model used in the control design process was the FGR introduced in Chapter 2. The un-augmented aircraft is unstable and exhibits many of the cross-couplings characteristics of a single main rotor helicopter. The under slung load was modelled as a 1000kg point mass with a 8m cable and simple drag model. The design condition was based on 40 knots level flight. The starting point was a 6<sup>th</sup> order differential equation modelling the small perturbation rigid motion of the aircraft. The 6 state rigid body vector  $x$  is given in table 5.2.

**Table 5.2: 6<sup>th</sup> order model states**

State	Description
$\theta$	Pitch attitude
$\theta_{\text{long}}$	Longitudinal sling angle
$v_x$	Forward velocity
$v_z$	Vertical velocity
$q$	Pitch rate
$\dot{\theta}_{\text{long}}$	Longitudinal sling angle rate

Figure 5.19 illustrates the control architecture of the longitudinal controller.



**Figure 5.19: Longitudinal control architecture**

where  $r$ ,  $d$ ,  $n$ , in figure 5.19 are the exogenous input vectors,  $z$  are the output vectors to be controlled and  $r$  is the reference, generally a step input in pitch attitude,  $\theta$ . A weighted mixed sensitivity H-infinity optimization was used in the design of the controller that allows a “stacking approach” to specify how the closed loop transfer functions behave [56]. A detailed explanation of the approach with further examples can be found in Postlethwaite [56]. The controller  $K_h$  stabilizes the nominal plant  $G$  and minimises the H-infinity norm of a weighted cost function:

$$K_h = \arg \min \left[ \begin{array}{c} W_1(I + GK)^{-1} \\ W_2(I + GK)^{-1} \\ W_3K(I + GK)^{-1} \end{array} \right]_{\infty}$$

The cost function penalises the tracking error in helicopter pitch attitude and sling angle through the sensitivity weight  $W_1$  and  $W_2$  and control usage through the control weight  $W_3$ .  $W_3$  can also be used to enhance robustness against additive plant error that could for example represent sensor uncertainty.

$W_1$  and  $W_2$  are low pass filters selected to shape the sensitivity function  $(I + GK)^{-1}$  and  $W_3$  is a high pass filter used to shape  $K(I + GK)^{-1}$  and tailor robustness and control activity [56]. The weights were selected to give good attitude tracking

characteristics and to attenuate the load sling angle oscillations. The following iterative design process was adopted to ‘tune’ the weights in the linear domain:

1. Select the initial weight based on existing controllers and past experience.
2. Use the MATLAB algorithm ‘*hinflmi*’ to derive the  $H_\infty$  controller matrix,  $K$ .
3. Evaluate the performance of the controller and re-tune if necessary.

The gains selected were as follows:

### Performance Weights

$$\theta_{\text{error}} : W_{1\theta} = \frac{6.5}{s + 0.05} \quad (\text{W1 in figure 5.19}) \quad \text{eqn 5.8}$$

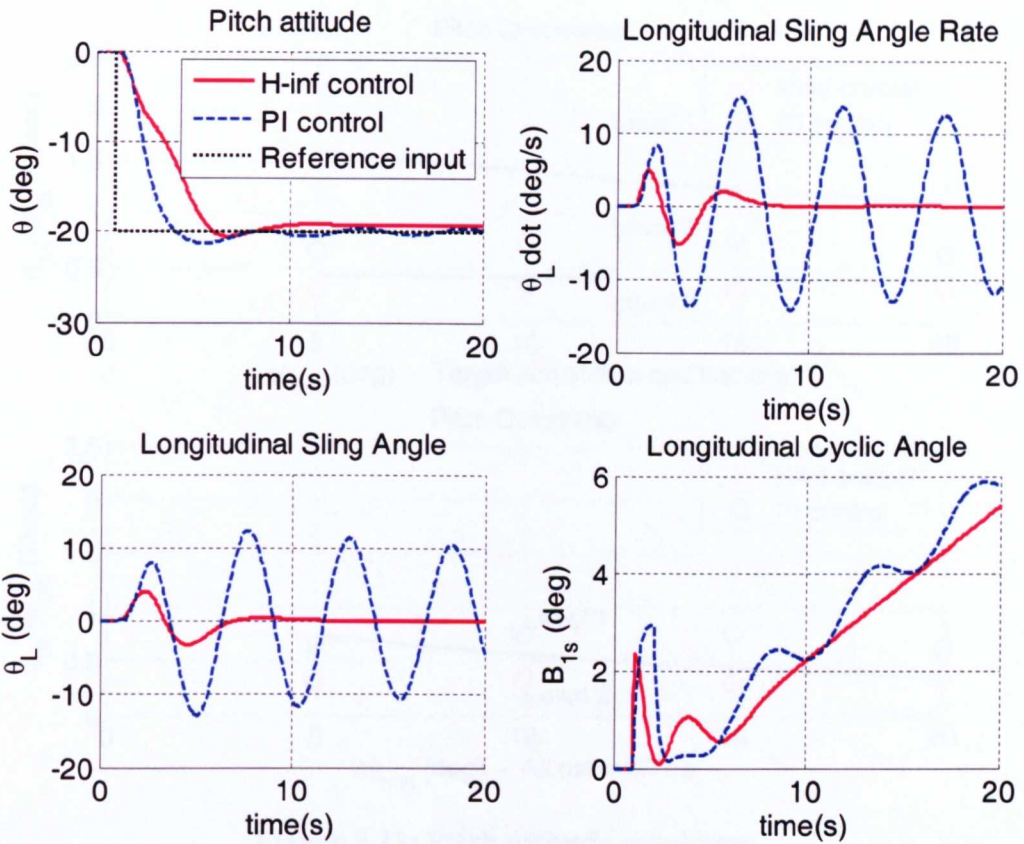
$$\theta_{\text{long}} : W_{2\theta_{\text{long}}} = 12 \quad (\text{W2 in figure 5.19}) \quad \text{eqn 5.9}$$

### Control Weights

$$W_{b1s} = \frac{2s + 0.002}{s + 4} \quad (\text{W3 in figure 5.19}) \quad \text{eqn 5.10}$$

Figure 5.20 shows the pitch attitude, resulting sling angle rate and angle and longitudinal cyclic angle after a pitch attitude step demand at 40kts, 200 ASL. In addition to the  $H_\infty$  controller, the figure also shows the ensuing response from a PI controller that gives a similar pitch attitude response for comparison. The PI controller was designed to give the best ACAH response and no emphasis was placed on load stabilisation. The result is a response that a conventional ACAH control helicopter would achieve. The comparison in figure 5.20 illustrates the advantage in having a multi-objective  $H_\infty$ .

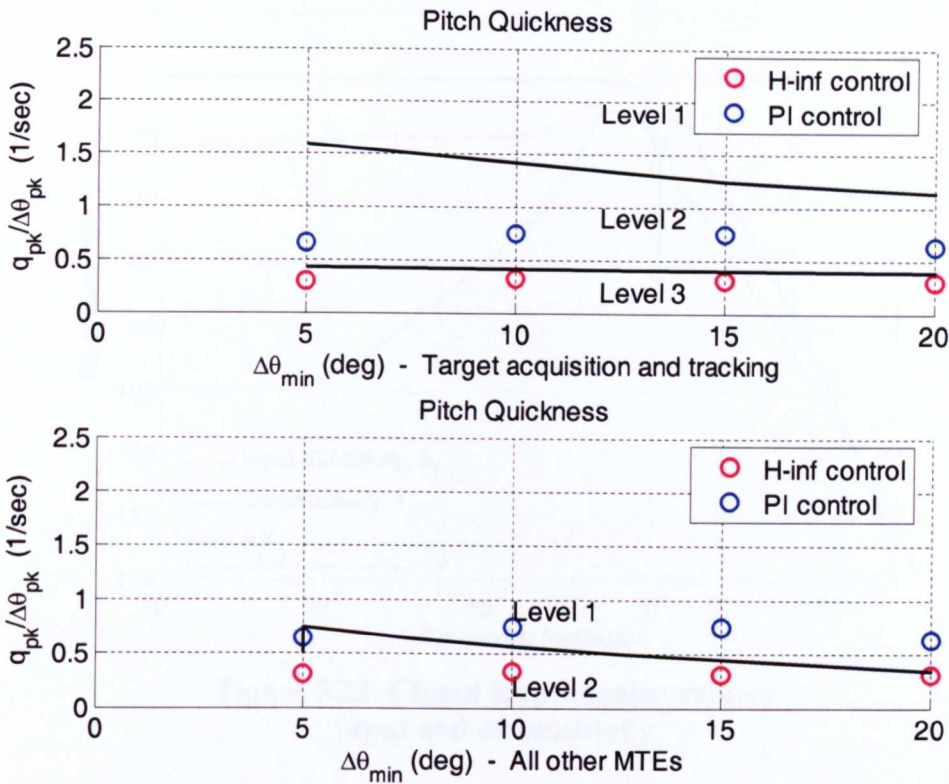




**Figure 5.20: Longitudinal ACAH slung load stabilisation**

From the figure it is evident that the  $H_\infty$  ACAH load stabilisation system was very effective at damping the load oscillations and reduced the initial sling oscillation by 50%. The sling angle is always increasing because the helicopter is trimmed at 40kts and the aerodynamic drag on the load causes the sling cable to trail. The  $H_\infty$  controller also uses less blade angle than the PI controller corresponding to less actuator travel and usage.

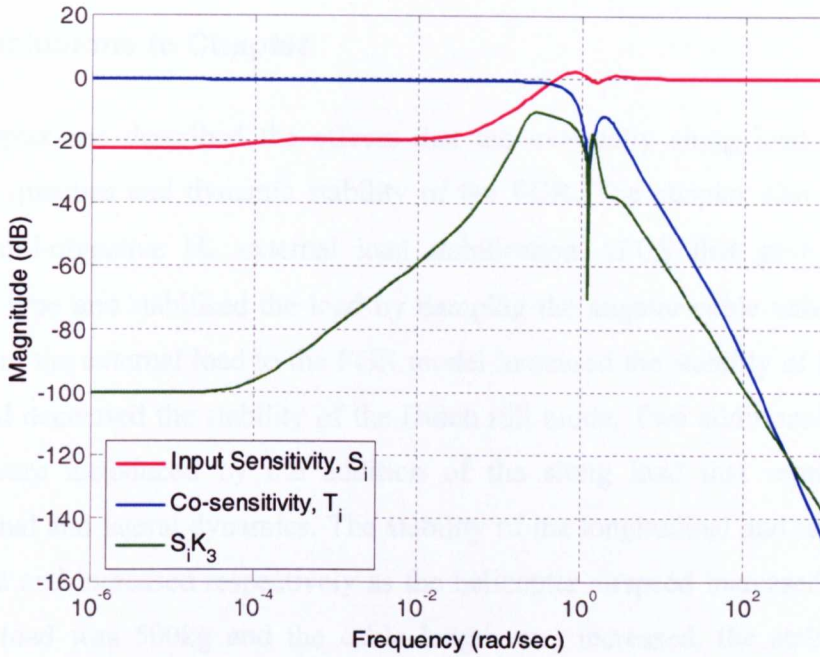
Flight control design often involves a balance between stability and agility and this situation is no exception. By increasing the stabilising of the slung load, the dynamic response of the system has been modified reducing the agility of the helicopter. The ADS-33 attitude quickness criterion was used to examine the reduction in agility. Figure 5.21 shows the attitude quickness for the  $H_\infty$  and PI control system with the ADS-33 target tracking and all other MTE requirements overlaid [2].



**Figure 5.21: Pitch attitude quickness with ADS-33 target tracking and all other MTE requirements overlaid [2]**

### 5.6.2 Controller Robustness

Any AFCS that is to be implemented on a real aircraft must be sufficiently robust as modelling, sensor errors and omissions will inevitably occur [59]. Figure 5.22 shows the closed loop linear system's singular values of input sensitivity function  $S$ , co-sensitivity function,  $T$  and the transfer function between plant outputs and plant inputs  $S_i K_3$  plotted against angular frequency.



**Figure 5.22: Closed loop singular values;  
Input and co-sensitivity**

$S$  is the closed-loop transfer function from the output disturbances to the outputs [59] defined as:

$$S = (I + GK)^{-1}, \quad \text{eqn 5.11}$$

where  $G$  is the plant and  $K$  is the controller gain in figure 5.16.

$T$  is the closed-loop transfer function from the reference signals to the outputs [59]:

$$T = (I + GK)^{-1} GK, \quad \text{eqn 5.12}$$

where  $G$  is the plant and  $K$  is the controller gain in figure 5.16.

The sensitivity function approximately defines the low frequency tracking capability and the bandpass frequency is between 0.4 and 3.5rad/s. The co-sensitivity function,  $T$  and the function  $S_i K_3$  give indications of the system's robustness to input multiplicative and additive uncertainty respectively. Both functions indicate that the controller is robust against uncertainties at high frequencies, where modelling errors are likely to occur [59].

## 5.7 Conclusions to Chapter

This chapter has described the effects that the externally slung load had on the handling qualities and dynamic stability of the FGR. The chapter also described a novel multi-objective  $H_\infty$  external load stabilisation AFCS that gave an ACAH response type and stabilised the load by damping the angular cable tether rate. The addition of the external load to the FGR model increased the stability of the phugoid mode and decreased the stability of the Dutch roll mode. Two additional rigid body modes were introduced by the addition of the slung load that represented the longitudinal and lateral dynamics. The stability of the longitudinal and lateral modes decreased and increased respectively as the helicopter airspeed increased. When the external load was 500kg and the cable length was increased, the stability of the longitudinal load mode decreased and the lateral load mode increased. However when the analysis was repeated with a 1000kg load the stability of the longitudinal mode increased which is contrary to the 500kg load case. This suggests that it is the combination cable length and load mass that contributes to the dynamic stability of the external load modes. Increasing the cable length of the load was found to increase the longitudinal stability. The piloted simulation carried out in the chapter indicated that the pilot felt that the addition of the external load to the system improved the handling qualities at low speed due to a perceived increase in damping in the longitudinal and lateral axes. The pilot also indicated that increasing the cable length increased the pilot workload due to the increased amplitude of the oscillations. Pitch attitude feedback was found to have a negligible effect on the load stability and damping, whilst increasing pitch rate feedback was found to increase the mode damping. The  $H_\infty$  controller effectively stabilised the external slung load and gave a pitch ACAH response type as intended. The extra load stability had a detrimental affect on the agility of the helicopter, almost halving the ADS-33 pitch attitude quickness results.

## Chapter 6

### THE AUTOMATIC CO-OPERATIVE LIFT CONTROL SYSTEM

#### 6.1 Introduction

The economic benefits of co-operative lift have already been discussed in the preceding chapters but the operational, safety and implementation issues have not been addressed until now. Co-operative lift requires close formation flying where the separation distance between the helicopters in the configuration is only twice that of the helicopter rotor diameter, making everyday manoeuvres such as turning, climbing and descending hazardous with extremely high pilot workload. The helicopters operate with an externally slung load supported by a horizontal spreader bar forming a highly coupled system. Add to this the presence of environmental disturbances such as wind gusts or turbulence and the inherent cross-coupling effects and handling qualities deficiencies associated with conventional non-augmented helicopters and safe effective co-operative lift operations become extremely difficult if not impossible to achieve. In addition to the high pilot workload involved, co-operative lift trials in the past that used helicopters with limited control augmentation have indicated that the helicopter flight envelope was reduced to a level far below that of a single helicopter operating alone. In 1971 Sikorsky carried out a co-operative feasibility study using two CH-54 Skycrane helicopters (figure 1.3) and came to the conclusion that co-operative lift was only suitable for low speed load repositioning and taxi type manoeuvres [25]. This chapter describes the automatic co-operative lift control (ACLC) system that was developed to overcome these problems, aiming to increase the safety, flight envelope and operational effectiveness of the co-operative lift configuration. The ACLC was developed using a full authority, active control technology (ACT) philosophy using a digital fly-by-wire AFCS. The main advantage of fly-by-wire is the ability to adapt the system's characteristics at each point in the aircraft's flight envelope through the use of control laws that are scheduled with flight condition.

Digital computing has allowed complex algorithms and modern control techniques such as multi-variable  $H_\infty$  to be implemented effectively taking advantage of active control technology performance benefits including:

- Advanced autopilots that provide a significant reduction in pilot workload
- Reconfiguration to allow mission continuation or safe recovery following battle damage
- Optimised handling qualities across the flight envelope
- Carefree handling, where the AFCS prevents the aircraft exceeding the manoeuvre envelope of the aircraft

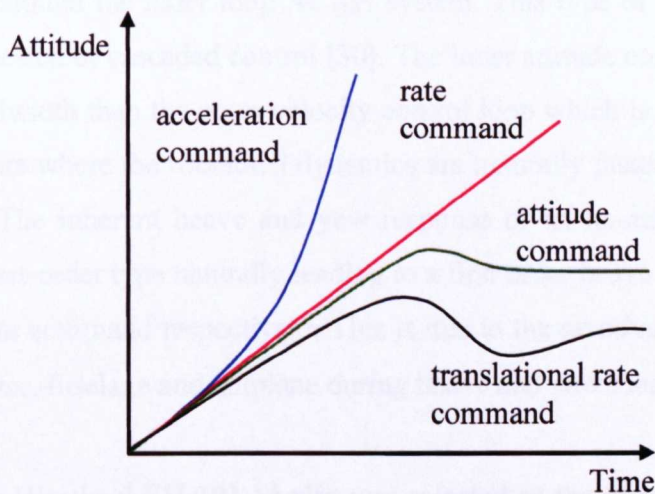
The practical implementation issues including the control system redundancy and integrity and examples of the AFCS hardware required for the ACLC are described later on in this chapter in section 6.8.

The aim of any AFCS is to ensure good handling qualities are attained by artificial means without changing the physical structure or aerodynamics of the vehicle. After all, it is more economically and operationally viable to add or update an AFCS than it is to adapt the physical structure and characteristics of the rotorcraft. A decision was made to design the ACLC described in this chapter using classical control techniques rather than using modern techniques such as the  $H_\infty$  controller described in the previous chapter. The main reason for adopting this approach was to increase the likelihood of the controller meeting CAA airworthiness control system requirements and the controller being implemented and flown on real helicopters in the shortest possible time frame. Modern control laws, including  $H_\infty$  control are less likely to be flight cleared by the CAA in a short time because it is still a relatively new area and there are few examples of  $H_\infty$  controllers that are already implemented on operational aircraft [59].

Classical aircraft control system design is based on the philosophy of successive loop closure. This means that although multiple variables are required to be controlled simultaneously, single-input-single-output (SISO) design techniques such as Bode and Root-Locus can still be used in a sequential design process tackling one axis at a time. In this manner a roll rate controller would be designed by first closing the roll

command loop before designing the pitch controller for the new closed-loop system that includes pitch command system. The loop closure design procedure is described later in Sections 6.3 and 6.4. The performance and handling qualities of the new controller can then be assessed using time and frequency domain analysis and the controller adjusted if required, leading to a highly iterative but effective design process. Non-linear specifications such as limiting of safety critical signals, mode switching, scheduling logic over the flight envelope and actuator models can also be included at this early stage in the design process to increase the accuracy of the handling qualities prediction.

The inclusion of an AFCS means that the response type of the augmented helicopter can be tailored to its specific role. The response-type relates to the character of the response in the first few seconds subsequent to a pilot applied step input. Figure 6.1 shows how the response-type attitude varies for three different types of control system.



**Figure 6.1: Attitude response-type following a step cyclic control input (Adapted from Ref [46])**

The rate command (RC) response is considered to be the simplest practical response type found in conventional helicopters [46]. ADS-33 allows for variations in the response away from the pure rate to include the variety of current helicopters that do not exist in the pre-defined categories but still exhibit satisfactory handling qualities. The basic requirement is that the initial and final cockpit controller force, following

an attitude change, are the same sign. Pilots find that translational response type controllers including ACAH and TRC much easier to fly than RC controllers. With TRC, the attitude loop is automatically closed relieving the pilot of higher gain stabilisation and in addition, the velocity feedback loop is automatically closed, thus reducing the piloting required to perform a steering task. This significantly reduces the pilot workload during high gain tasks, lending it perfectly to co-operative lift operations. There is however one main disadvantage of these translational response type systems; the additional stability is usually achieved with the sacrifice of manoeuvrability and agility [46].

Longitudinal and lateral velocity in helicopters is proportional to the vehicle pitch and roll dynamics. The larger the pitch or roll attitude, the bigger the longitudinal and lateral velocities. To achieve velocity control or TRC, a pitch and roll ACAH system is usually designed first and optimised to give a quick response with good handling qualities. Next, a longitudinal and lateral velocity command system is used to form an outer loop around the inner loop ACAH system. This type of control architecture is known as nested or cascaded control [30]. The inner attitude control loop must have a higher bandwidth than the outer velocity control loop which is not usually a problem in helicopters where the rotational dynamics are naturally faster than the translational dynamics. The inherent heave and yaw response of an un-augmented helicopter is usually a first-order type naturally leading to a first order heave rate command system and yaw rate command respectively. This is due to the aerodynamic damping effects from the rotor, fuselage and tailplane during heave and yaw manoeuvres.

The Agusta Westland EH-101 Merlin was selected as the test harness helicopter for the co-operative lift controller. The primary reason for this was because a Matlab Simulink model of the helicopter was available which would be compatible with previous SimMechanics slung-load and distributed simulation work completed in the project.



## 6.2 The Automatic Co-operative Lift Controller Objectives

The primary objectives of the ACLC were to reduce pilot workload during co-operative lift operations and increase safety by allowing the separation between the helicopters in the formation to be automatically maintained using a separation maintenance control (SMC) system. Separation control in a manual co-operative lift configuration consisting of two traditionally augmented helicopters would be performed by the rear helicopter pilot forming on the lead helicopter by attempting to synchronise the pilot controls and compensating for the under slung load dynamics and external disturbances [27]. Formation flying in good visual conditions is difficult enough and has inherent risks, but add a spreader bar and external load and the task becomes much more difficult with incredibly high pilot workload. To overcome this problem the controller philosophy was centred on the idea of having one pilot in the formation controlling both helicopters with the helicopter separation and flight formation maintained automatically thus reducing the pilot workload significantly, allowing the safe transportation of external loads in the region of 10 tonnes.

The main design characteristics of the co-operative lift system consist of the following:

1. One 'master' pilot controls both aircraft using master-slave, helicopter role assigned control. This eliminates the difficult target tracking and SMC task that would be faced by the rear pilot in the formation. It is important to note that in reality a slave pilot would still be required but only to fulfil the role as safety pilot. This would also reduce pilot fatigue on long missions, as the pilots could swap roles.
2. Both helicopters in the configuration feature a TRC response type controller that decouples the longitudinal and lateral helicopter dynamics, reducing the cross-coupling effects and pilot workload. The incorporation of TRC allows the pilot to easily maintain a target velocity and with the intrinsic possibility of position hold when the stick is centred, allowing the pilot to hover-hold making precision load pick up and drop off of loads easier to perform. This would be especially beneficial in degraded visual environments with the presence of atmospheric

disturbances and during load pick ups when ground crew attach the load to the helicopter whilst the aircraft is hovering close to the ground.

3. The SMC automatically maintains separation in the  $X_e$ ,  $Y_e$ ,  $Z_e$  inertial earth axis. This is the most difficult and dangerous aspect of a non augmented completely manual, co-operative lift operation. Automatic SMC reduces the pilot workload, eliminating pilot error and improves flight safety.

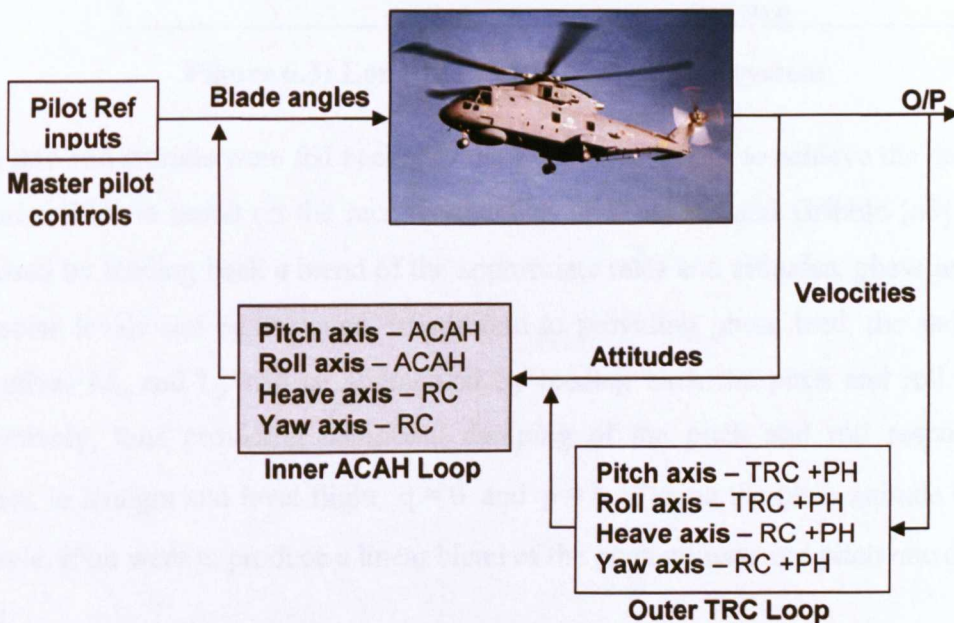
### 6.3 Design Procedure

The iterative design procedure adopted for the development of the ACLC is listed below:

1. A linear model of the EH-101 was obtained for control design and handling qualities analysis in the linear domain.
2. The inner loop consisting of ACAH in the pitch and roll and RC in heave and yaw axes was designed using classical control theory.
3. The inner loop of the AFCS was analysed in the linear domain to predict the helicopter handling qualities using ADS-33 design standard.
4. The inner loop was implemented on the non-linear EH-101 model for non-linear desktop simulation and analysis before piloted assessment in the HELIFLIGHT simulator.
5. With a satisfactory inner loop, the outer control loops were added to the AFCS to achieve TRC control with a cascaded loop structure.
6. Once the master and slave helicopters had desirable TRC controllers, a linear model consisting of two helicopters was developed for single pilot co-operative lift operation.
7. The helicopter  $X_e$ ,  $Y_e$  and  $Z_e$  SMC loops were simulated using desktop simulation before piloted assessment of the system in the HELIFLIGHT simulator using recommended ADS-33 MTEs reported later in Chapter 7.

## 6.4 Control System Architecture

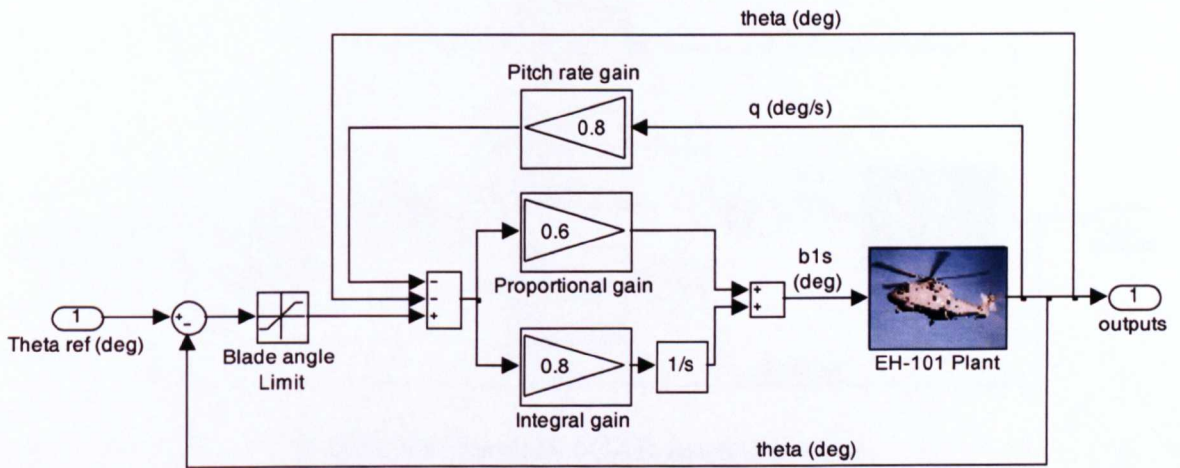
The three axes co-operative lift controller that was developed was applied to both helicopters in the configuration, allowing both helicopters to perform the role of master or slave. The advantage of using a common controller is that the helicopter roles could be swapped in flight. This would be beneficial during a long ferry mission as the pilots could swap roles to reduce pilot fatigue or if one helicopter had better visual cues than the other during a load pick up, then the helicopter roles could be changed to take advantage of this. The slave helicopter control system uses an additional sub-system that maintains separation control and ensures that the heading angle is the same as the master helicopter so that the formation of the flight is also maintained. The ACLC consists of an inner ACAH control loop in pitch and roll with RC in heading and heave axes. An outer inertial earth axis velocity command loop was formed around the inner loop to achieve translational rate command in the longitudinal and lateral axes which in combination with a heading and height-hold (HH) facility gave the helicopter position-hold (PH) functionality. Figure 6.2 shows the cascaded loop structure of the TRC in one of the helicopters in the co-operative lift controller.



**Figure 6.2: Co-operative Lift Cascaded loop control structure**

### 6.4.1 Inner Control Loop Design

The longitudinal ACAH control system structure is illustrated in figure 6.3 with the swashplate actuator dynamics included within the EH-101 plant model. The system consists of a classical proportional-integral (PI) controller with the pilot commanded pitch attitude as the reference signal input. The gains in the PI controller were selected with a combination of root locus (described in Chapter 5) and trial and error techniques. An ACAH system must yield a pitch or roll attitude proportional to the commanded input,  $\theta_{ref}$  or  $\phi_{ref}$  and in addition the system must regulate pitch and roll attitudes to their trim values when there are no commanded inputs.



**Figure 6.3: Longitudinal ACAH control system**

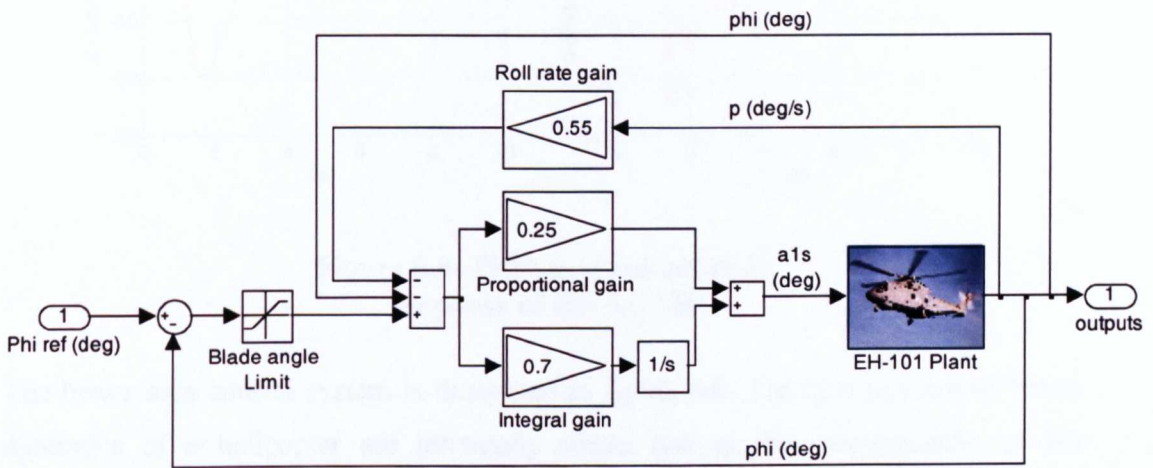
Pitch rate and attitude were fed back into the PI control system to achieve the desired response. This is based on the recommendation of Dudgeon and Gribble [60] who proposed by feeding back a blend of the appropriate rates and attitudes, phase lead at low-noise levels can be achieved. In addition to providing phase lead, the stability derivatives  $M_q$  and  $L_p$  will be augmented by feeding back the pitch and roll rates respectively, thus providing additional damping of the pitch and roll responses. Further, in straight and level flight,  $q \approx \dot{\theta}$  and  $p \approx \dot{\phi}$ . Taking the pitch attitude as an example, if one were to produce a linear blend of the pitch attitude and pitch rate of the form:

$$\theta + kq \approx \theta(1 + ks)$$

*eqn 6.1*

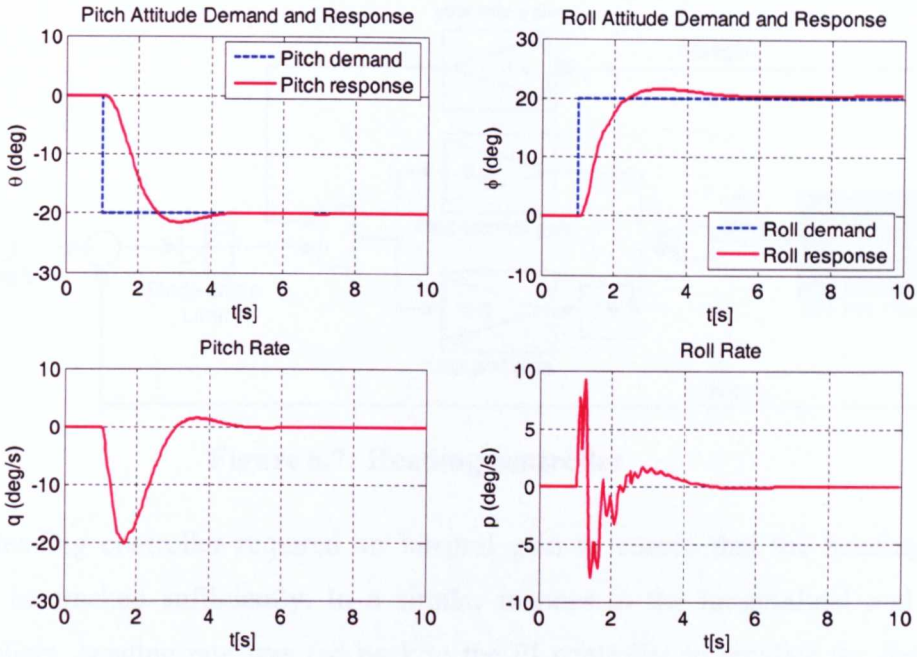
Then it is seen from equation 6.1 that a stable zero has effectively been introduced to the  $\theta$  response at  $k^{-1}$  rad/s [60].

Desktop simulation using linear models indicated that the pitch rate feedback has a similar effect to the derivative term in the PID controller but has the beneficial effect of adding less noise to the system than a conventional derivative gain would [60]. The lateral ACAH controller was developed in a similar manner and is illustrated with the in figure 6.4.



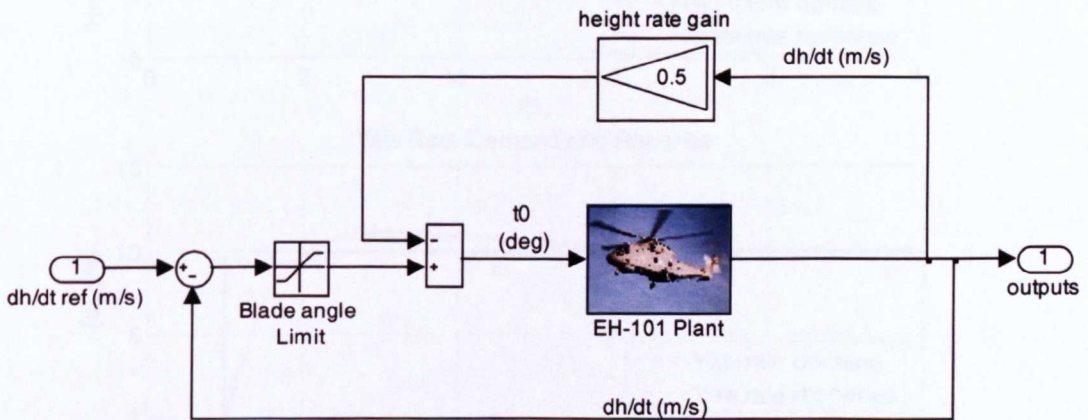
**Figure 6.4: Lateral ACAH control system**

It is more difficult to tune the pitch ACAH system and achieve a desirable pitch response in comparison to the roll ACAH. This is due to the different inertia and flight dynamics characteristics of the pitch axis. For example the horizontal stabiliser creates additional aerodynamic damping during pitching manoeuvres. The lower feedback gains in the roll ACAH (figure 6.4) compared to the pitch ACAH (figure 6.3) illustrates this point. Figure 6.5 shows the longitudinal and lateral step response to a step input. The pitch and roll axes show excellent steady-state tracking with a small overshoot of 5% steady-state.



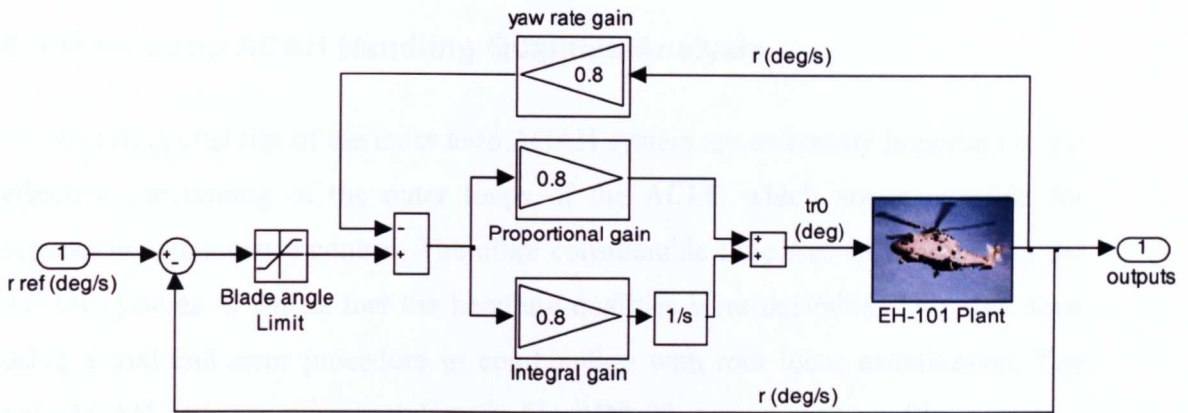
**Figure 6.5: Pitch and roll attitude response of the ACAH**

The heave axis control system is illustrated in figure 6.6. The non-augmented heave dynamics of a helicopter are inherently stable due to the aerodynamics of lift generation producing a first order type response. However, the introduction of further damping through velocity feedback improved the system considerably.



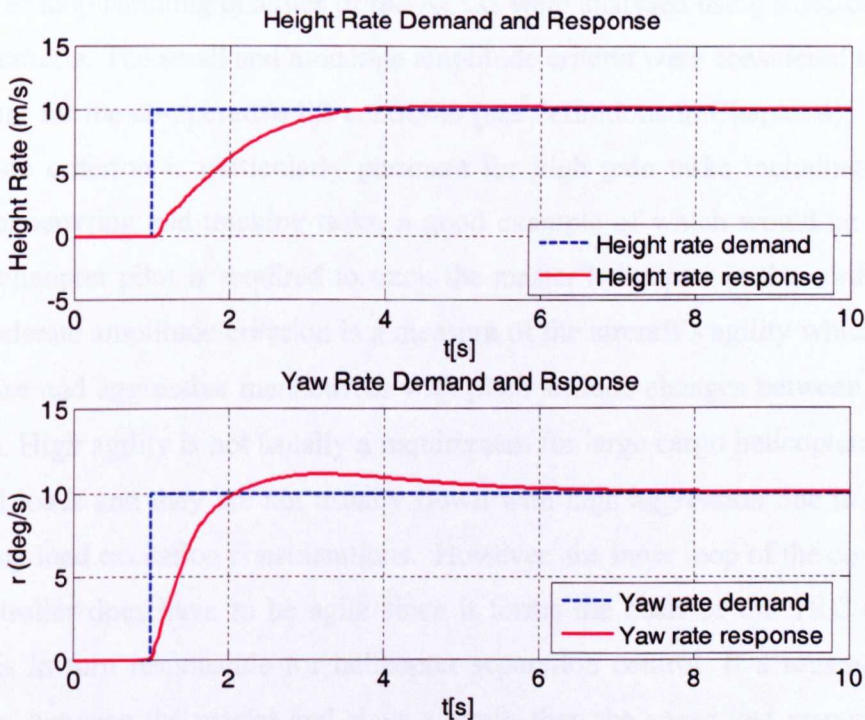
**Figure 6.6: Heave axis controller**

The yaw dynamics are also inherently stable in a similar manner to the heave dynamics but it was still necessary to introduce further damping on the yaw rate to artificially counteract the anti-torque effect of the main rotor. The heading control system is shown in figure 6.7.



**Figure 6.7: Heading controller**

The heading controller required an integral gain to ensure that the heading angle could be tracked sufficiently. In a similar manner to the longitudinal and lateral controllers, heading rate was fed back to the PI controller to emulate the derivative behaviour of a PID controller. Figure 6.8 below shows the inner loop height and yaw rate response to a step input.



**Figure 6.8: Height and yaw rate response to a step input**

## 6.5 Inner Loop ACAH Handling Qualities Analysis

The handling qualities of the inner loop ACAH system are extremely important to the effective functioning of the outer loops of the ACLC which are responsible for separation maintenance control. Therefore considerable time was spent in tuning the ACAH systems to ensure that the handling qualities were desirable. This was done using a trial and error procedure in combination with root locus examination. The only ACAH design requirement described in ADS-33 states that [2, pp. 9];

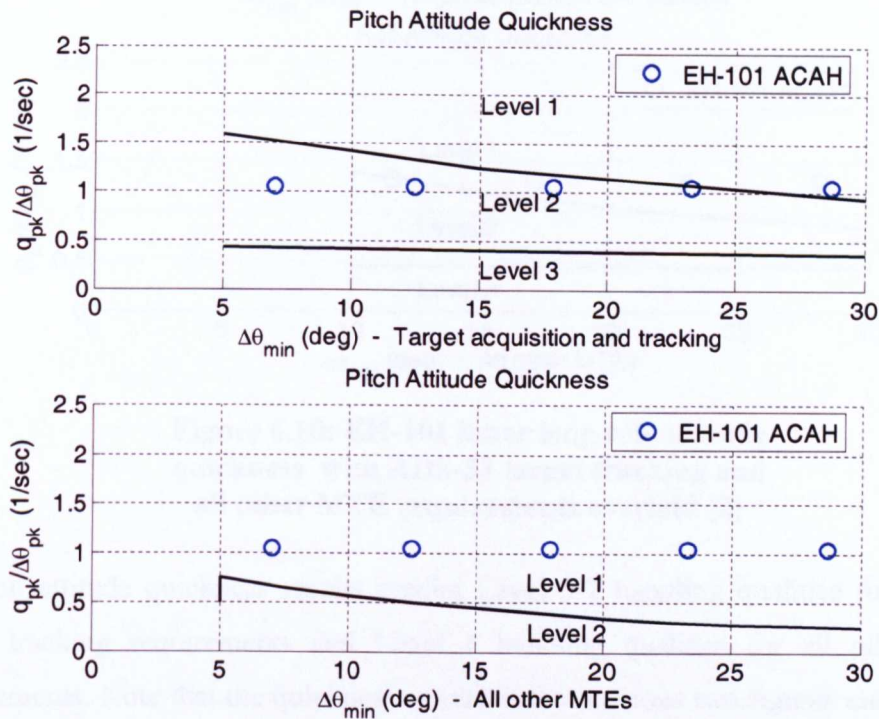
*“... if attitude command is specified as a required response type, a step cockpit controller force input should produce a proportional pitch attitude change within 6 seconds. However, the pitch attitude may vary between 6 and 12 seconds following the step input, if the resulting ground-referenced translational acceleration is constant or its absolute value is asymptotically decreasing towards a constant.”*

The inner loop handling qualities of the ACLC were analysed using selected ADS-33 design criteria. The small and moderate amplitude criteria were considered to be most important for the co-operative lift controller (see definitions in Chapter 4). The small amplitude criterion is particularly pertinent for high gain tasks including confined area manoeuvring and tracking tasks, a good example of which would be when the slave helicopter pilot is required to track the master helicopter in the configuration. The moderate amplitude criterion is a measure of the aircraft's agility which pertains to precise and aggressive manoeuvres with pitch attitude changes between 5 and 30 degrees. High agility is not usually a requirement for large cargo helicopters carrying external loads and they are not usually flown with high aggression due to structural and slung load excitation considerations. However, the inner loop of the co-operative lift controller does have to be agile since it forms the basis of the TRC controller which is in turn responsible for helicopter separation control. If a separation error develops between the master and slave aircraft, then the speed and response of the TRC and hence ACAH inner loop control, are responsible for eliminating this error and maintaining desirable separation tracking.



### 6.5.1 Inner Loop Attitude Quickness Results

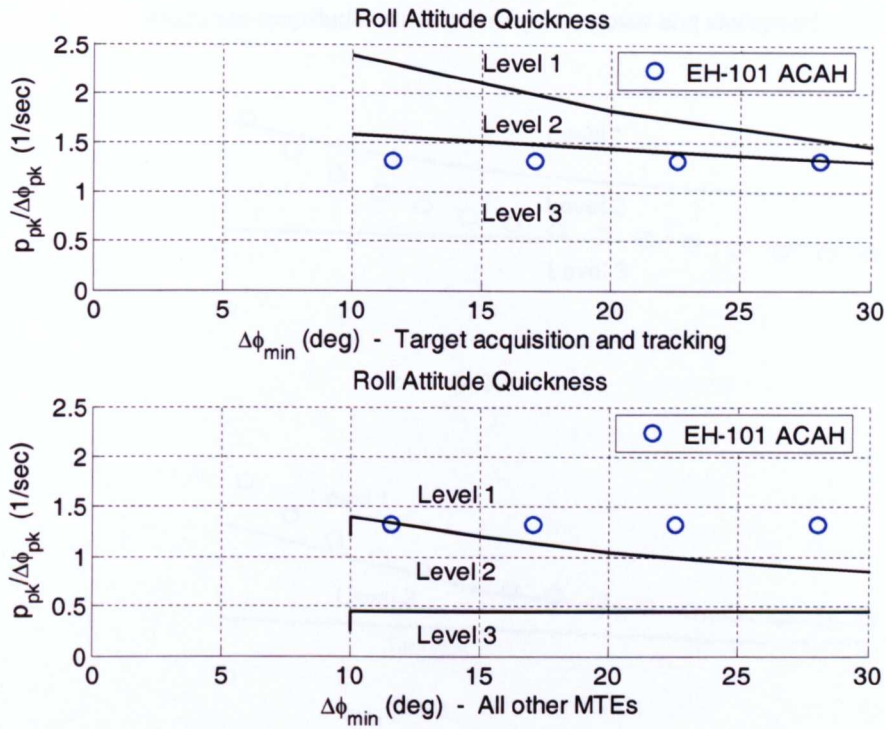
Figure 6.9 shows the pitch attitude quickness plots for the EH-101 ACAH inner loop with the ADS-33 requirements for target tracking and all other MTEs overlaid [2]. The quickness results displayed in the figure correspond to an EH-101 in a hover condition with an AUM 14200kg.



**Figure 6.9: EH-101 inner loop pitch attitude quickness with ADS-33 target tracking and all other MTE requirements overlaid [2]**

The attitude quickness results illustrated in figure 6.9 predict clear Level 2 handling qualities for the target tracking requirements and clear Level 1 handling qualities for all other MTE requirements. These results are consistent with a large transport helicopter operating at maximum AUM.

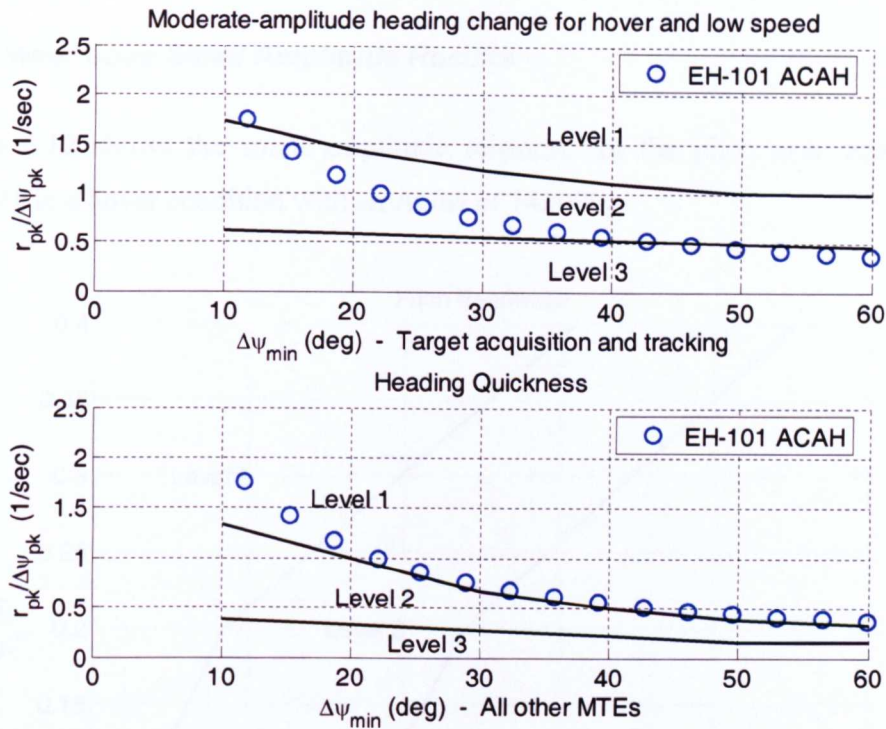
Figure 6.10 shows similar results for the roll attitude quickness plots for the EH-101 inner loop ACAH control system, again with the ADS-33 requirements for target tracking and all other MTEs overlaid.



**Figure 6.10: EH-101 inner loop roll attitude quickness with ADS-33 target tracking and all other MTE requirements overlaid [2]**

The roll attitude quickness results predict Level 3-2 handling qualities for the roll target tracking requirements and Level 1 handling qualities for all other MTE requirements. Note that the quickness results in the previous two figures are very flat in comparison to the previous quickness results calculated in Chapter 4 corresponding to the FGR and F-CH-47B which both had RC systems. This is typical of an ACAH controller where the attitude is determined by the pilot control input and not the rate as in rate command systems.

Figure 6.11 shows the yaw attitude quickness plots for the EH-101 inner loop ACAH with the ADS-33 requirements for target tracking and all other MTEs overlaid.

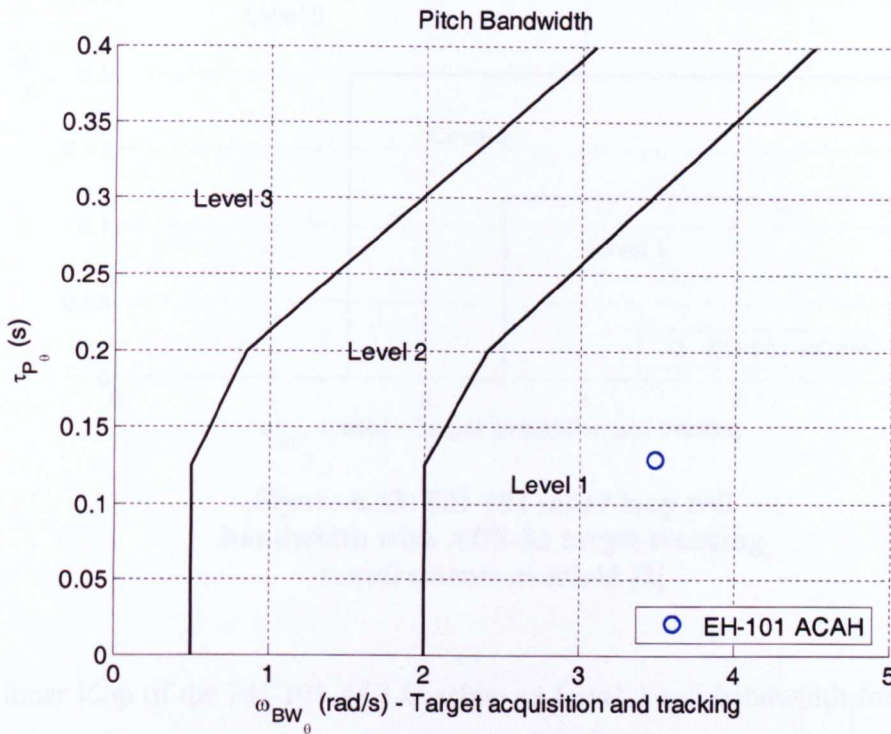


**Figure 6.11: EH-101 inner loop yaw attitude quickness with ADS-33 target tracking and all other MTE requirements overlaid [2]**

The yaw attitude quickness results in figure 6.11 indicate Level 2 handling qualities for small heading changes reducing to Level 2-3 at higher heading angle changes for the target acquisition and tracking requirements. Level 1 handling qualities were achieved when comparing the quickness results to all other MTE requirements.

### 6.5.2 Inner Loop Small Amplitude Results

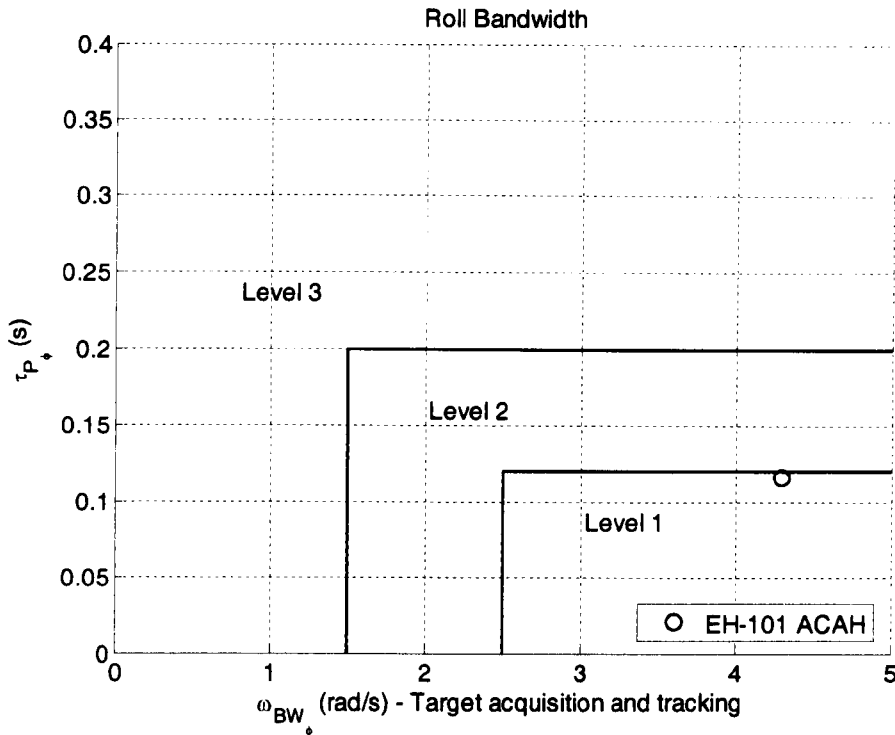
Figure 6.12 shows the small amplitude response for the pitch axis, again for an EH-101 in a hover condition with an AUM of 14200kg.



**Figure 6.12: EH-101 inner loop pitch bandwidth with ADS-33 target tracking requirements overlaid [2]**

The ADS-33 requirements for target acquisition and tracking have been overlaid. The plots indicate that the pitch axis achieved clear Level 1 handling qualities. Note that the more stringent target tracking requirements were used in the small amplitude analysis as the amount of available bandwidth was considered to be very important when considering the separation maintenance role of the controller.

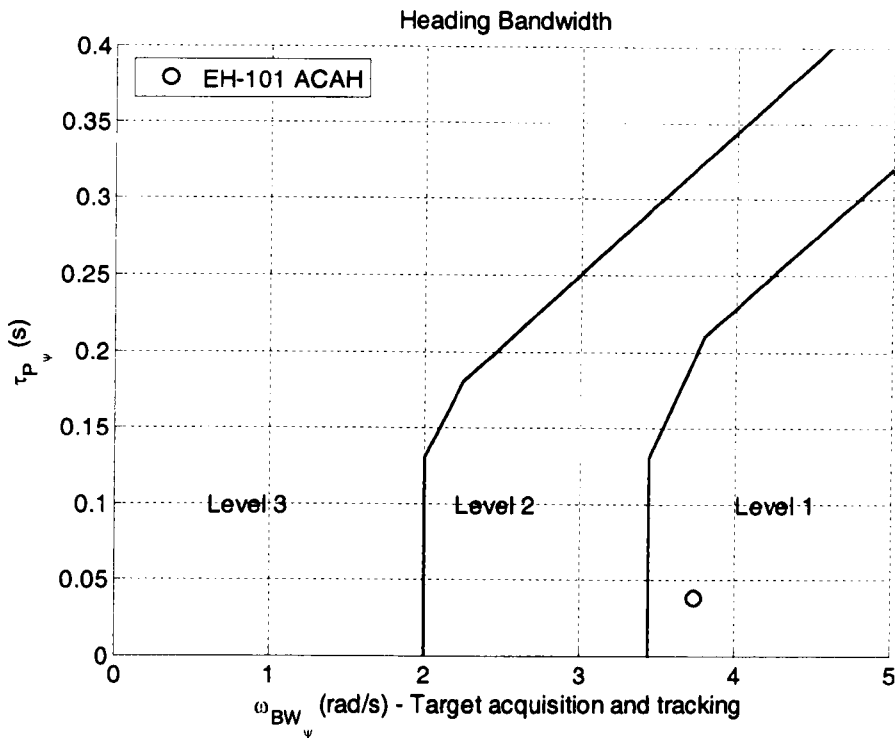
Figure 6.13 shows the small amplitude response for the roll axis, again for an EH-101 in a hover condition with an AUM of 14200kg. The ADS-33 requirements for target acquisition and tracking have been overlaid.



**Figure 6.13: EH-101 inner loop roll bandwidth with ADS-33 target tracking requirements overlaid [2]**

The inner loop of the EH-101 ACLC achieved Level 1 roll bandwidth for the target acquisition and tracking MTE requirements. A good roll bandwidth is important to the lateral separation maintenance function of the controller where the roll angle is proportional to the lateral translational velocity and consequently how quickly a separation error can be eliminated.

Figure 6.14 shows the small amplitude response for the yaw axis, again for an EH-101 in a hover condition with an AUM of 14200kg. The ADS-33 requirements for target acquisition and tracking have been overlaid.



**Figure 6.14: EH-101 inner loop heading bandwidth for target acquisition MTEs [2]**

The inner loop of the EH-101 ACLC achieved Level 1 heading bandwidth with respect to the ADS-33 target acquisition and tracking requirements.

The ACLC inner loop was also assessed against the ADS-33 inter axis requirements to establish the pitch-due-to-roll and roll-due-to-pitch coupling and both indicated Level 1 handling qualities. This is particularly important for a TRC system where a decoupled translational response is required in both the longitudinal and lateral axes to eliminate off-axis translational drift.

### **6.5.3 Stability Analysis of the ACLC Inner Loop and the Industrial Clearance of Flight Control Laws**

The aerospace industry has reached an advanced level of expertise and experience in flight control laws design and the development of flight control laws from concept to validation is a very complex, multidisciplinary task, making it a costly and expensive process [61]. In the past decade, the Group for Aeronautical Research and Technology in Europe (GARTEUR) has established action groups to investigate new and improved analysis techniques of flight control laws. The design process for modern AFCS is a complex, multi-disciplinary activity, which has to be transparent, correct and well documented, in order to allow certification of the aircraft [61]. In industry the design, validation and clearance of the flight control laws (FCLs) is based on a highly iterative process that was followed during the development of the co-operative lift controller. Essentially there are five main phases that can be identified [61]:

- 1. Off-line phase**, using desktop design, analysis and simulation.
- 2. Pilot-in-the-loop test phase**, using manned, real time simulation.
- 3. Iron-bird test phase**, with hardware in the loop.
- 4. Formal clearance phase** of the control laws.
- 5. Flight test phase.**

Thorough analysis of the results in phases 1 until 3 can be used to demonstrate that the full certification criteria are fulfilled. Enhanced identification of the weak areas of the controller in phase 1, can lead to less required analysis in phases 2 and 3, reducing the overall costs of the clearance process, particularly since the costs of analysis increase exponentially each phase [61].

The analysis criteria used in the industrial clearance process can be divided into four discrete classes [61]:

1. Linear stability criteria
2. Aircraft handling/PIO criteria
3. Nonlinear stability criteria
4. Nonlinear response criteria

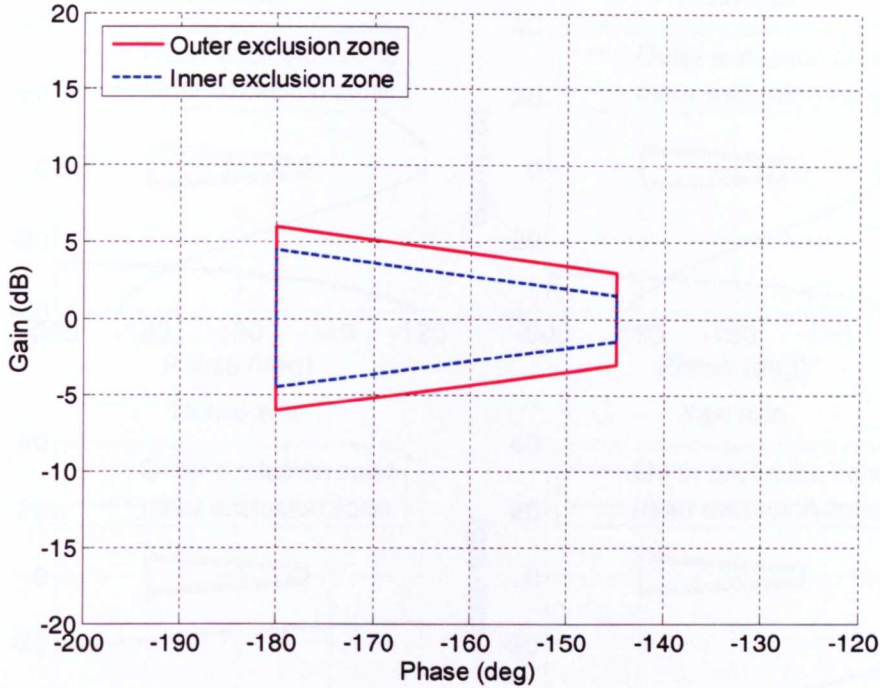
A complete clearance of the ACLC inner loop using all industrial criteria was not feasible during the research due to the limited time and resources available. It was therefore decided to use a small representative set of criteria to analyse a limited number of flight conditions for the assessment of the ACLC. The following two stability criteria were selected to achieve this [61]:

1. Stability margin criterion (class 1)
2. Unstable eigenvalue criterion (class 1)

#### **6.5.4 Stability Margin Criterion**

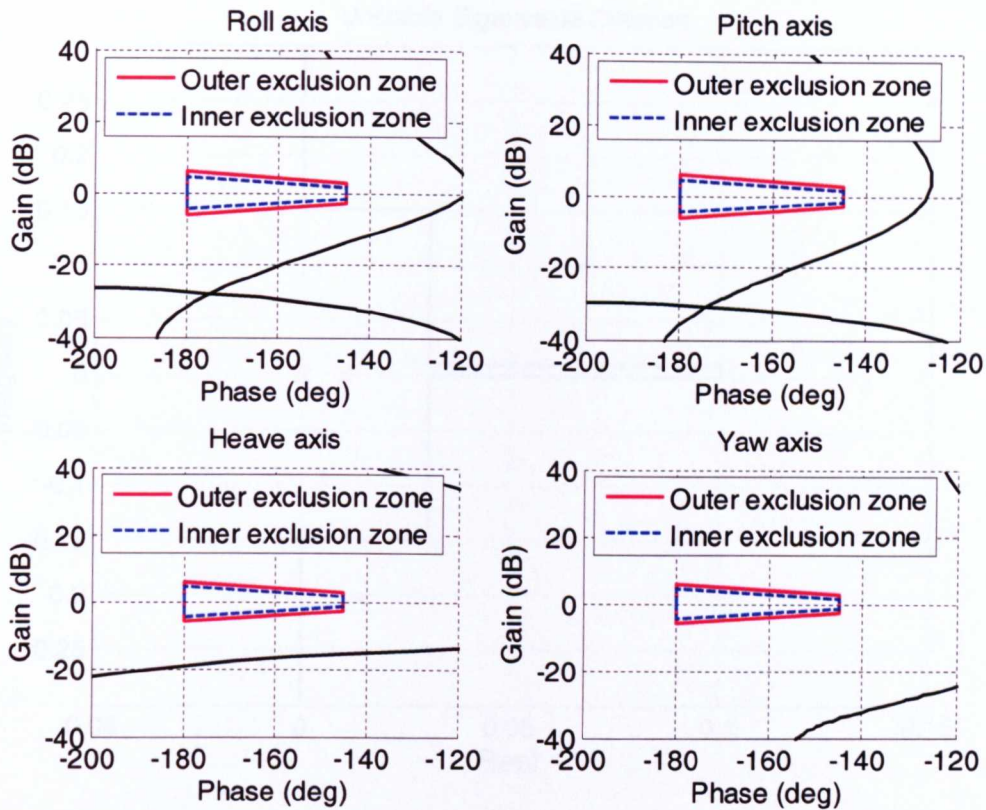
The stability margin criterion is used to prove that the aircraft is stable over the entire flight envelope with sufficient margin against instability for all known uncertainties (worst-case combinations). The linear stability margins for the open-loop frequency response in pitch, roll and yaw were calculated by breaking the loop at the input of each actuator and then plotting the results in Nichols diagrams [61], where the permitted phase and gain margins were shown as exclusion regions which must not be violated by the plot. In single loop analysis the open-loop frequency response is obtained by breaking the loop at the input of each actuator or sensor, one at a time, while leaving the other loops closed [62]. In the nominal case the Nichols plot should not violate the outer exclusion region which is represented by the red solid line in figure 6.15 corresponding to a minimum gain margin of  $\pm 6$  dB and a minimum phase margin  $\pm 35$  degrees. However when uncertainties are taken into account a boundary corresponding to  $\pm 4.5$  dB is used, as indicated by the blue dashed line in figure 6.15.





**Figure 6.15: Nichols stability margin boundaries [62]**

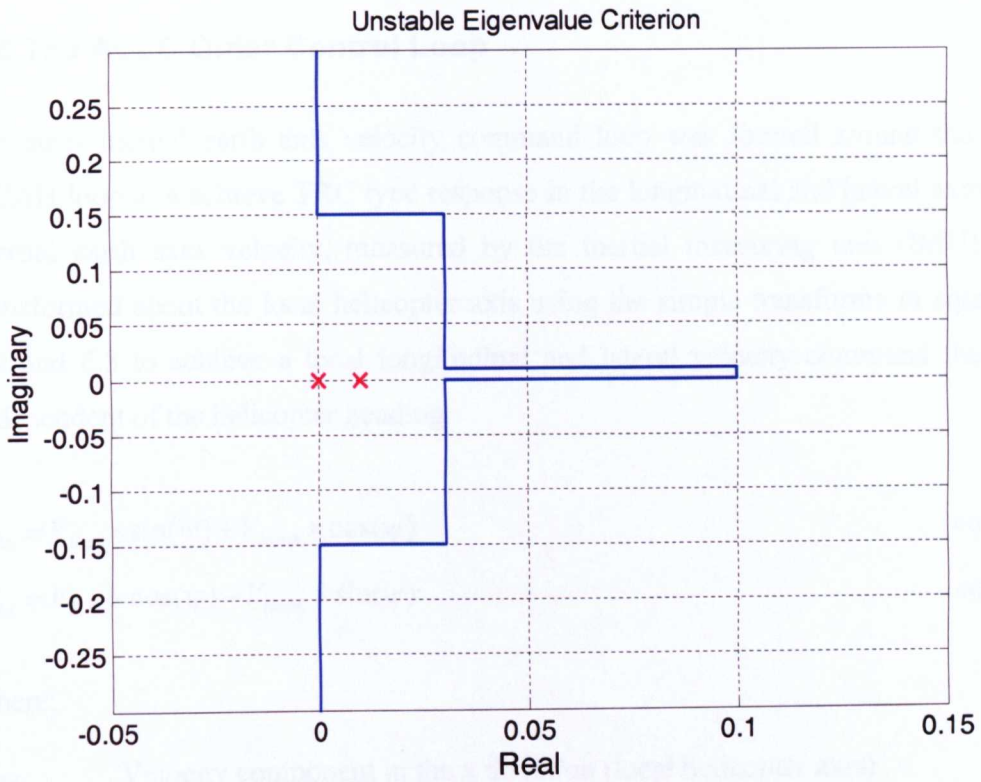
The criterion is passed if the frequency response locus does not pass the exclusion region. The boundaries are not sacrosanct and are not derived from theoretical calculations but are instead based on practical experience. Small violations of the boundary do not necessarily have to lead to flight restrictions if further investigations show that it is not required. Figure 6.16 shows the Nichols stability margin boundaries and frequency response loci for the pitch, roll, yaw and heave axes of the inner loop control system. All inner loop actuators and sensor models were included in the assessment. From the figure it is clear that there are no violations of the exclusion zones indicating that the inner loop is stable in all four flight axes.



**Figure 6.16: Nichols stability margin boundaries for ACLC inner loop for each flight axis**

### 6.5.5 Unstable Eigenvalue Criterion

The criterion is used to assess the worst cases of divergent modes (unstable eigenvalues). The worst case is defined as the largest positive eigenvalue. Not all eigenvalues in the right hand s-plane are considered as a filing criterion and unstable motion with a long time constant is allowed if the eigenvalues remain on the left side of the limiting boundary shown in figure 6.17 [62]. Figure 6.17 illustrates that no eigenvalues are outside the limiting value indicating that the ACLC inner control loop is stable according to the unstable eigenvalue criterion.



**Figure 6.17: Unstable eigenvalue criterion for the ACLC inner loop [62]**

## 6.6 The ACLC Outer Control Loop

An outer inertial earth axis velocity command loop was formed around the inner ACAH loop to achieve TRC type response in the longitudinal and lateral axes. The inertial earth axes velocity, measured by the inertial measuring unit (IMU), was transformed about the local helicopter axis using the simple transforms in equations 6.2 and 6.3 to achieve a local longitudinal and lateral velocity command that was independent of the helicopter heading.

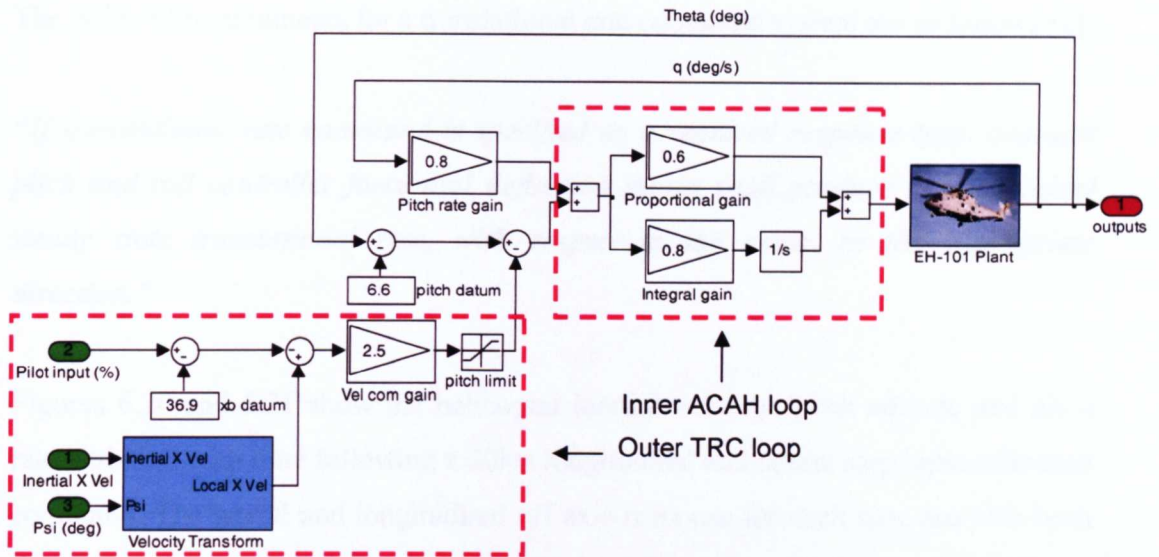
$$V_{lhx} = V_{East} \times \sin(\psi) + V_{North} \times \cos(\psi) \quad \text{eqn 6.2}$$

$$V_{lhy} = V_{East} \times \cos(\psi) - V_{North} \times \sin(\psi) \quad \text{eqn 6.3}$$

where;

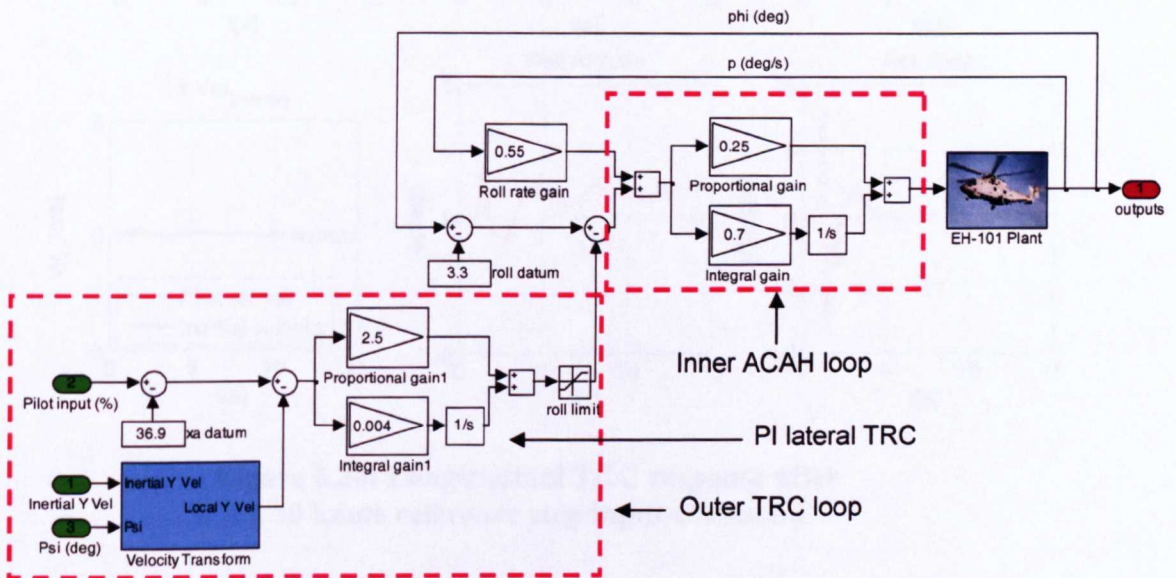
$V_{lhx}$	Velocity component in the x direction (local helicopter axis)
$V_{lhy}$	Velocity component in the y direction (local helicopter axis)
$V_{East}$	Velocity component in the East direction (inertial earth axis)
$V_{North}$	Velocity component in the North direction (inertial earth axis)
$\psi$	Heading angle

The longitudinal and lateral outer loop control architecture for the TRC system is illustrated in figures 6.18 and 6.19. The outer velocity command loop consists of a proportional gain in the longitudinal controller and a combination of proportional and integral gain in the lateral controller which was required to achieve good lateral tracking at speeds above 40kts. Pitch and roll attitude saturation limits were inserted to prevent the controller from demanding a helicopter attitude that was greater than 30 degrees which would be considered over aggressive during slung load operations. The pitch attitude limit was selected with the 5,000kg payload in mind and the nature of slung load operations where large inputs and pitch attitudes are not desired due to load excitation and structural load constraints. To ensure control harmonisation, a 30 degree attitude limit was also applied to the lateral TRC system. The velocity transform subsystem illustrated in figures 6.18 and 6.19 transforms the measured inertial velocity in an earth axis frame about rotorcraft axis to obtain a local helicopter axis longitudinal and lateral velocity command.



**Figure 6.18 Longitudinal controller with cascaded inner ACAH and outer TRC loops**

The pitch and roll datum constants represent the trim attitudes of the model and the xb and xa datum constants the trim stick positions for example 36.9% xb in hover. The gains in figures 6.18 and 6.19 were tuned using a trial and error technique.

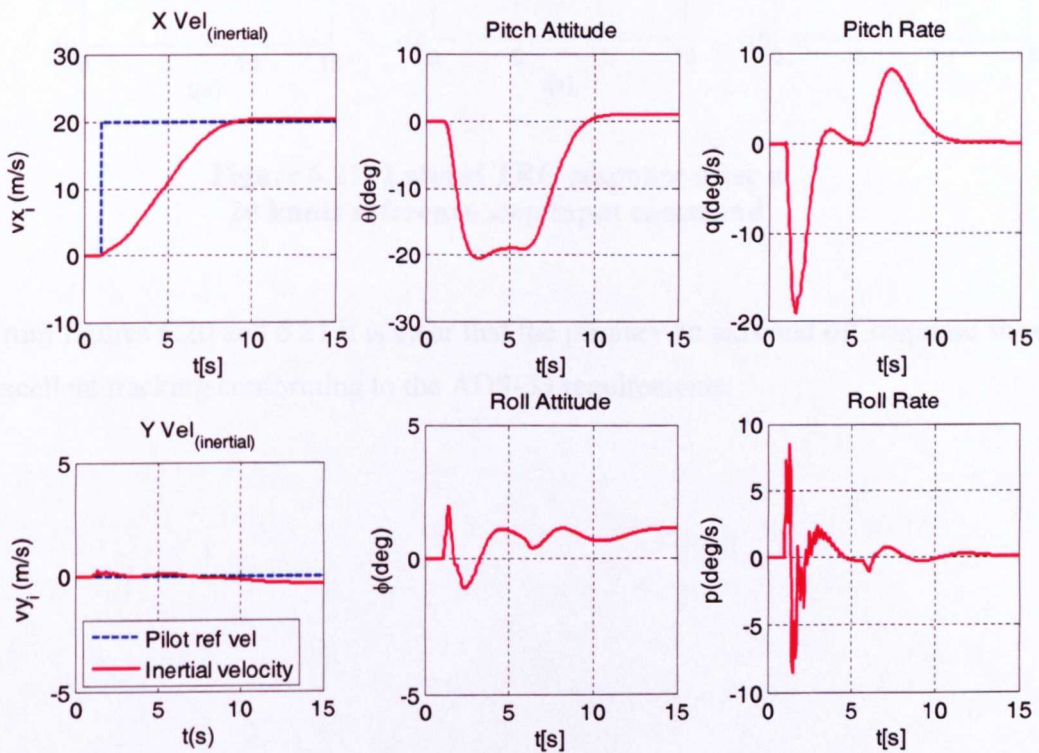


**Figure 6.19 Lateral controller with cascaded inner ACAH and outer TRC loops**

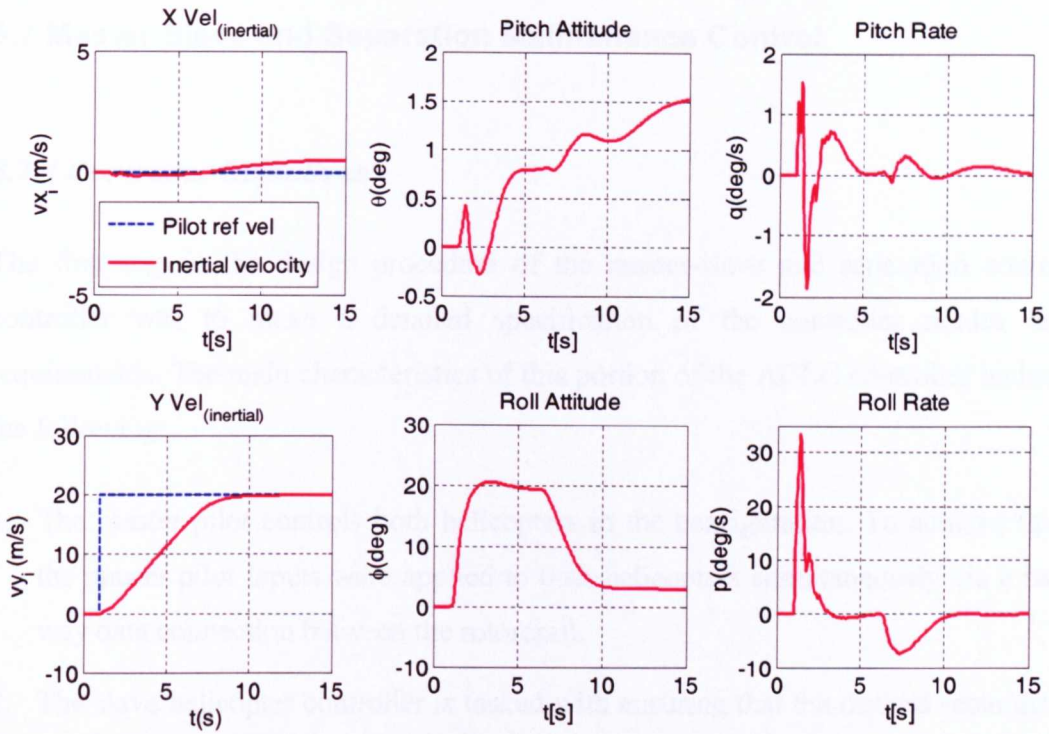
The ADS-33 requirements for a translational rate command system are as follows [2]:

***“If translational rate command is specified as a required response type, constant pitch and roll controller force and deflection inputs shall produce a proportional steady state translational rate, with respect to the earth, in the appropriate direction.”***

Figures 6.20 and 6.21 show the helicopter inertial velocity, pitch attitude and pitch rate variation with time following a 20kts longitudinal and lateral step input reference command. The lateral and longitudinal off axis response for each case has also been plotted to illustrate how the system has effectively been decoupled using the TRC.



**Figure 6.20: Longitudinal TRC response after a 20 knots reference step input command**



**Figure 6.21: Lateral TRC response after a 20 knots reference step input command**

From figures 6.20 and 6.21 it is clear that the primary on axis and off response shows excellent tracking conforming to the ADS-33 requirements.

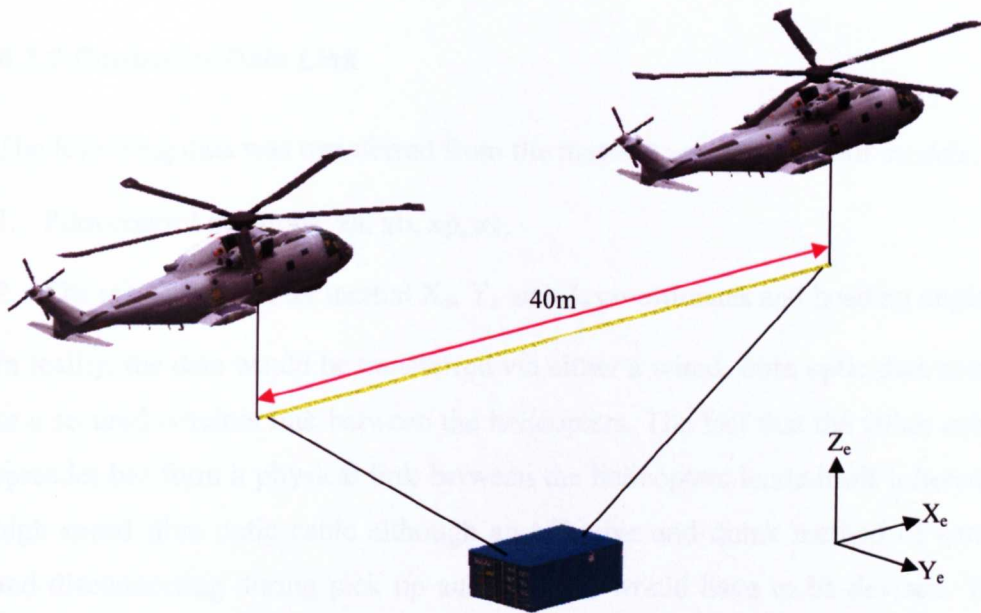
## **6.7 Master-Slave and Separation Maintenance Control**

### **6.7.1 Controller Objectives**

The first step in the design procedure of the master-slave and separation control controller was to make a detailed specification of the controller modes and requirements. The main characteristics of this portion of the ACLC controller include the following:

1. The master pilot controls both helicopters in the configuration. To achieve this, the master pilot inputs were applied to both helicopters simultaneously via a two way data connection between the rotorcraft.
2. The slave helicopter controller is tasked with ensuring that the desired separation in inertial  $X_e$ ,  $Y_e$  and  $Z_e$  planes between the slave and master helicopter CG is maintained at all times during manoeuvring. This was achieved by calculating the point in inertial space relative to the master helicopter where the slave helicopter should operate, the so called desired separation point (DSP). A feedback loop with DSP reference co-ordinates and the slave helicopter's actual co-ordinates was formed to achieve this.
3. The initial configuration was designed so that the master and slave helicopters were in-line with each other in a tandem configuration as shown in figure 6.22, with the  $X_e$  separation equal 40m and  $Y_e$  and  $Z_e$  equal to 0m.





**Figure 6.22: Tandem configuration**

The formation adopted with the Master helicopter operating at the rear was based on the assumption that it would be much more beneficial for the pilot to fly the aft helicopter in the formation in order to keep the slave helicopter in view at all times. If the control system failed or the helicopter separation distance became too small, the system could be disengaged, load jettisoned and evasive manoeuvres carried out.

4. The helicopters were also required to maintain the formation displayed in figure 6.22 during heading changes. This was achieved using a transform in the controller that transformed the position error about the local helicopter heading angle.
5. The incorporation of TRC allowed the pilot to easily maintain a target velocity and the inherent position hold functionality, allowed the pilot to hover-hold and make precision pick up and drop off of loads easier to carry out. This is especially beneficial in degraded visual environments with the presence of atmospheric disturbances such as turbulence or gusts.

### **6.7.2 Controller Data Link**

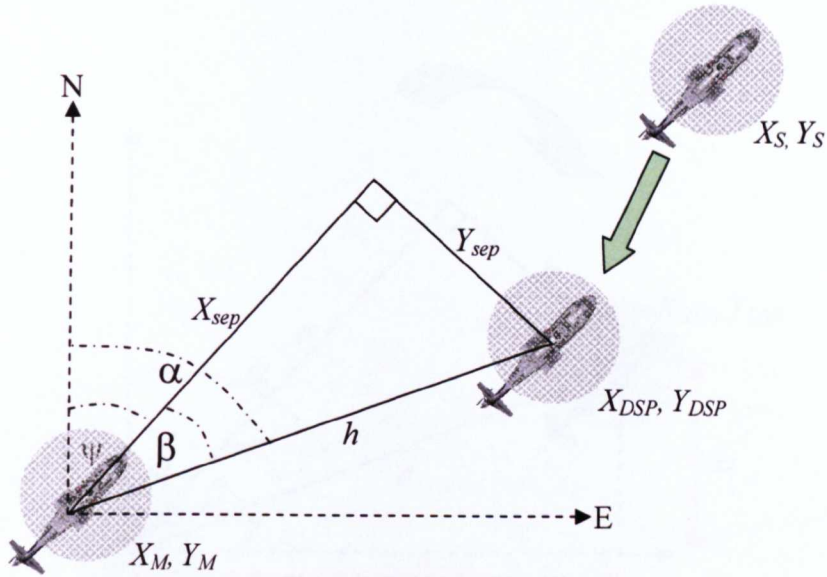
The following data was transferred from the master to slave rotorcraft models:

1. Pilot control positions,  $x_a$ ,  $x_b$ ,  $x_p$ ,  $x_c$ .
2. The master helicopter inertial  $X_e$ ,  $Y_e$  and  $Z_e$  co-ordinates and heading angle.

In reality, the data would be transferred via either a wired, fibre optic data connection or a secured wireless link between the helicopters. The fact that the tether cables and spreader bar form a physical link between the helicopters lends itself inherently to a high speed fibre optic cable although an effective and quick method of connecting and disconnecting during pick up and drop off would have to be devised. Wireless links remove the physical infrastructure that are required but do not usually have the same high speed data transfer and are not as easy to shield against interference or an electromagnetic pulse which would be an important military requirement.

### **6.7.3 The Desired Separation Point**

The desired separation point (DSP) represents the point in space that the slave helicopter must occupy in order to maintain the correct separation relative to the master helicopter. This point is continuously calculated and updated by the slave helicopter control system using position and heading data from the master helicopter. The error between the DSP and the slave helicopter's actual co-ordinates was then used to form a feedback control system that maintained the desired separation at all times. The desired separation point was calculated using the transformation shown in figure 6.23.



**Figure 6.23: DSP calculation (earth axis)**

where;

$$\alpha = \beta + \psi \quad \text{eqn 6.4}$$

$$h = \sqrt{X_{sep}^2 + Y_{sep}^2} \quad \text{eqn 6.5}$$

$$X_{DSP} = h \times \sin(\alpha) + X_M \quad \text{eqn 6.6}$$

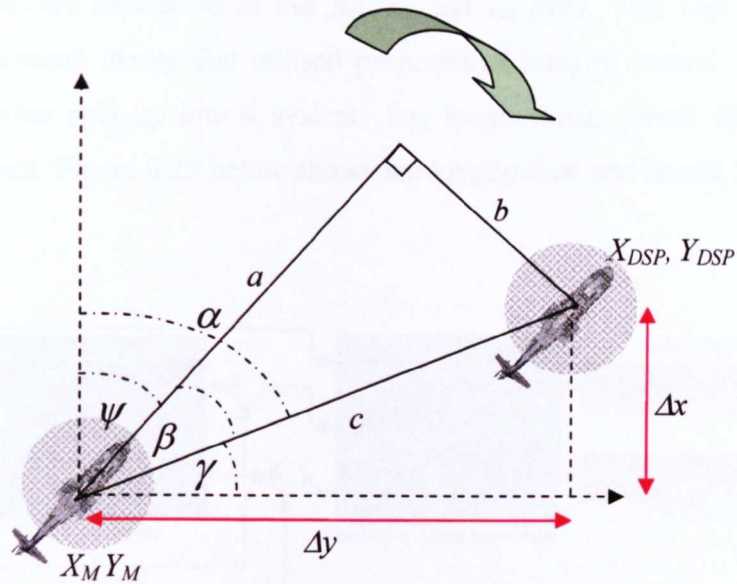
$$Y_{DSP} = h \times \cos(\alpha) + Y_M \quad \text{eqn 6.7}$$

$X_{sep}$  and  $Y_{sep}$  are the desired longitudinal and lateral separation distances (earth axis)

$X_S$  and  $Y_S$  are the x and y positions of the slave helicopter (earth axis)

$X_M$  and  $Y_M$  are the x and y positions of the master helicopter (earth axis)

The co-ordinates of the DSP were then transformed about the heading angle into local helicopter axes using the transformations illustrated in figure 6.24. The transformation was to ensure that a longitudinal or lateral stick displacement gave a longitudinal or lateral translation relative to the helicopter axis system independent of the helicopter heading angle.



**Figure 6.24: DSP earth to local helicopter axis transformation**

where;

$a$  = longitudinal separation (m)

$b$  = lateral separation (m)

$c$  = the distance between the master helicopter and the desired point  $X_{DSP}, Y_{DSP}$  (spreader bar length).

$$a = \tan^{-1} \left( \frac{\Delta y}{\Delta x} \right) \quad \text{eqn 6.8}$$

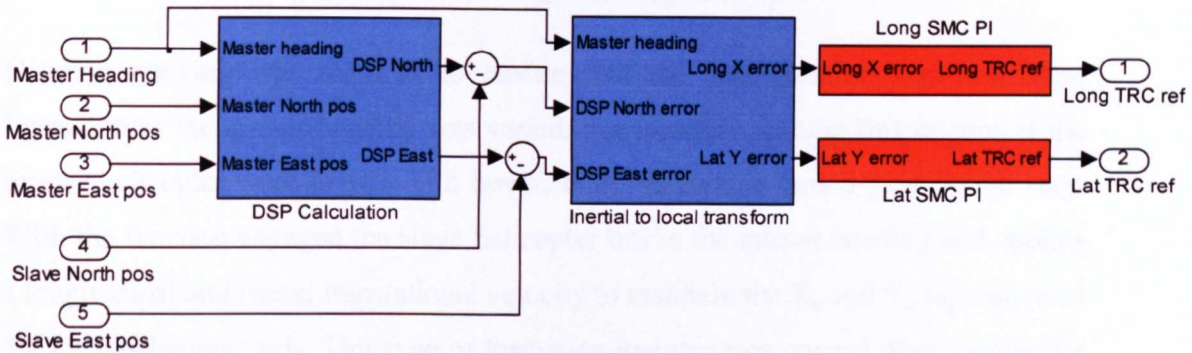
$$a = c \times \cos(\beta) \quad \text{eqn 6.9}$$

$$b = c \times \sin(\beta) \quad \text{eqn 6.10}$$

$$c = \frac{\Delta x}{\sin(\gamma)} \quad \text{eqn 6.11}$$

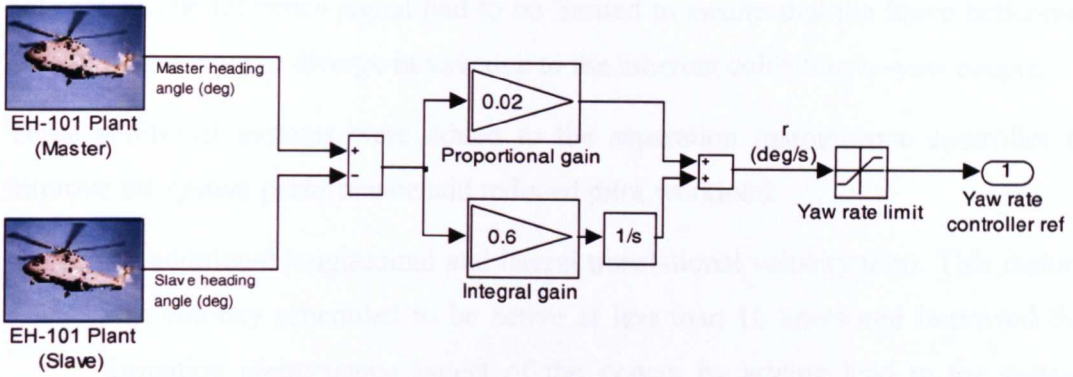
### 6.7.4 Separation Maintenance Control

The separation maintenance sub-controller of the ACLC was responsible for maintaining the desired separation in the  $X_e$ ,  $Y_e$  and  $Z_e$  axes. This was achieved through classical control theory that utilised proportional integral control. The sub-controller was further split up into 4 systems for; longitudinal, lateral, height and heading maintenance. Figure 6.25 below shows the longitudinal and lateral SMC sub systems.



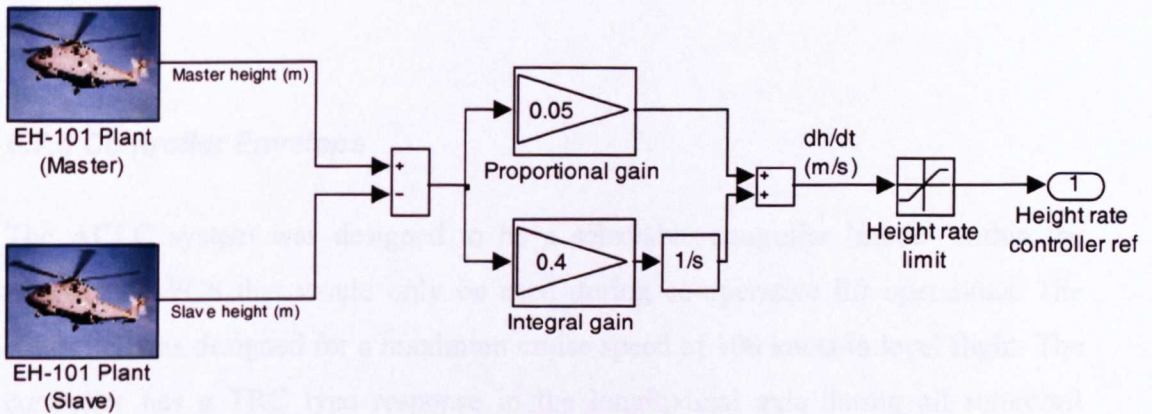
**Figure 6.25: Longitudinal and lateral separation control systems**

The inputs into the system were the master and slave helicopters' positions in an inertial earth axes co-ordinate system and the master helicopter's heading angle. The DSP subsystem calculated the position where the slave helicopter should be in inertial earth axes relevant to the master helicopter based on the longitudinal and lateral separation specified for the particular mission (figure 6.22). The separation distance between the helicopters could be changed in real-time if the helicopter formation needed to be changed. The DSP is then compared with the slave helicopter's actual position and the resulting error signal is converted from inertial earth axis to a local helicopter axis co-ordinate system using the master helicopter's heading angle (figure 6.24). Proportional integral control is then used in both the longitudinal and lateral axes to form the separation maintenance controller and the resulting reference signal drives the TRC system earlier in Section 6.6. The heading and height tracking functions were also controlled using classical proportional integral control. Figure 6.26 shows the heading tracking sub-controller.



**Figure 6.26: Heading tracking controller**

Heading tracking was required to ensure that the configuration kept the same formation as the master heading was varied. For example without this feature, if the master helicopter were to yaw in a hover, both helicopters would yaw on the spot. With the function engaged the slave helicopter tracks the master heading and applies a longitudinal and lateral translational velocity to maintain the  $X_e$  and  $Y_e$  separation in the local helicopter axis. This type of formation maintenance control does require the master helicopter's yaw rate to be limited using a saturation limit. Without this limit imposed and if the master helicopter yaw rate was very high, the slave would be unable to translate quickly enough longitudinally and laterally to keep the formation constant. Figure 6.27 shows the height tracking portion of the controller.



**Figure 6.27: Height tracking controller**

The height tracking controller monitored the height of the Master and Slave helicopter in the formation and used proportional and integral control to form a height rate reference signal which was fed into the height rate controller of the slave

helicopter. The reference signal had to be limited to ensure that the Slave helicopter did not over-torque or diverge in yaw due to the inherent collective-to-yaw couple.

Three additional systems were added to the separation maintenance controller to improve the system performance and reduced pilot workload:

1. An additional longitudinal and lateral translational velocity term. This feature was velocity scheduled to be active at less than 10 knots and improved the formation maintenance aspect of the system by adding lead to the system during low speed yaw manoeuvres. For example the following lateral lead reference demand was added to the lateral TRC where  $V_{lat\_lead}$  is the additional lateral translational velocity demand added,  $y_{sep}$  is the desired y separation and  $k_{lat\_lead}$  is a gain scheduled proportional gain:

$$V_{lat\_lead} = (\dot{\psi} \times y_{sep}) k_{lat\_lead}$$

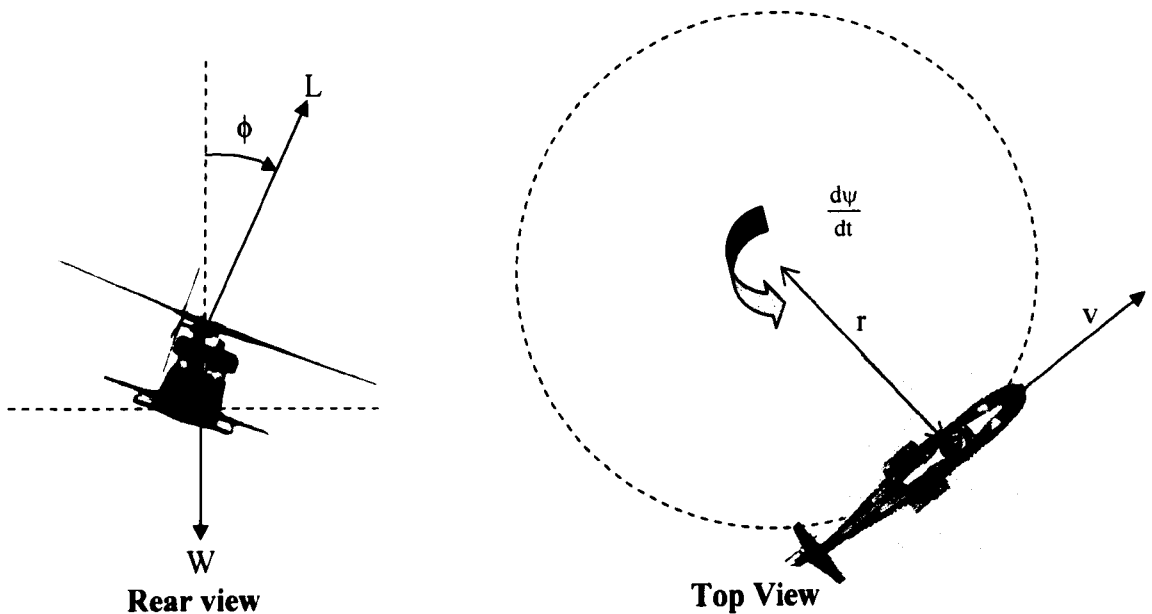
2. A height hold system toggled by a cockpit switch that maintained the helicopters height.
3. A heading hold system toggled by a cockpit switch that maintained the helicopters heading angle.

The system described in (1) above was included to improve the tracking performance of the controller, whereas points (2) and (3) were added later to reduce pilot workload.

### **6.7.5 Controller Envelope**

The ACLC system was designed to be a selectable controller ‘mode’ within the helicopter AFCS that would only be used during co-operative lift operations. The controller was designed for a maximum cruise speed of 100 knots in level flight. The controller has a TRC type response in the longitudinal axis during all rotorcraft speeds which is unusual for a helicopter control system. ADS-33 provides guidelines that the TRC response type should be used only for ground speeds up to 20kts and that the velocity per stick displacement should be relatively low. Conventional AFCS only use TRC at low speeds, typically less than 9kts [63], however it hypothesised that TRC would be the best type of response type for a co-operative configuration, since with the flight axes decoupled into  $X_e$ ,  $Y_e$  and  $Z_e$  axes, separation maintenance

control would be easier to implement and safer to operate. Only 'flat turns' can be carried out using TRC; these are carried out by the pilot applying pedal input to steer the rotorcraft with zero bank angle. This would not be practical or efficient at high speeds and an alternative method of lateral/heading control had to be established. With this in mind the lateral TRC was blended with an attitude command/turn-coordination system at speeds above 30kts. At high speed pilots of conventional helicopters fly co-ordinated turns by applying a small pedal input in addition to lateral stick to command an additional yaw rate in order to perform zero side slip turns. In the ACLC angular rate reference signals required to fly co-ordinated turns were provided by the turn co-ordination system. Figure 6.28 below shows simplified free body diagrams used to derive the turn-coordinator control law.



**Figure 6.28: Turn co-ordination derivation**

After resolving the vertical and horizontal force components in figure 6.28, the following equations were obtained:

Vertical forces:

$$L \cos \phi = W \quad \text{eqn 6.12}$$

Horizontal forces (horizontal component of lift force = centrifugal force)

$$L \sin \phi = \frac{mV^2}{R} \quad \text{eqn 6.13}$$



Substituting the helicopter weight and airspeed equations into equations 6.10 and 6.11 the following modified equilibrium equations can be obtained:

$$W = mg \quad \text{eqn 6.14}$$

$$V = \frac{d\psi}{dt} R \quad \text{eqn 6.15}$$

Equations 6.13, 6.14 and 6.15 were then combined to form the following equation for the rate of change of heading angle:

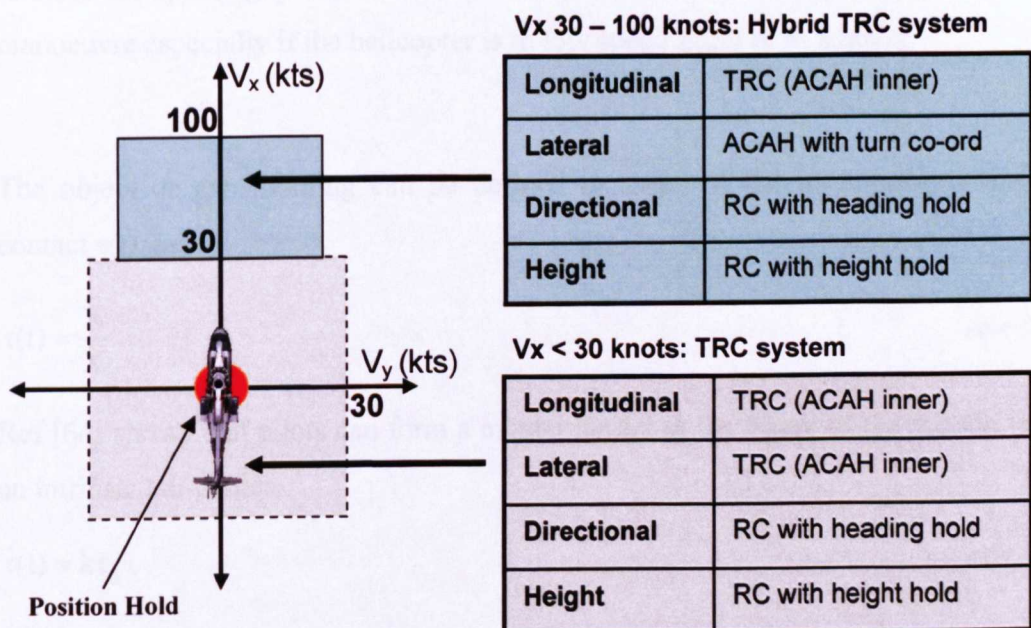
$$\frac{d\psi}{dt} = \frac{g}{v} \tan \phi \quad \text{eqn 6.16}$$

Equation 6.16 can be transformed into the following equation by assuming the pitch and roll attitude are constant during a level turn:

$$r = \frac{g}{v} \sin \phi \cos \theta \quad \text{eqn 6.17}$$

$$q = \frac{g}{v} \sin \phi \tan \phi \cos \theta \quad \text{eqn 6.18}$$

Equations 6.17 and 6.18 were applied to the turn-coordination system to generate a yaw and pitch rate command that were summed with the pilot inputs. Figure 6.29 below summarises the response type variation of the ACLC with speed:



**Figure 6.29: Controller envelope summary**

### 6.7.6 Tau Based Gap Closure System

The separation maintenance control system described in the previous section maintains the separation distance between the helicopters by eliminating the error signal between the desired separation point and the helicopter's current position. This section describes a more sophisticated experimental system of maintaining separation that was developed using an optical guidance theory called tau theory. Lee [3] suggested that an animal's ability to determine the time to close on an object does not depend on knowledge concerning the size of the object, the closing speed or distance. Instead he proposed that the 'looming' of the object, or the ratio of its size to the rate of growth of its image on the retina, is actually the fundamental optical variable used in nature. An example of this occurs in nature when a bird approaches and lands on the branch of a tree or in the case of a pilot, during an acceleration and deceleration manoeuvre when the pilot initialises the deceleration to hover. Tau theory has been applied to helicopter guidance at The University of Liverpool with considerable work carried out using tau principles to investigate how far pilots need to look ahead [64] and [65], how pilots perform the landing flare [66] and how pilots apply spatial judgement during the landing on a ship [67]. The latter two examples are broadly similar to the co-operative lift separation maintenance problem where the rear pilot has to close a spatial gap to maintain the desired separation. The manoeuvre required to close the spatial gap can be considered to be a mini acceleration and deceleration manoeuvre especially if the helicopter is in low speed flight or in a hover.

The object or gap looming can be defined in terms of the instantaneous time to contact  $\tau(t)$ , as:

$$\tau(t) = \frac{X}{\dot{X}} \quad \text{eqn 6.19}$$

Ref [64] shows that pilots can form a mental model of the future of the motion using an intrinsic tau-guide:

$$\tau(t) = k\tau_g \quad \text{eqn 6.20}$$

where  $k$  is a constant.

Examples of possible motion guides are the constant deceleration, velocity and acceleration guides:

$$1. \text{ Constant velocity, } \tau_g = t - T, (\dot{\tau}_g = 1) \quad \text{eqn 6.21}$$

$$2. \text{ Constant deceleration, } \tau_g = \frac{1}{2}(t - T), (\dot{\tau}_g = 0.5) \quad \text{eqn 6.22}$$

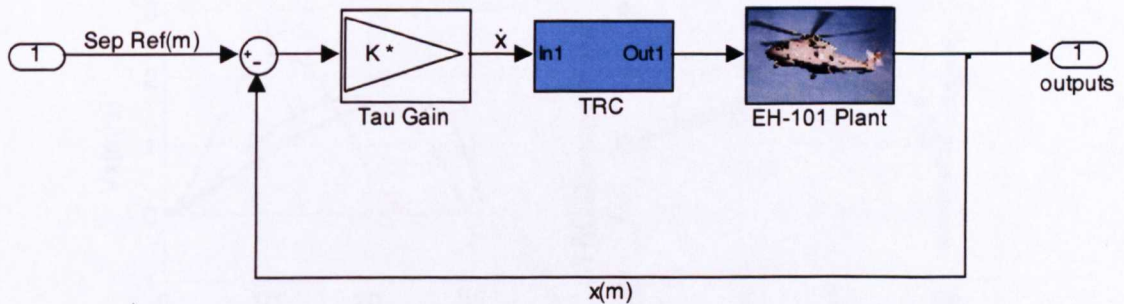
$$3. \text{ Constant acceleration, } \tau_g = \frac{1}{2}\left(t - \frac{T^2}{t}\right), \dot{\tau}_g = \frac{1}{2}\left(1 + \left(\frac{T^2}{t}\right)\right) \quad \text{eqn 6.23}$$

where  $T$  in the equations above is the total duration time of the manoeuvre.

Using equations 6.19, 6.20 and 6.23, the following equation can be obtained for  $\dot{x}$  (figure 6.30):

$$\dot{x} = \frac{2x}{k\left(t - \frac{T^2}{t}\right)} \quad \text{eqn 6.24}$$

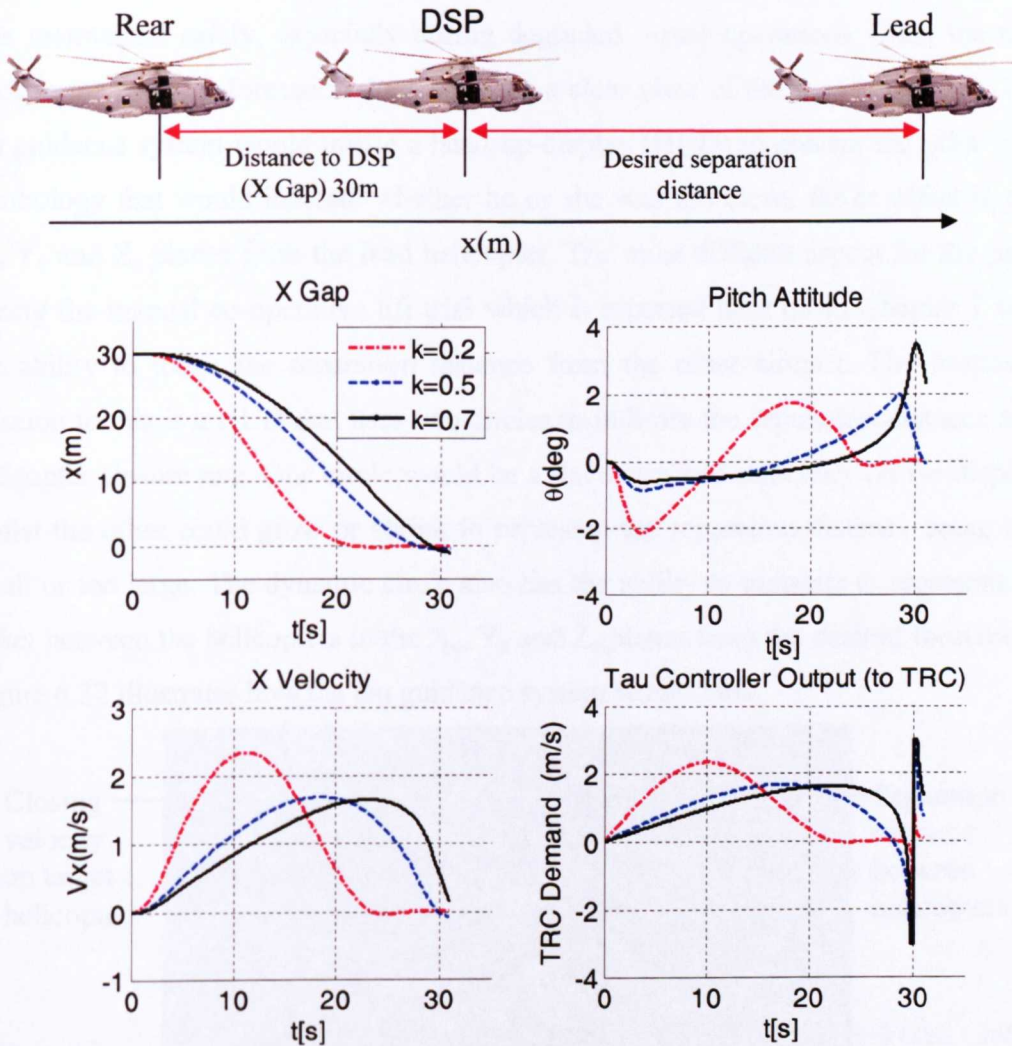
The tau controller gain was then implemented on the EH-101 Model so that the reference signal from the controller fed into the TRC system to command a velocity and reduce the separation distance as required. Figure 6.30 below shows the longitudinal tau separation maintenance controller:



**Figure 6.30: Longitudinal tau separation maintenance controller**

Equation 6.24 indicates that the tau gain  $K$  is a function of  $k$  and  $T$  defined earlier. These values must be defined in the controller for it to function properly. The value of big  $T$  depends on the size of the separation gap to be closed, for example if the separation between the helicopters is small then  $T$  would be small. The closer the

value of  $k$  is to unity, the closer the trajectory mirrors the constant acceleration guide, with a closure rate that increases proportionally with time. A low value of  $k$  corresponds to a control strategy whereby the pilot initiates the deceleration earlier in the manoeuvre. A large value of  $k$  close to unity corresponds to the maximum deceleration very late on in the manoeuvre. Figure 6.31 below shows an example of the controller in operation. In this example, both helicopters are considered to be hovering and the rear helicopter is 30m away from the DSP.



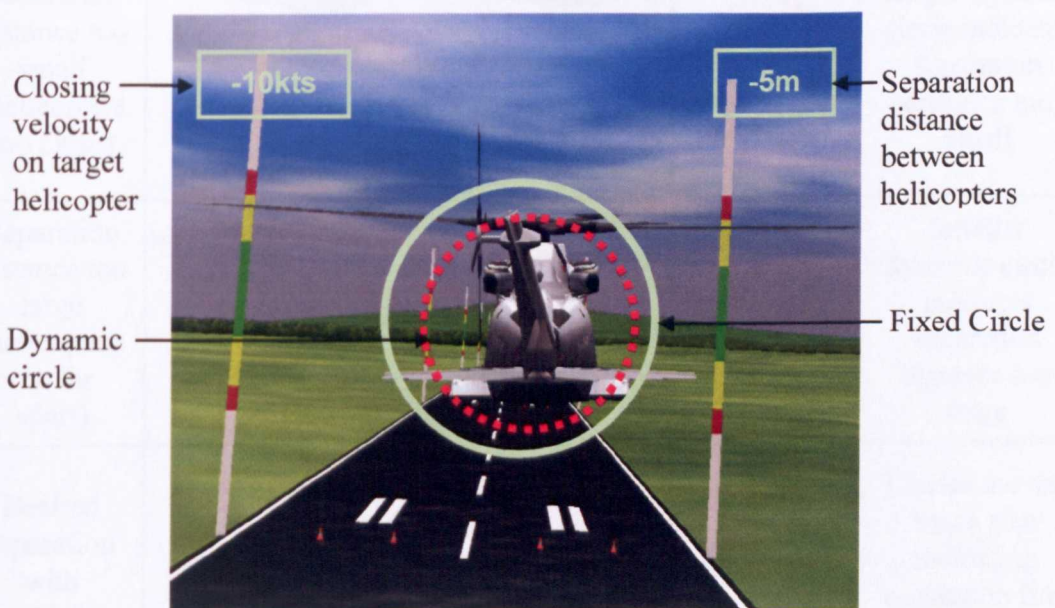
**Figure 6.31: Tau Separation Closure System**

The tau separation closure system (TSCS) is engaged at 0 seconds and the 30m gap between the rear helicopter and the DSP is reduced to zero by the TSCS driving the TRC with a reference signal. The value of  $T$  is specified as 30s and three different values of  $k$  are used to illustrate how the velocity profile can be varied corresponding to different levels of aggression. Due to time constraints the TSCS system was not

implemented into the ACLC for the piloted simulation trials, however the work completed in this section shows some promise and it is recommended that this be pursued in future research.

### 6.7.7 Tau Based Visual Guidance

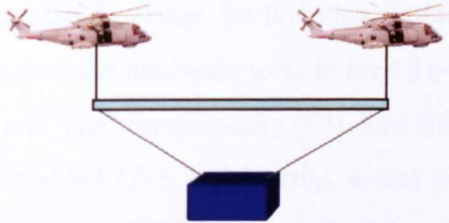

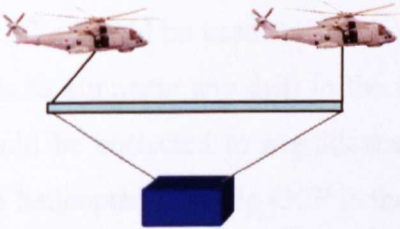

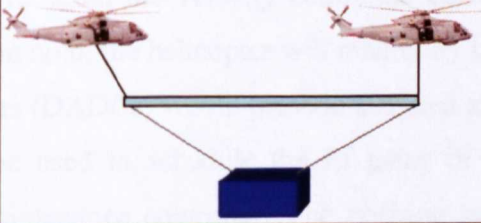

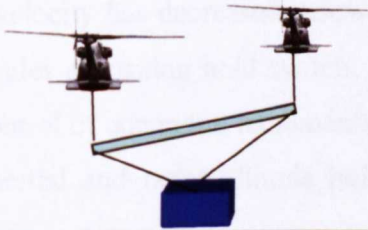
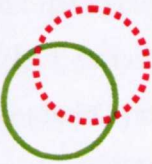
Another area where tau theory was explored was the concept of a tau based visual guidance system. This would be used to ensure the separation between the helicopters was maintained safely, especially during degraded visual operations when the rear pilot in the twin-lift formation does not have a clear view of the lead helicopter. The tau guidance system would utilise a head-up-display (HUD) to present the pilot with symbology that would indicate whether he or she was too close, far or offset in the  $X_e$ ,  $Y_e$  and  $Z_e$  planes from the lead helicopter. The most difficult aspect for the pilot during the manual co-operative lift trial which is reported later on in Chapter 7 was the ability to judge the separation distance from the other aircraft. The proposed solution to this is a HUD that uses two circles to indicate the separation distance and helicopter closure rate. One circle would be a fixed size and stationary on the display whilst the other could grow or shrink to represent the separation distance being too small or too large. The dynamic circle also has the ability to translate to represent an offset between the helicopters in the  $X_e$ ,  $Y_e$  and  $Z_e$  planes from the desired formation. Figure 6.32 illustrates how the tau guidance system would look.



**Figure 6.32: Tau based guidance system**

The green circle in figure 6.32 represents the circle that is fixed in the centre of the display. The red dotted circle size can be enlarged or reduced and translated laterally and vertically. If the separation distance between the helicopters is too large, then the red circle reduces in size, prompting the pilot to reduce the separation distance. The red circle enlarges as the separation distance is reduced until at the desired separation the green and red circles are congruent. If the separation distance becomes too small the red circle increases in size so that it looks larger than the green circle. If there is a lateral or vertical offset between the helicopters and the desired formation, then the red circle translates cueing the pilot to reduce the error offset. The HUD would also display closure velocity and separation distance. Table 6.1 summarises the HUD symbology as a function of helicopter separation and offset.

**Table 6.1: Summary of HUD symbology**

Relative Helicopter Position	Offset	HUD Symbology	Comments
Desired separation and offset			Congruent circles indicate desired separation and zero offset
Separation distance too small (helicopters too close)			Larger dynamic circle indicates separation distance too small
Separation distance too large (helicopters too far apart)			Smaller dynamic circle indicates separation distance too large
Desired separation with positive y and z offset			Circles are the same size indicating separation fine but offset in y and z present

It must be emphasised that the HUD guidance system itself is not driven by any tau based equations but instead operates on the error signal between the two helicopter positions and the desired separation distance. The pilot uses what can be described as ‘prospective control’ to evolve a safe separation distance between the helicopters. Tau provides the time to contact or close to an object or surface at the current closure rate. By providing extra closure rate cues in the form of the scalable red circle, the pilot can better judge his closure rate through direct object looming enabling him to more efficiently close on an object or in this case maintain the desired separation using tau principles. Due to time constraints the tau based guidance and separation control system was not implemented on the helicopters in the co-operative lift configuration. This would be one of several areas of research recommended for future work outlined in Chapter 8.

## **6.8 Controller Implementation**

The following section describes the technical implementation of the ACLC onto the real aircraft, based on the hardware used in the CH-47F Chinook Digital AFCS which also has ACAH and TRC functionality [63]. The full authority ACLC would require a sophisticated embedded GPS and inertial sensor such as the Honeywell Embedded GPS and Inertial Sensor (EGI<sup>®</sup>) to provide data required by the TRC based system. Dual Honeywell EGI<sup>®</sup>s would be used for the inertial and aircraft attitude data and would use GPS data to eliminate any drift in the inertial sensors. The velocity data from the EGI<sup>®</sup> would be corrected to a guidance and control point (GCP) that is selected to be at the helicopter CG. The GCP is the point about which the helicopter will manoeuvre when the velocity command control laws are active. For example during position hold, the helicopter will inherently turn around the CG point. Dual air data computers (DADCs) would provide airspeed and pressure altitude. The airspeed data would be used to schedule the PI gains of the primary control system and separation maintenance controller. The position hold system would become active when the ground velocity has decreased below 1 knot and the cyclic is in detent or when the pilot toggles a position hold switch. A cyclic HAT switch would then be used for precise control of one metre increments. The height hold system would use a combination of inertial and radar altitude hold. In inertial altitude hold an outer

integral loop is created by integrating the vertical velocity errors. This should work very well for short term hovering and manoeuvring flight over level terrain without the need for the radar altimeter [63]. Honeywell EGI<sup>®</sup> is accurate to +/- 5 foot per minute and there would be potential for a drift rate of 5 fpm limiting the practicality of the system for long duration hovering. For precise long duration hovering manoeuvres over terrain which is not flat, the radar altimeter can be used to close the outer position loop instead of the integrated vertical velocity eliminating the inertial drift.

The slave helicopter in the ACLC formation requires the master helicopter's control positions and inertial co-ordinates for its own separation and formation maintenance sub controllers. These would have to be broadcast from the master helicopter's EGIs and DADC using either a wireless link or physical cable link such as a fibre-optic or wire.

The main emphasis in modern control is based on digital computers with the use of inertial motion and air-stream units. Mechanical linkages between the pilot controls and aircraft control surfaces have been removed and replaced with electrical signal commands (fly-by-wire) or more recently by fibre optic light (fly-by-light). This greatly reduces the mechanical complexity of the system but increases the complexity of the flight control software. In order to achieve the same level of system redundancy as was achieved with the previous mechanical systems, multiple signal sources and several lanes of computing are required to provide the necessary redundancy and these are cross-monitored in order to isolate any failed equipment [68]. A comprehensive built-in-test capability is usually built in to ensure the aircraft is 'safe-to-fly' prior to each flight and to identify and locate existing failures. Most recent systems utilise triplex redundant architectures with reliance on both cross-lane and in-lane monitoring to achieve the required level of system integrity and therefore operational safety.



## 6.9 Conclusions to Chapter

This chapter has described the design process and operation of the ACLC system that was implemented on the EH-101 co-operative lift configuration. The handling qualities of the controller were investigated using desktop simulation and the ADS-33 handling qualities criteria. The stability of the system was assessed using the stability margin and unstable eigenvalue criteria and the system was found to be stable. The inner loop ACAH handling qualities predicted from the small and moderate amplitude criteria indicated Level 1 performance for the ADS-33 requirements for all MTEs with the exception of target acquisition. The chapter also described the flight control clearance procedure recommended by a GARTEUR group that was established to investigate new and improved analysis techniques of flight control laws. The separation maintenance control, turn co-ordination function, novel tau gap closure control system and HUD guidance system that allows the pilot to judge the separation distance and gap closure were also detailed. The Chapter did not consider the effect of modelling and sensor uncertainties on the controller performance. This was due to time constraints before the piloted simulation trials. This area would have to be revisited before any flight test phase and is one of the recommendations for future work in Chapter 8.

The following chapter assesses the handling qualities of the ACLC through two piloted simulation trials. The ADS-33 acceleration and deceleration and pirouette MTEs were used to assess the real-time performance of the ACLC to gain important subjective qualitative data that will be used to support the quantitative results described in this chapter.

## Chapter 7

### CO-OPERATIVE LIFT PILOTED SIMULATION TRIAL

#### 7.1 Introduction

Objective measurements and assessments in the form of quantitative data derived from desktop simulation are very important for demonstrating compliance with handling quality design standards like ADS-33 [2]. However, quantitative data alone is not sufficient to guarantee that a new helicopter or an AFCS upgrade on an existing fleet helicopter will be safe in achieving the operational objectives. For example, objective assessment alone concentrating on quantitative analysis may cover up gaps or potential handling quality ‘cliff edges’. Additional piloted tests with a more subjective orientation are therefore extremely important in the design process and can expose handling quality problems that were not apparent when considering quantitative data alone. This chapter describes two piloted simulation trials that were carried out using two ADS-33 MTEs: the acceleration and deceleration and pirouette.

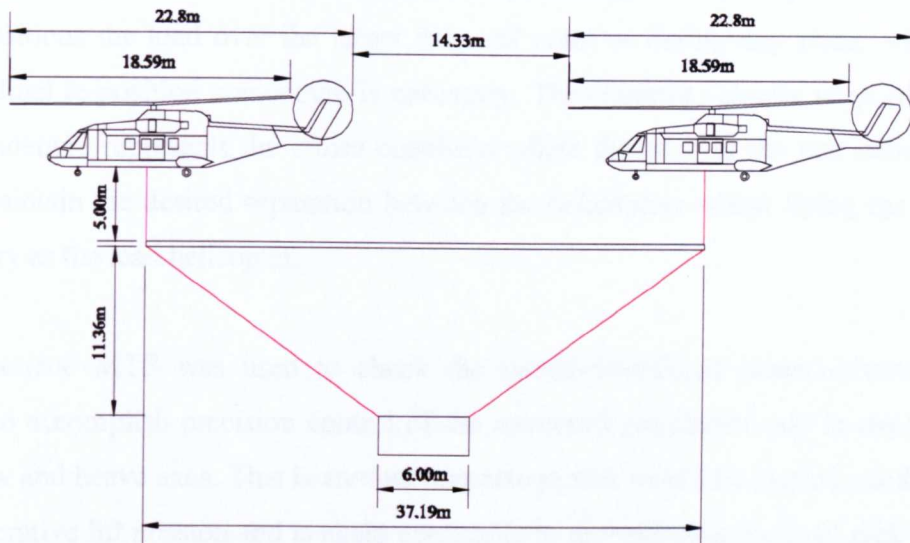
#### 7.2 The Piloted Simulation Trial Objective

The two main objectives of the trials were:

1. To investigate the handling qualities and pilot workload of a manual co-operative lift configuration without twin-lift control augmentation (ACLC) and to determine whether or not manual co-operative lift operations were possible with traditionally augmented helicopters.
2. To compare the non-augmented manual co-operative lift system with the ACLC system developed to determine if the system met the control objectives described in Chapter 6 and to see if the handling qualities and pilot workload were improved.

The co-operative lift model used in the trial was the same as the one introduced in Chapter 2, consisting of two helicopters in an in-line tandem formation carrying a

5000kg under slung load supported by a horizontal spreader bar. The separation dimensions are illustrated in the scale drawing in figure 7.1:



**Figure 7.1: Co-operative Lift Configuration**

### 7.3 The Mission Task Elements

Given the time constraints and considerable financial expense that is associated with piloted simulation trials, only two MTEs could be performed in the trial. Hence it was important that the selected MTEs would test a proportion of the flight envelope deemed most important and applicable to co-operative lift operations. If possible, the MTEs selected would test all four flight axes; the longitudinal, lateral, directional and heave dynamics over a range of speeds. With these factors in mind, the following two MTEs were selected:

1. The acceleration and deceleration MTE
2. The pirouette MTE

The acceleration and deceleration MTE was primarily used to investigate the longitudinal characteristics of the configuration but also had elements of lateral, directional and height tracking imposed through a series of spatial constraints and tracking requirements. The manoeuvre was performed at a range of speeds corresponding to different levels of aggression so that the pilot workload could be investigated using the Bedford workload scale (Appendix 3). The acceleration and

deceleration MTE is representative of a portion of a co-operative lift mission where the pilot must reposition longitudinally; this could be during the take off phase when the pilot has to position over the load for pick up, during the drop off phase when the pilot positions the load over the target drop off point or during any phase where a longitudinal re-position manoeuvre is necessary. The constant velocity proportion of the manoeuvre represents the cruise condition where the pilot in the rear helicopter must maintain the desired separation between the helicopters whilst flying the same trajectory as the lead helicopter.

The pirouette MTE was used to check the lateral-directional characteristics and ability to accomplish precision control of the rotorcraft simultaneously in the pitch, roll, yaw and heave axes. This is another manoeuvre that would be carried out during a co-operative lift mission and is again applicable to repositioning for load pick up or drop off. The manoeuvre had constraints on heading, height and position tracking.

ADS-33E stipulates that each MTE should be assessed by at least three test pilots so that an average handling qualities rating can be obtained. However, due to test pilot availability, and financial constraints, the MTEs in this section were flown using one pilot. The test pilot used in the simulation trial was an ex-Royal Navy test pilot who had accumulated thousands of hours of rotary wing experience throughout his career and had attended the British Empire Test Pilot School at Boscombe Down. The pilot also had previous experience of under slung load operations flying Westland Sea Kings and Chinook helicopters. He was also involved with the original development of the EH-101 and was therefore an ideal choice for the handling qualities analysis of the MCLC and ACLC.

#### **7.4 The Acceleration and Deceleration MTE**

The acceleration and deceleration manoeuvre is an aggressive hover/low speed manoeuvre that is derived from nap of the earth flying (NOE). Generally, the manoeuvre consists of two parts; a very aggressive acceleration from hover to target airspeed, immediately followed by an equally aggressive deceleration back to hover over a predetermined target point.

The manoeuvre was designed to evaluate:

- Pitch and heave axis handling qualities during aggressive manoeuvring near the limits of performance
- Undesired inter-axis coupling
- Harmony between pitch and heave axes controllers
- Response to collective inputs
- Emphasise complex speed and power management.

The ADS-33 definition of the acceleration and deceleration MTE states [2, pp. 37]:

*‘Starting from a stabilised hover, rapidly increase power to approximately the maximum and maintain altitude constant with pitch attitude. Hold collective constant during the acceleration to the target airspeed. Upon reaching the target airspeed, initiate a deceleration by aggressively reducing the power and holding altitude constant with pitch attitude. The peak pitch attitude should occur just before reaching the final stabilised hover.’*

Table 7.1 shows the desired and adequate performance levels specified by ADS-33.

**Table 7.1: ADS-33 Desired and Adequate Performance Requirements**

	<b>Desired</b>	<b>Adequate</b>
<b>Altitude +/-</b>	10ft	20ft
<b>Lateral Track +/-</b>	15ft	30ft
<b>Heading +/-</b>	10 deg	20 deg

The desired and adequate requirements are used by the pilot to assess the performance of the MTE prior to awarding the HQR. It is therefore imperative that the pilot can easily assess the performance against these requirements using visual cues available from the MTE test course. One of the advantages of flight simulation is that additional visual cues can be added to the test course to enhance this process and compensate for the reduced field of view. The additional cues can be quickly added and can even be better than those available for a MTE in reality. For example, for the acceleration and deceleration MTE, ADS-33 suggests that cones and flat markers

should be used to denote the test course and desired and adequate requirements. However in the trial, 150 foot poles with height markings were used to give the pilot better visual cues. Figure 7.2 shows a screen shot of the actual course adopted for the trial and figure 7.3 shows the course dimensions. The course was created using an airfield with the addition of 150 foot vertical poles either side of the runway that also displayed the desired and adequate height boundaries using 'traffic light' coloured bands. The poles also helped the pilot to determine the prescribed start and finish points. The length of the course was 5 poles in total, with 500ft between each post. ADS-33 does not specify the length of the course, only that a target velocity should be reached. The reason for specifying the course length in this trial was to add an additional aggression control. The lateral track requirements were indicated using cones on the runway.

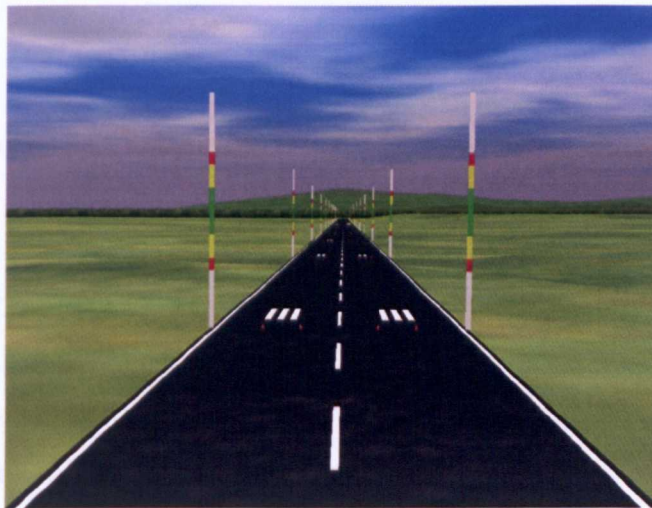


Figure 7.2: Acceleration and deceleration MTE course

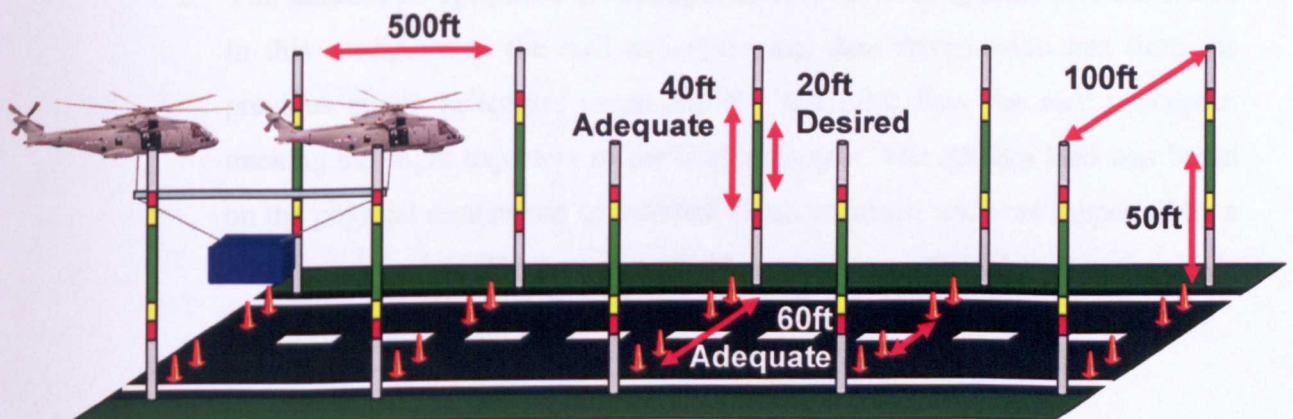


Figure 7.3: MTE course with dimensions

Ideally two pilots would have been used in the trial to simulate the manual configuration of the twin lift system, with one pilot in each of the two helicopters. However as stated previously there was only one pilot available and the lead helicopter in the formation had to be data driven using the technique described in section 3.5.2 in order to simulate the manual co-operative lift configuration. In this mode, the test pilot flew a single helicopter in the manoeuvre with the all up mass of the helicopter set to the total mass expected during the co-operative lift operation and the helicopter states were recorded. These were then used to drive the master or lead helicopter. The disadvantage of this configuration is that the forces and moments from the external load cannot be fed back to the lead helicopter and the slave pilot found it difficult to anticipate the lead pilot's manoeuvre because there was no verbal two way communication that would normally be present between two pilots.

#### **7.4.1 The MTE Test Conditions**

The acceleration and deceleration MTE was performed using four different helicopter configurations:

1. **A single EH-101 with base AFCS.** This single helicopter configuration was flown first and the flight data was recorded so that it could be used to drive the lead helicopter in the formation. The single EH-101 used a basic attitude augmentation SCAS in pitch and roll with rate command in collective and yaw. Although this controller is representative of the type used on the real helicopter, it is a lot simpler and does give a different response.
2. **The manual co-operative lift configuration with 5000kg load (MCLC load).** In this configuration the lead helicopter was data driven with data from the previous single helicopter sortie and the test pilot flew the rear helicopter, tracking the flight trajectory of the lead helicopter. The 5000kg load was based on the physical dimensions of standard cargo container and was supported by a 300kg spreader bar. The type of controller was the base SCAS used in the single EH-101 (described in point 1 above).

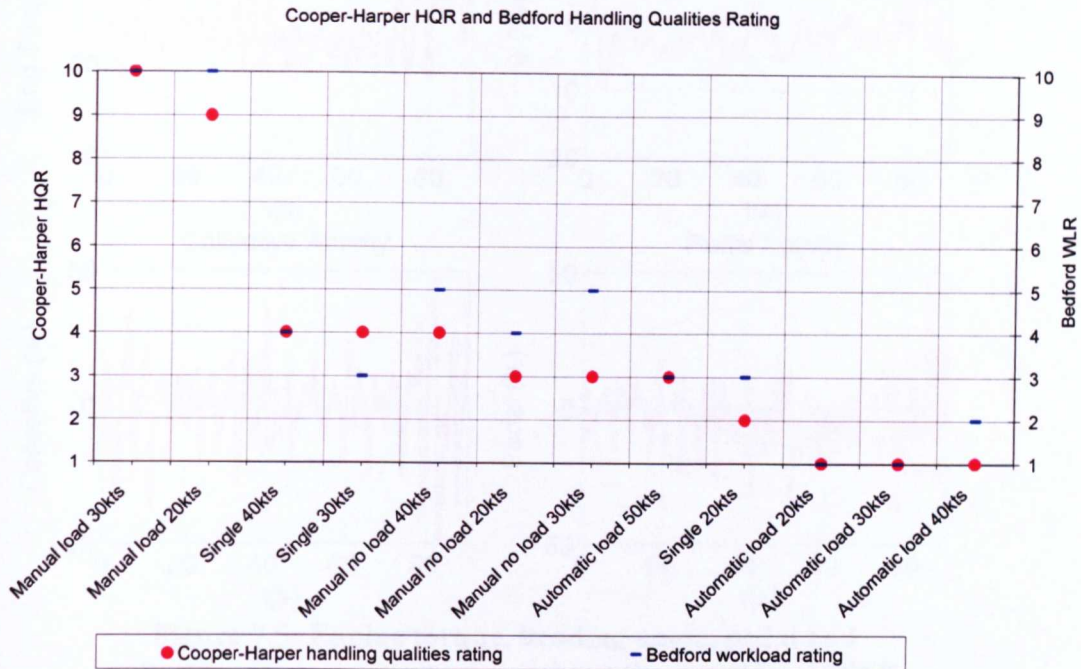
3. **The manual co-operative lift configuration with no load (MCLC no load).**  
This configuration was the same as the one described in the previous point, but without the under slung load and spreader bar, turning the task into a formation flying MTE.
4. **The automatic co-operative lift configuration with 5000kg load (ALCL load).** This is the automatic configuration where the pilot flies the rear (master) helicopter in the configuration and the lead (slave) helicopter maintains the specified separation between itself and the master automatically. The type of controller used was the ALCL master slave controller which had a TRC response type in longitudinal and lateral axis and rate command in directional and height. A detailed description of this controller can be found in Chapter 6.

After each manoeuvre, the Cooper-Harper handling qualities rating and Bedford workload rating were awarded by the pilot using an 'in-cockpit pilot questionnaire' (Appendix 3) which guides the pilot through the ratings in terms of:

- Task cues available
- Aggressiveness
- Task performance
- System characteristics
- Workload
- HQR
- PIO susceptibility



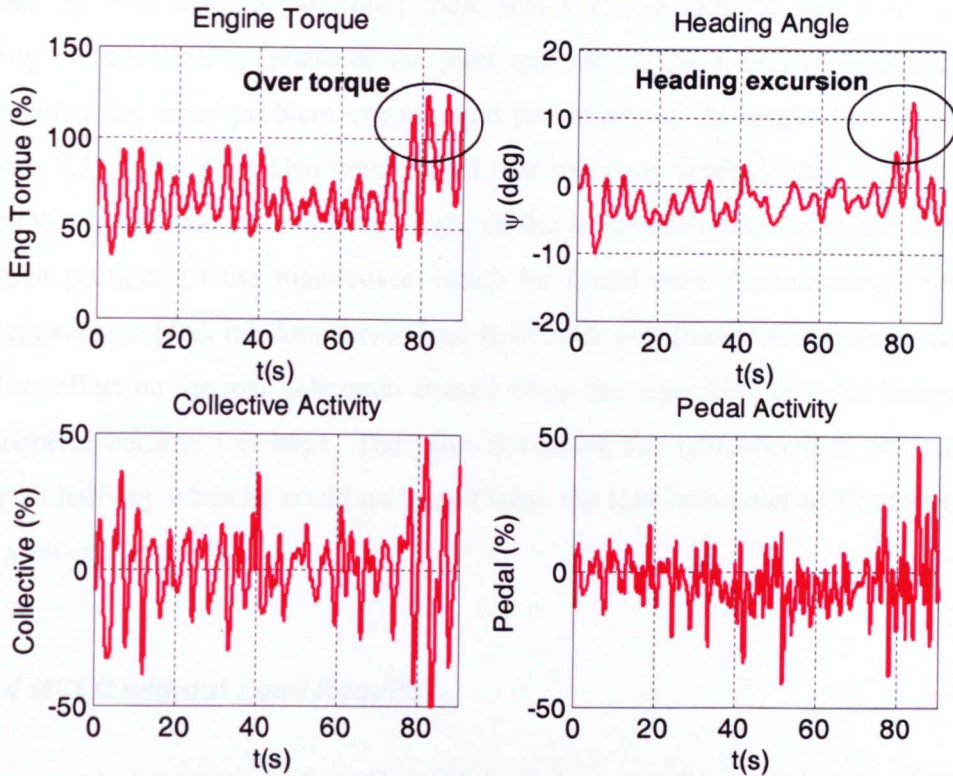
Figure 7.4 shows the Cooper-Harper handling qualities and Bedford workload rating awarded by the pilot during the acceleration and deceleration MTE in descending HQR order:



**Figure 7.4: Cooper-Harper HQR and Bedford workload ratings**

### 7.4.2 Single Helicopter Results

The single helicopter sorties were completed at 20, 30 and 40 knots and the pilot awarded HQRs of 2, 4 and 4 respectively, placing the baseline configuration in the Level 1 region. Bedford workload ratings of 3, 3, and 4 were awarded indicating Level 1 performance. The pilot commented that he encountered a handling quality cliff edge in directional control during the deceleration phase that was related to poor directional control authority when operating at high engine torque. Figure 7.5 illustrates the handling quality cliff edge and shows the engine torque, heading angle, pedal and collective control activity throughout the manoeuvre.



**Figure 7.5: Engine torque, heading angle, pedal and collective control activity throughout the accel/decel MTE (single EH-101 20kts)**

After 70 seconds, the pilot initialises the deceleration to hover phase of the manoeuvre corresponding to an increase in engine torque which eventually leads to an over-torque at 79 seconds. The increase in collective and torque during the deceleration period causes a 16 degree heading excursion due to the helicopter's high collective-to-yaw couple. With the helicopter now near a hover condition the pilot quickly lowers the collective to hover trim causing the helicopter to yaw aggressively in the opposite direction to the previous excursion due to decrease in engine torque. The pilot attempts to correct for this using full right pedal indicating reduced control authority.

### 7.4.3 MCLC Load Results

The pilot was only able to complete the 20 knots sortie and awarded the run with a HQR of 9 and Bedford workload rating of 10, indicating major deficiencies and a control loss at some portion of the operation. The pilot commented on three losses of tail rotor authority during the sortie and severe roll and directional excursions

associated with this. In particular, there was a severe lack of yaw control power during the deceleration phase as the pilot approached the limiting collective power replicating the same problem encountered previously in the single helicopter sortie (figure 7.5). The pilot also commented that the poor vertical field of view in the simulator meant that he lost visual sight of the lead helicopter during the high pitch attitude portions of the manoeuvre which he found very disconcerting. Since the system was coupled, the data driven lead helicopter was found to have an undesirable pulling effect on the rear helicopter caused when the separation distance between the helicopters became too large. The pilot attempted the manoeuvre at 30 knots but aborted halfway when he could no longer track the lead helicopter due to large heave and yaw excursions.

#### **7.4.4 MCLC without Load Results**

The manual co-operative lift sortie without the external load present (i.e. formation flying) was achievable at 20, 30 and 40 knots. This represented a standard formation flight task where the helicopters were in a tandem inline configuration. The HQRs awarded were 3, 3 and 4 respectively and Bedford workload ratings 4, 5 and 5 suggesting there would be insufficient spare capacity for additional tasks such as navigation and system management. The pilot commented that he would find the manoeuvre easier if an offset echelon configuration was used instead of the tandem formation, the main reason for this being that the lead helicopter fuselage is visible giving better pitch cues.

#### **7.4.5 ACLC Load Results**

The final sortie involved the twin lift ACLC system. The helicopter formation was kept the same as the previous sorties, but this time the pilot flew the rear master helicopter and commanded both helicopters in the configuration. The separation distance between the helicopters was tracked and kept constant by the ACLC system. The sortie was initially performed at 20, 30 and 40 knots and the pilot awarded HQR 1 and Bedford workload rating 1 for all manoeuvres indicating excellent highly desirable performance with no pilot compensation required for desired performance

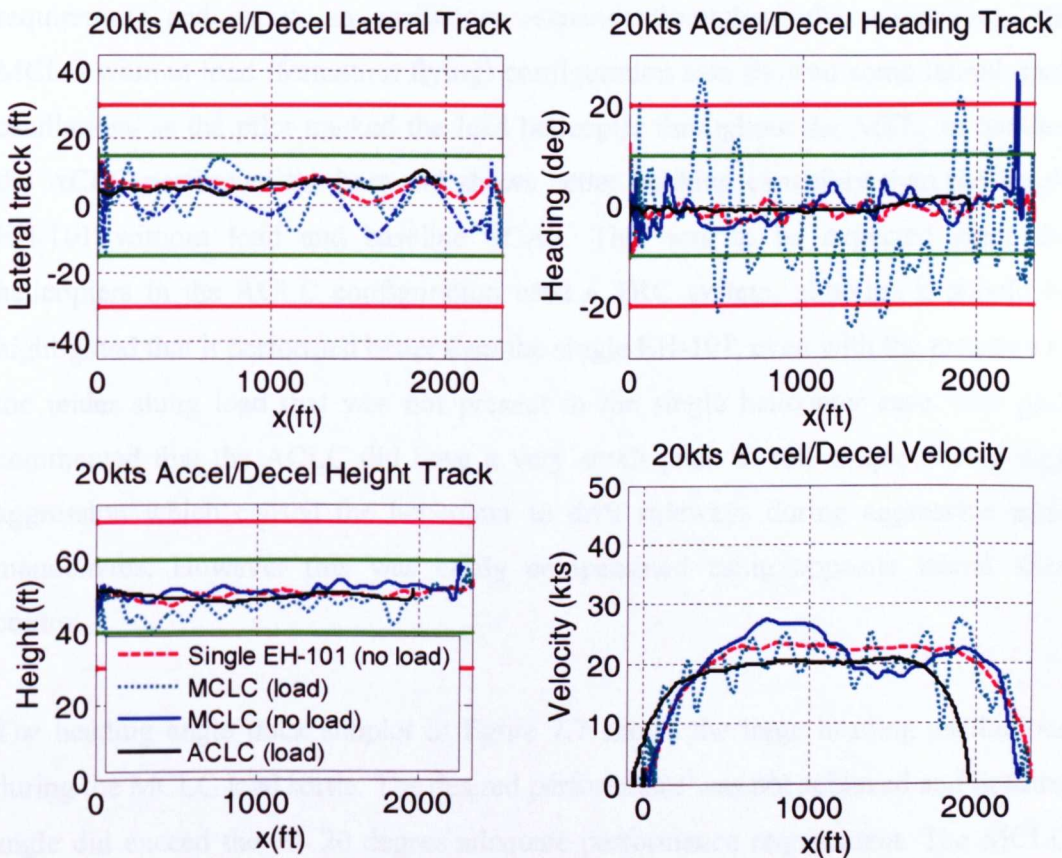
and insignificant workload. With excellent performance demonstrated at low speed, the sortie was then expanded to 50 knots which represented extremely high aggression given the spatial constraints and presence of the external load. The pilot awarded a HQR and Bedford workload rating of 3 for the 50 knots case indicating there was still enough spare capacity for all additional tasks even at such high aggression. The pilot commented that flying the configuration from the rear with the automatic pilot in front was disconcerting since he naturally focussed on what the lead helicopter was doing rather than concentrating on the outside world visual cues available to him. Figure 7.6 shows the pilot's eye view through the centre cockpit window during the manoeuvre with the automatic slave helicopter visible. The pilot recommended that the manoeuvre should be flown in echelon configuration to reduce this problem and improve the visual cues available to the pilot.



**Figure 7.6: Pilot view out of the centre cockpit window**

### 7.4.6 Task Performance

Figure 7.7 shows the lateral track, height track, heading and velocity throughout the MTE for the 20 knots case as a function of distance along the MTE course. The red and green lines represent the adequate and desired performance requirements used in the task performance analysis. These correspond to the physical course dimensions displayed in figure 7.3.



**Figure 7.7: 20 knots acceleration and deceleration MTE performance**

Figure 7.7 shows results for the following configurations described earlier in Section 7.4.1:

1. Single EH-101 without load.
2. MCLC with 5000kg load.
3. MCLC without load.
4. ACLC with 5000kg load.

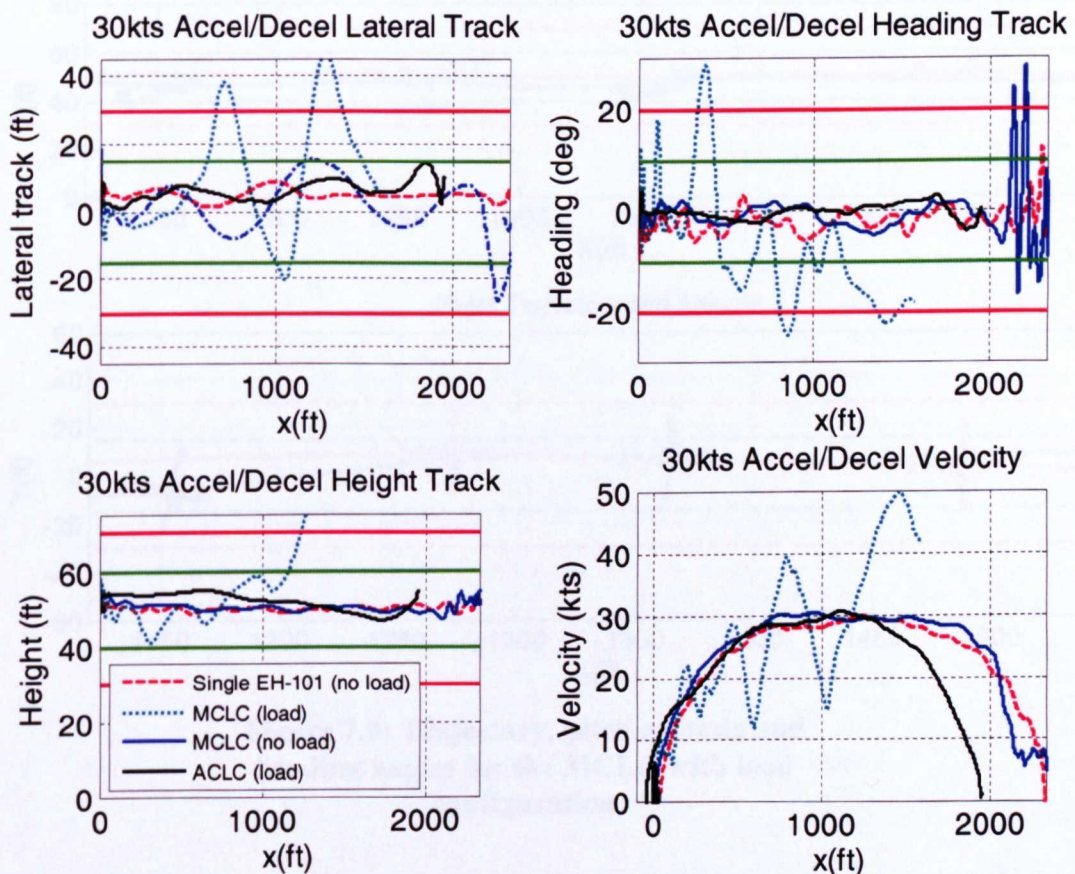
The complex multi-body, distributed simulation nature of the CLM meant that the model was not started in a perfect trim condition and the first 20 feet in the manoeuvre was taken up during initialisation when the pilot brought the configuration to a stable trimmed hover. This explains why there were some erratic heading angle and lateral track fluctuations during this period and these were not included in the desired and adequate performance analysis. The lateral track subplot shows that all of the configurations met the desired MTE performance criterion. The MCLC with 5000kg load configuration came closest to breaching the  $\pm 20$  feet lateral tracking requirement and shows an oscillatory response throughout the manoeuvre. The MCLC without load (formation flying) configuration also showed some lateral track oscillations as the pilot tracked the lead helicopter throughout the MTE. In contrast the ACLC performed the best and shows better tracking capability than the single EH-101 without load and baseline SCAS. This was to be expected since the helicopters in the ACLC configuration used a TRC system, although it should be highlighted that it performed better than the single EH-101, even with the presence of the under slung load that was not present in the single helicopter case. The pilot commented that the ACLC did have a very small pitch to roll couple during high aggression which caused the helicopter to drift sideways during aggressive pitch manoeuvres. However this was easily compensated using opposite lateral stick control.

The heading angle track subplot in figure 7.7 shows the large heading oscillations during the MCLC load sortie. The desired performance was not achieved and heading angle did exceed the  $\pm 20$  degree adequate performance requirement. The MCLC configuration without load also exceeded the adequate standard during the deceleration to target hover phase of the MTE. The reason for this was described earlier in section 7.4.2 and can be attributed to poor yaw control authority during high torque manoeuvres. The ACLC tracked the desired heading angle best compared to the other configurations.

The height track subplot shows that all of the configurations investigated were within the desired requirements. The MCLC load configuration performance was worse with four height oscillations throughout the manoeuvre which the pilot attributed to the

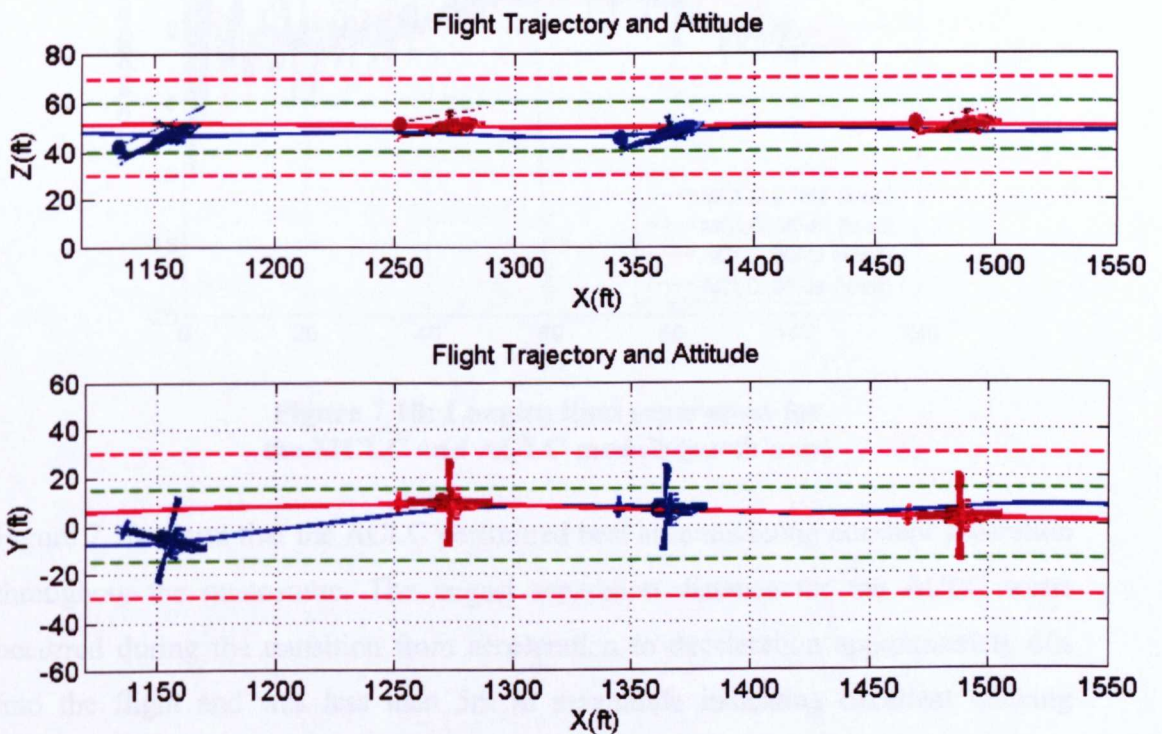
interaction of the load dynamics. There was a particularly large oscillation during the deceleration phase which correlates with the heading excursion during the increased torque activity. The ACLC tracked the desired height requirements best and showed no height oscillations even with the presence of the external load.

The velocity track subplot shows that the pilot found velocity control difficult for both MCLC configurations. He commented after the trial that the inline formation adopted provided few visual cues corresponding to the pitch attitude and therefore velocity of the lead helicopter and suggested that the echelon formation would be better suited to the task. The ACLC shows excellent velocity tracking which is expected from a TRC response type. Figure 7.8 shows the lateral track, height track, heading and velocity throughout the MTE for the 30 knots case as a function of distance along the MTE course.



**Figure 7.8: 30 knots acceleration and deceleration MTE performance**

The pilot aborted the 30 knots MCLC load sortie when the vertical separation distance between the helicopters became too large and he could no longer track the lead helicopter. The figure shows this occurred 1000 feet into the manoeuvre which was approximately half way into the acceleration and deceleration MTE i.e. during the steady state portion of the manoeuvre. Prior to the failure the velocity subplot indicates that the pilot found it very difficult to track the lead helicopter's velocity profile as indicated by the large oscillatory nature. Some of these velocity oscillations *would have been induced by the rear helicopter being physically pulled along by the lead* as the longitudinal separation became too great. Figure 7.9 illustrates this flight condition by showing the flight path trajectories, pitch attitudes and heading angles of the helicopters during one portion of the manoeuvre for the MCLC load configuration (between 1125-1550ft). Side and top down views are provided to show the vertical and lateral trajectories.



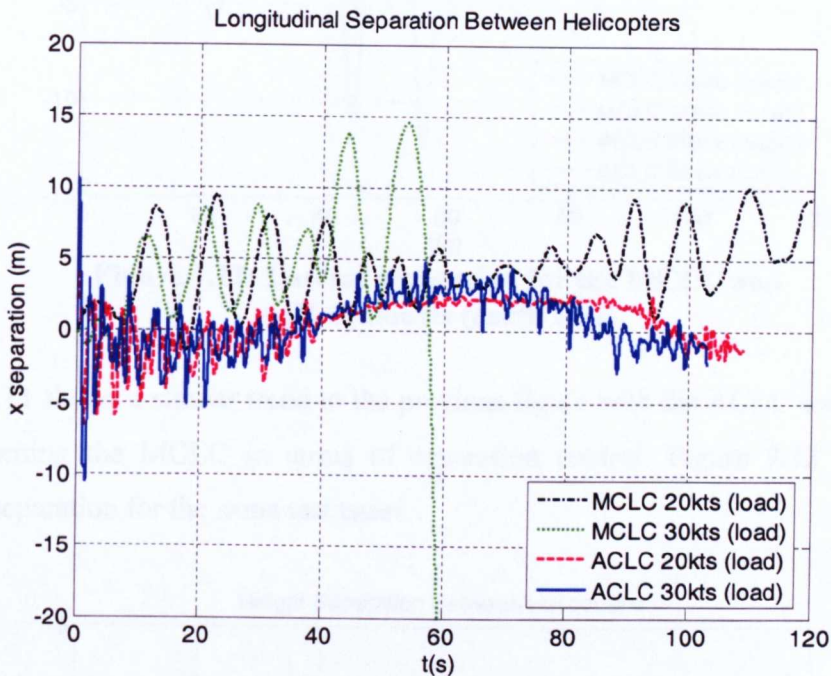
**Figure 7.9: Trajectory, pitch attitude and heading angles for the MCLC with load configuration**

The lead helicopter in the co-operative lift formation is coloured red and rear helicopter blue. The red and green dotted lines represent the adequate and desired requirements respectively. The figure clearly shows the high nose up pitch attitude



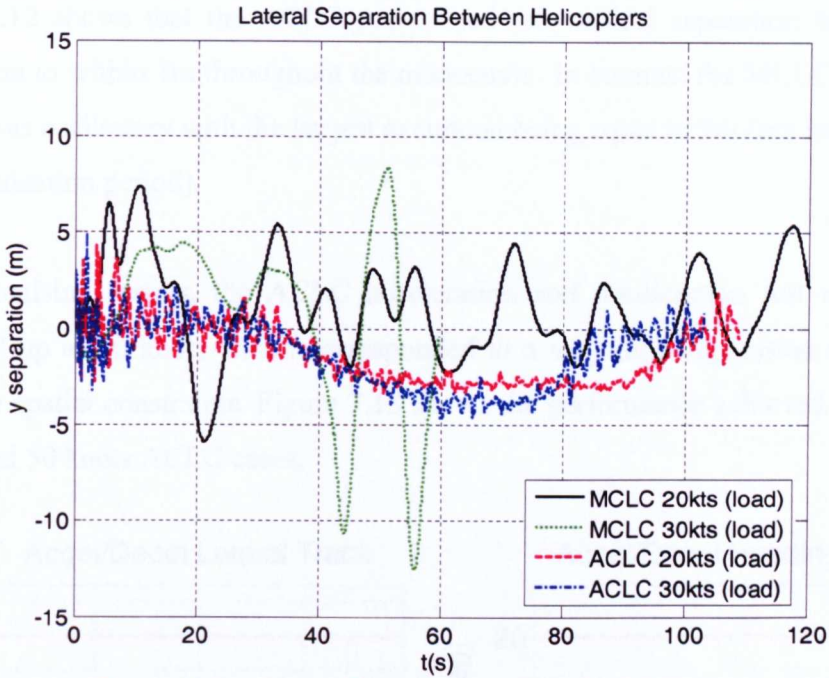
encountered by the rear helicopter and also illustrates a lateral excursion with a heading deviation.

Figure 7.10 shows the longitudinal separation in earth axis between the helicopters during the acceleration and deceleration MTE for the 20 and 30 knots runs for the MCLC and ACLC load conditions. The first 10 seconds of the figure show the separation variation during the initialisation of the model and can be disregarded.



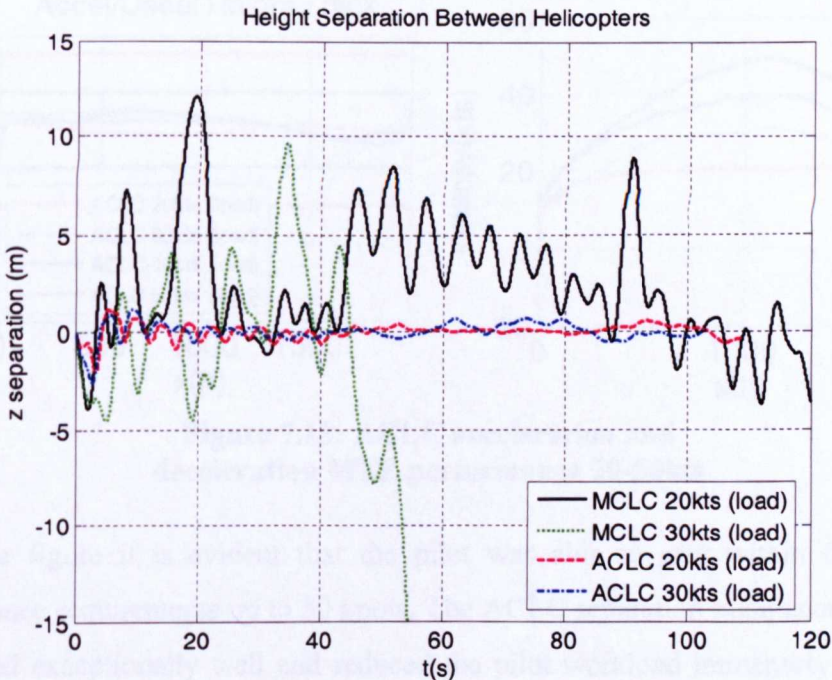
**Figure 7.10: Longitudinal separation for the MCLC and ACLC models (earth axis)**

Figure 7.10 shows that the ACLC performed best at maintaining constant separation throughout the manoeuvre. The largest separation distance for the ACLC sortie occurred during the transition from acceleration to deceleration approximately 60s into the flight and was less than 5m in magnitude indicating excellent tracking performance. The pilot failed to complete the 30 knots MCLC sortie which is evident from the very large separation distance at 60s. The x separation for the MCLC sortie oscillated as the pilot attempted to track the lead helicopter unlike the ACLC which was less oscillatory. Figure 7.11 shows the lateral separation between the helicopters during the acceleration and deceleration MTE for the 20 and 30 knots runs for the MCLC and ACLC load conditions.



**Figure 7.11: Lateral separation for the MCLC and ACLC models (earth axis)**

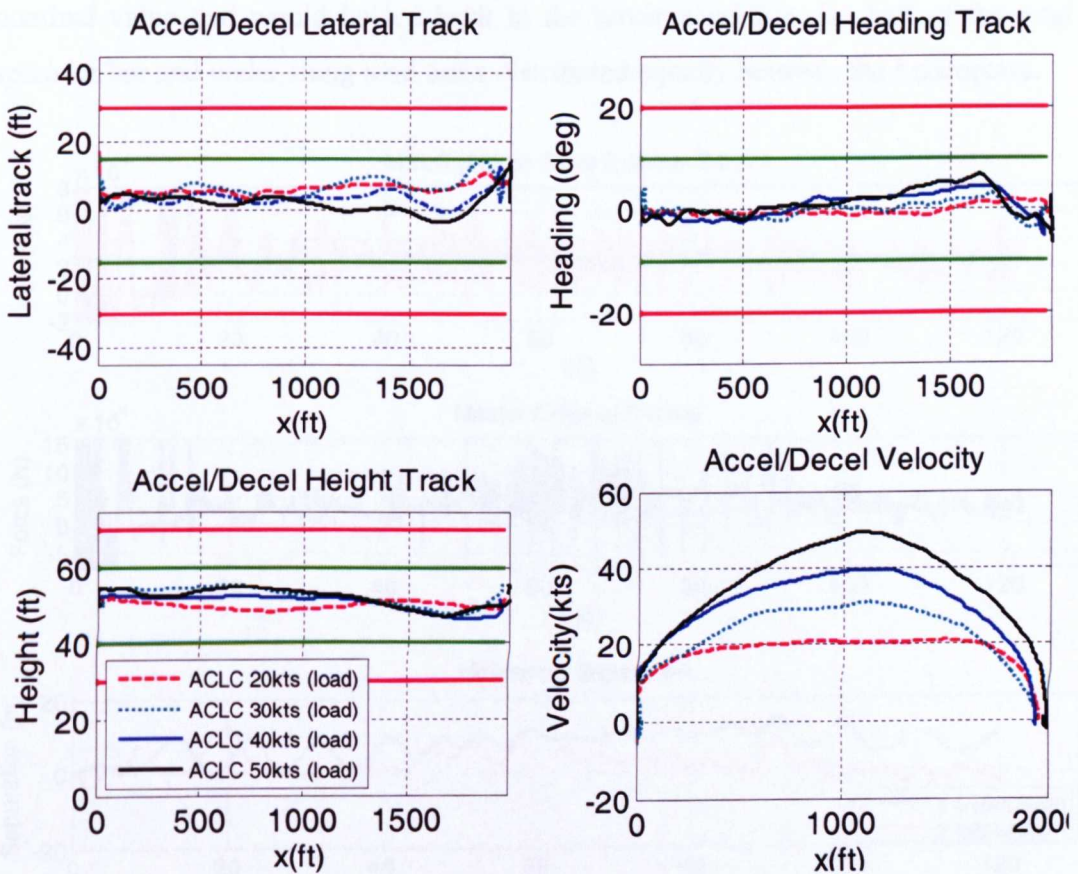
Figure 7.11 shows a similar trend to the previous figure with the ACLC configuration outperforming the MCLC in terms of separation control. Figure 7.12 shows the vertical separation for the same test cases.



**Figure 7.12: Vertical separation for the MCLC and ACLC models (earth axis)**

Figure 7.12 shows that the ACLC maintained the vertical separation between the helicopters to within 1m throughout the manoeuvre. In contrast the MCLC separation control was oscillatory with the largest excursion being equal to 9m (not including the 10s initialisation period).

With promising results, the ACLC acceleration and deceleration test matrix was expanded up to 50 knots which corresponded to a very high aggression manoeuvre given the spatial constraints. Figure 7.13 shows the performance achieved for the 20, 30, 40 and 50 knots ACLC cases.

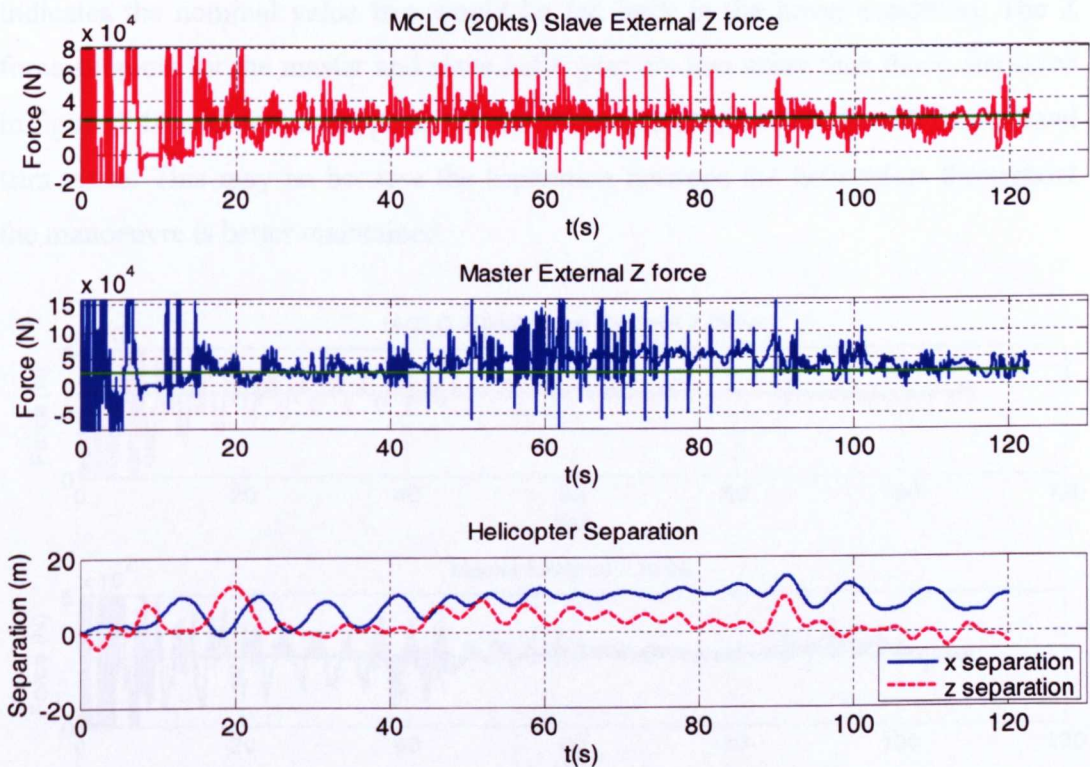


**Figure 7.13: ACLC acceleration and deceleration MTE performance 20-50kts**

From the figure it is evident that the pilot was able to stay within the desired performance requirements up to 50 knots. The ACLC separation maintenance system performed exceptionally well and reduced the pilot workload immensely. This was particularly noticeable in the longitudinal vertical axis where the pilot found it most difficult to track the lead helicopter.

### 7.4.7 Load Dynamics

The forces and moments fed back to the lead and chase helicopter CG from the spreader bar and under slung load were also recorded to see the variation throughout the manoeuvre. Figure 7.14 shows the external Z force from the spreader bar and under slung load that is fed into the master and slave helicopters during the 20 knots MCLC sortie. The first 18 seconds of data can be disregarded since this was the initialisation period when model was not in trim as explained earlier. The figure also shows the longitudinal and vertical separation between the helicopters during the manoeuvre which correlate with the force variation. The green line indicates the nominal value that would be fed back in the hover condition, i.e. half of the total spreader bar and under slung load mass distributed equally between the helicopters.



**Figure 7.14: External Z force for MCLC (20knots, 5000kg load)**

The figure shows that the forces fed back to the helicopters follow the nominal green line during the initial and end hover portions of the manoeuvre as expected. There are however numerous spikes in the force data that last for around one time step. These spikes are present in both helicopters at exactly the same time step.

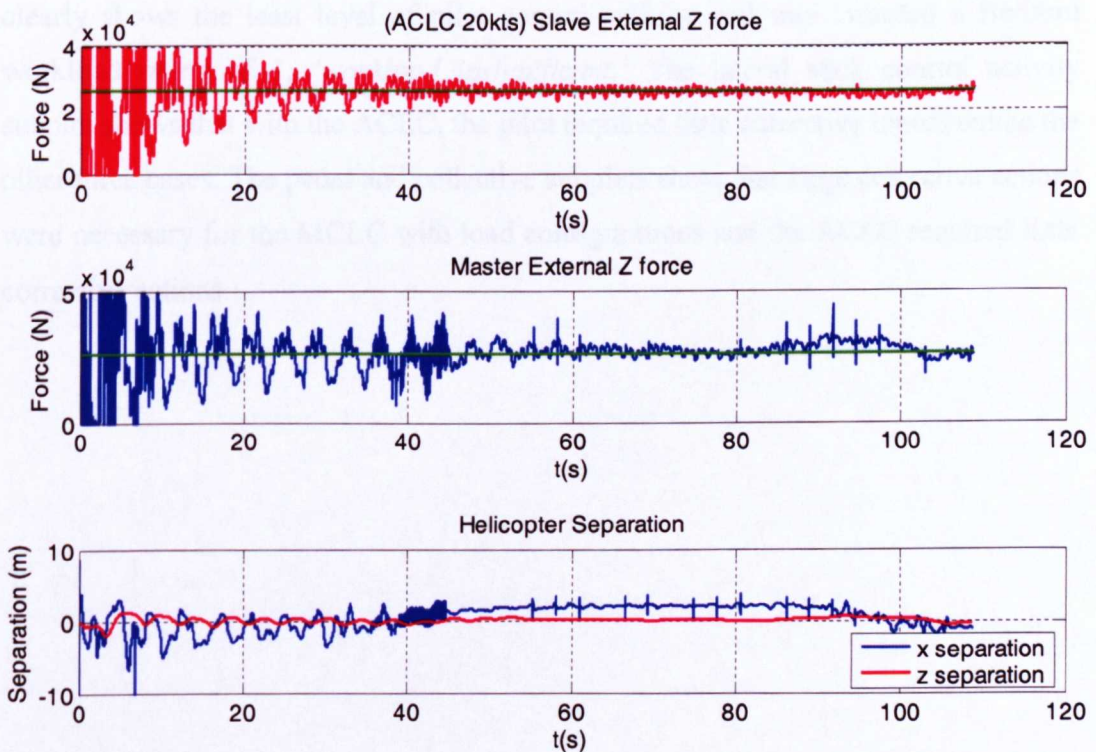
Using the relationship,  $F=ma$ , the acceleration caused by the spikes is approximately:

$$\frac{F}{m} = a = \frac{110000 \text{ N}}{142000 \text{ kg}} = 0.78 \text{ m/s}^2$$

If the acceleration is applied over one time step (0.0056s), then the applied velocity would be:

$$\text{velocity} = \text{acceleration} \times \text{time} = 0.78 \times 0.0056 = 0.0044 \text{ m/s}$$

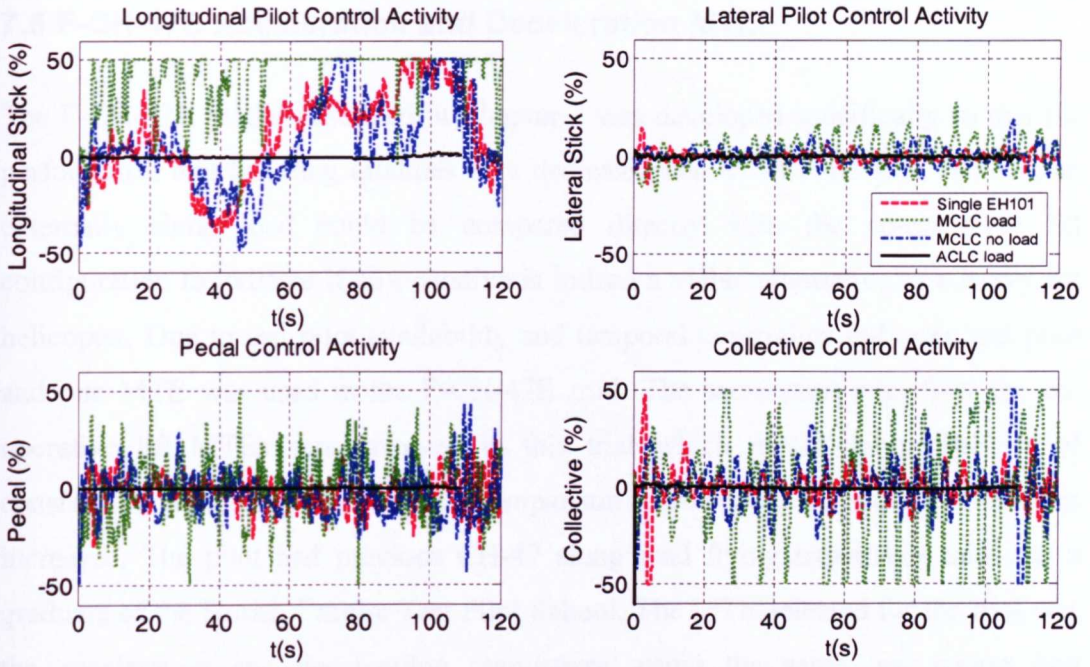
The effect of these force spikes on the trajectory of the helicopter can therefore be considered to be negligible. Figure 7.15 shows the Z forces fed back to the helicopters and the helicopter X and Z separation for the ACLC at 20 knots. Again, the green line indicates the nominal value that would be fed back in the hover condition. The Z force subplots for the master and slave helicopter are less noisy than those displayed in figure 7.14 with less data spikes and the force data correlates well with the nominal trim value. This may be because the separation between the helicopters throughout the manoeuvre is better maintained.



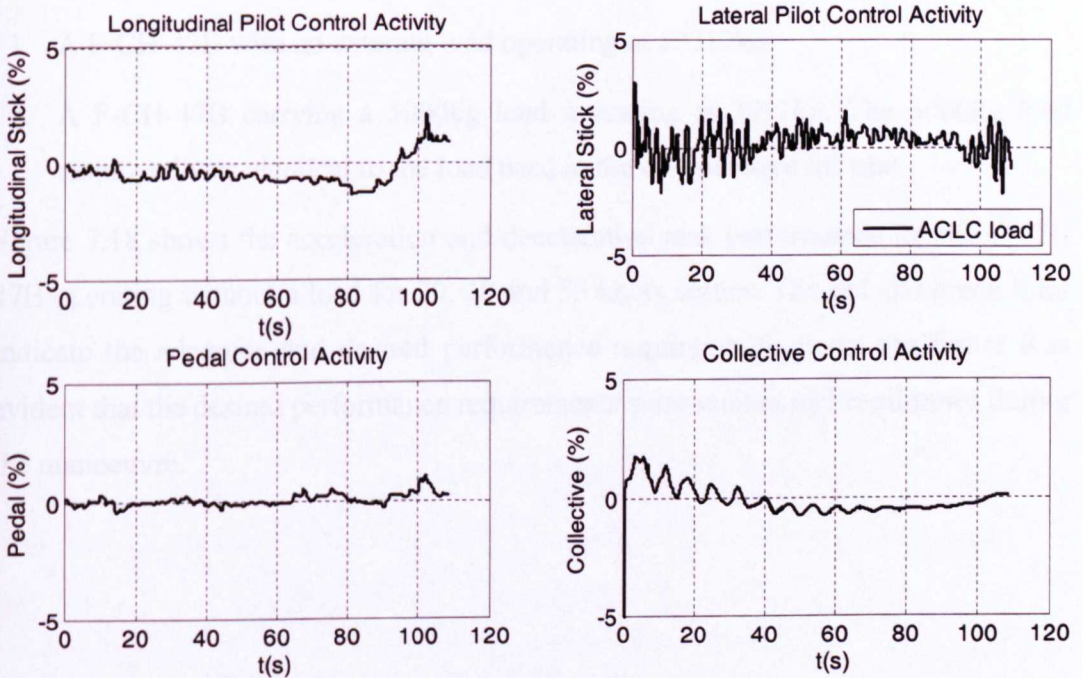
**Figure 7.15: External Z force for ACLC (20knots, 5000kg load)**

### 7.4.8 Control Activity

The pilot's control activity is a good indicator of the ease and precision with which a pilot is able to perform the desired task and it can also be proportional to the pilot workload with high stick activity usually correlating with high workload. Figure 7.16 shows the longitudinal stick, lateral stick, pedal and collective activity throughout the acceleration and deceleration MTE for the 20 knots sortie with the single helicopter, MCLC and ACLC with and without load. The longitudinal pilot control activity subplot shows that the highest control activity in terms of stick deflections occurred during the MCLC with load sortie. During the sortie, the pilot applied positive back stick which correlates with previous results that indicate the rear helicopter was indeed being 'pulled' along by the lead. The Bedford workload scale rating awarded to the sortie was 9; *'extremely high workload. No spare capacity.'* which correlates well with the high level of stick activity. The single EH-101 and MCLC without load configurations show similar levels of activity and were both awarded the same Bedford workload scale ratings of 4; *'insufficient spare capacity for easy attention for additional tasks.'* Figure 7.17 shows an isolated plot of the control activity for the ACLC with load sortie which is displayed in figure 7.16. The ACLC with load sortie clearly shows the least level of pilot control activity and was awarded a Bedford workload rating of 1, *'workload insignificant.'* The lateral stick control activity subplot shows that with the ACLC, the pilot required little corrective inputs unlike the other three cases. The pedal and collective subplots show that large corrective actions were necessary for the MCLC with load configurations and the ACLC required little corrective actions.



**Figure 7.16: Control activity during the 20 knots acceleration and deceleration MTE**



**Figure 7.17: Control activity during the 20 knots acceleration and deceleration MTE for the ACLC**

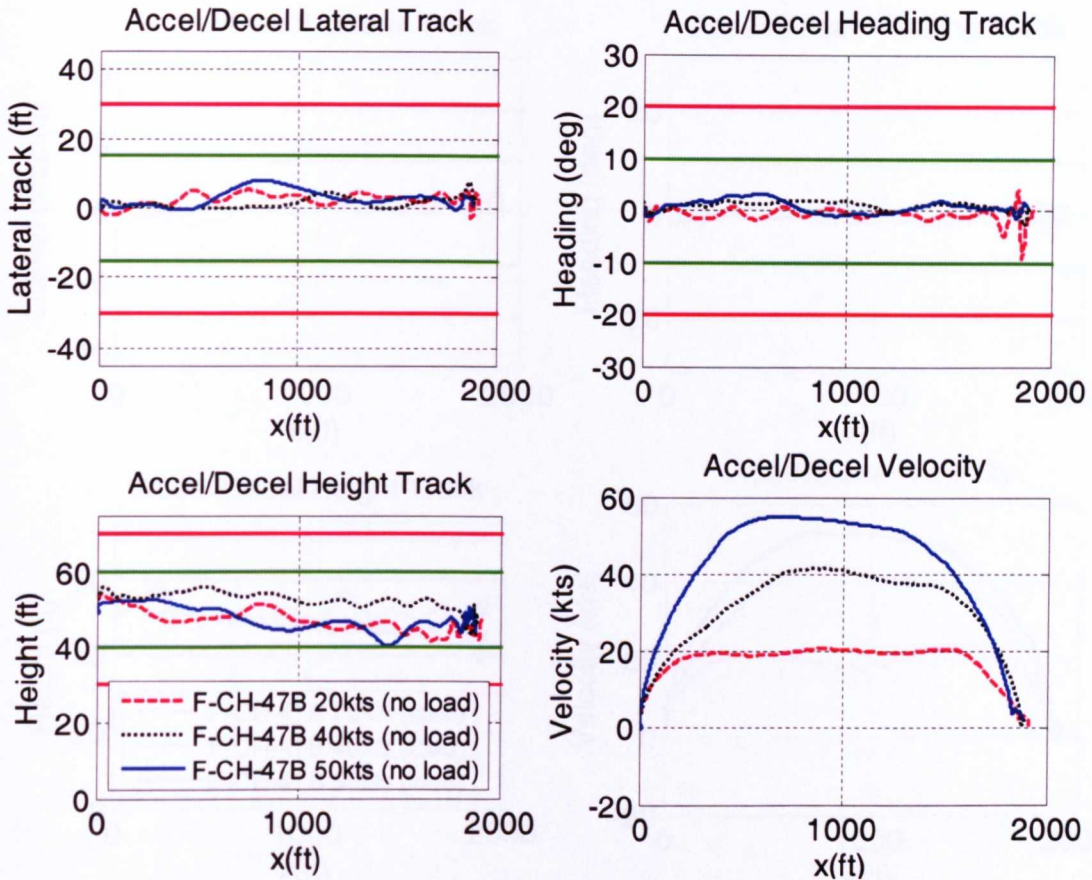
## 7.5 F-CH-47B Acceleration and Deceleration MTE

The F-CH-47B model described in Chapter 2 was developed specifically so that the performance and handling qualities of a dedicated heavy lift helicopter carrying an externally slung load could be compared directly with the co-operative lift configuration to indicate if co-operative is indeed a viable alternative to a heavy lift helicopter. Due to test pilot availability and temporal constraints only one test pilot and one MTE was used in the F-CH-47B trial. The same pilot who flew the co-operative lift MTEs was involved in this trial which meant the probability of consistent and meaningful ratings for comparison between the two configurations was increased. The pilot had previous CH-47 slung load flying experience and was a graduate of the British Empire Test Pilot School. The MTE selected for the trial was the acceleration and deceleration manoeuvre, using the same test course and performance requirements as the ones used for the previous co-operative lift trial. The ADS-33 requirements illustrated in figure 7.3 and table 7.1 were adopted. Two different F-CH-47B helicopter test configurations were flown in the trial:

1. A F-CH-47B with no external load operating at 12317kg.
2. A F-CH-47B carrying a 5000kg load operating at 7091kg. The 5000kg load employed was identical to the load used in the co-operative lift trial.

Figure 7.18 shows the acceleration and deceleration task performance for the F-CH-47B operating without a load for 20, 40 and 50 knots sorties. The red and green lines indicate the adequate and desired performance requirements. From the figure it is evident that the desired performance requirements were maintained at all times during the manoeuvre.

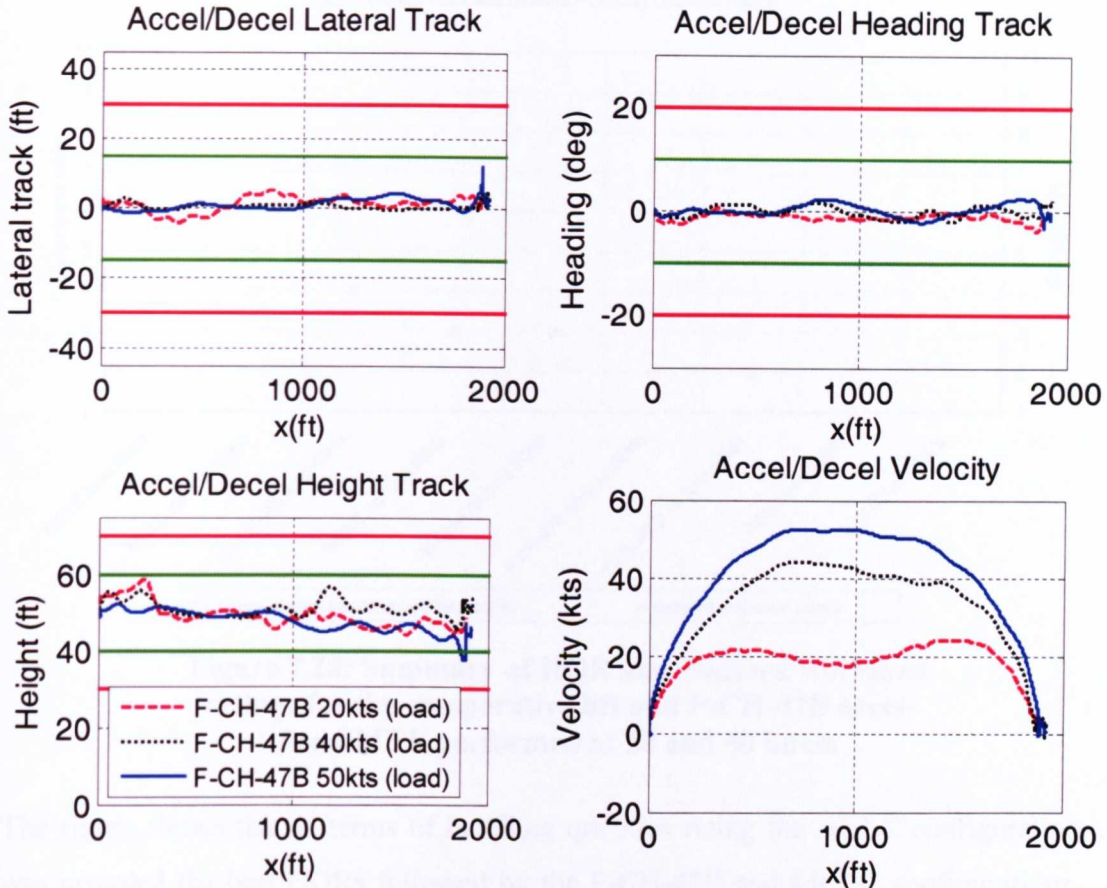




**Figure 7.18: F-CH-47B acceleration and deceleration MTE performance, no load**

The pilot awarded the three sorties HQRs of 2, 2 and 3 indicating Level 1 handling qualities and Bedford workload ratings of 2, 2 and 6. The pilot also commented that the simulation model was representative of the real aircraft. Figure 7.18 indicates that the pilot found height control most difficult which he attributed to a slightly over agile heave response.

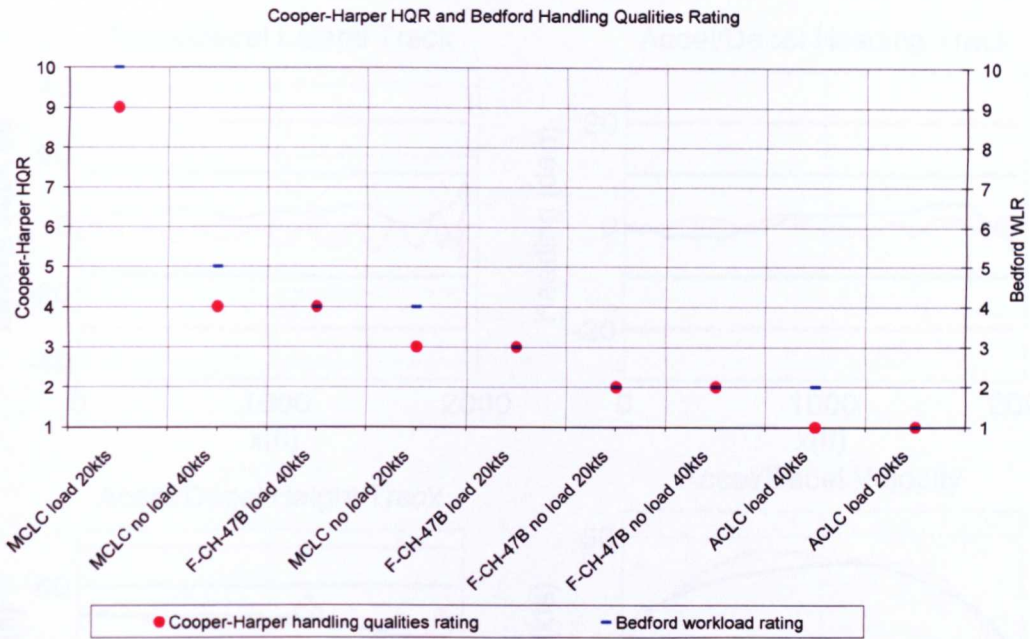
Figure 7.19 shows the acceleration and deceleration task performance for the F-CH-47B operating with a 5000kg load and 5m tether cable at 20, 40 and 50 knots.



**Figure 7.19: F-CH-47B acceleration and deceleration MTE performance, with load**

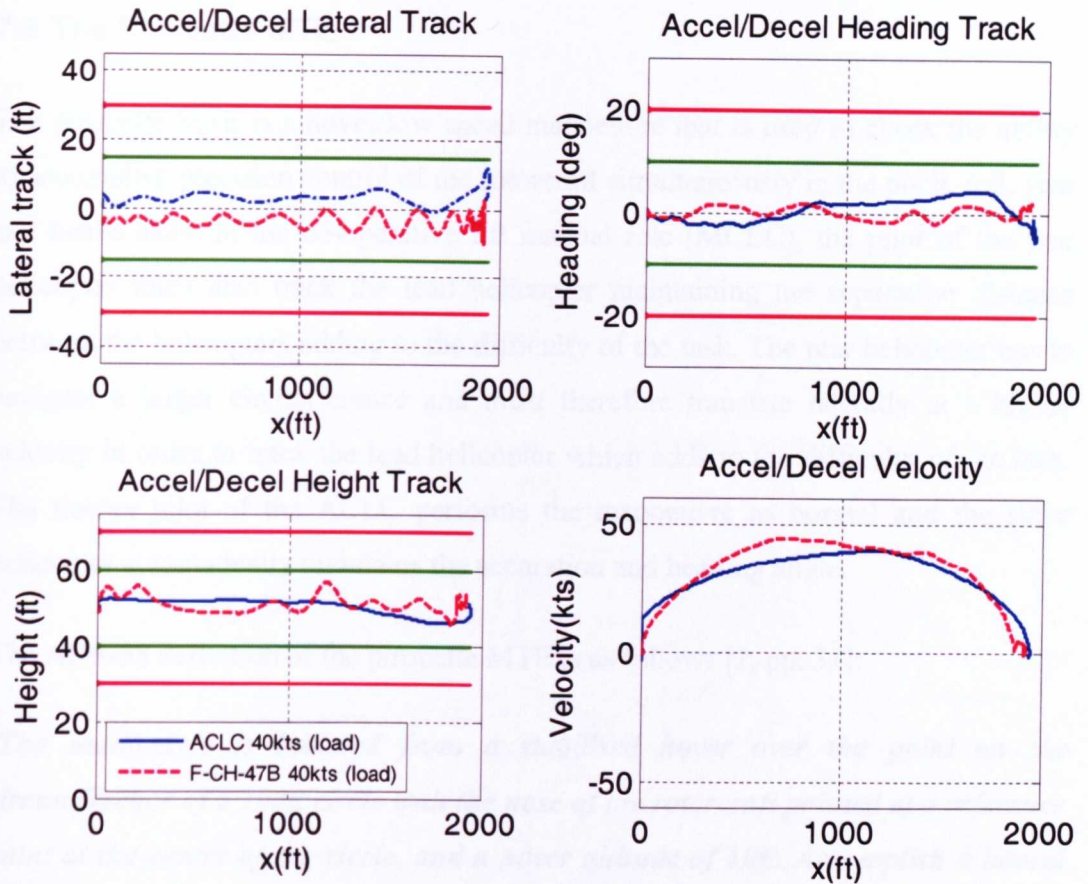
The pilot awarded HQRs of 3, 4 and 4 indicating that the addition of the external load did have a slight detrimental effect on the handling qualities of the F-CH-47B. There was one height excursion beyond the desired height requirement at the end of the manoeuvre during the high aggression 50 knots case. The pilot commented that speed control was also more difficult than the no load case due to the dynamics of the load and that he could ‘feel’ the external load dynamics through the motion cues of the simulator, which he felt in his experience was like a light load with poor lateral damping. The pilot awarded Bedford workload ratings of 3, 4 and 6 for each of the three speeds, indicating slightly higher workload than the previous no load case.

Figure 7.20 shows a summary of the HQR and Bedford workload ratings for the co-operative lift and F-CH-47 configurations for the 20 and 40 knots MTEs. The data points have been sorted into descending HQR order.



**Figure 7.20: Summary of HQR and Bedford workload ratings for the co-operative lift and F-CH-47B accel-decel MTE performed at 20 and 40 knots**

The figure shows that in terms of handling qualities rating the ACLC configuration was awarded the best HQRs followed by the F-CH-47B and MCLC configurations. Figure 7.21 shows the task performance plots for the ACLC and F-CH-47B for the 40 knots acceleration and deceleration MTE, both performed carrying the same 5000kg external load.



**Figure 7.21: ACLC and F-CH-47B acceleration and deceleration MTE performance (40kts 5000kg load)**

Figures 7.20 and 7.21 indicate that for the acceleration and deceleration test case considered, the ACLC is a viable alternative to a dedicated heavy lift cargo helicopter such as the CH-47 when considering the handling qualities, task performance and pilot workload achieved. However, more MTEs would have to be performed over a wider flight envelope to conclusively prove that the co-operative lift could replace heavy lift operations.

## 7.6 The Pirouette MTE

The pirouette MTE is a hover/low speed manoeuvre that is used to check the ability to accomplish precision control of the rotorcraft simultaneously in the pitch, roll, yaw and heave axes. In the co-operative lift manual role (MCLC), the pilot of the rear helicopter must also track the lead helicopter maintaining the separation distance between the helicopters adding to the difficulty of the task. The rear helicopter has to navigate a larger circumference and must therefore translate laterally at a higher velocity in order to track the lead helicopter which adds to the difficulty of the task. The master pilot of the ACLC performs the manoeuvre as normal and the slave helicopter automatically maintains the separation and heading angle.

The ADS-33 definition of the pirouette MTE is as follows [2, pp. 31]:

*'The manoeuvre is initiated from a stabilised hover over the point on the circumference of a 100ft circle with the nose of the rotorcraft pointed at a reference point at the centre of the circle, and a hover altitude of 10ft. Accomplish a lateral translation around the circle, keeping the nose of the rotorcraft pointed at the centre of the circle and the circumference of the circle under a selected point on the rotorcraft. Maintain essentially constant lateral groundspeed throughout the lateral translation. Terminate the manoeuvre with a stabilised hover over the starting point.'*

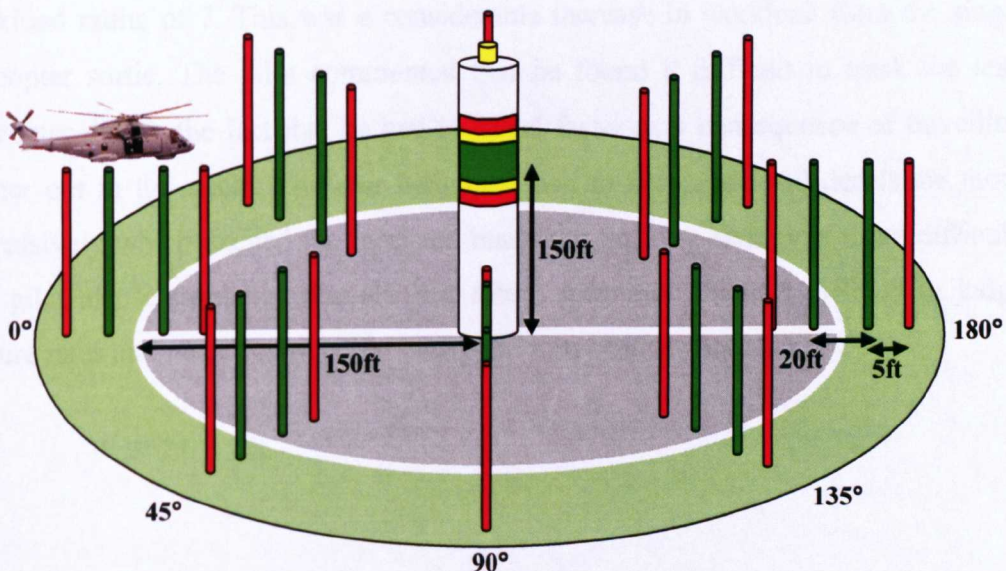
The ADS-33 MTE description above is aimed at a conventional helicopter operating without a slung load; consequently, the spatial dimensions had to be adapted to accommodate the large co-operative lift configuration. The manoeuvre height was changed to 150ft and the circumference of the circle enlarged to 150ft. The pirouette MTE is inherently difficult to perform in the HELIFLIGHT simulator due to the limited field of view both laterally and vertically. The increase in manoeuvre height added to the visual problem as the view out of the chin windows did not show what was directly below the rotorcraft and a simple circle on the ground could not be used as a visual cue. In a similar fashion to the previous acceleration and deceleration MTE, the problem was overcome to an extent by adding extra visual cues to the visual simulation environment that would help the pilot to distinguish the correct

circular track and desired and adequate performance standards. The extra visual cues consisted of: 120ft vertical coloured pole markers spaced at 45 degrees around the circumference of the circle to show the desired and adequate circumferential track limits, a lighthouse structure in the centre of the circle complete with coloured bands to help with the heading and height performance and white lines on the ground at 90 degree intervals to help the pilot determine where on the circle he was at any time. ADS-33 states a complete circle must be carried out, however because the course was enlarged this was deemed unnecessary and the pilot was only required to completed half of the circle. Table 7.2 below shows the desired and adequate performance requirements

**Table 7.2: ADS-33 desired and adequate performance requirements**

	Desired	Adequate
<b>Maintain a selected reference point on the helicopter within +/- X ft of the circumference of the circle</b>	10ft	15ft
<b>Maintain heading so that the nose of the helicopter points at the centre of the circle within +/- X deg</b>	10 deg	15 deg
<b>Altitude +/-</b>	10ft	15ft

Figure 7.22 shows the test course used for the pirouette MTE with the lighthouse at the centre of the circle and the vertical poles at every 45 degrees outlining the circumference of the circle.



**Figure 7.22: Pirouette MTE course**

### **7.6.1 The MTE Test Conditions**

The pirouette MTE was performed using three different helicopter configurations, similar to those used in the previous acceleration and deceleration MTE:

1. A single EH-101 with base AFCS.
2. The manual co-operative lift configuration with 5000kg load (MCLC load)
3. The automatic co-operative lift configuration with 5000kg load (ACLCL load)

After each manoeuvre, the pilot awarded the sortie with a Cooper-Harper HQR and Bedford workload rating using the 'in-cockpit pilot questionnaire' (Appendix 3).

### **7.6.2 Single Helicopter Results**

Due to the time constraints, only one single helicopter sortie was completed. The helicopter position data were recorded and later used to drive the lead helicopter in the MCLC configuration. The pilot awarded the single EH-101 with baseline SCAS a Cooper-Harper HQR and Bedford workload rating of 5. He commented that the visual cues available were not sufficient and did impact the performance of the sortie.

### **7.6.3 MCLC Load Results**

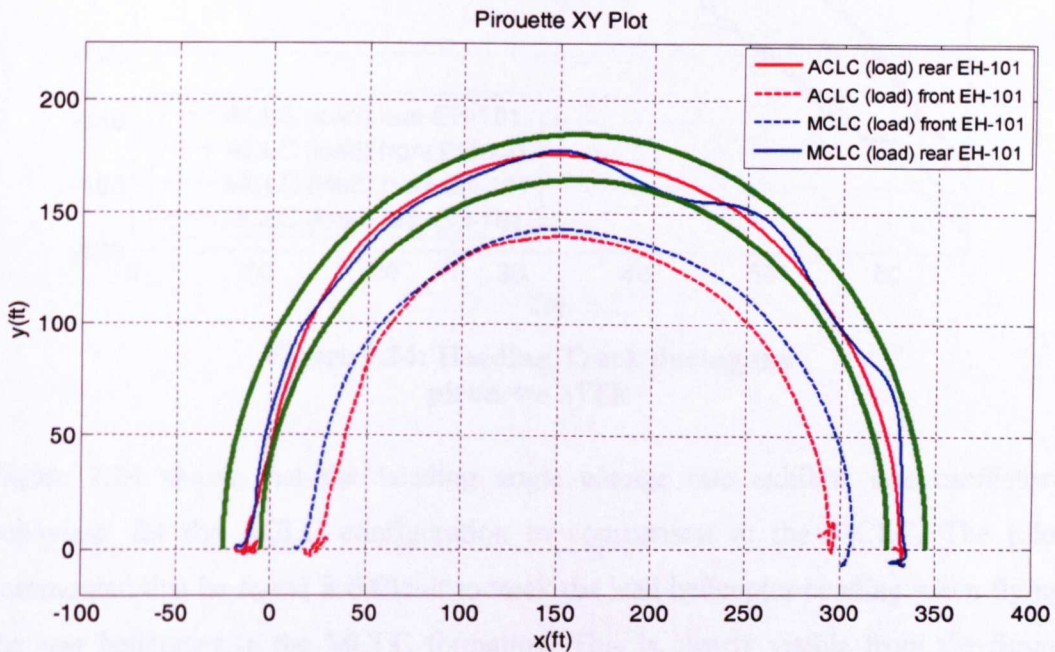
The pilot awarded the MCLC sortie a Cooper-Harper HQR of 6 and Bedford workload rating of 7. This was a considerable increase in workload from the single helicopter sortie. The pilot commented that he found it difficult to track the lead helicopter due to the fact that he had to travel faster as a consequence of travelling further out in the circle. The rear helicopter had to accelerate and decelerate more aggressively which excited the load and made the tracking task even more difficult. The pilot also commented that the line astern formation made it difficult to judge closure rates and made forward and backward movements very tricky.

### 7.6.4 ACLC Load Results

The pilot flew the rear helicopter in the ACLC with the front helicopter in automatic slave mode. The ACLC significantly improved the handling qualities and reduced the pilot workload and the pilot awarded a Cooper-Harper HQR and Bedford workload rating of 2. The main problem with the ACLC configuration was the limited field of view available to the pilot. The pilot commented that having to continuously ignore the lead helicopter which had different motions due to the ACLC controller being active was very disconcerting.

### 7.6.5 Task Performance

Figure 7.23 shows an XY plot of the MCLC and ACLC throughout the manoeuvre.

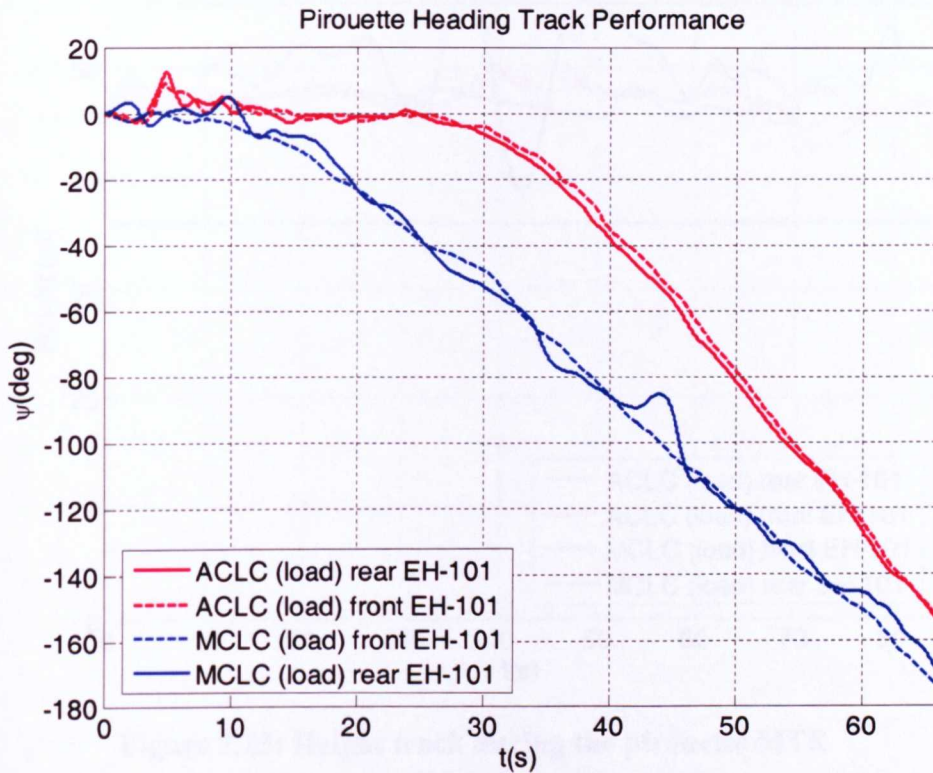


**Figure 7.23: XY plot during the pirouette MTE**

The figure shows the half of the pirouette course that was completed by the pilot. The MCLC and ACLC configuration results are displayed in blue and red respectively and the rear and front helicopters in the formation are illustrated in solid and dashed line styles respectively. The green lines indicate the circumferential track requirements for desired performance for the rear helicopter. From the figure it is evident that the ACLC tracked the course much better than the MCLC. The MCLC



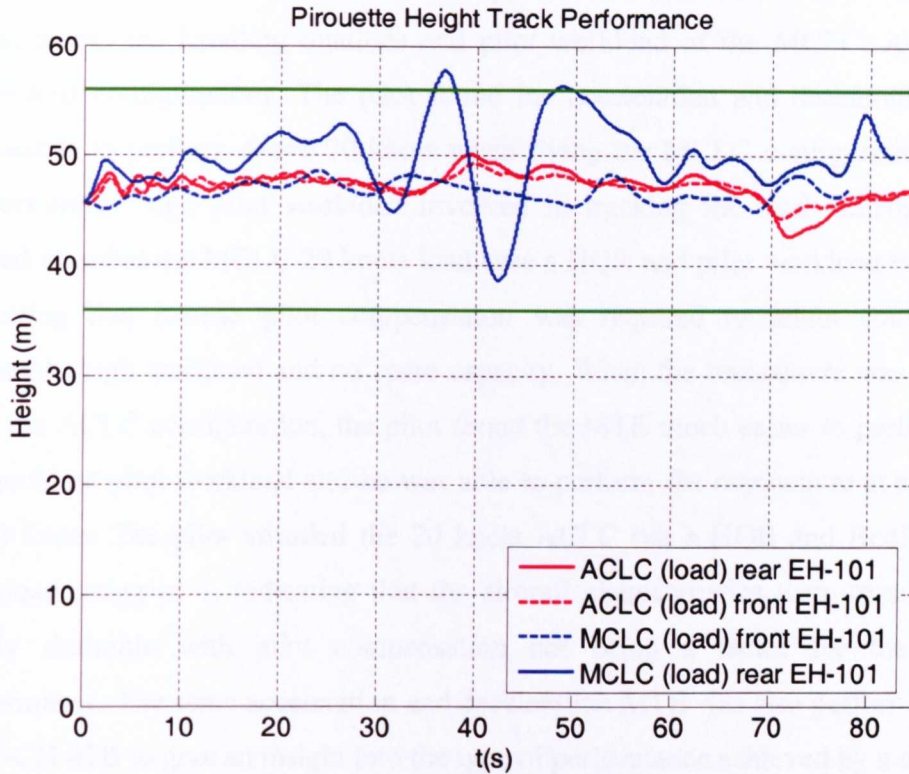
configuration remained within the desired requirements throughout the manoeuvre but oscillated about the desired requirements on two occasions. Figure 7.24 shows the heading angle variation for the front and rear helicopters in the MCLC and ACLC configurations with time.



**Figure 7.24: Heading Track during the pirouette MTE**

Figure 7.24 shows that the heading angle change rate exhibits less oscillatory behaviour for the ACLC configuration in comparison to the MCLC. The pilot commented that he found it difficult to track the lead helicopter heading when flying the rear helicopter in the MCLC formation. This is clearly visible from the figure which shows oscillatory behaviour. The figure also shows that the pilot was able to perform the manoeuvre a lot quicker with the ACLC configuration indicating that the ACLC did not only improve the task performance in terms of performance requirements and pilot workload but also gave the pilot increased confidence to carry out the MTE quicker.

Figure 7.25 shows the height track for the front and rear helicopters of the MCLC and ACLC configurations during the pirouette MTE.



**Figure 7.25: Height track during the pirouette MTE**

Figure 7.25 indicates that the ACLC configuration tracked the target height the best with a maximum height excursion of  $-5\text{m}$ . The front slave helicopter in the ACLC configuration tracked the rear helicopter extremely well with the largest height difference equal to  $2\text{m}$ . In contrast, the front helicopter in the MCLC configuration did not track the target height as effectively and the pilot found tracking the lead helicopter very difficult as indicated by the oscillatory nature of the line representing the rear helicopter. The rear helicopter in the MCLC made two excursions beyond the desired performance levels during the manoeuvre.

## 7.7 Conclusions to Chapter

This chapter described the three ADS-33 piloted simulation trials that were carried out to assess the handling qualities and pilot workload of the MCLC, ACLC and F-CH-47B configurations. The pilot found the acceleration and deceleration MTE impossible to perform above 20 knots when flying the MCLC configuration due to the extremely high pilot workload involved in tracking the lead helicopter. The pilot awarded the MCLC 20 knots load case a HQR and pilot workload rating of 9 indicating that intense pilot compensation was required to retain control with extremely high workload and no spare capacity. When the manoeuvre was repeated with the ACLC configuration, the pilot found the MTE much easier to perform with insignificant pilot workload and he was able to perform the manoeuvre at speeds up to 50 knots. The pilot awarded the 20 knots ACLC run a HQR and Bedford pilot workload rating of 1, indicating that the aircraft characteristics were excellent and highly desirable with pilot compensation not being a factor for the desired performance. The same acceleration and deceleration MTE was also performed using the F-CH-47B to give an insight into the type of performance achieved by a dedicated heavy lift helicopter in comparison to a co-operative lift configuration. The pilot awarded the F-CH-47B 20 knot sortie a HQR and Bedford workload rating of 3 indicating that the performance achieved was worse than the ACLC but better than MCLC demonstrating that an ACLC configuration could be used in place of a heavy lift helicopter. This was for one sample MTE and more MTEs over a wider flight envelope would be required to determine if co-operative lift operations could be used to replace heavy lift helicopters.

The pilot found that the pirouette manoeuvre was difficult to perform with the MCLC load configuration and awarded a HQR and Bedford workload rating of 6 and 7 respectively. These ratings indicated very objectionable but tolerable deficiencies with adequate performance requiring extensive pilot compensation. The fact that the rear helicopter in the formation had to travel a circumferentially larger distance meant that the rear helicopter had to translate with larger velocities making the tracking task even more difficult. The pilot awarded the ACLC sortie a HQR and Bedford workload rating of 2 with negligible deficiencies and low workload. The pilot

recommended that the formation adopted for the co-operative lift configuration should be changed from a tandem inline formation used in the trials to an echelon configuration with a lateral offset between the two helicopters. This would provide the rear pilot in the formation better visual cues and reduce the likelihood of the front helicopter motion distracting the pilot. In both trials the pilot commented that the motion cues helped the co-operative lift simulation task.

## Chapter 8

### CONCLUSIONS AND RECOMMENDATIONS

The objective of this research was to take a holistic view of helicopters operating external loads and investigate new ways of expanding the operational effectiveness of such configurations. Several helicopter slung load models were developed in the course of the research to meet this objective including the FGR, F-CH-47B and EH-101 co-operative lift configuration.

The FGR model was used to investigate what effects the addition of the external load had on the handling qualities and stability of the helicopter. The investigation indicated that the external load changed the natural frequency and modal shapes of the helicopter's low frequency modes and introduced two additional rigid body modes which represented the longitudinal and lateral rotational degrees of freedom. The external load increased the stability of the phugoid mode and decreased the stability of the Dutch roll mode. The stability of the longitudinal and lateral load modes decreased and increased respectively as the helicopter airspeed was increased and the general stability of the load modes was dependent on the particular permutation of tether cable length and load mass. The ADS-33 hover board piloted simulation trial of the FGR indicated that the external load did not adversely affect the low speed pilot handling qualities. In fact, the pilot commented that he felt the addition of the load improved the low speed handling qualities due to a perceived increase in the system damping.

The FGR model was also used to examine the effect of conventional classical feedback control and more modern multi-objective control systems on the helicopter handling qualities and external load stability and dynamics. Linear analysis indicated that helicopter pitch attitude feedback was found to have a negligible effect on the stability of the external load, whilst feeding back the pitch rate did increase the load damping by a small amount. The multi objective  $H_\infty$  system developed successfully

stabilised the sling angle rate as intended and gave an ACAH response type. The  $H_\infty$  system was compared to a PI system that gave a similar steady state response and it was discovered that the pitch attitude quickness of the  $H_\infty$  system was almost half that of the PI system. This indicated that the extra load stability came at the cost of a reduction in the helicopter agility as expected.

The EH-101 co-operative lift model was developed using a novel distributed simulation technique that involved significant software and hardware modifications to the existing HELIFLIGHT simulator architecture. The result was a distributed simulation system that could simulate multiple helicopters and external loads in real-time for piloted simulation using the motion simulator. The EH-101 co-operative lift model was successfully verified against another model developed by Westland Helicopters using an entirely different modelling approach. A data communication link between the helicopters in the configuration was modelled so that control and positional data could be passed in both directions for the ACLC. The ACLC that was developed featured several novel features including separation and flight formation maintenance control. The issue of flight certification was also addressed using the recommendations from a GARTEUR group established to investigate new and improved analysis techniques of flight control laws. The complete clearance of the ACLC inner loop using all the recommended industrial criteria was not feasible during the research due to the limited time and resources available. The ACLC did however pass a small representative set of criteria using the stability margin and unstable eigenvalue criterion and was also developed using classical control theory to improve the likelihood of the control system passing the CAA flight certification process. The ACAH inner loop of the ACLC achieved Level 1 handling qualities for the ADS-33 small, moderate and large amplitude criteria, for all mission task elements with the exception of target acquisition and tracking. The tau based separation maintenance gap closure control system showed some promise in the desktop analysis performed and it is recommended that this be pursued more in the future and tested using piloted simulation.

Two piloted simulation trials of the EH-101 co-operative lift model were conducted using the ADS-33 acceleration and deceleration and pirouette MTEs. The trials indicated that manual co-operative operations lift using two helicopters with traditional AFCS was not feasible due to the extremely high pilot workload involved in tracking the lead helicopter of the coupled system. The pilot awarded the manual acceleration and deceleration MTE a HQR and Bedford workload rating of 9 indicating that intense pilot compensation was required to retain control with extremely high workload and no spare capacity. When the same manoeuvre was repeated using the ACLC, the pilot awarded a HQR and Bedford workload rating of 1 indicating that the aircraft characteristics were excellent and highly desirable with insignificant workload. This meant that the ACLC system significantly improved the co-operative lift handling qualities from the Level 3 to Level 1 region. The pilot was able to perform the acceleration and deceleration at speeds up to 50 knots corresponding to very high aggression and still rated the configuration with a HQR and Bedford workload rating of 3. The pilot suggested that the co-operative lift configuration should be flown in echelon formation rather than the in-line tandem formation that was adopted for the trials so that the pitch attitude of the lead helicopter could be better judged. The pilot found the pirouette MTE much easier to perform with the ACLC in comparison to the manual configuration. The rear helicopter in the twin-lift formation had to travel a circumferentially larger distance during the pirouette which meant that the rear helicopter also had to translate quicker than the lead helicopter to maintain formation which added to the difficulty of the tracking task. The pilot awarded the manual configuration a HQR and Bedford workload rating of 6 and 7 respectively. This indicated very objectionable but tolerable deficiencies with little spare capacity. In contrast the pilot awarded the ACLC configuration with a HQR and Bedford workload rating of 2 with negligible deficiencies and low workload.

The F-CH-47B Chinook model was developed specifically so that the EH-101 co-operative lift model could be compared with a dedicated heavy lift helicopter by means of piloted simulation using the HELIFLIGHT simulator. The F-CH-47B non-linear response and stability derivatives correlated well with the NASA simulation model upon which it was based. Due to time and financial constraints only one ADS-

33 MTE was performed using the F-CH-47B: the acceleration and deceleration manoeuvre. The pilot awarded the 20 knot sortie a HQR and Bedford workload rating of 3 indicating that the performance achieved was better than the manual co-operative lift configuration but worse than the ACLC. The trial demonstrated that if effective co-operative lift operations were to be adopted and used in place of dedicated heavy lift cargo helicopters, then a level of control augmentation similar to the ACLC would be required. More analysis and MTEs would have to be performed before one could definitively agree that co-operative lift could replace or at least support dedicated heavy lift helicopters but the work completed in this thesis certainly supports this outlook.

Recommendations for future work include developing the tau based separation gap closure controller and separation cue HUD further. The separation cue HUD in particular is something that is practical and relatively easy to implement and test. The pilot commented during the co-operative lift trials that it was very difficult to judge the correct longitudinal, lateral and vertical separation from the other helicopter and the extra cues from the HUD concept would greatly aid the pilot in this area.

The ACLC developed in this thesis did not consider the effect of uncertainties from modelling approximations, sensors errors and data link latency due to time constraints imposed by the piloted simulation trials. This is one area that would have to be revisited before any flight test phase to examine the robustness and performance of the controller in more detail.

This research did not consider the complex problem of vortex wake interaction between the helicopters in the configuration or the interaction of the vortex wake on the spreader bar or the load. The modelling of these aerodynamic interactions using computational fluid dynamics (CFD) would be extremely useful before any flight test phase to predict any interference effects and it is strongly recommended that this area of research be followed up in a future project.



## References

- [1] Kendrick, S. A. and Walker, D. J., "The Modelling Simulation and Control of Helicopters Operating With External Loads," *proceedings of the 62nd American Helicopter Society Annual Forum*, Vol. 2, pp. 1022-1035, Phoenix, Arizona, USA, 2006.
- [2] Anon., "Aeronautical Design Standard-33E-PRF: Performance Specification Handling Qualities Requirements for Military Rotorcraft," *US Army AMCOM, Design Standard Report*, Redstone, Alabama, USA, March 21, 2000.
- [3] Lee, D. N., "The Optic Flow-field: The Foundation of Vision," *Philosophical Transactions of the Royal Society of London, Series B, Biological Sciences*, Vol. 290, Issue 1038, pp. 169-179, 1980.
- [4] Lucassen, L. R. and Sterk, F. J., "Dynamic Stability Analysis of a Hovering Helicopter With A Sling Load," *Journal of the American Helicopter Society*, Vol. 10, pp. 6-12, 1965.
- [5] Szustak, L. S. and Jenny, D., "Control of Large Crane Helicopter," *Journal of the American Helicopter Society*, Vol. 16, pp. 11-12, 1971.
- [6] Dukes, T. A., "Manoeuvring Heavy Sling Loads Near Hover, Part 1: Damping the Pendulous Motion," *Journal of the American Helicopter Society*, Vol. 18, pp. 11-22, 1973.
- [7] Poli, C. and Cromack, D., "Dynamics of Slung Bodies Using a Single-Point Suspension System," *AIAA, Journal of Aircraft*, Vol. 10, pp. 80-86, 1973.
- [8] Cliff, E. M. and Bailey, D. B., "Dynamic Stability of a Translating Vehicle with a Simple Sling Load," *AIAA, Journal of aircraft*, Vol. 12, pp. 773-777, 1975.
- [9] Feaster, L., "Dynamics of a Slung Load," *Master Thesis*, Massachusetts University, 1975.
- [10] Feaster, L., Poli, C., and Kirchhoff, R., "Dynamics of a Slung Load," *AIAA Journal of Aircraft*, Vol. 14, pp. 115-121, 1977.
- [11] Prabhakar, A. and Sheldon, D., "Dynamic Stability of a Helicopter Carrying an Underslung Load," *Royal Military College of Science, Department of Mechanical Engineering*, Technical Note RCMS TN-AM-78, 1976.
- [12] Prabhakar, A., "Stability of a Helicopter Carrying an Underslung Load," *Vertica*, Vol. 2, pp. 121-143, 1978.

- [13] Nagabhushan, B. L., "Systematic Investigation of Models of Helicopter with a Slung Load," *Master Thesis*, Virginia Polytechnic Inst. and State University, VA, 1977.
- [14] Nagabhushan, B. L., "Low-Speed Stability Characteristics of a Helicopter with a Sling Load," *Vertica*, Vol. 9, pp. 345-361, 1985.
- [15] Nagabhushan, B. L., Cliff, E., "Manoeuvred Stability of a Vehicle with a Towed Body," *proceedings of the 9th AIAA Atmospheric Flight Mechanics Conference*, paper 9, San Diego, California, 1982.
- [16] Cicolani, L. S., and Kanning, G., "Equations of motion of Slung Load Systems with Results for Dual Lift," *NASA TM 102246*, February 1990 (accessed via the NASA technical report server).
- [17] Cicolani, L. S., McCoy, A. H., Tischler, M. B., Tyson, P.H., "Flight Test Identification and Simulation of a UH-60A Helicopter and Slung Load," *Technical report, NASA/TM-2001-209619*, USAAMCOM-TR-01-A-001, (accessed via the NASA technical report server).
- [18] Stuckey, R. A., "Mathematical Modelling of Helicopter Slung-Load Systems," *Technical Report*, Aeronautical and Maritime Research Laboratory, Australia, 2001, (accessed via [www.dsto.defence.gov.au](http://www.dsto.defence.gov.au)).
- [19] Bisgaard, M., Bendtsen, J. D., and Cour-Harbo., "Modelling of Generic Slung Load System," *proceedings of the AIAA Modelling and Simulation Technologies Conference and Exhibit*, paper code: AIAA 2006-6816, Keystone, Colorado, USA, 2006.
- [20] Gabel, R. and Wilson, G., "Test Approaches to External Sling Load Instabilities," *Journal of the American Helicopter Society*, Vol. 3, pp. 44, 1968.
- [21] Hone, H., "Flight Load Investigation of Helicopter External Loads," *Technical Report*, U.S. Army Air Mobility Research and Development Laboratory 1975, (accessed via <http://stinet.dtic.mil>).
- [22] Briczinski, S. and Karas, G., "Criteria for Externally Suspended Helicopter Loads," *U.S. Army Air Mobility Research and Development Laboratory*, USA AMRDL-TR-71-61, 1971, (accessed via <http://stinet.dtic.mil>).
- [23] Hamers, M., "Flight Director for Handling of Helicopter Sling Loads," *proceedings of the 31st European Rotorcraft Forum*, paper 119, Florence, Italy, 2005.
- [24] Sheridan, P. F., "Feasibility Study for Multiple Helicopter Heavy Lift Systems," *Vertol Aircraft Corporation*, Report. R-136, 1957.
- [25] Curtiss, H. C., Jr and Warburton F.W., "Stability and Control of The Twin Lift Helicopter System," *Journal of the American Helicopter Society*, Vol. 30, pp. 14-23, 1985.

- [26] Rodriguez, A. and Athans, M., "Multivariable Control of a Twin Lift Helicopter System Using the LQG/LTR Design Methodology," *NASA Ames and Langley Research Centre, Laboratory for Information and Decision Systems, Massachusetts Institute of Technology*, April 1986, (accessed via <http://ntrs.nasa.gov/search.jsp>).
- [27] Hess R. A., Tran. P. M., "Pilot/Vehicle Analysis of a Twin – Lift Helicopter Configuration in Hover", *AIAA, Journal of Guidance*, Vol. 11, pp. 465-472, 1988.
- [28] Menon, P. K. A., Prasad J. V. R., and Schrage D. P., "Nonlinear Control of a Twin-Lift Helicopter Configuration," *AIAA, Journal of Guidance*, Vol. 14, No. 6, pp. 1287-1293, 1991.
- [29] Reynolds, H., K. and Rodriguez, A., "H-infinity Control of a Twin Lift Helicopter System," *proceedings of the 31st IEEE Conference on Decision and Control*, Tucson, Arizona, USA, pp. 2442-2447, 1992.
- [30] Mittal, M., Prasad. J. V. R., "Three dimensional Modelling and Control of a Twin-Lift Helicopter System," *AIAA, Journal of Guidance*, Vol. 16, No. 1, pp. 86-95, 1993.
- [31] Meier, W. H. and Olson, J. R., "Efficient Sizing of a Cargo Rotorcraft," *AIAA, Journal of Aircraft*, Vol. 25, pp. 538-543, 1987.
- [32] Stepniewski, W. Z., "Factors Shaping Conceptual Design of Rotary Wing Aircraft," *presented at the 37th American Helicopter Society Annual Forum*, New Orleans, LA, USA, 1981.
- [33] Du Val, R. W., "A Real-Time Multibody Dynamics Architecture For Rotorcraft Simulation," *proceedings: The Challenge of Realistic Rotorcraft Simulation*, pp. 9.1-9.12, London, UK, 2001.
- [34] Prouty, W.P, *Helicopter Performance, Stability and Control*, First Edition, Krieger Publishing Company, 1995.
- [35] Howlett, J. J., "UH-60A Black Hawk engineering simulation program: Volume I," NASA CR-166309, 1981, (accessed via <http://ntrs.nasa.gov/search.jsp>).
- [36] Bailey, F. J., "A Simplified Theoretical Method of Determining the Characteristics of a Lifting Rotor in Forward Flight.," NACA report 716, 1941, (accessed via <http://ntrs.nasa.gov/search.jsp>).
- [37] Peters, D. A. and He, C. J., "Finite State induced flow models Part II, Three dimensional rotor disc," *AIAA, Journal of Aircraft*, Vol. 2, pp. 323-333, 1995.
- [38] Weber, J. M., Tung, Y. L., and Chung, W., "A Mathematical Simulation Model of a CH-47B Helicopter," *NASA Ames Research Centre*, Vol. 1 & 2, M. F. C., Ed., 1984, (accessed via <http://ntrs.nasa.gov/search.jsp>).

- [39] Yamakawa, G. A. and Miller, L. G., "Airworthiness and Qualification Test, Phase D, CH-47B," *Army Aviation Systems Test Activity Edwards AFB CA*, pp. 66-23, 1970, (accessed via <http://stinet.dtic.mil>).
- [40] Albion, N., Leet, J. R., and Mollenkof, A., "Ground Based Simulation of CH-47C Helicopter," Boeing Company, Vertol Division D8-2418-1, 1969, (accessed via <http://stinet.dtic.mil>).
- [41] Padfield, G. D. and White, M. D., "Flight Simulation in Academia; HELIFLIGHT in it's First Year of Operation," *The Aeronautical Journal of the Royal Aeronautical Society*, Vol. 107, pp. 529-538, 2003.
- [42] Cooper, G. E., and Harper, R. P. Jr., "The Use of Pilot Ratings in the Evaluation of Aircraft Handling Qualities," NASA TM D-5133, 1969, (accessed via <http://stinet.dtic.mil>).
- [43] Woomer, C.W. and Williams, R.L., "Environmental Requirements for Simulated Helicopter/VTOL Operations from Small Ships and Carriers," *Piloted Simulation Techniques*, AGARD-CP-249, Paris, Advisory Group on Aerospace Research and Development, 1978.
- [44] Rolfe, J. M. and Staples, K. J., *Flight Simulation*, Cambridge Aerospace Series, Cambridge University Press, ISBN 0 521 3751 9.
- [45] Hosman, R. J. A. W., and van der Vaart, J.C., "Thresholds of Motion Perception and Parameters of Vestibular Models Obtained from Test in a Motion Simulator. Effects of Vestibular and Visual Motion Perception on Task Performance.," *Memorandum M-372*. Delft University: Technishce Hogeschool Delft.
- [46] Padfield, G. D., *Helicopter Flight Dynamics: The Theory and Application of Flying Qualities and Simulation Modelling*, AIAA Educational Series, 1996.
- [47] Key, D. L., "Handling Qualities Specifications for U.S. Military Helicopters", AIAA, *Journal of Aircraft*, Vol. 19, No. 2, pp.138-144, 1982.
- [48] Ockier C. J., "Evaluation of the ADS-33D Handling Qualities Criteria Using the BO 105 Helicopter," German Aerospace Centre Report, 1998.
- [49] Tyson, P. H., Cicolani, L. S., Tischler, M. B., et al, "Simulation Prediction and Flight Validation of UH-60A Black Hawk Slung-Load Characteristics," *presented at the 55th American Helicopter Society Annual Forum*, 1999.
- [50] Stevens, B. L., Lewis, F. L, *Aircraft Control and Simulation*, John Wiley and Sons, Inc., Second Edition, ISBN 0-471-37145-9.
- [51] Bolton, W., *Control Systems*, Newnes, 2002, ISBN 0-7506-5461-9.
- [52] Walker, D. J., "Multivariable control of the longitudinal and lateral dynamics of a fly-by-wire helicopter," *Control Engineering Practice Journal*, Vol. 11, pp. 781-795, 2002.

- [53] Postlethwaite, I., Smerlas, A., Walker D.J., Gubbels A.W., and Baillie S.W., S. M. E., Howitt J., Horton R.I., " $H_\infty$  control: From desk-top design to flight test with handling qualities evaluation," *proceedings of the 54th Annual Forum American Helicopter Society*, pp. 1313-1324, 1998.
- [54] Simon, D., *Optimal State Estimation: Kalman,  $H_\infty$  and Non-linear Approaches*, John Wiley and Sons, 2006, ISBN 978-0471708582.
- [55] Green, M. and Limbeer D., *Linear Robust Control*, Prentice Hall, 1995, ISBN 0-13-102278-4.
- [56] Skogestad, S and Postlethwaite, I., *Multivariable Feedback Control Analysis and Design*, Second Edition, John Wiley and Sons, 2005, ISBN-13 978-0-470-01168-3.
- [57] Glover, K., Doyle, J. C., "State-space Formulae for All Stabilising Controllers That Satisfy an  $H_\infty$  Norm Bound and Relations to Risk Sensitivity," *Systems and Control Letters 11*, pp. 167, 1988.
- [58] Doyle, J. C., Glover, K., Khargonekar P.,P. and Francis, B.A., "State-Space Solutions to Standard  $H_2$  and  $H_\infty$  control problems," *IEEE Transactions on Automatic Control*, Volume AC 34, pp. 831-847, 1989.
- [59] Turner, C. W., Walker. D. J., Alford A.G., "Design and ground-based simulation of an  $H_\infty$  limited authority flight control system for the Westland Lynx Helicopter," *Aerospace Science and Technology Journal*, Vol. 5, pp. 221-234, 2001.
- [60] Dudgeon, G. J. W. and Gribble, J. J., "Helicopter Attitude Command Attitude Hold Using Individual Channel Analysis and Design," *AIAA, Journal of Guidance, Control and Dynamics*, Volume 20, pp. 962-971, 1997.
- [61] Fielding, C., and Varga, A., Bennani, S and Selier, M., *Advanced Techniques for Clearance of Flight Control Laws*, Springer, First Edition, 2004, ISBN-10 35404440542.
- [62] Bates, D. G. and Kureemun, R., "Improved Clearance of a Flight Control Law Using Mu-Analysis Techniques," *Journal of Guidance, Control, and Dynamics*, Vol. 26, no. 6, pp. 869-884, 2003.
- [63] Einthoven, P., Miller, D., Irwin, J., McCurdy, B., Bender, J., Blanken, C., Lawler, M., "Development of Control Laws for the Chinook Digital AFCS Program," *proceedings of the 62nd American Helicopter Society Annual Forum*, Phoenix, Arizona, USA, 2006.
- [64] Padfield, G. D., Clark G., "How long do pilots look forward? Prospective visual guidance in terrain-hugging flight," *proceedings of the 31st European Rotorcraft Forum*, Florence, Italy, 2005.

- [65] Padfield, G. D. and Bradley, R., "How Do Helicopter Pilots Know When to Stop, Turn or Pull up?" *Journal of the American Helicopter Society*, Vol. 48, part 2, pp. 108-119, 2003.
- [66] Jump, M. and Padfield, G. D., "Tau Flare or Not Tau Flare: That is the Question: Developing Guidelines for an Approach and Landing Sky Guide," *proceedings of the AIAA Guidance, Navigation and Control Conference*, San Francisco, California, United States of America, 2005.
- [67] Voskuijl, M., "Rotorcraft Flight Control for Improved Handling, Loads Reduction and Envelope Protection," Masters Thesis, The University of Liverpool, 2007.
- [68] Fielding, C., "The Design of Fly-By-Wire Control Systems," *BAE Systems Report, Aerodynamics (W427D)*, Warton Aerodome, Preston, (accessed via: [http://www.ukacc.group.shef.ac.uk/Lecture/2001\\_Lecture.pdf](http://www.ukacc.group.shef.ac.uk/Lecture/2001_Lecture.pdf)).
- [69] Corwin, W. H., Sandry-Garza, D. L., Biferno, M.H., Boucek, G. P., Logan, A. L., Jonsson, J. E., Metalis, S. A., "Assessment of Crew Workload Measurement Methods, Techniques, and Procedures," Volume I, Wright Patterson Air Force Base, USA, 1989, (accessed via <http://stinet.dtic.mil>).

# APPENDIX 1

## F-CH-47B CHINOOK MODEL

The CH-47B helicopter was modelled in FLIGHTLAB [33] for heavy slung load analysis using data obtained from several sources [39], [40], and was given the designation F-CH-47B. The main features of the model include the following;

1. Three dimensional aerodynamic loads derived from rotor off wind tunnel tests.
2. An articulated blade element rotor with equivalent hinge offset and hinge lag dynamics.
3. A three state rotor inflow and rotor interference model.
4. An accurate representation of the mechanical mixing control system.
5. A simple engine model with power dynamics.
6. The complete CH-47B SAS including; the longitudinal and lateral SAS, longitudinal cyclic trim (LCT), differential-collective-pitch-trim (DCPT) and directional SAS with sideslip, turn co-ordination and yaw rate damping.

### A1.1 Rotor System Properties

The rotor cross section, mass distribution and inertia data for the VR6 blade used in the CH-47B cross section were not available in the public domain. However a complete set of data describing the UH-60 NACA 0012 aerofoil which resembles the VR6 was accessible. This data was scaled up appropriately to represent the VR6; the blade chord was scaled up from 1.73 to 2.1 feet and the correct blade twist angle of 1 to -12 degrees corresponding to the VR6 was applied and the blade mass distribution scaled up. Table A1.1 shows the rotor parameter values used in the F-CH-47B model.

**Table A1.1: F-CH-47B Rotor System  
Parameters**

<b>Feature</b>	
Number of Blades	3
Blade	NACA 0012
Chord	2.1 ft
Sweep	0 to -12 deg
Inertia	Modified FGR
Mass distribution	Modified FGR
Flap hinge offset	1 ft
Lead-lag hinge offset	1.3 ft
Lag damper spring stiffness	0
Lag damper damping coefficient	20000 ft lbf sec/rad
Induced Velocity model	Three state model
Rotor 1 hub location	[7.33 0 8.62]ft
Rotor 2 hub location	[46.33 0 13.36]ft
Blade Tip loss factor	0.97
Orientation of hub 1	[0 171 0]ft
Rotor speed	23.562 rad/s (225/230 rpm)
Max Rotor speed (auto rotation)	244rpm
Rotor radius	30 ft
Blade pitch range -aft	-19.3 to +39.3deg
Blade pitch range -fwd	-22.5 to +36.2deg
Coning stop angle	30deg
Collective pitch	1 to 18deg
Rotor disc loading	8.84lb/ft <sup>2</sup>
Rotor interference model	Three state interference model with velocity decay constant

The FLIGHTLAB blade aerodynamic load component models a two dimensional aerodynamic segment that produces forces and pitching moment as nonlinear function of velocity and Mach number. It computes the air velocity expressed in the local coordinate, given the inertial, wind and induced velocity. The aerofoil table on the inputs are lift, drag and pitch moment coefficient for angles of incidence  $-90^\circ$  to  $90^\circ$  and side slip angles  $-180^\circ$  to  $180^\circ$ .

FLIGHTLAB was also used to model an enhanced version of Peters/He finite state dynamic wake models for a 3-D non-uniform unsteady rotor induced flow solution. The theory is based on unsteady potential theory of Peters and He [37]. The model is derived from first principles and is formulated in state space consistent with all flight



dynamics modelling. The finite state dynamic wake model has the sophistication of the vortex wake for modelling accuracy and also offers efficiency in satisfying the stringent computational demands of flight simulation. The model works well for steady and manoeuvring flight conditions and features:

1. tip vortex distortion effect in the finite state dynamic wake model to overcome the poor prediction of rotorcraft off axis response
2. modelling of vortex ring state and extending the simulation to be applicable across the flight envelope
3. the swirl due to in-plane lift which is important in prop-rotor modelling

The Peters 3-state interference model computed the off-rotor induced velocity by vortex wake model for interference for either prescribed wake or free wake.

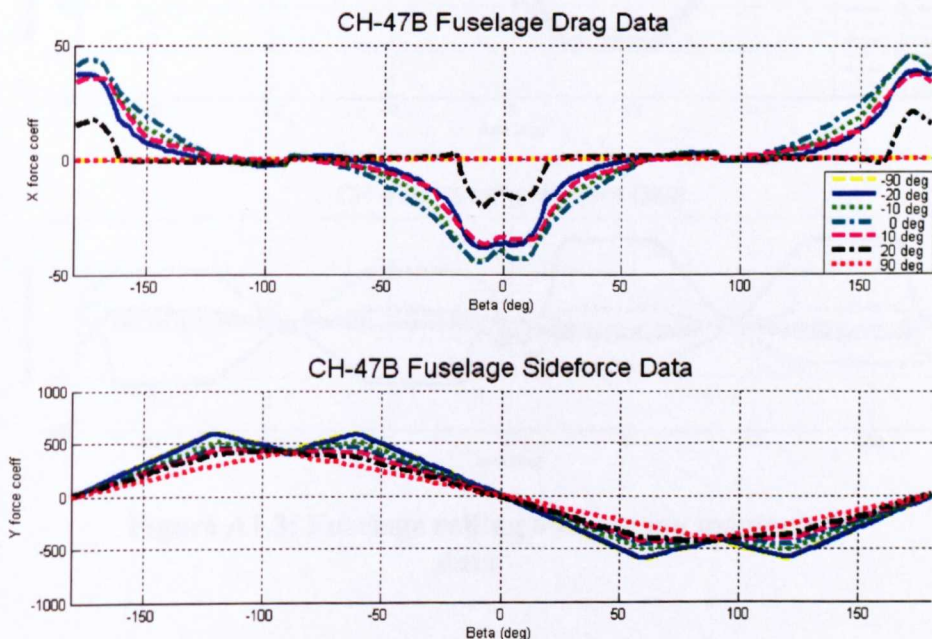
## **A1.2 Fuselage Properties**

The fuselage data implemented was generated from rotor-off wind tunnel tests performed by NASA Ames. The forces and moments were represented in the helicopter body reference frame and were normalised by the fuselage dynamic pressure. The aerodynamic data was calculated from the function tables by linear interpolation on fuselage angle of attack  $\alpha$  and sideslip angle  $\beta$ . The function tables consist of X, Y, Z (surge, sway, heave) fuselage forces and L, M, N (rolling, pitching and yawing) fuselage moments. Table A1.2 on the following page shows the fuselage data used in the FLIGHTLAB model.

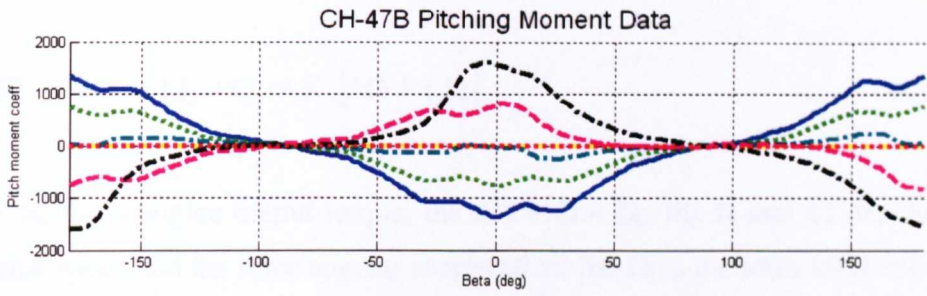
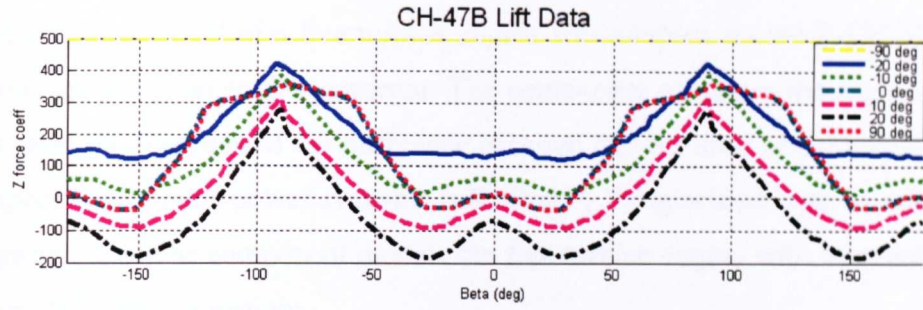
**Table A1.2: F-CH-47B Fuselage Properties**

Feature	
Most forward CG	[25.86 0 1.94]ft
Weight Empty CH-47D CG	[26.076 0 1.94]ft
Weight Empty CH-47B	[26.29 0 1.94]ft
Most aft CG	[26.51 0 1.94]ft
Total Vehicle Mass	33000lbm
Total Roll moment of inertia	34000 slug-ft <sup>2</sup>
Total Pitch moment of inertia	202500 slug-ft <sup>2</sup>
Total Yaw moment of inertia	191000 slug-ft <sup>2</sup>
Total X-Y product of inertia	0 slug-ft <sup>2</sup>
Total X-Z product of inertia	149000 slug-ft <sup>2</sup>
Total Y-Z product of inertia	0 slug-ft <sup>2</sup>
Air load measurement point	[26.29 0 1.94]ft
Ref Area	1ft <sup>2</sup>
Ref Length	1 ft
Pilot eye position	[6.47 -0.64 0.43]ft
Un-deflected gear length	2.366 ft

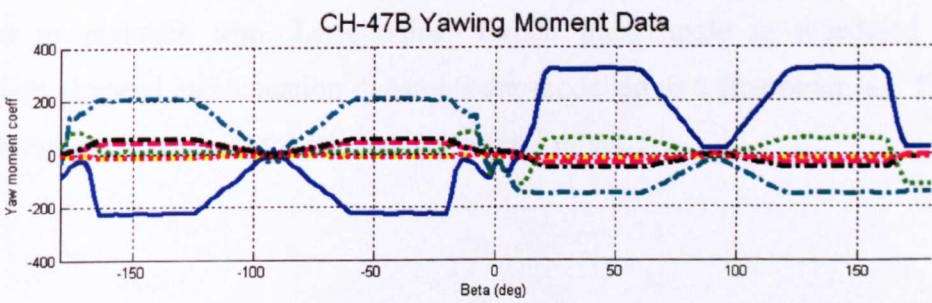
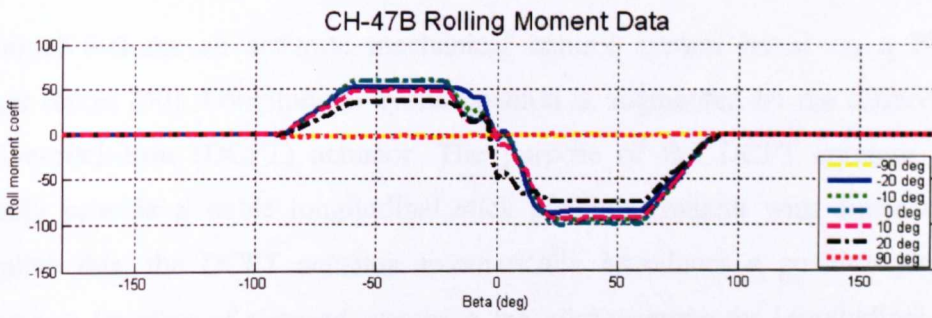
The fuselage drag data was modified to incorporate the extra drag from the landing gear and rotor hub using a drag estimate procedure adopted by Prouty [34]. Figures A1.1, A1.2 and A.1.3 show the F-CH-47B fuselage drag, side-force, lift, pitching moment, rolling moment and yawing moment as a function of  $\alpha$  and  $\beta$ .



**Figure A1.1: Fuselage drag and side-force data**



**Figure A1.2: Fuselage lift & pitching moment data**



**Figure A1.3: Fuselage rolling and yawing moment data**

### A1.3 Engine Properties

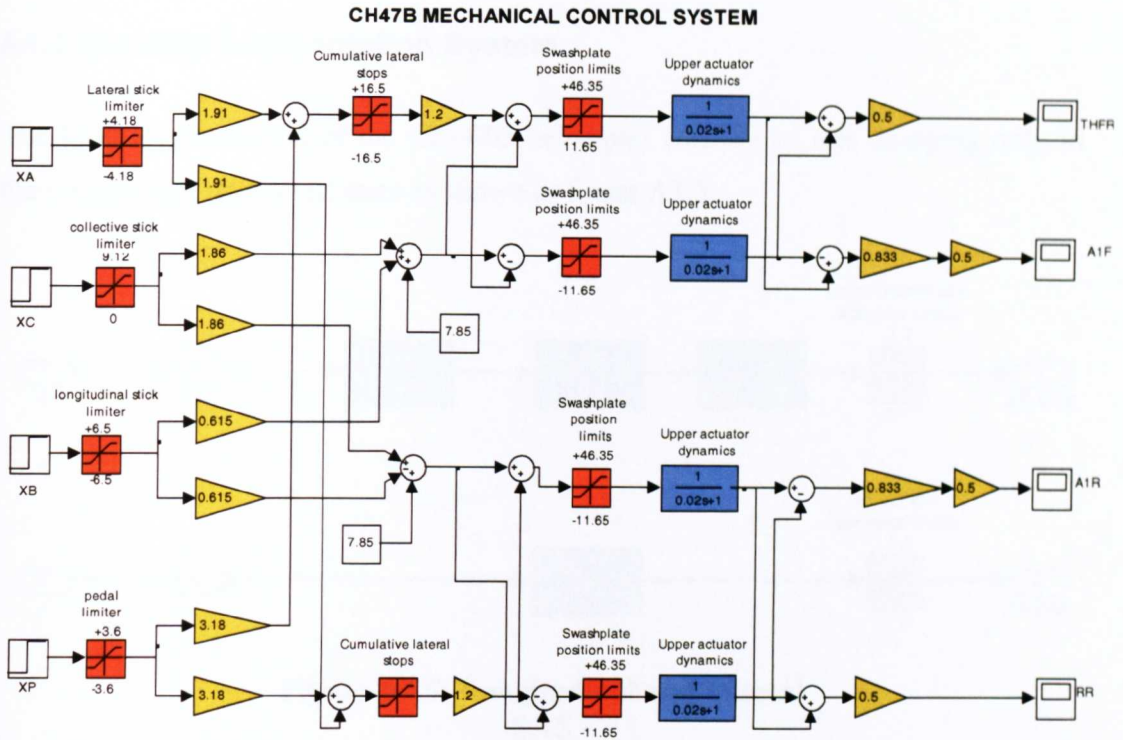
A simple engine model of a free turbine engine was adopted for the F-CH-47B that functions more like an engine governor. The component computes the engine output torque from the feedback of the difference between current rotor speed and the rotor ideal speed. The engine power available is limited by the specified input as a function of flight altitude. The component models the free turbine engine with a second order ordinary differential equation:

$$(\tau_1\tau_2)\ddot{Q}_e + (\tau_1 + \tau_3)\dot{Q}_e + Q_e = K_3[\Delta\Omega + \tau_2\dot{\Omega}] \quad \text{eqn A1.1}$$

where the  $Q_e$  is engine output torque; the  $\Delta\Omega = \Omega - \Omega_i$ ; the  $\Omega$  and  $\dot{\Omega}$  are the rotor rotational speed and the rotor angular acceleration; the  $\Omega_i$  is the rotor ideal speed; the  $\tau_1, \tau_2, \tau_3$  are the engine time constants; the  $K$  is the droop law constant.

### A1.4 Mechanical Control System

The model features an accurate mechanical control system based on a NASA technical report [40]. Longitudinal cyclic position is augmented by the differential-collective-pitch-trim (DCPT) actuator. The purpose of the DCPT actuator is to artificially provide a stable longitudinal stick position gradient with airspeed. To accomplish this, the DCPT actuator automatically introduces a positive pitching moment as a function of airspeed, requiring the pilot to move the longitudinal stick forward to maintain trim. Longitudinal Cyclic pitch angle is scheduled with equivalent airspeed and actuation dynamics are modelled as a first-order lag. Figure A1.4 shows a schematic of the mechanical control mixer.

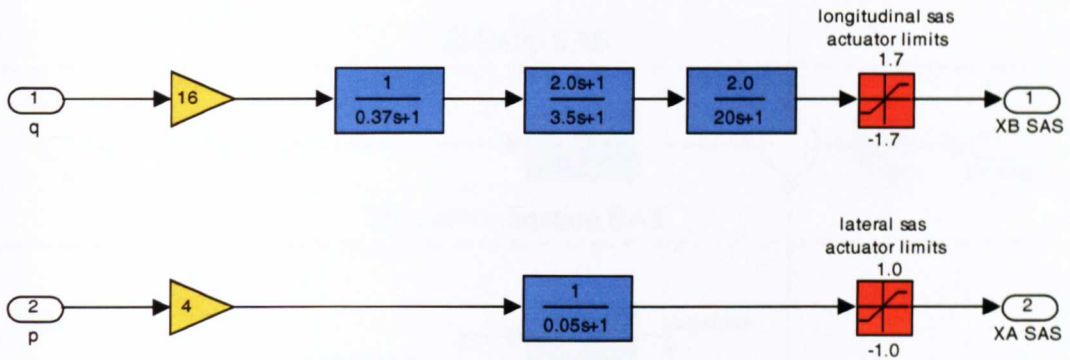


**Figure A1.4: CH-47B mechanical controls**

After the control stop limiting downstream of the cockpit control-position limiting, control positions are converted from inches to degrees of equivalent swashplate. First stage control mixing (longitudinal and vertical, lateral and directional) is followed by cumulative lateral stop limiting (of the authority of differential lateral and combined lateral inputs). The resultants of (vertical and lateral) second stage mixing are limited at the swashplate prior to driving the swivelling and pivoting upper-boost actuators. To prevent bind up in the swashplates, and ensure that they move smoothly, each is driven by a combination of swivelling and pivoting motion and swashplate displacement is the sum of the two inputs.

## A1.5 Stability Augmentation System

The basic augmentation of the CH-47B helicopter consists of rate damping only in the longitudinal and lateral axes as shown in figure A1.5:



**Figure A1.5: Longitudinal and Lateral SAS**

The longitudinal SAS consists of pitch-rate feedback through cascaded first-order lag, lead-lag and washout filters. The lateral SAS comprises a single first-order lag applied to roll rate.

Directional SAS yaw damping uses simple filtering with a change from a first-order lag in cascade with a lead-lag at 40 knots to a first-order lag in cascade with a washout filter applied to yaw rate as shown in figure A1.6 Turn co-ordination is implemented with a first-order lag on helicopter roll rate.

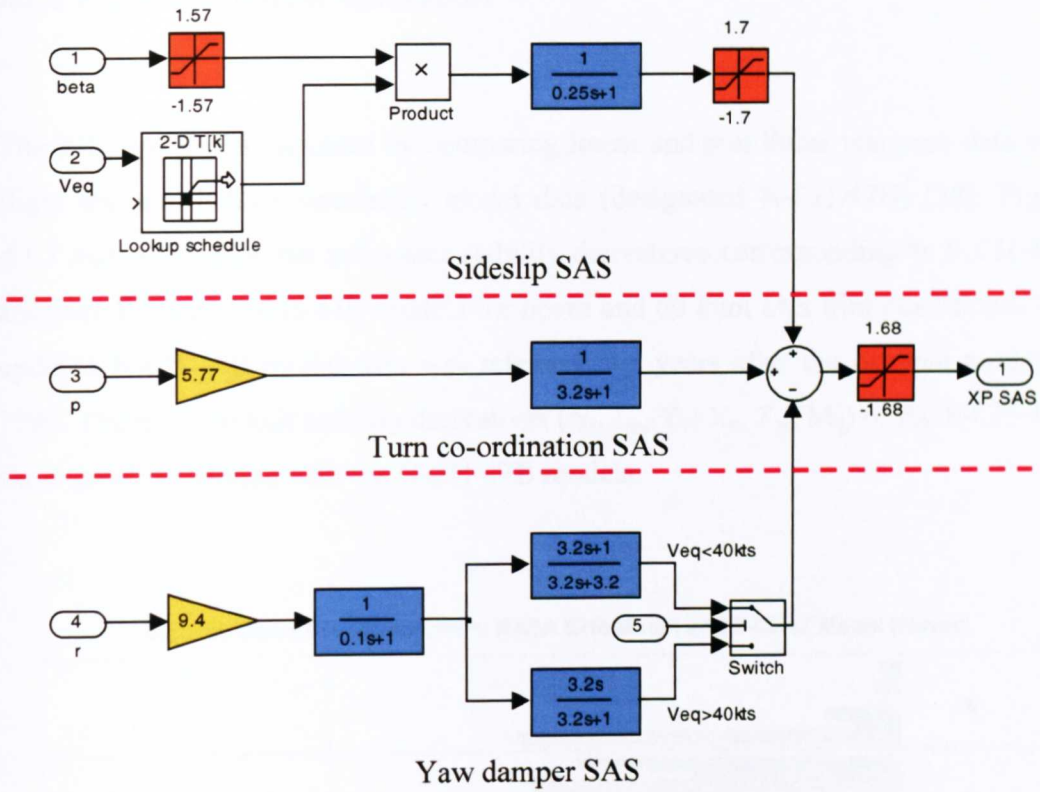
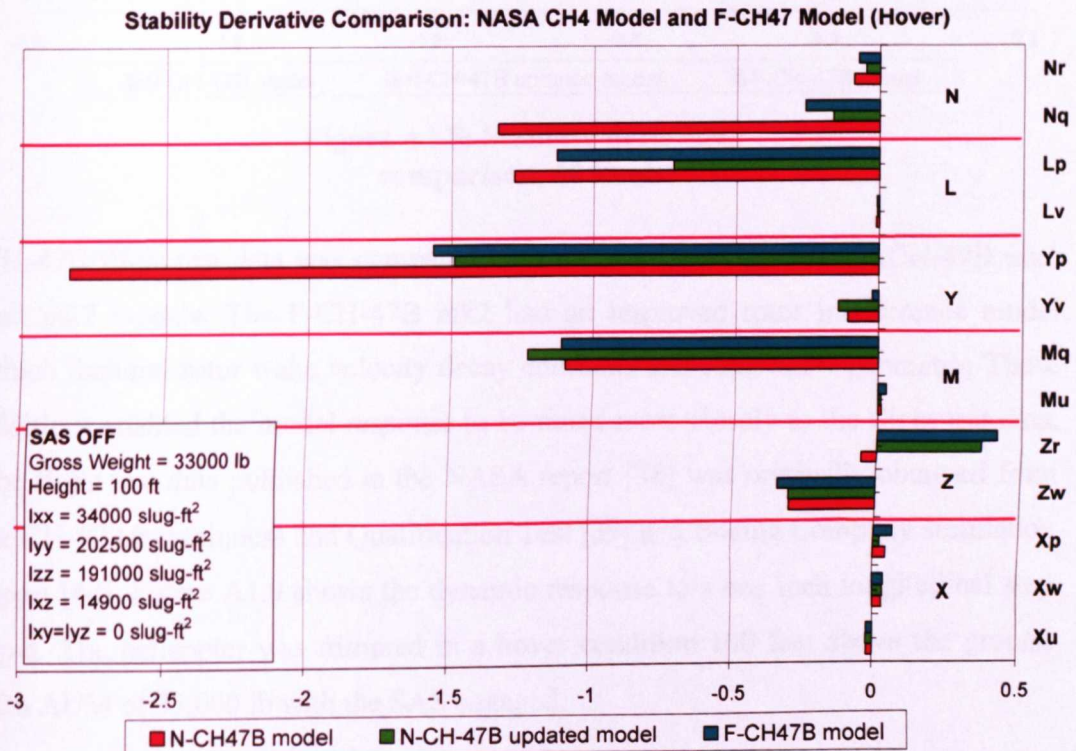


Figure A1.6: Directional SAS

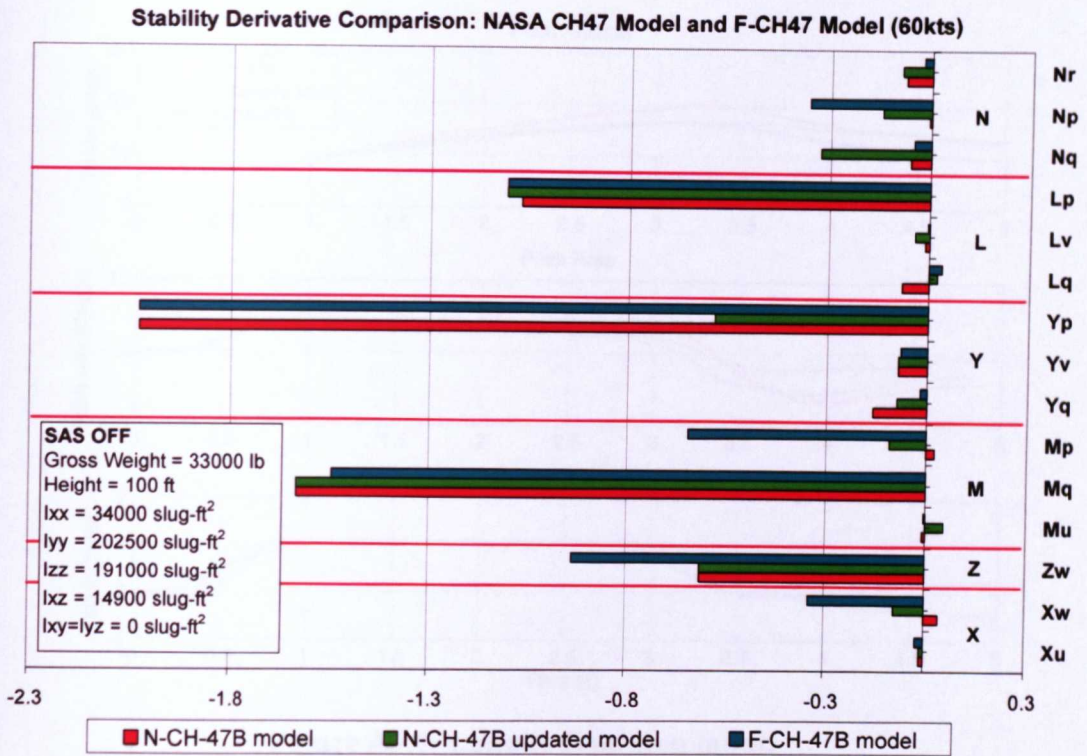
### A1.6 F-CH-47B Model Validation

The F-CH-47B was validated by comparing linear and non linear response data with flight test and NASA simulation model data (designated N-CH-47B) [38]. Figure A1.7 and A1.8 show the helicopter stability derivatives corresponding to F-CH-47B and two different N-CH-47B models for hover and 60 knot IAS trim conditions. The updated N-CH-47B model data was released two years after the original model in 1986. The main on axis stability derivatives ( $N_r$ ,  $L_p$ ,  $Y_v$ ,  $X_u$ ,  $Z_w$ ,  $M_q$ ) of the F-CH-47B show good correlation with the N-CH-47B models.



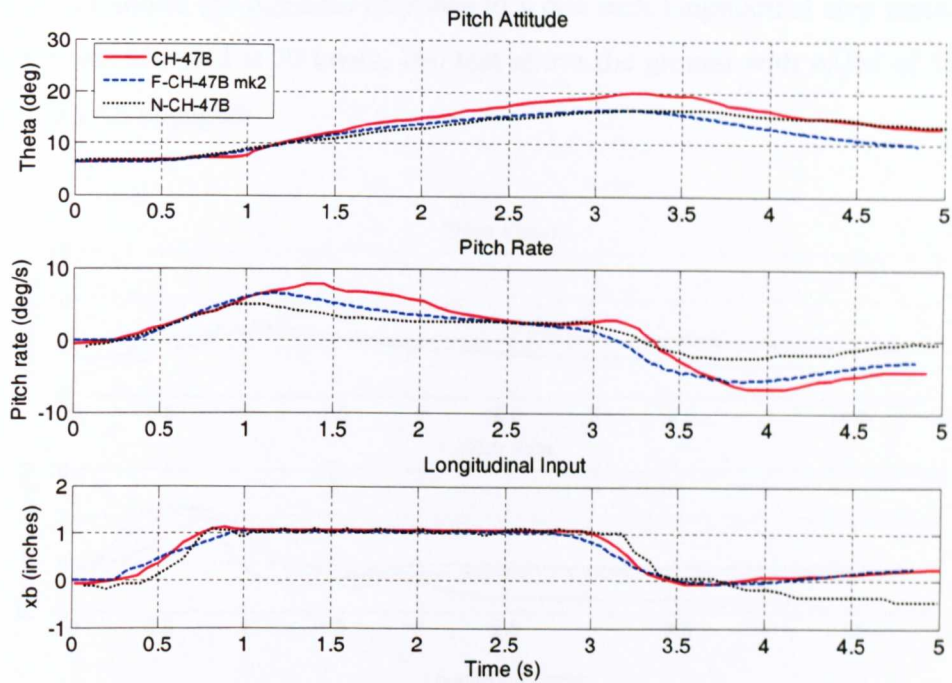
**Figure A1.7: Stability derivative comparison, hover**





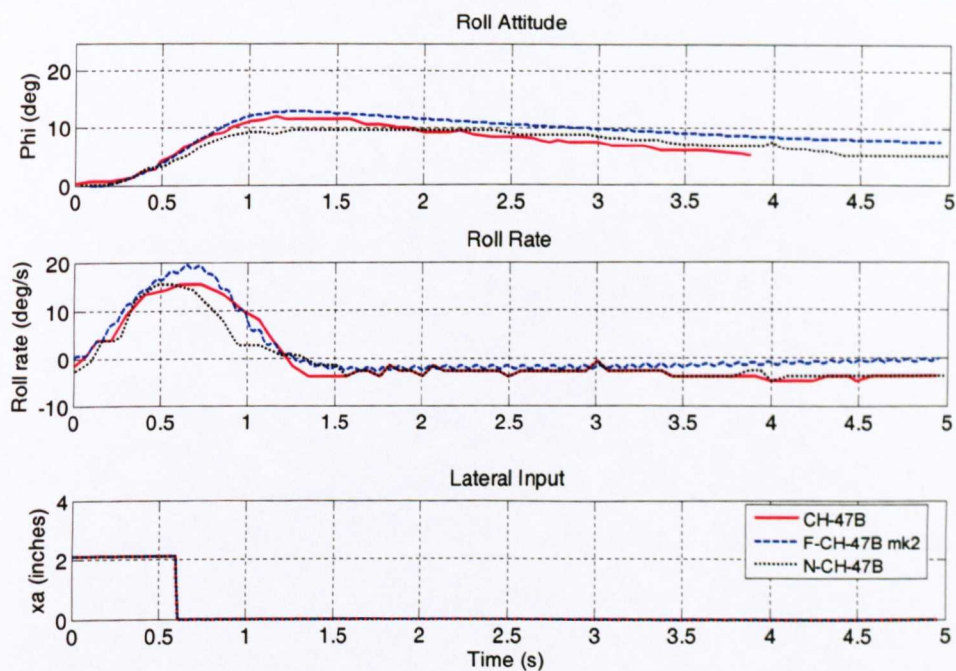
**Figure A1.8: Stability derivative comparison, 60 knots**

CH-47B flight test data was compared with the N-CH-47B and the F-CH-47B mk1 and mk2 models. The F-CH-47B mk2 had an improved rotor interference model which featured rotor wake velocity decay constants and rotor skew geometry. These additions enabled the model response to be tuned more closely to the flight test data. The flight test data published in the NASA report [38] was originally obtained from the CH-47 Airworthiness and Qualification Test [39] and Boeing Company simulation report [40]. Figure A1.9 shows the dynamic response to a one inch longitudinal step input. The helicopter was trimmed in a hover condition 100 feet above the ground with AUM of 33,000 lb with the SAS engaged:



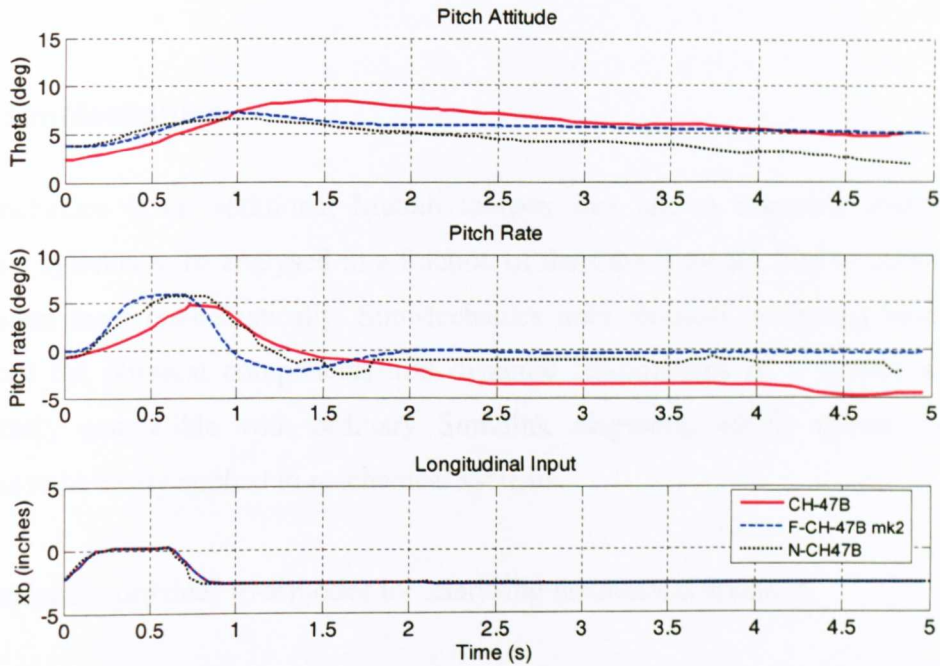
**Figure A1.9: Longitudinal step input, 33000lb, SAS on**

Figure A1.10 shows the dynamic response to a one inch lateral step input. The helicopter was trimmed at 35 knots, 100 feet above the ground with AUM of 33,000 lb with the SAS engaged.



**Figure A1.10: Lateral step input, 35 knots, 33,000lb, SAS on**

Figure A1.11 shows the dynamic response to a one inch longitudinal step input. The helicopter was trimmed at 70 knots, 100 feet above the ground with AUM of 33,000 lb with the SAS engaged:



**Figure A1.11: Lateral step input, 35 knots, 33,000lb, SAS on**

## **A p p e n d i x 2**

### **SIMMECHANICS MULTI-BODY SIMULATION**

#### **A2.1 SimMechanics**

SimMechanics is an additional Matlab toolbox that allows complex multi-body dynamic systems to be analysed in a fraction of the time it would take to derive and implement them mathematically. SimMechanics uses physical modelling blocks to represent the physical components and dynamic relationships of a system and is completely compatible with ordinary Simulink diagrams, which allows control systems to be easily applied to mechanical systems.

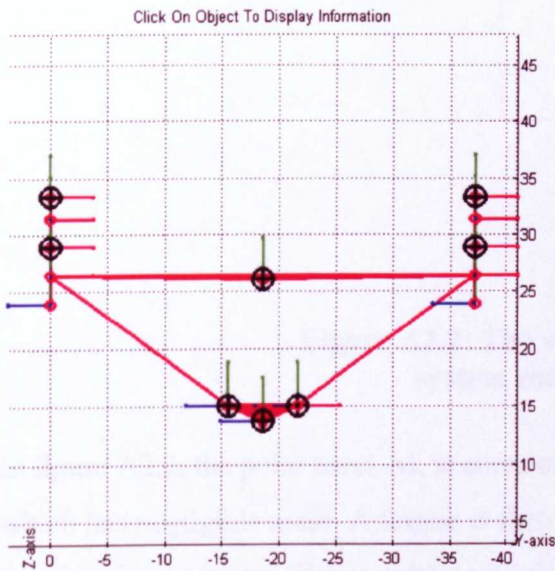
SimMechanics provides four modes for analyzing mechanical systems:

1. Forward Dynamics calculates the motion of the mechanism resulting from the applied forces/torques and constraints.
2. Inverse Dynamics finds the forces/torques necessary to produce a specified motion for open loop systems.
3. Kinematics does the same for closed loop systems by including the extra internal invisible constraints arising from those structures.
4. Trimming searches for steady or equilibrium states of a system's motion with the Simulink trim command. It is mostly used to find a starting point for linearization analysis.

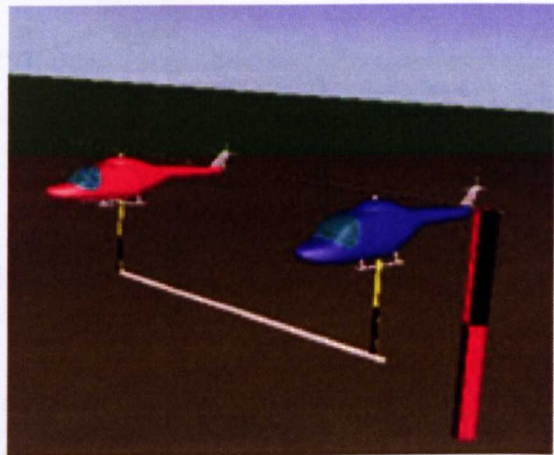
The user must build separate models for each type of analysis because of the different mechanical variables that have to be specified for each analysis. For example in forward dynamics mode, the initial conditions for positions, velocities and accelerations including the all the forces acting on the system are required to find the solution. However in inverse dynamics or kinematics mode, the positions, velocities

and accelerations of the independent degrees of freedom must be completely specified.

SimMechanics also allows the complex dynamics to be visualised in three dimensions using two different methods. In the first, the Matlab Handle Graphics tool is utilised, which uses standard Matlab graphics with some additional SimMechanics features to visualise the system. This proved to be extremely valuable during the development of the mechanical system, since the visualisation automatically updated when components were added allowing the components and locations to be visualised. The second visualisation method uses the Matlab Virtual Reality Toolbox to build components of a complex system in a hierarchical method allowing virtual ‘worlds’ to be developed using the virtual reality modelling language (VRML). Figure A2.1 shows how the co-operative lift system modelled visually using the two different visualisation techniques described:



SimMechanics graphics

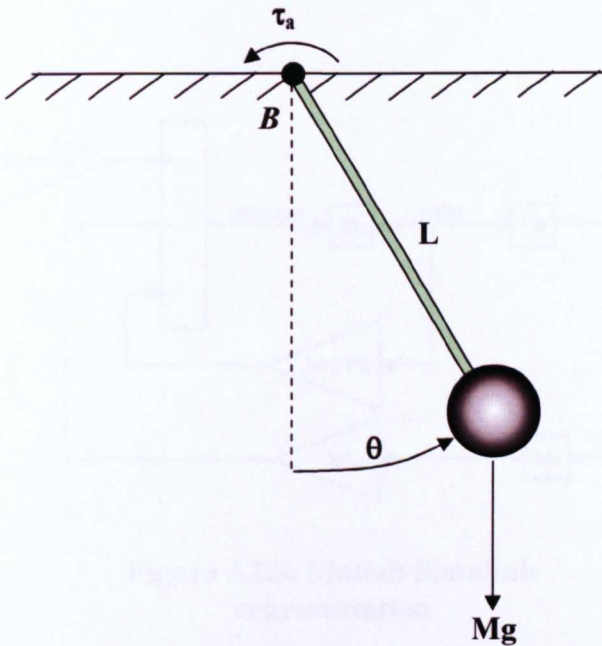


VRML graphics

**Figure A2.1: Matlab SimMechanics and Matlab Virtual Reality toolbox graphics representations of the co-operative lift model**

## A2.2 SimMechanics Example

The following section illustrates how a simple pendulum system can be modelled in three different ways; mathematically from first principles, using Matlab Simulink and Matlab SimMechanics. The external slung load dynamics for a single line and mass system is analogous to a simple pendulum making this example particularly relevant. There is usually an offset between the helicopter's centre of gravity and cable attachment adding to the complexity of the dynamics. The pendulum system investigated is illustrated in figure A2.2:



**Figure A2.2: The simple pendulum system considered**

In figure A2.2, the point mass,  $M$ , is connected to the pivot by a rigid arm of length  $L$ , which has negligible mass. A torque is then applied to the system and the bearings in the pivot have viscous friction with coefficient  $B$ .

After drawing the free-body diagram the equations of motion for the pendulum can be derived as:

$$J\dot{\omega} + B\omega + MgL\sin\theta = \tau_a(t)$$

The moment of inertia for a point mass is given by  $J=ML^2$  and the previous equation can be re-written as:

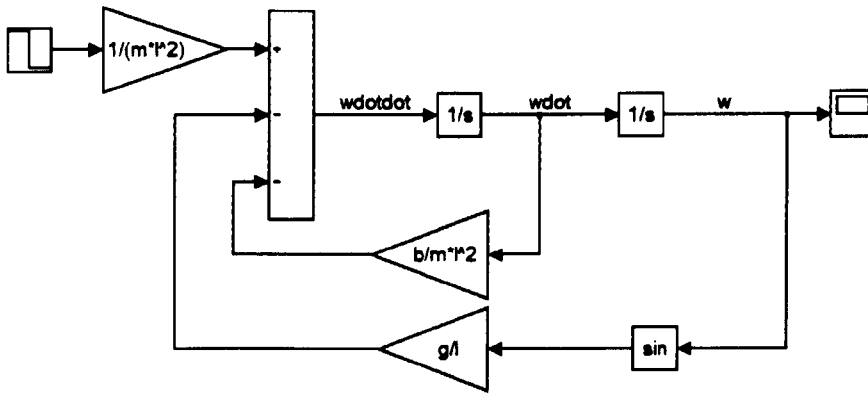
$$ML^2 \dot{\omega} + B\omega + MgL \sin \theta = \tau_a(t)$$

Introducing  $\omega = \dot{\theta}$ , the equation of motion can be re-written as:

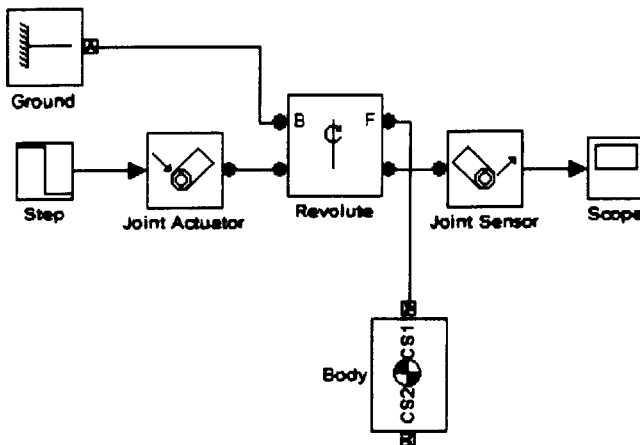
$$\dot{\theta} = \omega$$

$$\dot{\omega} = -\frac{g}{L} \sin \theta - \frac{B}{ML^2} \omega + \frac{1}{ML^2} \tau_a(t)$$

Figures A2.3 and A2.4 show the Matlab Simulink and SimMechanics representatives of the system:

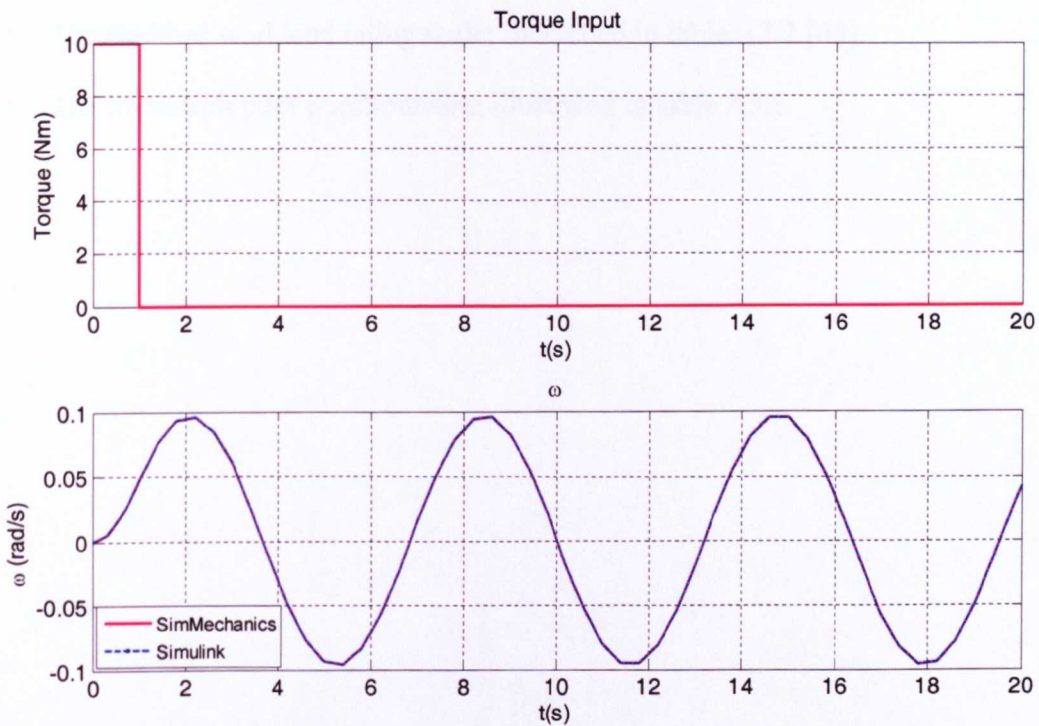


**Figure A2.3: Matlab Simulink representation**



**Figure A2.4: Matlab SimMechanics representation**

Figure A2.4 illustrates one of the advantages of using Matlab SimMechanics over Matlab Simulink to model multi-body dynamic systems. The physical structure of the system is visible during model development which aids the construction process. In contrast, the Simulink system shown in figure A2.3 must be first derived mathematically and does not provide an insight into the physical structure of the system during the build procedure. Figure A2.5 shows the angular response to a torque step input for the two different modelling methods, where  $m=1\text{kg}$ ,  $l=10\text{m}$ ,  $g=9.81\text{m/s}^2$ , and  $b=0\text{Ns/m}$ .



**Figure A2.5: Pendulum angular response to a torque step input for SimMechanics and Simulink representations**

From the figure it is evident that SimMechanics gives the same response as the Simulink mathematically derived system. This illustrates how SimMechanics can also be used to check mechanical systems that have been derived manually.



## **A p p e n d i x 3**

### **PILOT RATING SCALES**

This section provides examples of the three pilot rating scales that were used in the piloted simulation trials. They were:

1. The Cooper-Harper handling qualities rating scale; illustrated in table A3.1 [42].
2. The Bedford workload rating scale; illustrated in table A3.2 [69].
3. The in-cockpit pilot questionnaire; illustrated in table A3.3.

Table A3.1: Cooper-Harper Handling Qualities Rating Scale

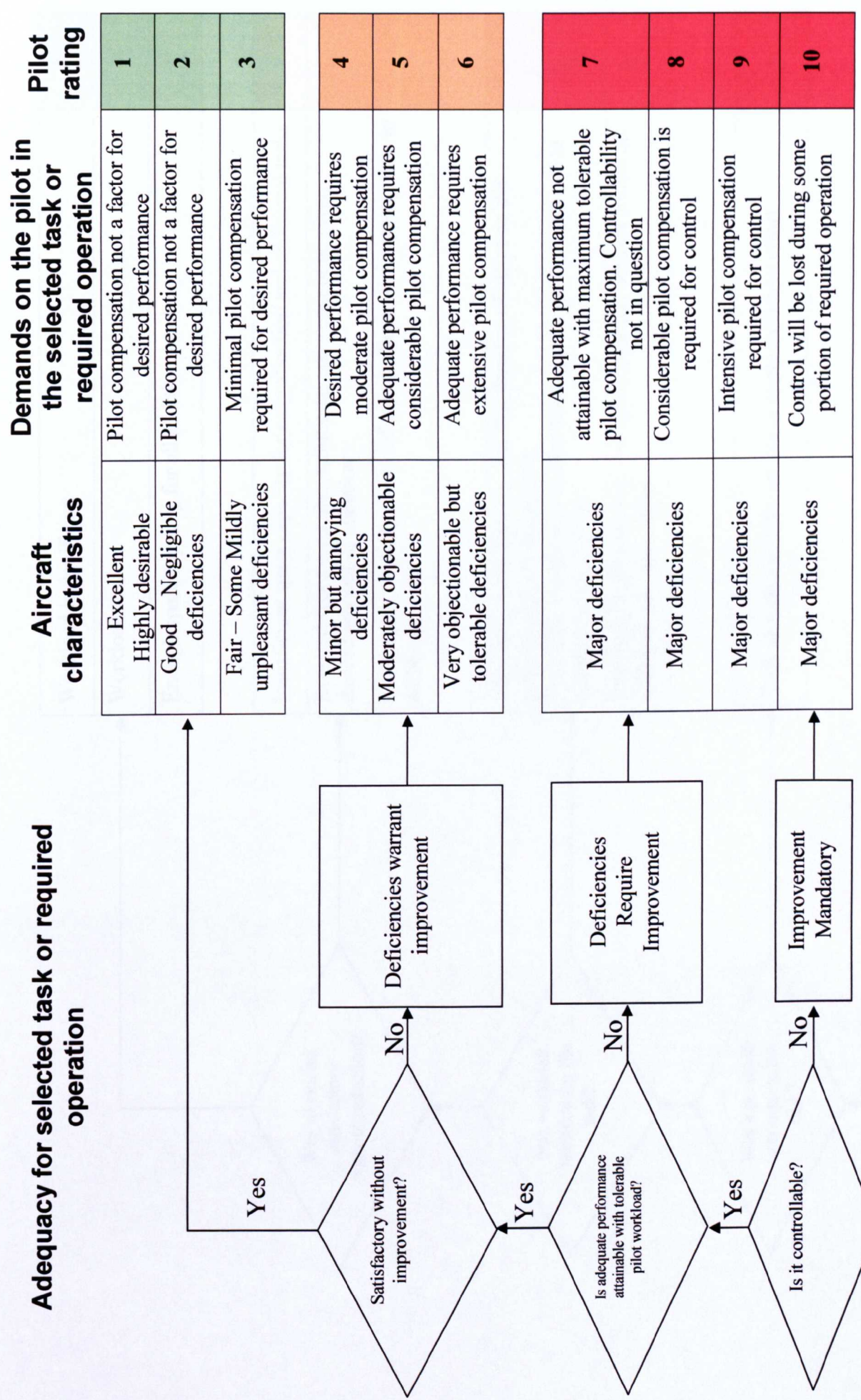
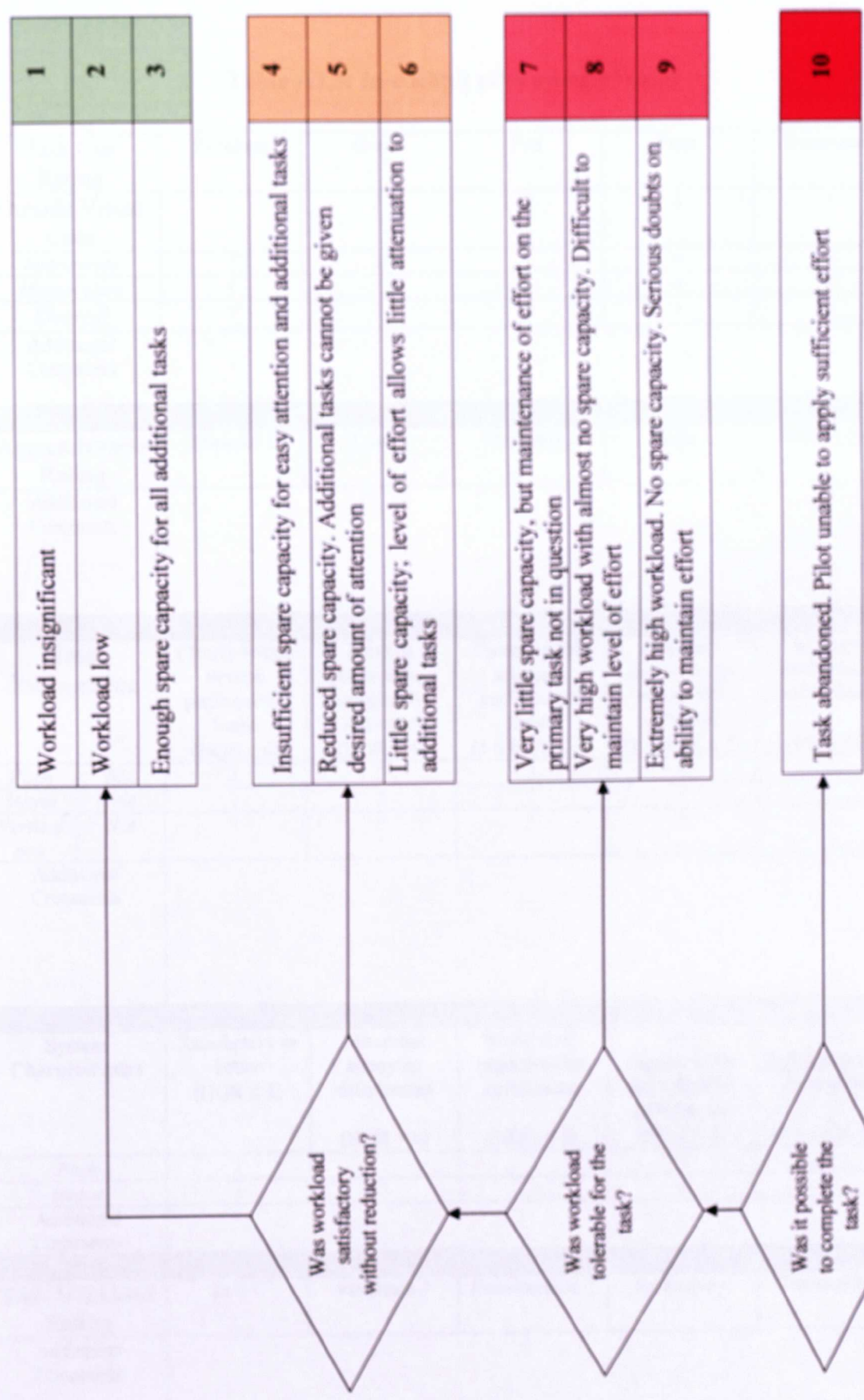


Table A3.2: Bedford Workload Rating Scale



**Table A3.3: In-cockpit pilot questionnaire**

<b>Task Cue Rating</b>	Excellent	Good	Fair	Poor	Inadequate
<b>Outside Visual Cues</b>	1	2	3	4	5
<i>Instruments</i>	1	2	3	4	5
<i>Motion Cues</i>	1	2	3	4	5
<b>Overall</b>	1	2	3	4	5
<b>Additional Comments</b>					
<b>Aggressiveness Rating</b>					
<b>Aggressiveness Rating</b>	Minimal 1	Low 2	Moderate 3	High 4	Maximum 5
<b>Additional Comments</b>					
<b>Task Performance</b>					
<b>Task Performance</b>	Clearly within desired performance limits (HQR ≤ 4)	Desired performance marginally achieved (HQR ≤ 4)	Clearly within adequate performance limits (5 ≤ HQR ≤ 7)	Adequate performance marginally achieved (5 ≤ HQR ≤ 7)	Adequate performance not achieved (HQR ≥ 7)
<i>Pitch</i>	N/A	1	2	3	4
<i>Heave</i>	N/A	1	2	3	4
<i>Vertical pos.</i>	N/A	1	2	3	4
<b>Additional Comments</b>					
<b>System Characteristics</b>					
<b>System Characteristics</b>	Satisfactory or better (HQR ≤ 3)	Minor but annoying deficiencies (HQR = 4)	Moderately objectionable deficiencies (HQR = 5)	Very objectionable but tolerable deficiencies (HQR = 6)	Major deficiencies but controllable (7 ≤ HQR ≤ 9)
<i>Pitch</i>	1	2	3	4	5
<i>Heave</i>	1	2	3	4	5
<b>Additional Comments</b>					
<b>Task Workload Rating</b>					
<b>Task Workload Rating</b>	Low 1	Moderate 2	Considerable 3	Extensive 4	Intolerable 5
<b>Additional Comments</b>					

HQR (Cooper-Harper)										
	1	2	3	4	5	6	7	8	9	10
Main reasons for rating										
PIO Rating										
	1	2	3	4	5	6	N/A			
Main reasons for rating										
Influencing factors				--	-	0	+	++		
Primary Response (overall)	Pitch									
	Heave									
	Stability									
	Coupling effects due to inceptor or H/C									
	Vehicle limits									
Inceptor	Mech. Char. (breakout, friction, freeplay)									
	Control char. (shaping, force feel, harmony)									
	Sensitivity response./displacement									
Additional Comments										